PERFORMANCE EVALUATION OF CHIRP SPREAD SPECTRUM SYSTEM AND LAND MOBILE SATELLITE SYSTEM BY COMPUTER SIMULATION

by

Junghwan Kim

Dissertation submitted to the Faculty of the

Virginia Polytechnic Institute and State University

in partial fulfillment of the requirements for the degree of

Doctor of Philosophy

in

Electrical Engineering

APPROVED:

Timothy Pratt, Chairman

Charles W. Bostian

Kai-Bor Yu

Jerry E. Mann

Richard O. Claus

July, 1988

Blacksburg, Virginia

PERFORMANCE EVALUATION OF CHIRP SPREAD SPECTRUM SYSTEM AND LAND MOBILE SATELLITE SYSTEM BY COMPUTER SIMULATION

by

Junghwan Kim

Timothy Pratt, Chairman

Electrical Engineering

(ABSTRACT)

The work presented in this dissertation examines the performance of two satellite radio communication systems by computer simulation. Two simulations were separately performed for a spread spectrum chirp system as an analog communications system, and for the Land Mobile Satellite System (LMSS) channel as a digital communications system.

For the simulation of analog communications, a spread spectrum system using chirp techniques called 'Coded Multiple Chirp Spread Spectrum' was proposed as a simple, cost-effective alternative for conventional spread spectrum systems. Its application as a spread spectrum overlay service on analog FM-TV was examined through the mutual interference analysis and spectral analysis using software programming.

For the simulation of digital communications, various digital modulation schemes as well as channel encoding, block interleaving/deinterleaving, and differential encoding techniques were used for a thorough performance evaluation of a Land Mobile Satellite System under fading conditions. For this purpose, an LMSS fading channel simulator capable of simulating diverse fading characteristics for a satellite channel was designed and tested to yield various performance measures such as symbol error rate and average bit error rate.

Acknowledgements

I am sincerely grateful to Dr. Timothy Pratt, my advisor, for his constant encouragement, invaluable and timely advice, and guidance right through the course of the work reported here.

I thank Dr. Charles W. Bostian, for his guidance and countless support through the second part of this work. I also thank Dr. Tri T. Ha, my former advisor, for his support through the first part of this work. Also I wish to acknowledge with sincere appreciation the financial support of NASA Lewis Research Center and NASA Jet Propulsion Laboratory from 1986 to 1988.

In addition, I would like to thank the following people : for his help in Trellis decoder programming, , a long time colleague, for his help and advice during study, and the members of Satcom Group for their support and comradery, for her help in typing figures.

Finally, the appreciation for the patience and understanding of my old parents in my country my wife, my daughter, and all of my family, cannot be expressed in words. Their quiet and heartfelt support has been a significant factor in my undertaking and completing this work.

Table of Contents

List of Illustrations

I. Introduction

Ever since the appearance of the first geosynchronous communication satellite INTELSAT I in 1965, the practical implementation of the idea proposed by Arthur C. Clarke in 1945, communication technology has gradually changed to digital from analog. In order to meet the increasing demand for complicated digital services as well as well-established analog ones, it has been necessary to design and analyze systems in a timely, cost-effective manner. The resulting design, analysis, and optimization of performance have been very demanding and difficult.

Over the past decades, a large body of computer-aided modeling techniques has been developed to facilitate the design process of complex communication systems. Nowadays, these techniques constitute a new and challenging part of communications engineering. In modeling of communication links, either satellite or terrestrial, performance evaluation and trade-off analyses are the central issues. These objectives can be accomplished by using models of devices and systems and either prototype hardware or computer simulation. Except for some idealized and oversimplified cases, evaluation of the performance of complex communication links in closed form using analytical techniques alone is extremely difficult. In addition, the former approach is generally expensive, time consuming, and inflexible. These are the major reasons why computer simulation is preferred.

However, there are many situations where the explicit needs of hardware experiments cannot be met by computer simulation, even though digital simulation provides a useful and effective adjunct to direct analytical evaluation of communication link performance. Hence, a proper blend of analytic modeling and simulation can be regarded as the key to successful performance evaluation. This approach is especially useful when the satellite communications link experiences fading that cannot be fully predicted by the computer simulation, requiring practically measured data for effective analysis.

In this thesis, the performance of satellite communications links employing two typically different communications schemes, i.e., analog communications and digital communications, was evaluated by computer simulation. For this purpose, two separate simulation programs that could simulate a spread spectrum system using chirp techniques and a Land Mobile Satellite System under fading conditions were created and tested.

For the first simulation, a spread spectrum system using chirp techniques was selected to investigate the feasibility of multiple access using chirp, an analog communication technique combined with spread spectrum in a satellite communication link. In this research, a cost-effective, simple-structured chirp spread spectrum system called "Coded Multiple Chirp Spread Spectrum", that requires no complex synchronization was proposed. Then, a spread spectrum overlay service on an existing analog FM-TV channel using the same satellite transponder was evaluated by computer simulation. The first part of the introduction is devoted to this topic.

For the second simulation, the Land Mobile Satellite System (LMSS) using several digital modulation schemes was selected as the counterpart to analog communications. In this simulation, an LMSS channel simulator which could simulate fading effects as well as basic satellite link components such as nonlinear amplifiers, channel encoding, and differential encoding was created and tested. The latter part of this introduction is devoted to this subject.

The pulsed FM or chirp modulation technique, invented by B. M. Oliver at Bell Labs in 1951 and formulated by C. E. Cook in 1958, has been widely used in radar systems as a solution for the conflicting requirements of simultaneous long-range measurements and high range resolution [1]. The range resolution is obtained by transmitting a long frequency modulated pulse that is time compressed in the receiver into a much narrower pulse. The distributed energy in the long pulse is coherently processed in a matched filter receiver to yield a short pulse of enhanced amplitude [1-2]. A detailed account of the chirp concept and the relevant mathematics has since been given by many authors [1-5].

The physical constraint of building delay lines that have dispersion characteristics which provide the required high time-bandwidth product has been overcome recently by using surface acoustic wave (SAW) devices and other types of dispersive delay lines (DDL). Chirp has now become an effective tool for producing small, low cost, lightweight spread spectrum systems for communication and ranging systems, as well as for radar [1].

Spread spectrum techniques have made the use of small earth terminal satellite networks commercially valuable for low data rate users. The low power spectral density of spread spectrum signals allows the use of very small antennas without significant interference to adjacent satellites when transmitting, while the processing gain allows the rejection of signals received from adjacent satellites when receiving. Among the four basic types of spread spectrum techniques, chirp systems have been shown to have advantages over other techniques like direct sequence (DS), frequency hopping (FH), time hopping (TH), and various hybrids. No coding is necessary with chirp, in principle, and thus no code synchronization is necessary either. In addition, multiple access can be achieved with simple sweep rate changes rather than by using different pseudo random sequence codes [6];[7]. The high vulnerability of chirp systems to deliberate jamming has been the major obstacle to their application for military use. Thus, the technique has received little attention.

In a chirp system, all non-chirp type interfering signals and noise at the input of the pulse compression filter appear at the output either with the same mean power or with decreased power. However, the desired chirp signal gets enhanced by the processing gain, resulting in the rejection of the interference and noise. The possibility of relatively simple equipment implementation makes the chirp spread spectrum system attractive for low data rate, bursty commercial communication systems.

The feature that permits the simple implementation of chirp for low data rate satellite communications is the absence of a synchronization loop in the receiver. In all other spread spectrum systems, the receiver must synchronize to the PN (Pseudo Noise) sequence used to spread the original data. If data rates are low and the messages are short, the receiver may take many seconds to synchronize to the received signal, in order to receive a message less than a second in length. The lower the data rate and the longer the PN sequence, the more pronounced this problem becomes, and very low throughput is achieved. A bursty system, in which messages are transmitted infrequently to a given receiver, makes the problem even worse, because receiver synchronization cannot be maintained between transmissions. It is in this application that the chirp system has the best performance, since no receiver synchronization is needed, and throughput can be maintained at 100%.

The following two chapters(Chapter II and III) are devoted to the description of design and analysis of spread spectrum systems using chirp. In Chapter II, several chirp spread spectrum systems are studied, using different modulation techniques. These included within-chirp, and multiple-chirp, where single or multiple chirps modulate the carrier amplitude, frequency or phase. Based on the preliminary study, the proposed coded multiple chirp spread spectrum system is described in detail, together with a performance analysis through computer simulation. In addition, the possibility of spread spectrum multiple access (SSMA) using the proposed system was also evaluated as the final step.

Chapter III starts with the analysis of the mutual interference between the overlay chirp signal and the existing traffic, an analog FM-TV signal, for a spread spectrum overlay service.

Based on an analytic approach for mutual interference, various computer simulation models were designed for the FM-TV signal with or without preemphasis. Using simulation, spectral analyses as well as satellite link analyses were performed to find the proper overlay position of the chirp signal in the limited satellite transponder bandwidth. Once the optimal overlay position was found, the possibility of application to VSAT (very small aperture terminal) networks was finally examined.

Mobile telecommunication services that provide voice and data communication to mobile users have been available only in metropolitan areas because of the restricted service range of terrestrial-based cellular systems. The ever increasing demand for similar services throughout a wide geographical area has led to a study of mobile satellite systems using geostationary satellite by NASA (National Aeronautics and Space Administration). The Land Mobile Satellite System (LMSS), initially discussed by Knouse [1,2], is being studied as a possible cost-effective program for providing mobile communication to rural areas [3]. The first phase of NASA's technology development program for LMSS is called the Mobile Satellite Experiment(MSAT-X) which is managed by the Jet Propulsion Laboratory (JPL). This program provides leading technology in the development of spectrally efficient modulation, voice processing schemes, and fade resistant coding. A good review is given by Naderi et al. [4].

For the successful implementation of an LMSS, the proper selection of modulation and coding schemes is essential. However, this selection must be made after a thorough investigation of the LMSS channel, because the LMSS channel exhibits some challenging propagation problems caused by fading due to multipath and shadowing (vegetative and otherwise). This fading results in performance degradation and thus extra link margin is needed to maintain the desired performance. Contrary to the well known behavior of multipath fading in unobstructed line of sight (LOS) paths, the corresponding behavior of a

satellite path which experiences fading caused by vegetative shadowing is not well verified, and the MSAT-X experiments are currently attempting to characterize path statistics [4].

In recent years, because of its relative importance in the LMSS channel, numerous efforts have been made to characterize vegetative shadowing by using analytical methods or by a simulation approach through hardware. These efforts can be classified into two categories: propagation experiments, and modeling and simulation of propagation effects.

The experimental studies were performed with the intention of characterizing earth-space propagation for land mobile operations. At least five different investigators have made measurements. Among these efforts, the pioneering work was performed by Garry Hess [5] using the ATS-6 satellite. He was followed by Roy Anderson[6] using same the satellite. More recent measurements have been made by W. Vogel [7] and CRC (Communication Research Centre) of Canada. The lack of satellites operating at the frequencies of interest led Vogel to use stratospheric balloons and the CRC to use a tethered balloon and a helicopter to carry a transmitter for simulating a distant satellite source. The latest phase of the CRC program has used the L-band transponder on the MARECS-A satellite. Based on their measurements and analyses [5-19], the following preliminary conclusions were made:

- The signal statistics are heavily dependent on the vegetation present, and lowering the elevation angle has the same effect as increasing shadowing, thus making the mean attenuation higher.
- The time plots of received signal strength show only small variation in open terrain but deeper fading occurs in the presence of vegetation and man-made blockage.
- Compared to multipath fading with terrestrial sources, satellite signals fade at a lower rate but fades tend to last longer.

The modeling and simulation efforts of propagation effects [20-40] were undertaken mainly because there were few analytical results for LMSS signal dynamics. Several simulators have been developed to synthesize an LMSS signal whose dynamics can be analyzed. These

include a hardware simulator at CRC, two simulators at JPL, one implemented in hardware and the other in software, and one software simulator developed at Virginia Tech. All LMSS simulators have the same basic configuration, such that the diffuse process for the multipath fades is generated either in hardware or in software. Most of those simulators were designed only to simulate the fading model in the LMSS channel.

The JPL hardware simulator [21-23] was designed to perform end to end evaluation of LMSS communication links and has been used to evaluate bit error rates of GMSK and 2-bit MSK modulation under various fading conditions, and to test NBFM (narrow band FM). However, this simulator did not have a simulation capability for vegetative shadowing. The Virginia Tech simulator was developed using the same basic configuration as the JPL simulator, but its primary concern was vegetative shadowing and a different approach from other simulators was used to account for this factor : a scaled version of a lognormal, universal data set that is based on empirical data [43].

Almost all previous research has been concentrated on the modeling and analysis of propagation effects, because of their importance in the LMSS channel. By virtue of tremendous efforts and investment, remarkable results have been achieved. However, the major goal of LMSS lies in the successful implementation of an end to end system using a satellite. Because of the relative importance of fading characteristics, little attention has been devoted to the modeling and simulation of an end to end evaluation. In this respect, only a few results can be found in the literature, and most of those results were obtained by hardware simulations [23-41].

However, once the fading statistics are verified, it will be obvious that the next step in LMSS experiments will be a performance evaluation of a communication link in the presence of fading. As a result, this topic is becoming an area of active research.

For an effective performance evaluation of an LMSS communication link at the system level, it is essential to have a powerful simulation tool using software rather than prototype hardware when the aspects of flexibility, and cost-effectiveness are considered. This tool can use modeling procedures which are frequently used to simulate ordinary satellite communication links. Regardless of the simulation method, the component modules that perform specific functions must be carefully defined. These functions are basically as follows:

1. create and store a sequence of samples that represent the modulated signal.

2. filter the sequence of samples.

3. operate on the filtered signal according to the channel nonlinearity and fading characteristics.

4. demodulate the signal to observe the effect of the channel.

In turn, these functions can be represented with a sequence of signal processing operations; sampled values of encoded signals from an information source are generated, and operated on by a series of functional modules that simulate the effects of modulation, filtering, nonlinearity, fading, demodulating, and decoding.

Once a properly structured simulation program that meets the system requirements is available, the modulation schemes must be determined. Simulating fading effects is the major difficulty in an LMSS channel simulation . The choice of the modulation technique, i.e., which digital modulation scheme is best in the fading satellite channel, is an important factor in simulation. Generally speaking, noncoherent modulation is preferred because of its structual simplicity and relative robustness. However, it is not yet reported which noncoherent technique exhibits the best performance under fading conditions. In this research, rather than selecting an unproved noncoherent techniques, the well-known coherent digital modulation

techniques like QPSK and MSK were used at first, then the possibility of using noncoherent techniques like differential GMSK(Gaussian MSK) and TCM(trellis coded modulation) 8-differential PSK was also checked.

Generation of fading statistics is also an important factor in LMSS channel simulation. These characteristics can be modeled in two ways: by analytical modeling, and by using a measured data set. From the simulation point of view, the former may seems desirable because of its flexibility in the generation of artificial fades. Also this method has been preferred in hardware simulation. However, the statistical model which is frequently used may be valid only under special environmental situations; therefore the simulation result may not be generalized. In this research, instead of using an analytically defined fading model, stored data sets that have been measured by other researchers were employed.

Based on the modeling procedures and considerations for the choice of digital modulation techniques and the method of furnishing the fading characteristics, a fading channel simulator was designed. With this simulator, the performance of LMSS channel was evaluated through various performance measures such as average bit error rate, bit by bit error rate, and word error rate.

For the detailed description of this second topic, the LMSS fading channel simulator, see the three chapters (Chapter IV, V, and VI) following the chirp spread spectrum part of this thesis. In Chapter IV, a brief review of digital modulation techniques such as QPSK, MSK . TCM-8 PSK, and GMSK is presented along with the differential versions of the last two techniques. In addition, satellite path fading, including vegetative shadowing is also briefly discussed.

Chapter V is devoted to the description of the modeling procedures of the LMSS fading channel simulator. With the various digital modulation schemes reviewed, methods of system level modeling are described first. Advantages and disadvantages of various system

configurations are discussed here. Then component modeling procedures are described in detail. The major components are the modules for the encoder/decoder, the modem (modulator and demodulator), nonlinearity, the fading simulator, and the performance evaluator.

Finally in Chapter VI, results of sample simulations are analyzed and discussed by comparing the error rate for various link conditions and fading effects.

II. Chirp Spread Spectrum System

2.1. Review of Chirp Spread Spectrum Systems

Because of its inherent capability of interference rejection, the chirp modulation technique is a strong candidate for use in spread spectrum communication systems. A number of authors have proposed chirp signals for the representation of binary digital information by assigning an increasing frequency expanded pulse known as 'up-chirp' to a binary '1' and decreasing frequency expanded pulse known as 'down-chirp' to a binary '0' (or vice-versa) [2],[7],[8]. The degree of orthogonality between these two signals determines the possibility of overlapping time-frequency regions, and thus the efficiency of bandwidth utilization. Berni and Greg [9] compared BPSK, chirp and FSK and found that chirp signalling performance is between the performance of BPSK and FSK from the power and bandwidth utilization viewpoints [2]. Hirt and Pasupathy [10] investigated the effect of designing chirp signals with continuous phase at bit transitions, but the use of these techniques increases the receiver complexity.

The use of up and down-chirp signal for the spread spectrum system was suggested in 1962 by Winkler [7]. Dayton [11] found that these signals gave excellent performance in

multipath situations due to the narrow compressed pulse width. In addition, various applications such as high-frequency data transmission [12] and air-ground satellite communication [13] have been reported [14]. Recently Baier et al. [15] suggested the so called 'PN chirp' technique, which is the combination of chirp modulation with pseudonoise (PN) (or pseudo-random) shift keying (PSK) using a fixed tap matched filter. A similar suggestion was also proposed independently by M. Kowatsch et al. [16]. The advanced version of their proposal in 1983 [16] proposed a PN-chirp spread spectrum system which combines standard linear FM surface acoustic wave (SAW) devices, DDL, and an external code modulator. But this proposed system [15] still has the disadvantage of some hardware complexity and a need for synchronization, even though it offers high flexibility by avoiding the use of a programmable matched filter [15].

In the foregoing paragraphs, we have discussed the application of the chirp (or linear FM modulation) technique in binary digital data communication systems and in various spread spectrum communication systems. Of the abundant applications of chirp, though, none are directly applicable for the purposes of our study, because of the complexity in practical implementation in a satellite link or the nature of the purely theoretical analysis in those proposals. Because of these difficulties, we have investigated some possible techniques using chirp modulation and PN coding, in an attempt to find the most feasible scheme. The desired features were selective addressing of a large number of potential users operating in a common band-limited channel, and good system performance measured by low probability of errors in data transmission.

We have reviewed several ways in which chirp can be used to provide spread spectrum coding of a communication link. We classify the systems under consideration at large as class I: 'Within-chirp Modulation', and class-II: 'Multiple Chirp Modulation', as illustrated in Fig. 1 and Fig. 2a. The term 'Within Chirp Modulation' is used because a single chirp is modulated by a finite length PN code within a chirp period, whereas the term 'Multiple Chirp Modulation' arises because multiple chirps are generated within the finite length of a PN code.

Also we can further classify the 'Within chirp Modulation (class I) as the Amplitude (I-1), Frequency (I-2), and Phase (I-3) versions that are depicted in Fig. 1. Note that all three systems need synchronization in the receiver and the anticipated complexity of this synchronization (which was already mentioned in M. Kowatsch's proposal [14]) make these systems less desirable for our purpose of a relatively simple configuration. The other category, 'Multiple Chirp Modulation', can also be classified as the Multi-chirp (II-1), Time Delay (II-2), and Frequency Hop (II-3) as shown in Fig. 2.

The proposed system II-1, multi-chirp, is basically similar to the ordinary binary chirp system because it uses up and down-chirps according to the input digital data. This system does not need synchronization in its receiver. Instead, a code correlator which looks for a specific code word can detect the desired code asynchronously. For multiple access, the easiest way is to assign different chirp slopes to the various users. Another system, II-2, time delay, uses a variable time delay to generate a sequence of chirps with time delays set by a PN code, within each input data bit duration. This system needs a complementary PN sequence in the receiver for synchronization, and a window with the proper time delay in order to find the pulses at the dechirper output at the correct times. Therefore synchronization, and thus the windowing procedure, may be the major difficulties in practical implementation because of their complexity. The proposed system II-3, frequency hop, uses the method of frequency hopping. The transmitter generates the sequence of chirps with shifted center frequencies and this frequency shift in a chirp signal produces a time delay at the output of the dechirper. If the idea of hopping is applied to the phase, it is also possible to design a similar system to the frequency hopping case, but this does not appear to be feasible. Unless the compression filter has excellent phase coherence, comparison of phase at the compressor output from pulse to pulse will be difficult. Fig.2b. shows some typical waveforms for the multiple chirp schemes illustrated in Fig.2a.

Until now, we have proposed six kinds of spread spectrum chirp systems and studied the possibilities of practical implementation. If we set the design goal as a simple structured, low cost earth station, systems which need complex synchronization can be excluded from

SPREAD SPECTUM CHIRP SYSTEM

class I : within chirp modulation

I-1. AM

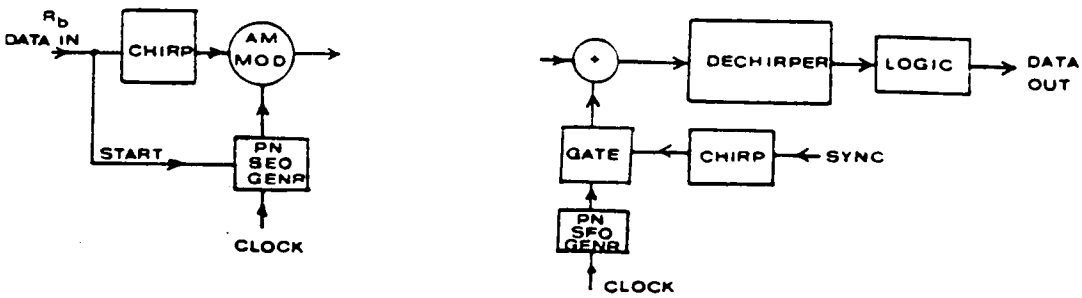

I-2. FM

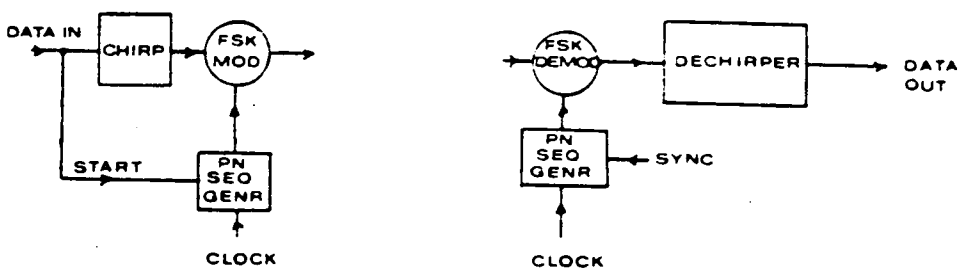

I-3. PM

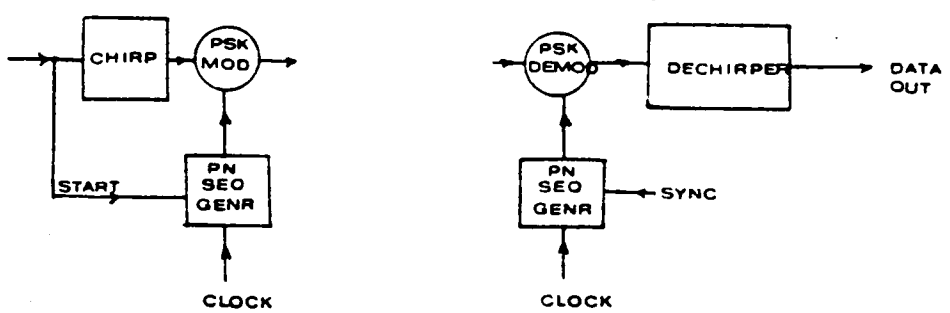

Figure 1. Within Chirp Modulations

Class Ⅱ : multiple chirp modulation

Ⅱ-1. Multi-chirp

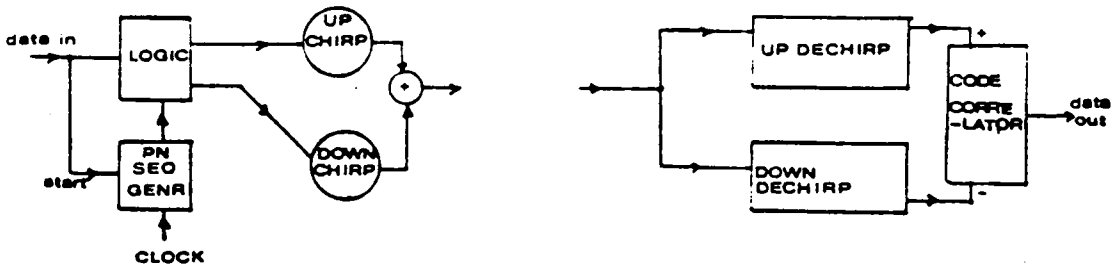

Ⅱ-2. Time delay

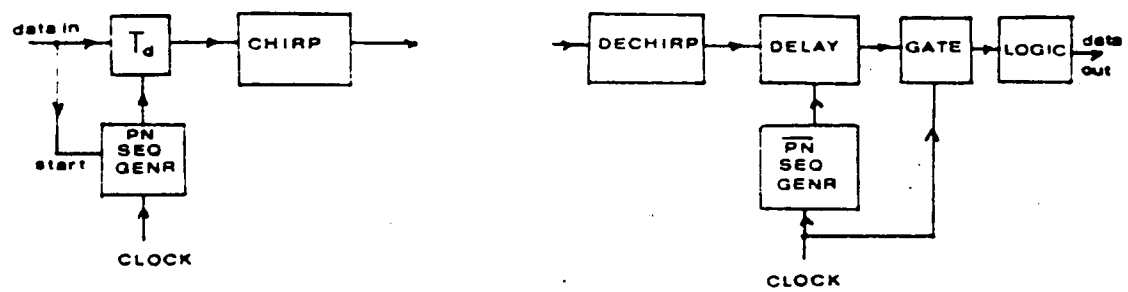

Ⅱ-3. Frequency hop

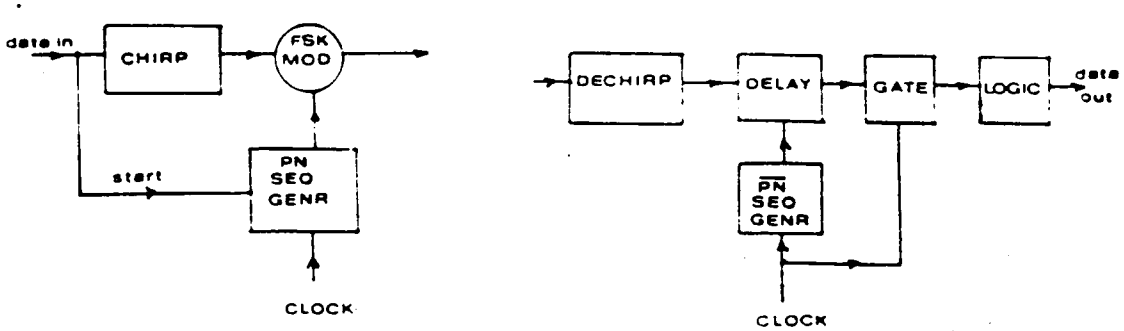

Figure 2a. Multiple Chirp Modulations

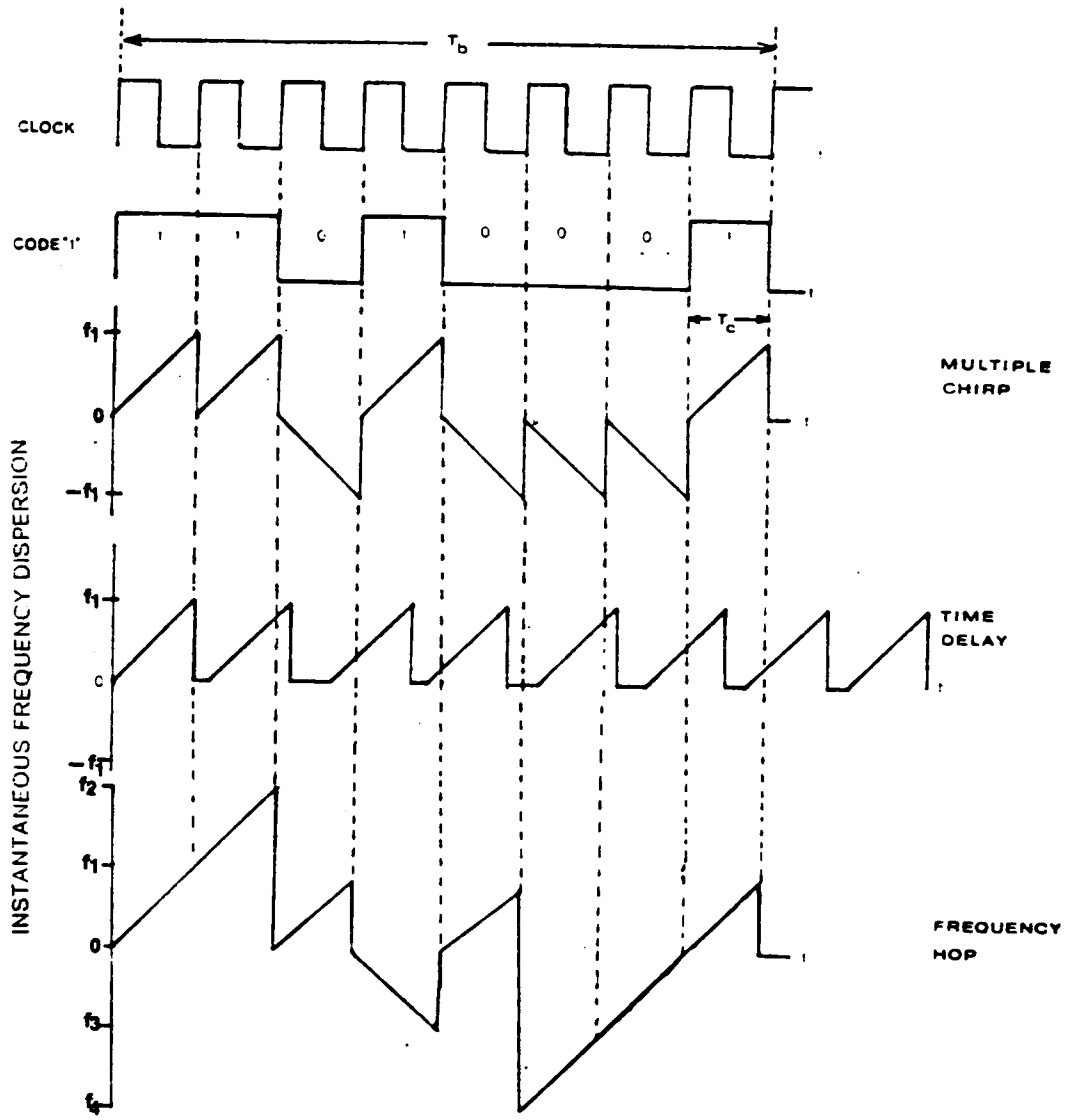

Figure 2b. Typical Waveforms of Multiple Chirp Modulations

consideration. Therefore five of the systems with the exception of multi-chirp system II-1, are considered non-starters. Once it can be proven that the 'multi-chirp system' exhibits the proper performance, this system seems to be the most feasible because it doesn't require additional synchronization in its receiver and it uses the proven binary chirp modulation scheme which was proposed by Winkler [7].

This preferred system is depicted in Fig. 2a (II-1), with multiple chirps for signalling. The signal consists of a sequence of chirp pulses, typically using two slopes, one up and one down. The sequence is chosen for good cross-correlation and autocorrelation properties, so that other sequences entering the decoder produce minimal output. Because this system uses the typical binary chirp system configuration in its modem, the anticipated performance will be between that of BPSK and FSK, as was pointed out by Berni and Greg [9]. Strictly speaking, because no synchronization is required, this system is very similar to a non-coherent FSK system using codewords. However, whereas a FSK system would have a single frequency narrow band filter to detect a wanted tone, the chirp system uses a 'dechirp' filter (a pulse compressor) to detect the presence of a wanted chirp.

Let's call the preferred system a 'Coded Multiple Chirp Spread Spectrum System', because the transmission of a single data bit is achieved by sending a sequence of chirp pulses. The sequence could be made up of any combination of chirp slopes, but the use of a single slope with up and down-chirps permits all receivers in a network to use the same pulse compression filter, with notable cost savings when many receivers are built. Detailed description of the system is left to the next section for convenience.

2.2. *Coded Multiple Chirp Spread Spectrum System*

2.2.1. Basic System Concept

The block diagram of the proposed system called 'Coded Multiple Chirp Spread Spectrum' is shown in Fig. 3a. In the transmitting section, the input binary data stream with a relatively slow data rate (compared with the chip rate of a PN code) is sorted into logical ones and zeros by the 1/0 selector at the data input, and encoded with a finite length PN code (16 or 32 chips) with a specified chip rate. After encoding, a sequence of up-chirps or down-chirps is generated by pulsing an up or down-chirp generator (a SAW dispersive delay line (DDL)). These encoded data are summed, amplified and transmitted. Because each data bit is now represented by a sequence of chirp slopes, the bandwidth of the data has been spread. In this scheme, a single data bit duration is equal to the total number of chip durations of the PN code word. Typical waveforms and spectra for this system are shown in Fig. 3b. By using multiple chirps to constitute a code word, it is possible to use different slopes for each user. However the use of single slope with up and down-chirp enables the selection of single dechirper filter (SAW DDL), and thus reduces the cost of device. If all the users in the network use the same sloped chirp, the multiple access can be accomplished by assigning different code words which promise good autocorrelation and cross-correlation, for example, Kasami or Gold codes with medium length. [17] [18]

We have modeled the receiving system in two steps: the dechirper and the digital code word correlator. In the dechirper, the received multiple-chirp word entering the receiver passes through the RF and IF stages and is converted to polar binary data using a pair of dechirpers and a pair of threshold (envelope) detectors. In the dechirping process, the wanted input signal corresponding to one chip duration is compressed with a predetermined compression gain and thus has enhanced amplitude. These compressed outputs from a pair

Coded Multiple Chirp.S.S System

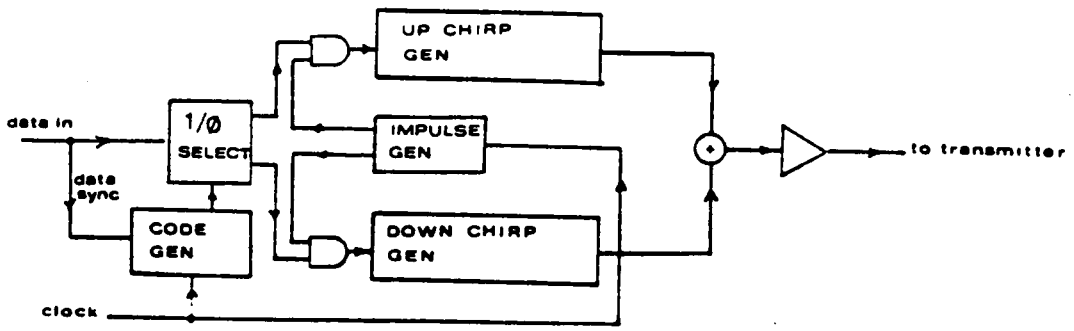

< Modulator >

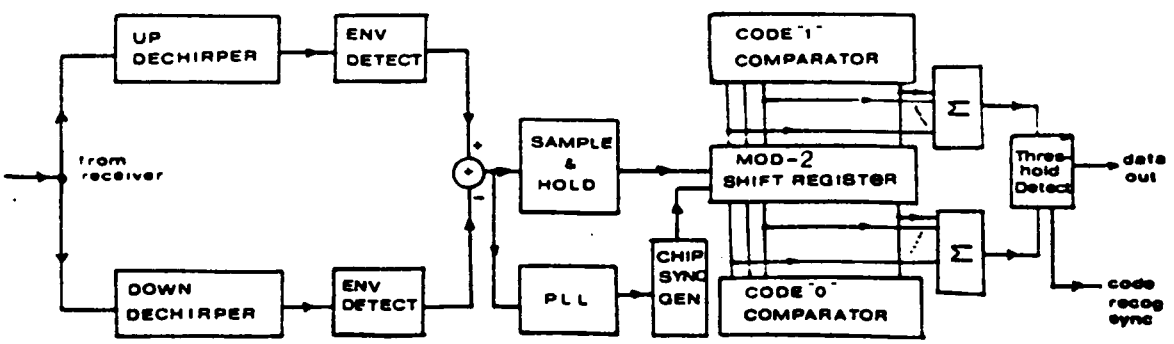

< Demodulator >

Figure 3a. Coded Multiple Chrip Spread Spectrum System (proposed)

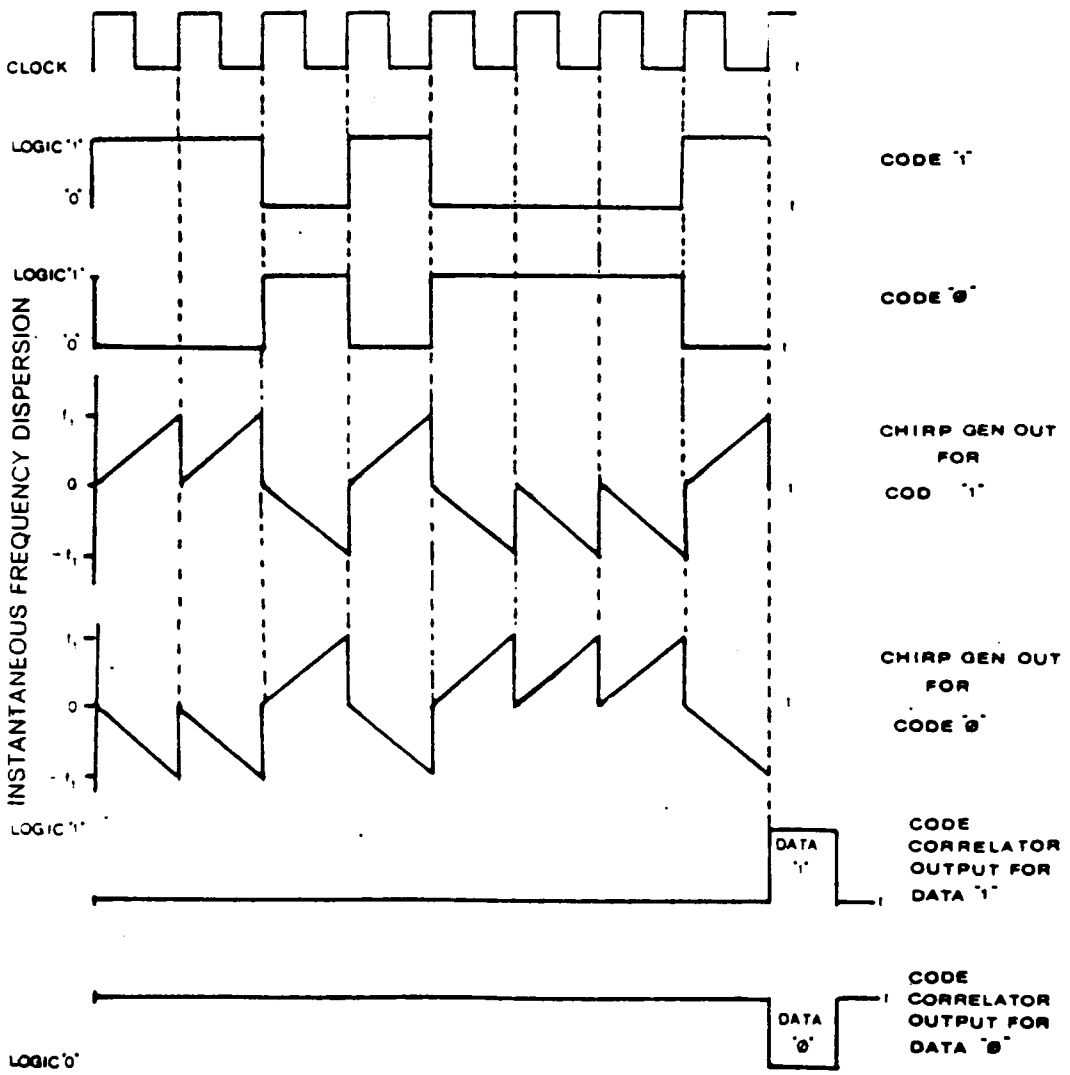

Figure 3b. Typical waveforms of Coded Multiple Spread Spectrum System

of dechirpers, each assigned to detect a particular up- and down-chirp, are summed (in reality, one channel output is inverted then summed) to be processed by a sample and hold (S/H) circuit before code recongination by the digital code word correlator. Because only one of the two dechirpers produces a large output at the end of a given chip duration, even in an interfering situation, the summer gives a positive or negative polarized output to the sample and hold circuit. The sample and hold circuit acts as a threshold detector and passes stable binary data corresponding to the chip state (one or zero) to the word correlator.

The sample-hold circuit output is in the form of polar binary pulses, each of one chip duration, corresponding exactly to the data driving the chirp generators in the transmitter. The chips have been recovered from the spread spectrum signal without any form of synchronization, and are always present whenever the receiver picks up a chirp signal with the correct slope.

The second step is a code word correlator followed by an analog threshold decision circuit, which determines whether a word is present in the correlator. The dechirper (or chirp compression filter) and detector behave like a non-coherent FSK system. The digital word correlator behaves like a unique word detector used in TDMA systems. Synchronization at the bit and word level are required for correct sampling and read-in of the binary word, as in any other binary data transmission system. The input binary data from the S/H output and the self-generated chip synchronization clock driven by a phased locked loop (PLL) are simultaneously given to the digital word correlator. The digital word correlator consists of a pair of word comparators and modulo-2 shift registers with the same length as the code word. After the nth (where n is the length of the shift register) shift, the register contents are compared, and the results are summed and detected by an analog threshold detector. If a code word is present in the shift register, the output will be $\pm$ n. If the spread spectrum system is operated with many simultaneous users in the channel, interference from other users will be the limiting factor in causing degradation of system performance expressed in bit errors in the detected data stream. If we use the same chirp slope for all users, the signals must be separated by the differences between their code words.

2.2.2. Performance Analysis

The performance analysis is organized as follows. Section one introduces the system parameters and waveform definitions for the proposed system. Section two briefly describes the correlation aspects of up and down-chirps; in addition, the cross-correlation of desirable codes are studied. Finally, as a general error criterion, chip error probability at the dechirper output is investigated. Then the probability of word (or code) error and corresponding word (code) miss probability are also described under the constraint of a finite length of code. Finally, the possibility of multiple access using chirp is examined.

System Parameters and Waveform Definitions.

The following are the system parameters necessary to define general expressions for the waveform of a coded multiple chirp spread spectrum signal.

R_b: input(binary) data bit rate
T_b: input(binary) data duration (= $1/R_b$)
R_c: chip rate of the word (or code sequence)
($R_c >> R_b$)
T_c: chip duration
μ: chirp slope (or dispersive slope)
G_p: processing gain (or pulse compression ratio)
d(t): input data signal (binary NRZ)
G(t): word (or code) sequence with period $N = 2^n - 1$ (n: shift register length)
P: transmitted power of signal
ΔF: chirp frequency sweep range

Then the general expression of the voltge wave form for a single chirp duration is given by

$$S_c(t) = \sqrt{2P}\, d(t)G(t) \cos(\omega_c t + \frac{1}{2}\mu t^2 + \theta_o) \tag{2.1}$$

where ω_c: carrier radian frequency

θ_o: Initial phase in radians

Crosscorrelation of Up Chirp and Down Chirp

Because the proposed system uses the chirp technique along with a code sequence to spread the spectrum, it is necessary to find the correlation between up and down-chirps at first, even though the relationship between a series of chirps coded by finite length sequences is needed finally. The autocorrelation and the typical spectrum of chirp are well defined in the relevant papers by Cook [19] or by Klauder et al [1]. So they are not described here.

Assuming only one chirp slope (but negative for down-chirp, if positive slope is assigned to up-chirp) is used, the up-chirp signal is given by

$$U(t) = \begin{cases} e^{j(\omega_c t + \frac{1}{2}\mu t^2)} & -\frac{T}{2} \le t \le \frac{T}{2} \\ 0 & |t| > \frac{T}{2} \end{cases} \tag{2.2}$$

and the down-chirp signal is given by

$$D(t) = \begin{cases} e^{j(\omega_c t - \frac{1}{2}\mu t^2)} & -\frac{T}{2} \le t \le \frac{T}{2} \\ 0 & |t| > \frac{T}{2} \end{cases} \tag{2.3}$$

The cross-correlation C(τ) between U(t) and D(t) is defined as [20]

$$C(\tau) \equiv < U(t)D(t - \tau) > \tag{2.4}$$

for $t \geq 0$, and under the assumption the U(t) and D(t) are periodic over T, the cross-correlation $C(\tau)$ is given by

$$C(\tau) = \frac{1}{T}\int_{-T/2+\tau}^{T/2} e^{j(\omega_c t + \frac{1}{2}\mu t^2)} e^{-j[\omega_c(t-\tau) - \frac{1}{2}\mu(t-\tau)^2]} dt \tag{2.5}$$

$$= \frac{1}{T} e^{j(\omega_c \tau + \frac{1}{2}\mu\tau^2)} \int_{-T/2+\tau}^{T/2} e^{j[\mu t^2 - \mu t\tau]} dt$$

$$= \frac{1}{T} e^{j(\omega_c \tau + \frac{1}{4}\mu t^2)} \int_{-T/2+\tau}^{T/2} e^{j[\sqrt{\mu}\, t - \frac{\sqrt{\mu}}{2}\tau]^2} dt$$

(By setting $\sqrt{\mu}\, t - \frac{1}{2}\sqrt{\mu}\, \tau = \sqrt{\frac{\pi}{2}}\, x$)

$$= \sqrt{\frac{\pi}{2\mu T^2}}\, e^{j(\omega_c \tau + \frac{1}{4}\mu\tau^2)} \int_{-X_1}^{X_2} e^{j\frac{\pi}{2}x^2} dx$$

where $X_1 = \sqrt{\Delta FT}\,[1 + \frac{\tau}{T}]$

$$X_2 = \sqrt{\Delta FT}\,[1 - \frac{\tau}{T}]$$

then

$$C(\tau) = \frac{1}{\sqrt{4\Delta FT}}\, e^{j(\omega_c \tau + \frac{1}{4}\mu\tau^2)} [\{C(X_2) + C(X_1)\} + j\{S(X_2) + S(X_1)\}] \tag{2.6}$$

and

$$|C(\tau)| = \frac{1}{\sqrt{4\Delta FT}} [\{C(X_2) + C(X_1)\}^2 + \{S(X_2) + S(X_1)\}^2]^{\frac{1}{2}} \tag{2.7}$$

where C(X) and S(X) are Fresnel cosine and sine integrals respectively. It is also possible to find identical expression to $C(\tau)$ as above for the $t < 0$ case.

For large values of ΔFT, C(X) and S(X) are approximately 0.5. Then

$$|C(\tau)| = \frac{1}{\sqrt{2\Delta FT}} \qquad -T \le \tau \le T \tag{2.8}$$

therefore, the cross-correlation approaches 0 for large processing gain (or compression gain) G_p (over 100 approximately). This also implies that the quasi-orthogonality of up and down-chirp signals during one chip duration approaches orthogonality if the processing gain G_p is sufficiently large. Under this condition, the performance of a chirp system is almost identical to the noncoherent orthogonal binary FSK system [2]. Fig. 4 shows an example of autocorrelation and cross-correlation of a chirp signal.

autocorrelation

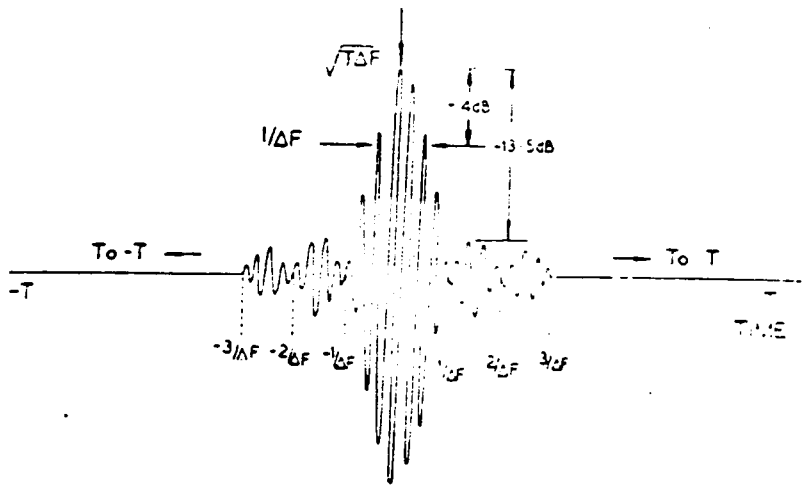

Crosscorrelation

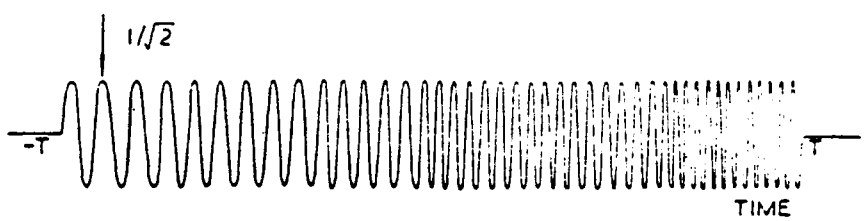

Figure 4. Autocorrelation and Cross-correlation of Chirp.

Cross-Correlation Between Code (Word) Sequences

For effective spread spectrum multiple access (SSMA), the following methods can be considered for the proposed chirp system:

- Using N different codes for N users as in CDMA.
- Using multiple chirp slopes with frequency dispersion variation or time dispersion variation.
- A mixture of multiple slope and multi-code.

Because the single slope chirp is regarded as the only economical way for simple and practical implementation, the most desirable method of achieving multiple access is by varying the code sequences of the network users. Under this condition, the selection of the codes plays an important role in deciding the performance of the system. The Gold code [17] or Kasami Code [18] are strong candidates for our purposes, in that they show low cross-correlation between any pair of codes. Besides, both of them meet the general requirement of the code sequence that interference due to a different code be far less than the code's autocorrelation, and any two codes having the same period must satisfy a lower bound in cross-correlation [21]. For a detailed description of these codes, see D. Sarwate and B. Pursley [22].

For an asynchronous system using code sequences for multiple access, such as the proposed coded multiple chirp spread spectrum system, the cross-correlation of sequences is a key parameter. The aperiodic cross-correlation function of two sequences X and Y is generally given by [22],

$$C_{X,Y}(\ell) = \begin{cases} \sum_{j=0}^{N-1-\ell} X_\ell Y_{j+\ell}\,, & 0 \le \ell \le N-1 \\ \sum_{j=0}^{N-1-\ell} X_{j-\ell} Y_j\,, & 1-N \le \ell \le 0 \\ 0\,, & |\ell| \ge N \end{cases} \tag{2.9}$$

where X, Y : Code sequence having same period N
N : Code length, $N = 2^n - 1$
n : Shift register length
ℓ : Relative time delay between sequences X and Y

and the lower bound of the aperiodic cross-correlation function is

$$|C_{X,Y}(\ell)| \leq [C_X(0)C_Y(0)]^{1/2} \tag{2.10}$$

Also, the peak aperiodic cross-correlation magnitude for two sequences is

$$C_C = \max[|C_{X,Y}(\ell)|;\ 0 \leq \ell \leq N - 1, X \neq Y] \tag{2.11}$$

whereas the aperoidic autocorrelation magnitude is written as

$$C_a = \max[|C_X(\ell)|;\ 0 \leq \ell \leq N - 1] \tag{2.12}$$

From the result [23], if there are K users in a multiple access system, with K unique sequences with the same period $N = 2^n - 1$, (the Gold or Kasami codes have period $N = 2^n - 1$), the following condition must be satisfied to ensure the effective multiple access.

$$\frac{(2N-1)}{N}\left(\frac{C_C^2}{N}\right) + \frac{2(N-1)}{N(K-1)}\left(\frac{C_a^2}{N}\right) \geq 1 \tag{2.13}$$

Chip Error Probability (Dechirper BER)

The performance of the proposed coded multiple chirp S.S. system can be expressed in terms of two probability measures; chip error probability for the dechirper and word (code) miss probability for the digital code-correlator. False alarms, in which a data bit is produced in the absence of a received codeword also contribute to errors in system performance. In this section, the probability of error of the chips in the dechirper will be found and discussed.

For the derivation of probability of chip error, the following justifications are necessary.

1. The performance of binary chirp signaling is identical to that of orthogonal noncoherent binary FSK because the cross-correlation of up and down-chirps is negligible, assuming large compression gain G_p.
2. If the justification above is reasonable, multiple chirps, which are derived from a series of up and down-chirps, give a code sequence which can be viewed as a binary FSK signal waveform.
3. By assuming the noise is AWGN and that interference from other chirp signals behaves as a Gaussian random variable, the generally accepted analysis of noncoherent binary FSK can be used to find the probability of chip error in the proposed chirp system. [2], [24], [25]

Under the assumption that the above three justifications are admissible, the system performance, as measured by probability of chip error rate, (denoted by P_e or bit error rate (BER)) can be found by either of the following two methods.

1. Method 1; Direct use of the P_e of noncoherent binary FSK
2. Method 2; Derivation of the expression for the P_e in binary noncoherent FSK in the presence of interfering signals

Method 1 gives a simple expression for P_e even though it is valid only when the compression gain is sufficiently large. Method 2 gives a more accurate expression without any restrictions. Here, in this report, only the results are written for convenience. For more detailed procedures, see Couch [26] for method 1 and Appendix A of Ramanan [2] for method 2.

By method 1, the P_e of the dechirper is given by [26]

$$P_e = \frac{1}{2} e^{-\rho} \tag{2.14}$$

where

$\rho = E_b/2N_o$
E_b; average energy per bit
N_o; two sided noise power spectral density

By method 2, P_e is given by [2]

$$P_e = Q[\sqrt{\rho(1-\sqrt{1-\alpha^2})}\ , \sqrt{\rho(1+\sqrt{1-\alpha^2})}\ ] - \frac{1}{2} e^{-\rho} I_0(\rho\alpha) \tag{2.15}$$

where Q (X, Y); standard Q function [114]

$\rho = E_b/2N_o$
$\alpha = 1/G_p$
$I_o(X)$: modified Bessel function of 1st kind.
G_p; processing gain

Note that the P_e of the dechirper derived in both methods above assumes that the signal power as well as the noise power is the same for each case of up-chirp and down-chirp. In addition, noise is assumed to be AWGN and interference used in method 2 is assumed to be a Gaussian random variable.

Fig.5a shows the P_e of the dechirper when it is calculated by method 1 assuming AWGN in the channel, and that the dechirper is identical to a noncoherent binary FSK system. Fig.5b [2] shows a comparison of the calculated P_e curves by method 1 and method 2 for several compression ratios. From Fig. 5b, it can be seen that for large time-bandwidth products, hence for large compression ratios, noncoherent FSK (orthogonal) and chirp signals (quasi-orthogonal) have nearly identical performance.

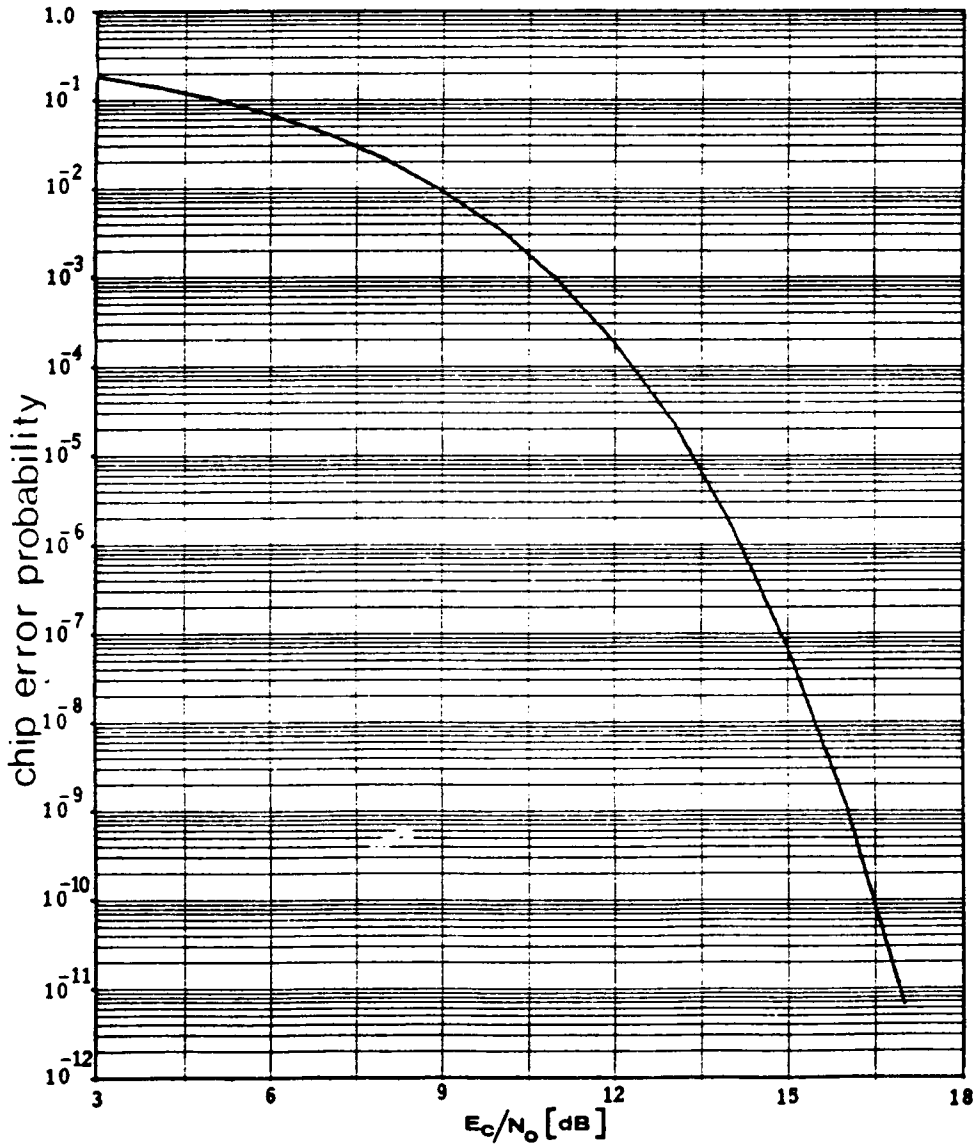

Figure 5a. BER [Chip Error Prob] of Dechirper. [Prior to Code Correlator]

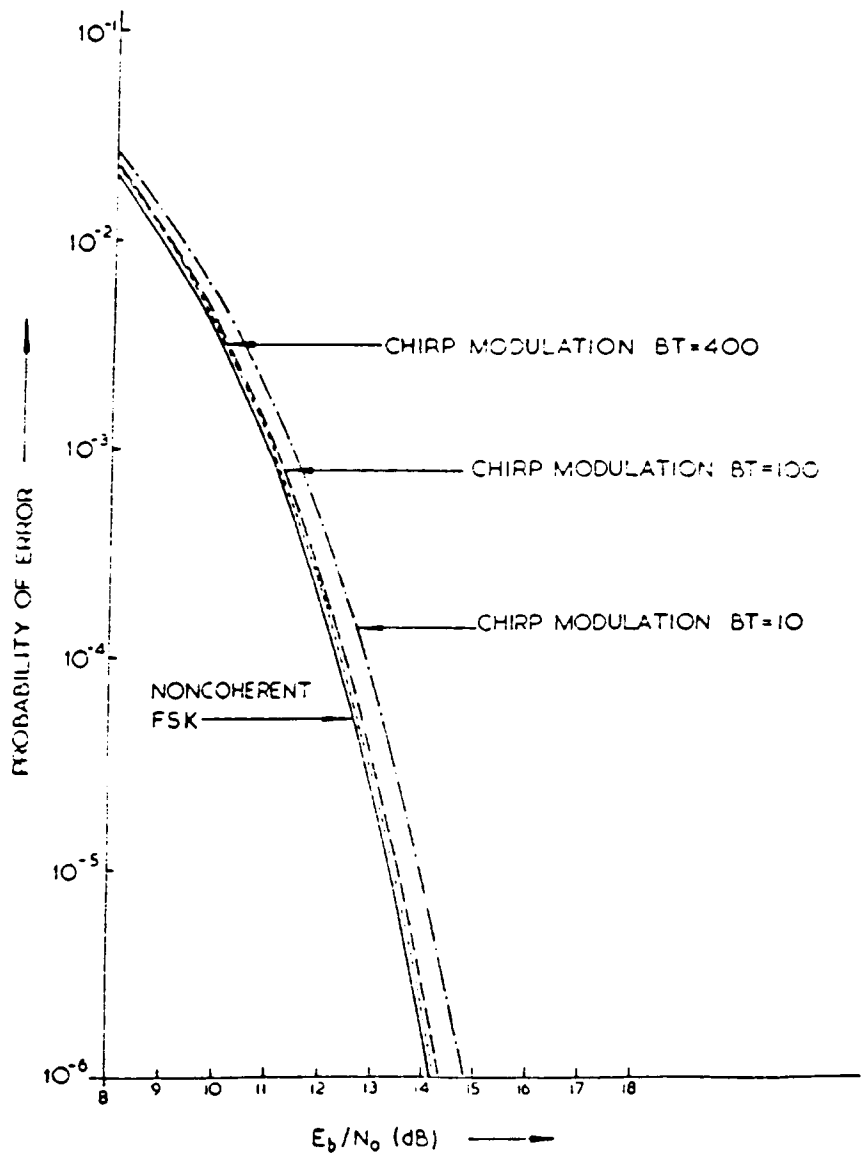

Figure 5b. Probability of error versus E_b/N_o for noncoherent FSK and chirp signals of different time-bandwidth products.

Performance of Digital Code Correlator

A digital code correlator is used to determine whether the received code (word) sequence is matched with the unique word stored in the comparator. Because the proposed digital code correlator uses the same idea as a unique word (UW) detector used in TDMA systems [27], the performance of our correlator can be directly formulated from that of a UW detector (correlator) used in the INTELSAT system [28]. Because two identical code correlators are used to detect a binary '0' and binary '1', the probability of a word (code) error for an individual code (word) correlator is found initially, and then the joint probability of error can be determined.

Let's find the probability of word error P_e for a single code correlator by the result of Feher [29]. The probability that an N bit (chip) word is received correctly is given by [29]

$$P = \sum_{l=0}^{E} \binom{N}{l} p^l (1-p)^{N-l} \tag{2.16}$$

where N is the word length, E is the number of errors to reach the code correlator threshold, 'p' is the bit (chip) error probability which was previously defined as the P_e of dechirper. In addition 'l' is the number of possible error bits received from the dechirper, under the constraint that l < E.

Because the probability of correct word detection is given by P, the probability of word miss Q, for a given threshold E is gven by

$$Q = 1 - P = \sum_{l=E+1}^{N} \binom{N}{l} p^l (1-p)^{N-l} \tag{2.17}$$

The above probability of word miss Q is a function of code length N and dechirper bit (chip) error rate, so there can be plenty of cases to calculate. In Fig. 6, the probability of word miss Q as a function of dechirper BER p is illustrated for N = 16, 32, 64, and 128, with E =

0, 1, 2, and 3. It is seen that code miss rates can be made quite low, even for fairly high bit-error rates of the dechirper, especially for large value of N [29]. However medium length codes like N = 16 or 32 are recommended because of shift register size restriction.

Another measure of system performance is word false alarm rate F. A word false alarm occurs when bit patterns due to random noise are allowed to enter the code correlator. There exists a small but finite probability that random patterns will accidentally correspond to the unique code and cause the erroneous production of a correlation detection. The probability of a false alarm F is given by the probability of accidental occurrence of the unique code in the wrong location within the number of errors E established by the unique code threshold and expressed by [27]

$$F = 2^{-N}\sum_{l=0}^{E}\binom{N}{l} \tag{2.18}$$

Fig. 7 illustrates the dependence of F on code length and bit (chip) error probability of the dechirper. In this figure, unique code false alarm probability, F, and unique code miss probability, Q, are drawn as a function of selected bit (chip) error rate and code matching ratio M/N, where M is the number of bits in the received sequence of a code that must match the unique code stored in the correlator [27]. (M is the threshold of the word presence detector which follows the correlator and is triggered by the correlation between an incoming bit pattern and the stored code sequence.)

Chirp Spread Spectrum Multiple Access

The method of varying chirp slope either by time dispersion or by frequency dispersion, or using a unique pseudo-random code can be employed for multiple access with chirp spread spectrum. In addition, hybrid versions of those methods can be considered. In other spread spectrum methods like direct sequence (DS) and frequency hopping (FH), the number of users

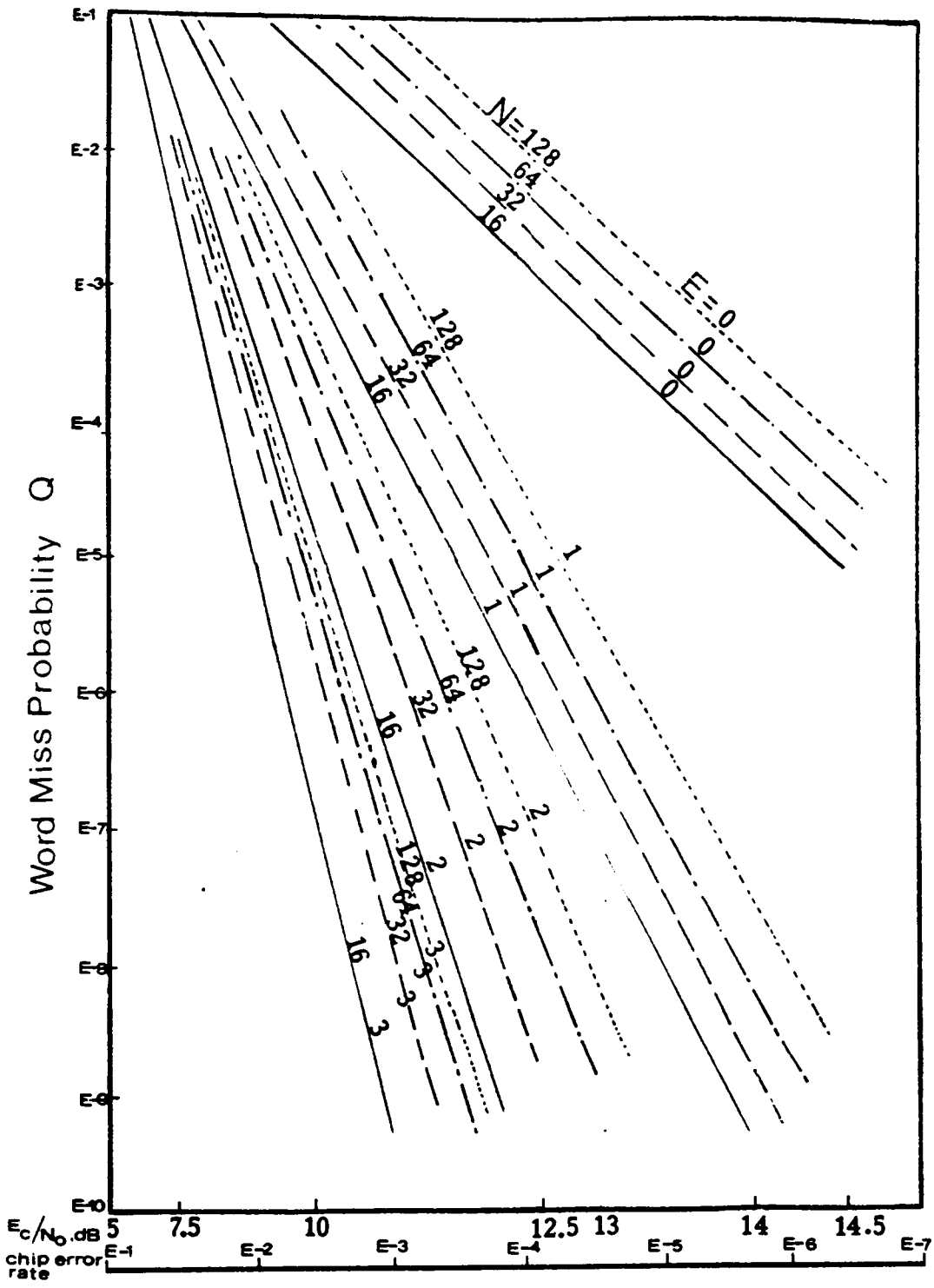

Figure 6. Word Miss Probability vs Dechirper BER.

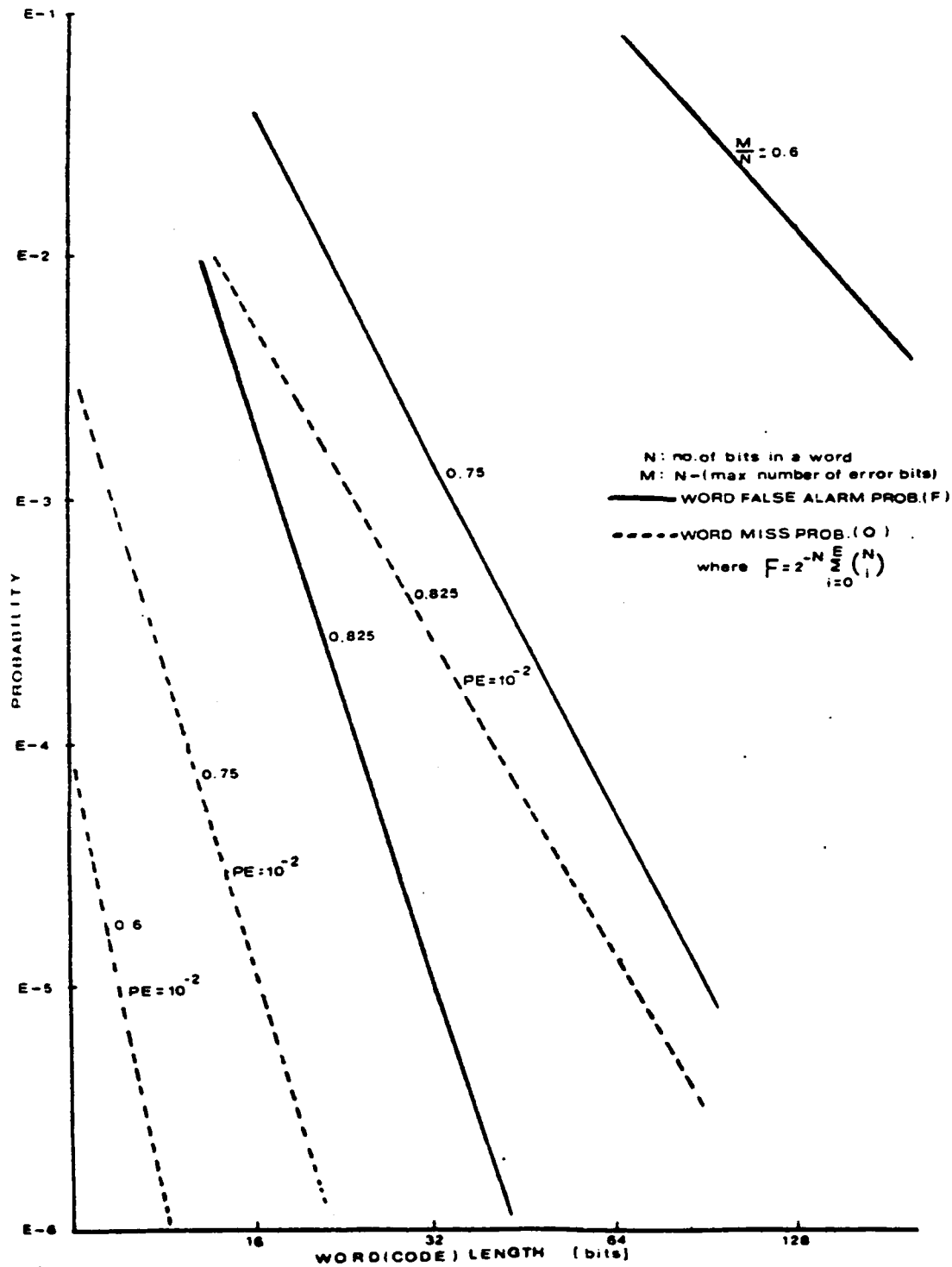

Figure 7. Word False Alarm Probability vs Miss Probability

who can access the transponder simultaneously is limited by the cross-correlation achievable between the codes used. If the method of slope variation is used, the major decision factor for the number of simultaneous users (n) will be the cross-correlations of different sloped chirp waveforms.

The signal selection to keep low cross-correlation between the simultaneous multiple sloped chirps must involve taking signals with differing time-bandwidth products, because the actual difference between the products determines the degree of orthogonality. Overall system performance depends on the influence of all the interfering signals in any one channel. From this point of view, the number of simultaneous users is dictated by the following three factors, regardless of slope varying method:

1. The time-bandwidth product of individual signals
2. The minimum difference in the time-bandwidth products used
3. The summation of n-1 distorted outputs has to be below a certain desired level for any given user for satisfactory operation.

The analysis of cross-correlation [2] between a desired chirp slope and an unwanted slope confirms the dependence of cross-correlation on the above mentioned time bandwidth product. Therefore, proper adjustments between slopes may allow multiple access to a certain degree. However, this scheme using differently sloped chirps is not considered a good choice for practical applications, because varying time-bandwidth products result in a different data rate for multiple users if the time dispersion is varied, and different bandwidth utilization in the limited transponder bandwidth. In addition, different SAW devices are needed for all the multiple users. From this point of view, spread spectrum multiple access using chirp with varying chirp slopes seems to be a bad choice. This conclusion is in agreement with reference [2], where it was shown that only 5 users could share a typical transponder using multiple slope chirp.

If we use the method of assigning unique codes for multiple users, while keeping the same chirp slope for all users, multiple access is possible. The performance of this scheme

is no different from other conventional spread spectrum techniques, and the merit of a relatively simple implementation in the chirp system will be retained. The alternative choice of combining slope variation and a unique code also seems undesirable because the system gets complicated. In conclusion, spread spectrum multiple access using many slopes in a chirp system is not considered desirable, even though it is possible, compared with other spread spectrum techniques. In this situation, spread spectrum overlay on an existing service seems to be the proper alternative to keep the inherent advantages of chirp.

2.3. Summary

While chirp is extensively used in radar systems, it has not been considered efficient for communications. However, recent demands for simple, low cost systems, especially for VSAT network, make the chirp spread spectrum system more attractive than any other spread spectrum technique because of its simplicity in practical implementation without requiring complicated synchronization schemes.

The proposed coded multiple chirp spread spectrum system using a pair of dechirpers for binary '0' and binary '1' and a code correlator meets those requirements of current demands, and its performance in terms of chip error rate is similar to that of noncoherent FSK using codewords. In addition, the word miss miss probability can be made quite low even for the fairly high chip error rate.

However, when the proposed spread spectrum system using chirp is analyzed in multiple access, it turns out to be inappropriate even though it is possible. We recommended applying this system for spread spectrum overlay with other existing signal using same satellite transponder for effective use of bandlimited channels. This technique is discussed in the next chapter.

III. Spread Spectrum Chirp Overlay Service

3.1. Overlay Service -- An Overview

Spread spectrum overlay is a kind of practical implementation of "frequency reuse" by adding a comparatively low data rate signal to an existing high traffic channel. This service can increase the capacity of an existing satellite transponder, and hence it can provide additional service and function to existing users in the satellite network. Because the primary concern is the effective reuse of the existing system without causing any harmful interference to the users already occupying the transponder, minimizing the possible occurrence of mutual interference between the existing signal and the overlay signal is the key factor in this service.

The performance degradation of existing signals caused by overlay can be kept to a minimum by reducing the transmitted power of the overlay signal. The data rate of overlay signals then must also be reduced to maintain the desired bit energy to noise density ratio. In this situation it is obvious that the overlay signal experiences relatively high level interference from the existing signal, and spread spectrum techniques are a proper choice to reject this interference, thereby achieving effective frequency reuse.

In this study of spread spectrum overlay, the existing signal being sent through the transponder is confined to analog FM-TV. Other possible choices such as FDM telephone and data were not studied. FM-TV is probably the most susceptible signal to interference from a chirp overlay, because both signals are frequency modulated, so the FM-TV demodulator is capable of demodulating the chirp signal directly.

This chapter is organized as follows. Section 3.2 introduces the fundamental analysis of interference between analog FM-TV signals and chirp signals by modeling the FM-TV signal in various forms. Section 3.3 describes the procedures of modeling the FM-TV signal in practical form by using multi-level step functions, or random multi-level step functions. In these procedures, some results of computer simulations are illustrated and analyzed both in the time and frequency domains. Then, based on our interference analysis for an FM-TV signal and a chirp signal, a satellite link analysis for C band is performed to find the proper C/I ratio in a practical situation. A comparative study of C/I ratio and optimum overlay position within the analog FM-TV bandwidth, and a performance analysis of an analog FM-TV system with chirp overlay conclude this chapter.

3.2. *Interference Analysis I (General Approach)*

For effective overlay service between existing analog FM TV and spread spectrum chirp systems, mutual interference between the two signals must be studied. It is first necessary to define the type of signals used and the receivers for these two systems. What is needed is a good description, in the frequency domain, of a FM-TV signal. Unfortunately, there exists no finite description or definition of this form that we could find in the literature. Therefore, modeling the TV signal appears to be a major difficulty in our study.

In this section, the demodulation process in analog FM TV (TV) and the proposed spread spectrum chirp system are briefly reviewed as a preliminary stage. Then, for a defined chirp signal and frequency discriminator in the TV receiver, various case studies of interference into the analog FM-TV channel were conducted, using an analytical approach. As another phase of the interference study, the interference caused by FM-TV signals into the chirp channel was also investigated. In this analysis, because we had no definition of the FM-TV signal and its corresponding spectrum, computer simulations as well as analytic expressions were used to support the analysis.

3.2.1. Demodulation of FM-TV Signal and Chirp

The process of FM-TV demodulation recovers the baseband signal as a TV video signal. A frequency discriminator or PLL demodulator, which follows the receiver IF stage, is used for this purpose. Only the frequency discriminator is considered for our purpose. The received FM-TV signal is converted into baseband form after RF amplification and IF amplification. The FM discriminator is usually followed by a deemphasis filter and a video amplifier. In the situation when there is interference added to the FM-TV signal, an error voltage will appear at the discriminator output

according to the intensity and phase relation of the interference signal to the FM-TV signal. This phenomenon will be explicitly dealt with in the next section.

While interference to the FM-TV signal reception can be analyzed through the FM discriminator output, the other aspect of interference in an overlay service is analog FM-TV interference into the chirp signal channel of the proposed coded multiple chirp spread spectrum system. Because the interference power from the FM-TV signal is generally at a much higher level than the received chirp system, the performance of the chirp compression filter and the receiver IF filter preceding the dechirper input play an important role in this interference analysis. Obviously, the output of the dechirper filter (compressor) must spread the input interference signal into a wider duration of time for effective detection of the compressed chirp pulse.

3.2.2. Chirp Interference to Analog FM-TV Signal

In previous section, principle of the demodulation process of an analog FM-TV signal was briefly reviewed. Because the FM discriminator output is expressed as a voltage, the response of the discriminator of an FM-TV receiver for various inputs must be studied before practical modeling of analog FM-TV signal can begin. In this preliminary analysis, we found a formula for FM discriminator output with a general message signal which frequency modulates the carrier. This formula can be applied to any kind of message information, video or audio, that is used in an FM system. Fig. 8 and Fig. 9 illustrate examples of the time waveform of FM discriminator output error voltage for an unmodulated TV carrier and a modulated carrier with chirp interference, under various input signal to interference ratios.

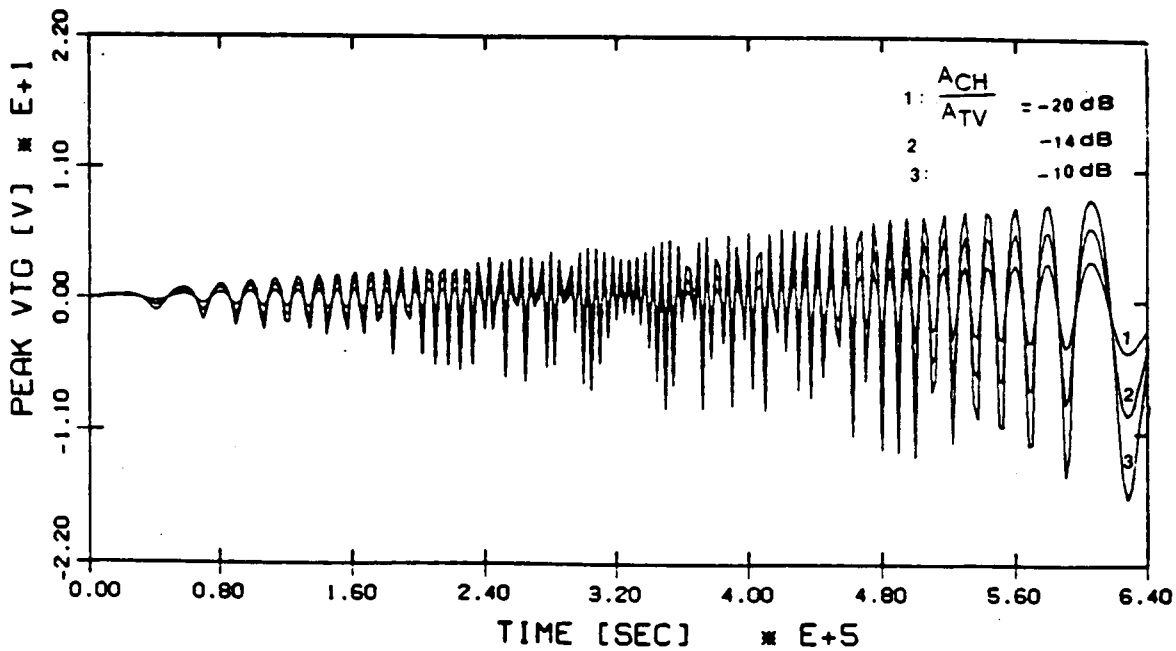

Figure 8. Time waveform of FM discriminator output error voltage for unmodulated FM-TV carrier plus chirp interference

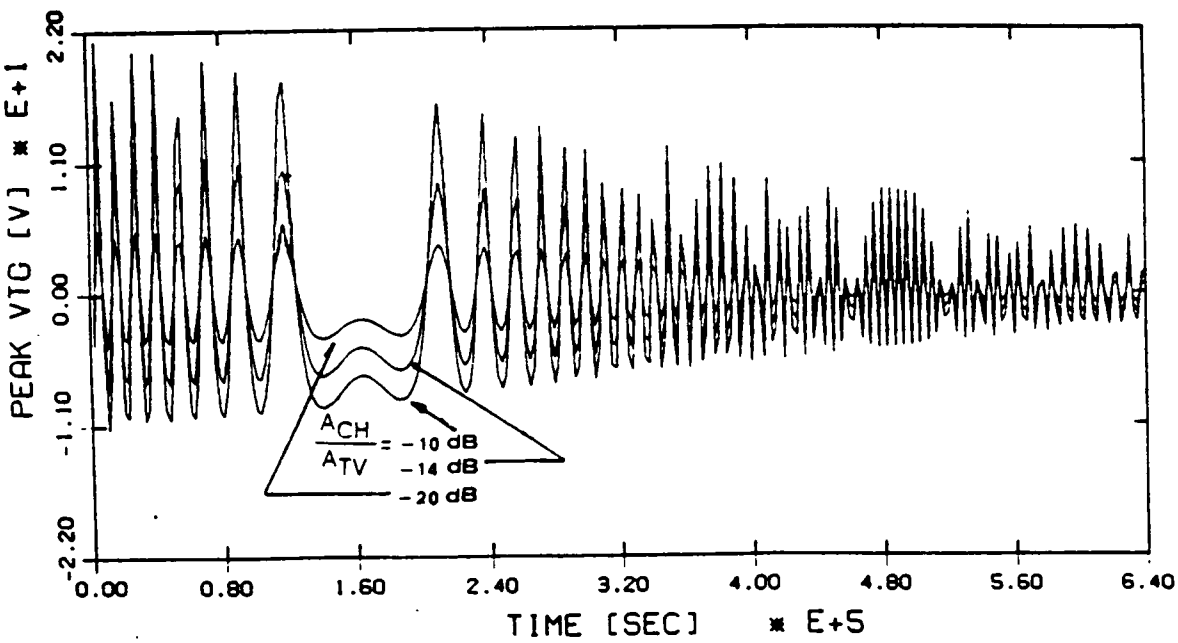

Figure 9. Time waveform of FM discriminator output error voltage for FM-TV carrier(m(t) = 0.5V dc) plus chirp interference

<1> General Expression of FM discriminator Output Under Interference.

To see the effect of interference to the FM signal, we need to find general expressions for error phase, instantaneous frequency deviation and corresponding error voltage at the FM discriminator output caused by the interference.

If the desired FM signal is expressed as

$$w(t) = A\cos[\omega_1 t + \phi(t)] \tag{3.1}$$

where A: FM carrier amplitude

ω_1: FM carrier radian frequency

$\phi(t)$: FM carrier phase

and interference is expressed as

$$i(t) = R\cos[\omega_2 t + \psi(t) + \hat{\mu}] \tag{3.2}$$

where R: interference carrier amplitude

ω_2: interference carrier radian frequency

$\psi(t)$: interference carrier phase

$\hat{\mu}$: initial phase

then, the input signal to the FM discriminator is the sum of the above two signals, written as

$$\begin{aligned} s(t) &= w(t) + i(t) \\ &= A(t)\cos[\omega_1 t + \Phi(t) + \beta(t)] \end{aligned} \tag{3.3}$$

where $A^2(t) = \{A + R\cos[\Phi(t)]\}^2 + \{R\sin[\Phi(t)]\}^2$

$$\Phi(t) = \omega_d t + \psi(t) - \phi(t) + \hat{\mu}$$

$\omega_d = \omega_2 - \omega_1$: carrier frequency difference

$\beta(t)$: error phase

In detail, the error phase caused by interference will be

$$\beta(t) = \tan^{-1} \frac{R \sin[\omega_d t + \psi(t) - \phi(t) + \hat{\mu}]}{A + R \cos[\omega_d t + \psi(t) - \phi(t) + \hat{\mu}]} \tag{3.4}$$

and the corresponding instantaneous frequency deviation is

$$\Delta f = \frac{d}{dt}\beta(t) = \frac{R}{A} \frac{\Phi'(t)[\frac{R}{A} + \cos\Phi(t)]}{[1 + \left(\frac{R}{A}\right)^2 + 2\left(\frac{R}{A}\right)\cos\Phi(t)]} \tag{3.5}$$

therefore, the error output voltage for the FM discriminator with slope k_D is

$$S_o(t) = \frac{1}{2\pi} k_D \left(\frac{R}{A}\right) \frac{\Phi'(t)[\frac{R}{A} + \cos\Phi(t)]}{[1 + \left(\frac{R}{A}\right)^2 + 2\left(\frac{R}{A}\right)\cos\Phi(t)]} \tag{3.6}$$

<2> Complete formula of FM discriminator Error Output

Based on the general expression in Eq.(3.6) above, the general case FM discriminator output error voltage for any FM-TV carrier and energy dispersal signal and linear chirp interference can be written as:

$$S_o(t) = \frac{1}{2\pi} k_D \left(\frac{A_{CH}}{A_{TV}}\right) \cdot \left[\omega_d + \mu t - 2\pi f_d m(t) + d_2'(t) - d_1'(t)\right] \cdot \left[\frac{A_{CH}}{A_{TV}} + \cos\left(\frac{1}{2}\mu t^2 + d_2(t) - 2\pi f_d \int^t m(\alpha)d\alpha - d_1(t) + \omega_d t + \hat{\mu}\right)\right]$$

$$\left[1 + \left(\frac{A_{CH}}{A_{TV}}\right)^2 + 2\left(\frac{A_{CH}}{A_{TV}}\right)\cos\left(\frac{1}{2}\mu t^2 + d_2(t) - 2\pi f_d \int^t m(\alpha)d\alpha - d_1(t) + \omega_d t + \hat{\mu}\right)\right] \quad (3.7)$$

where

A_{TV} : TV-carrier amplitude (cf. $W(t) = A_{TV}\cos[\omega_1 t + \phi(t)]$)

A_{CH} : chirp interference amplitude (cf. $i(t) = A_{CH}\cos[\omega_2 t + \frac{1}{2}\mu t^2]$)

ω_1 : TV carrier radian frequency

ω_2 : chirp carrier radian frequency

$\omega_d = \omega_2 - \omega_1$; carrier frequency difference (radian)

K_D : FM discriminator slope [Volt/Hz]

μ: chirp slope [Hz/sec]

f_d : TV signal peak frequency deviation [Hz]

m(t); active TV video signal (message signal)

$d_1'(t)$: differentiation of energy dispersal signal used in TV signal

$d_2'(t)$: differentiation of energy dispersal signal used in interference (chirp)

$\phi(t) = 2\pi f_d \int_0^t m(\alpha)d\alpha$: TV carrier phase

$\hat{\mu}$: initial phase offset of interference.

NOTE: This expression is the same as the $S_o(t)$ of case 4 described in detail in a later page, except for the initial phase $\hat{\mu}$ in chirp interference term.

<3> Case Study of Interference Effect.

With the formula previously derived, the effect of chirp interference on a TV signal in various cases was studied as follow:

1. Case 1. [No interference, used as a reference case]

   When there exists no interference, there will be no phase error, thus no frequency deviation and no error output voltage from the FM discriminator (FM DISC).

   input to FM DISC: $X_r(t) = A_{TV}\cos[\omega_1 t + \phi(t)]$

   where $\phi(t) = 2\pi f_d \int_0^t m(\alpha)d\alpha$

   phase error : 0

   instantaneous frequency deviation : 0

   FM DISC output error voltage : 0

2. Case 2. [unmodulated carrier plus chirp interference]

   a. input to FM-DISC :

$$X_r(t) = A_{TV}\cos\omega_1 t + A_{CH}\cos\left[\omega_2 t + \frac{1}{2}\mu t^2\right] \tag{3.8}$$

   b. phase error :

$$\beta(t) = \tan^{-1}\left[\frac{A_{CH}\sin\left(\omega_d t + \frac{1}{2}\mu t^2\right)}{A_{TV} + A_{CH}\cos\left(\omega_d t + \frac{1}{2}\mu t^2\right)}\right] \tag{3.9}$$

   c. instantaneous frequency deviation :

$$\Delta f = \frac{A_{CH}(\omega_d + \mu t)\left[\frac{A_{CH}}{A_{TV}} + \cos\left(\frac{1}{2}\mu t^2 + \omega_d t\right)\right]}{A_{TV}\left[1 + \left(\frac{A_{CH}}{A_{TV}}\right)^2 + 2\left(\frac{A_{CH}}{A_{TV}}\right)\cos\left(\frac{1}{2}\mu t^2 + \omega_d t\right)\right]} \quad (3.10)$$

d. FM DISC error output voltage :

$$S_o(t) = \frac{1}{2\pi} K_D \left(\frac{A_{CH}}{A_{TV}}\right) \frac{(\omega_d + \mu t)\left[\frac{A_{CH}}{A_{TV}} + \cos\left(\frac{1}{2}\mu t^2 + \omega_d t\right)\right]}{\left[1 + \left(\frac{A_{CH}}{A_{TV}}\right)^2 + 2\left(\frac{A_{CH}}{A_{TV}}\right)\cos\left(\frac{1}{2}\mu t^2 + \omega_d t\right)\right]} \quad (3.11)$$

NOTE: 1. As a first approximation, assuming $A_{CH} << A_{TV}$ then,

$$S_o(t)_{approx} = \frac{1}{2\pi} K_D \left(\frac{A_{CH}}{A_{TV}}\right)(\omega_d + \mu t)\cos\left(\frac{1}{2}\mu t^2 + \omega_d t\right) \quad (3.12)$$

3. Case 3. [Frequency Modulated TV Carrier plus chirp interference]

a. input signal to FM DISC :

$$X_r(t) = A_{TV}\cos[\omega_1 t + 2\pi f_d \int_0^t m(\alpha)d\alpha] + A_{CH}\cos[\omega_2 t + \frac{1}{2}\mu t^2] \quad (3.13)$$

where $2\pi f_d \int^t m(\alpha)d\alpha = \phi(t)$

m(t): active TV message signal

b. phase error :

$$\beta(t) = \tan^{-1}\left[\frac{A_{CH}\sin[\gamma(t)]}{A_{TV} + A_{CH}\cos[\gamma(t)]}\right] \quad (3.14)$$

where $\gamma(t) = \psi_{CH} - \phi_{TV} + \omega_d t$

$= \frac{1}{2}\mu t^2 - 2\pi f_d \int^t m(\alpha)d\alpha + \omega_d t$

$\psi_{CH} = \frac{1}{2}\mu t^2$; chirp interference phase

c. instantaneous frequency deviation :

$$\Delta f = \left(\frac{A_{CH}}{A_{TV}}\right) \frac{[\omega_d + \mu t - 2\pi f_d n(t)]\left[\frac{A_{CH}}{A_{TV}} + \cos[\gamma(t)]\right]}{\left[1 + \left(\frac{A_{CH}}{A_{TV}}\right)^2 + 2\left(\frac{A_{CH}}{A_{TV}}\right)\cos[\gamma(t)]\right]} \quad (3.15)$$

d. FM DISC output error voltage :

$$S_o(t) = \frac{1}{2\pi} K_D \left(\frac{A_{CH}}{A_{TV}}\right) [\omega_d + \mu t - 2\pi f_d m(t)] \frac{\left[\frac{A_{CH}}{A_{TV}} + \cos[\gamma(t)]\right]}{\left[1 + \left(\frac{A_{CH}}{A_{TV}}\right)^2 + 2\left(\frac{A_{CH}}{A_{TV}}\right)\cos[\gamma(t)]\right]} \quad (3.16)$$

Note: For approximation of $S_o(t)$ assuming $A_{CH} << A_{TV}$, use the following formula:

$$S_o(t)_{approx} = \frac{1}{2\pi} K_D \left(\frac{A_{CH}}{A_{TV}}\right)[\omega_d + \mu t - 2\pi f_d m(t)]\cos[\gamma(t)] \quad (3.17)$$

where $\gamma(t) = \frac{1}{2}\mu t^2 - 2\pi f_d \int_0^t m(\alpha)d\alpha + \omega_d t.$

4. Case 4. [Case 3 with an added energy dispersal signal]

a. input signal to FM-DISC :

$$X_r(t) = A_{TV}\cos\left[\omega_1 t + 2\pi f_d \int_0^t m(\alpha)d\alpha + d_1(t)\right] + A_{CH}\cos\left[\omega_2 t + \frac{1}{2}\mu t^2 + d_2(t)\right] \quad (3.18)$$

b. Phase Error :

$$\beta(t) = \tan^{-1} \frac{A_{CH} \sin [Z(t)]}{A_{TV} + \cos [Z(t)]} \tag{3.19}$$

where $Z(t) = \phi_{CH_d} - \phi_{TV_d}$

$$= \frac{1}{2}\mu t^2 + d_2(t) - 2\pi f_d \int_0^t m(\alpha)d\alpha - d_1(t) + \omega_d t$$

$$\psi_{CH_d} = \psi_{CH} + d_2(t)$$

$$\phi_{TV_d} = \phi(t) + d_1(t)$$

$d_1(t)$, $d_2(t)$: Energy dispersal signals

c. Instantaneous frequency deviation :

$$\Delta f = \left(\frac{A_{CH}}{A_{TV}}\right) \frac{[\omega_d + \mu t - 2\pi f_d m(t) + d_2'(t) - d_1'(t)]\left[\frac{A_{CH}}{A_{TV}} + \cos[z(t)]\right]}{\left[1 + \left(\frac{A_{CH}}{A_{TV}}\right)^2 + 2\left(\frac{A_{CH}}{A_{TV}}\right)\cos [Z(t)]\right]} \tag{3.20}$$

where $d_1'(t) = \frac{d}{dt} d_1(t)$, $d_2'(t) = \frac{d}{dt} d_2(t)$

d. FM DISC output error voltage :

$$S_o(t) = \frac{1}{2\pi} K_D\left(\frac{A_{CH}}{A_{TV}}\right) \frac{[\omega_d + \mu t - 2\pi f_d m(t) + d_2'(t) - d_1'(t)]\left[\frac{A_{CH}}{A_{TV}} + \cos [Z(t)]\right]}{\left[1 + \left(\frac{A_{CH}}{A_{TV}}\right)^2 + 2\left(\frac{A_{CH}}{A_{TV}}\right)\cos [Z(t)]\right]} \tag{3.21}$$

NOTE: For approximation of $S_o(t)$ assuming $A_{CH} << A_{TV}$, use the following formula:

$$S_o(t) = \frac{1}{2\pi} K_D \left(\frac{A_{CH}}{A_{TV}} \right) [\omega_d + \mu t - 2\pi f_d m(t) + d_2'(t) - d_1'(t)] \cos [z(t)] \qquad (3.22)$$

where

$$z(t) = \frac{1}{2}\mu t^2 + d_2(t) - 2\pi f_d \int_0^t m(\alpha)d\alpha - d_1(t) + \omega_d t \qquad (3.23)$$

3.2.3. Simulation of FM discriminator output under chirp interference

In the previous section, some useful basic formula were found for the FM discriminator output in the presence of chirp interference. In addition, Fig. 10 and Fig. 11 show the simple case of the error voltage output of an FM discriminator when the FM-TV message signal has a simple form like an average dc voltage. In this section, a more complicated but more general form of the FM-TV message signal is used as the TV message signal, to determine a realistic result for the FM discriminator output. Even though a more practical form of TV message signal with preemphasis filtering is simulated in a later part of this chapter, this section presents results for an interference analysis with a simpler form of signal.

In the simulation here, the reference TV video signal which we are using is a staircase voltage between 0.25 and 0.75 volts, with duration of 35 μs. On a TV screen this video signal would produce a series of vertical bars of decreasing brightness, with a seven step gray scale. To test the accuracy of the simulation, a staircase signal was converted into the corresponding FM wave, without any bandpass filtering, and then processed through the receiver simulation. The resulting video output was plotted, giving the result in Fig. 10 and Fig. 11. Fig. 10 shows the transmitted staircase function and Fig. 11 illustrates the video output after low pass filtering with 4.2 MHz cutoff frequency, the

theoretical bandwidth for NTSC video signals. Note that in Fig. 11 the transients caused by the instantaneous step in the original signal in Fig. 10 cause the receiver filter to ring at the expected frequency. In the above simulation, the FFT routine used 2048 samples of the 64 μs waveform. This sampling rate will theoretically reproduce all FM signal components up to 16 MHz.

The chirp signal was then overlaid on the FM-TV signal, and the error in the video staircase waveform at the receiver (FM discriminator) was calculated and plotted. As mentioned earlier, when sampled at 2048 or 4096 samples in 64 μs, aliasing does not appear and the resulting interference is small. Fig. 12 shows the error waveform for a 26 μs chirp signal swept through 10 MHz. The chirp signal was set 26dB below the video signal, measured as a peak voltage ratio. The largest interference occurs at the end of the chirp signal, with a peak level of 0.005V, relative to a 1.0V nominal video signal. It is unlikely that this low level interference would be visible on a TV screen, and would appear as very small random dots if it could be seen. To check whether the chirp signal produced significant interference in the video signal spectrum between 3 and 4 MHz, where the chrominance information is transmitted, additional simulations were performed. Fig. 13 shows the resulting spectrum of this interference component. For comparison purposes, Fig. 14 shows the calculated spectrum of the video staircase signal. The interference power level is well below that of the video signal, and has a very flat spectrum, indicating that chrominance interference should be very small.

From the above results, there appears to be very little interference at the video output of the TV system when a chirp signal is overlaid on an FM-TV signal, as carried by many satellite transponders. The interference peaks are more than 40dB below the FM-TV video signal when the chirp RF signal is 20dB below the FM-TV carrier, showing good interference suppression by the FM carrier. In the simulation procedure, the effect of deemphasis in the video receiver was ignored for convenience at this time. In general, deemphasis in the receiver will help to reduce the effect of interference peaks because of its low pass filter action. However, in a later part of this chapter, when a practical interference model is used, preemphasis in the transmitter was added to get more practical simulation results.

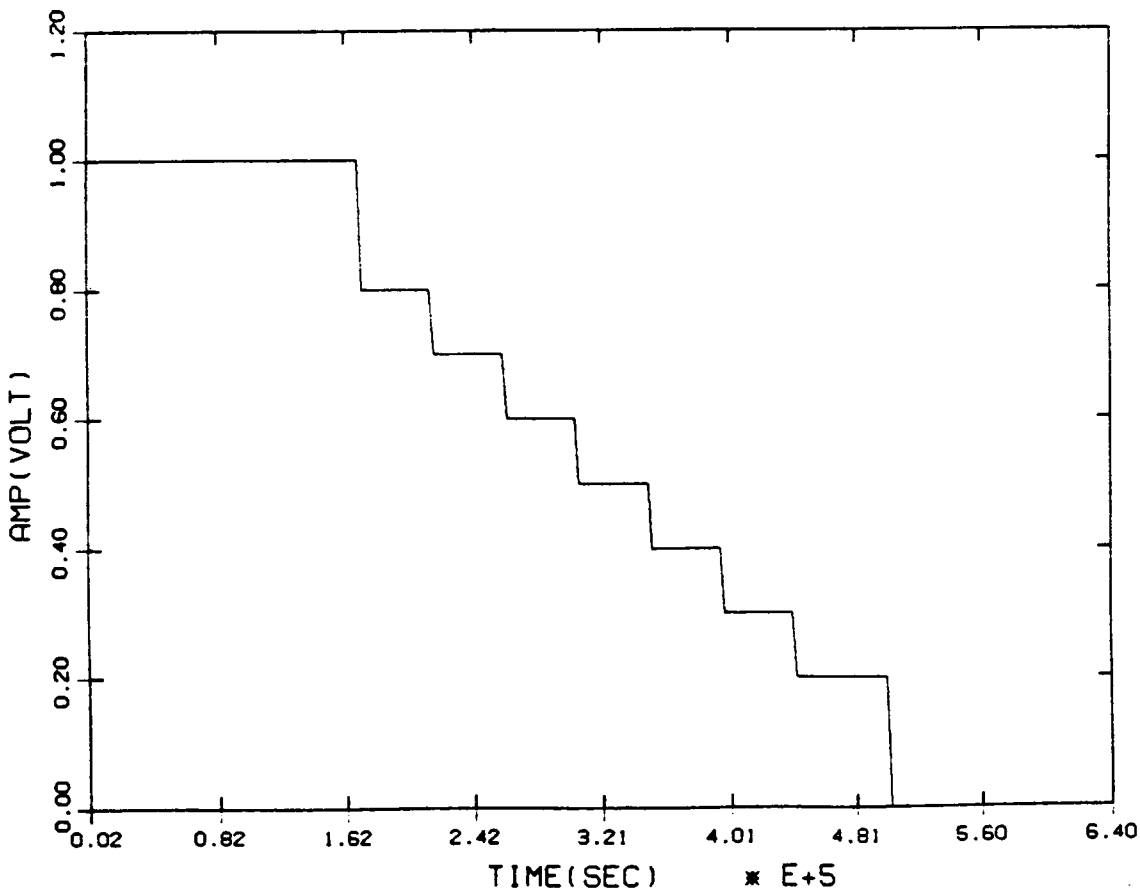

Figure 10. Simulated 9 step staircase function (time plot)

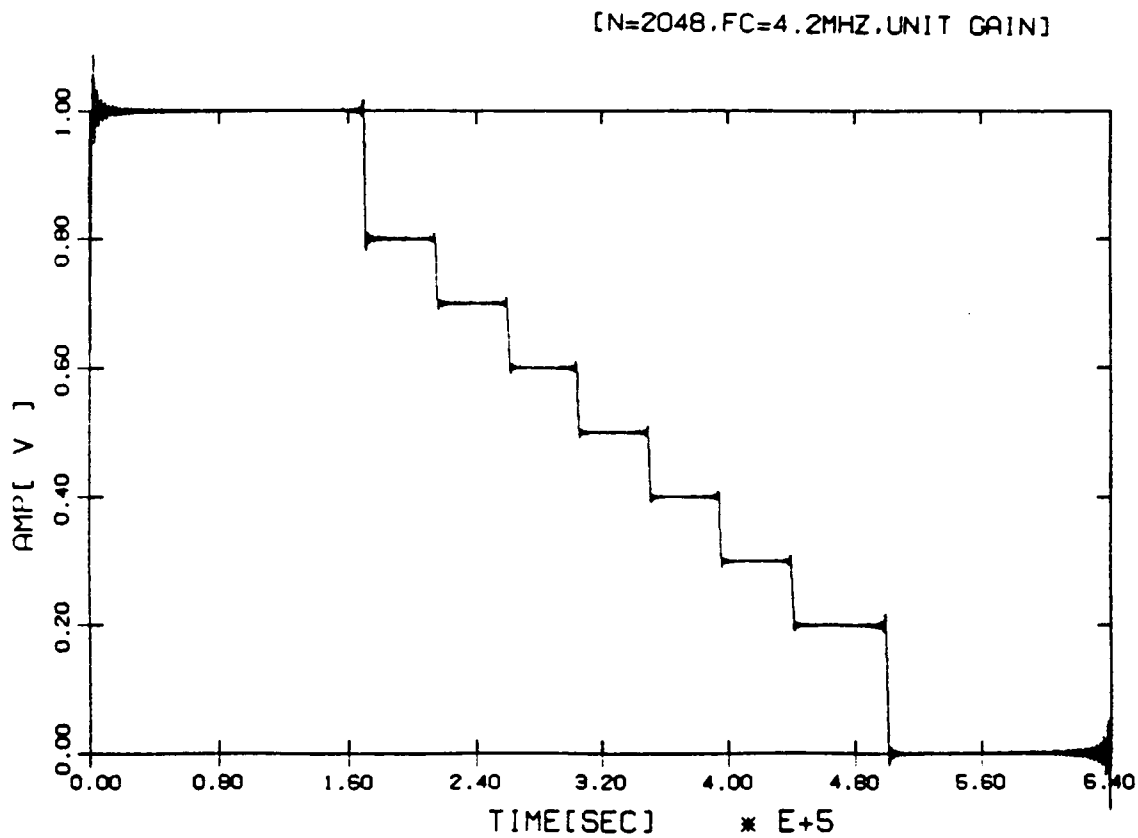

Figure 11. Received and lowpass filtered simulated 9 step staircase function

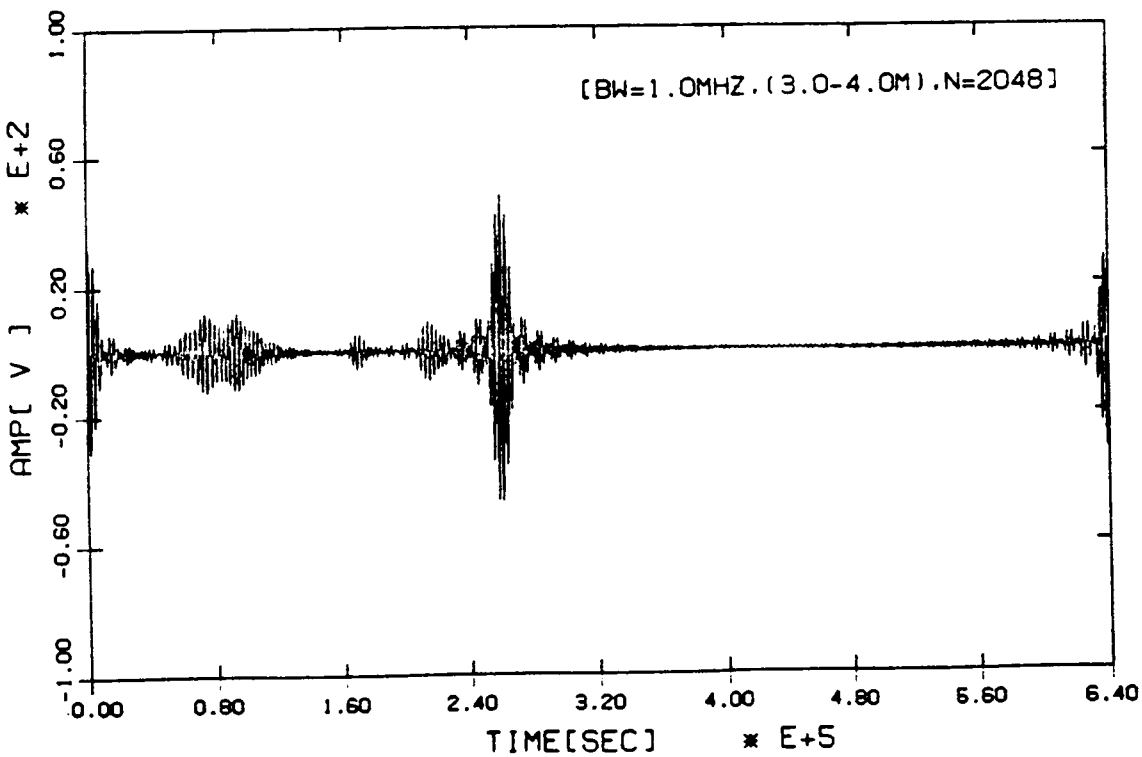

Figure 12. Error output voltage of FM discriminator after bandpass filtering

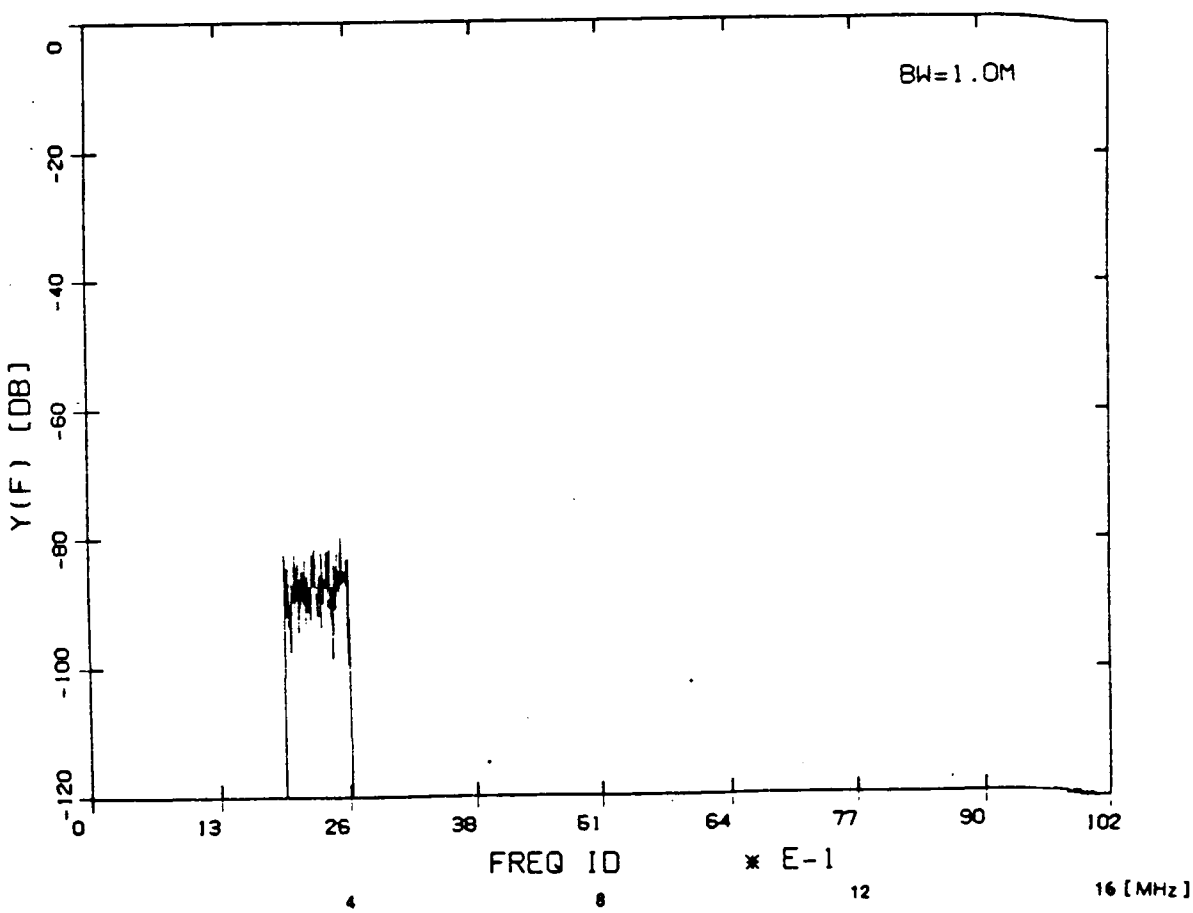

Figure 13. Specttrum of error output after bandpassing filtering (3-4 MHz)

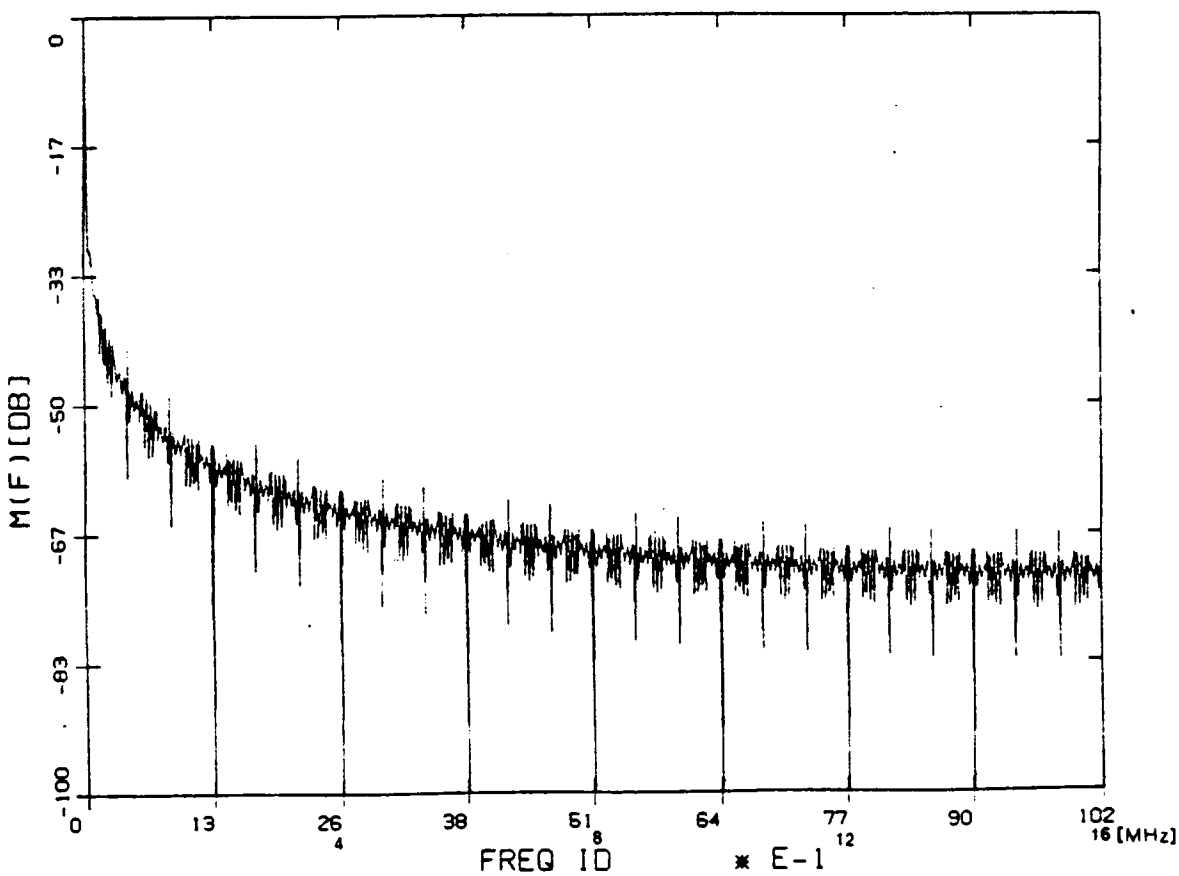

Figure 14. Spectrum of 9 step staircase function

3.2.4. Analog FM-TV signal interference on chirp demodulation

As another phase of the mutual interference study, the analog FM-TV signal can be modeled as interference in a chirp signal overlay service. To see the effect of such interference, we evaluated the output of a dechirper (compression filter) for the desired signal (chirp) and for the interference (FM-TV signal). For simplicity, detailed procedures are omitted, and only the results are described here.

Let the desired chirp signal be:

$$f(t) = \begin{cases} e^{j(\omega_c t + \frac{1}{2}\mu t^2)} & -T_o < t < T_o \\ 0 & |t| > T_o \end{cases} \tag{3.24}$$

and the unwanted interference analog FM-TV signal be:

$$I(t) = \begin{cases} A_I\, e^{j[\omega_c t + \Phi(t)]} & -T_1 < t < T_1 \\ 0 & \text{elsewhere} \end{cases} \tag{3.25}$$

then the compressed output of the desired chirp signal is given by

$$g(t) = \sqrt{\frac{2\mu T_o^2}{\pi}}\ \frac{\sin \mu t T_o}{\mu t T_o}\ e^{j[\omega_c t - \frac{1}{2}\mu t^2 + \frac{\pi}{4}]} \tag{3.26}$$

and its real part is written as:

$$\mathrm{Re}[g(t)] = \sqrt{\frac{2\mu T_o^2}{\pi}}\ \frac{\sin \mu t T_o}{\mu t T_o} \cos\left[\omega_c t - \frac{1}{2}\mu t^2 + \frac{\pi}{4}\right] \tag{3.27}$$

whereas the compressed output for analog FM-TV interference is

$$J(t) = A_i\sqrt{\frac{\mu}{2\pi}}\, e^{j(\omega_c t+\frac{\pi}{4})}\int_{-T_1}^{T_1} d\tau\; e^{j[\Phi(\tau)-\frac{\mu}{2}(t-\tau)^2]} \tag{3.28}$$

and its real part is written as

$$Re[J(t)] = tA_i\sqrt{\frac{\mu}{2\pi}}\int_{-T_1}^{T_1}\cos\left[(\omega_c t+\frac{\pi}{4})-\frac{\mu}{2}(\tau-t)^2+\Phi(\tau)\right]d\tau \tag{3.29}$$

In all the above equations, μ, ω_c, $\Phi(t)$ are the same as in the definitions in Section 3.2.2. Based on the equation for the desired output g(t) for chirp and unwanted outputs J(t) for analog FM-TV interference, a computer simulation was performed under the following conditions:

chirp frequency dispersion	: 10.0 MHz
chirp time duration	: 26 μs
chirp dispersion slope	: 10.0/26.0 MHz/μs
FM-TV message signal	: 0.5V dc
FM-TV signal duration	: 64 μs
FM-TV signal max freq. devn	: 10.0 MHz
initial IF frequency	: 70.0 MHz
interference signal amplitude	: 0.1V, 0.2V, 0.5V.

For convenience of simulation, the message signal of the analog FM-TV was chosen as 0.5V dc, which is the average dc level of a video signal in a conventional analog FM-TV system. Fig. 15 and Fig. 16 show the outputs of the compression filter. Fig. 15 is the typical output of a compressor to the desired chirp signal. Fig. 16 illustrates the output of the compressor when simulated FM-TV signal interference with an amplitude 0.1V dc is applied. As can be expected from chirp theory, the mismatched (unwanted interference) signal is widely spread into a long time duration, while the matched signal (chirp) is compressed into a short time. From this result, it is possible to expect that

the interference from the TV signal can be effectively suppressed below a certain desired level if the proper conditions are provided in the overlay service.

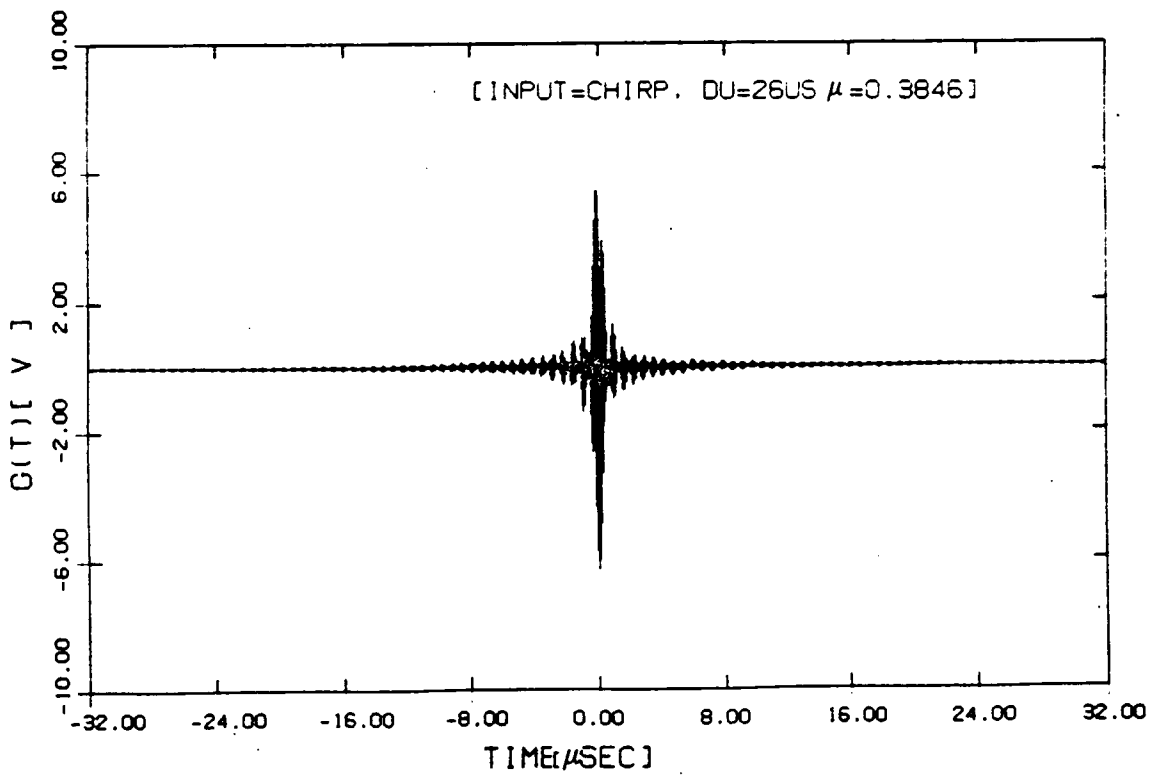

Figure 15. Typical compression filter output for chirp signal input

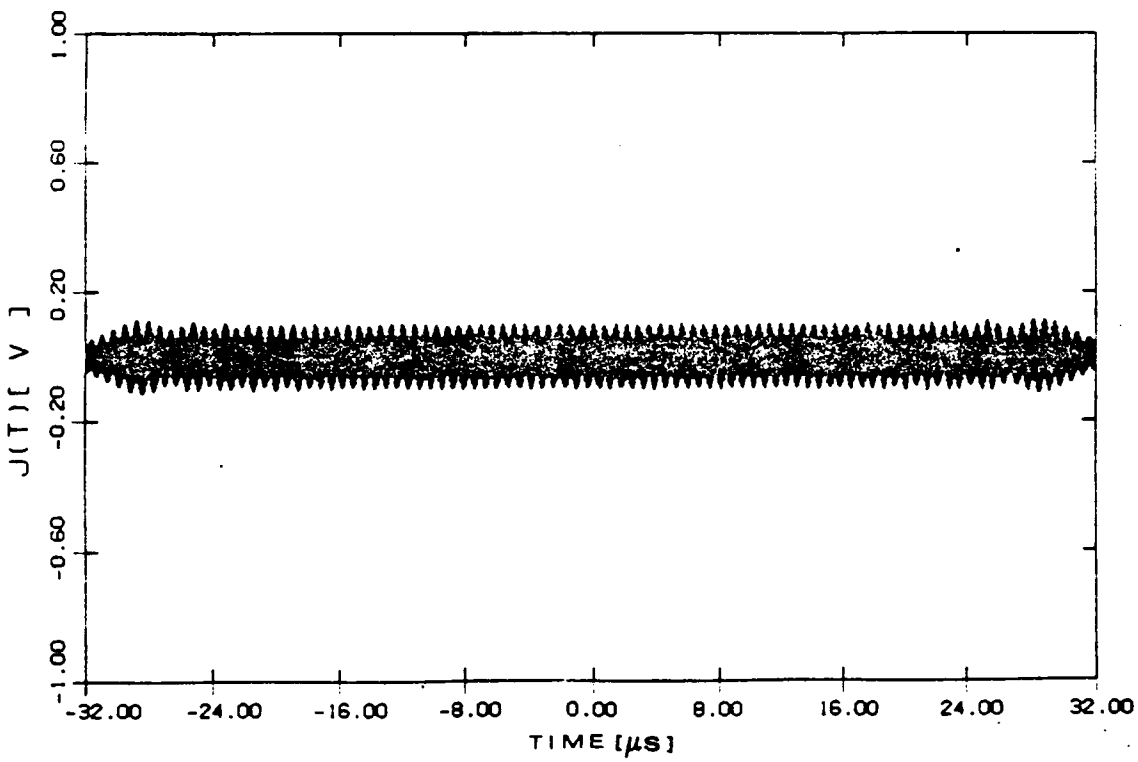

Figure 16. Compression filter output for FM-TV signal with amplitude of 0.1V

3.3. *Interference Analysis II (Practical Modeling and Simulation)*

So far, we have investigated the principle of an overlay service between analog FM-TV and a chirp spread spectrum system by finding the general expression of the FM-TV demodulator output error voltage when a chirp signal is interfering with the FM-TV signal, and vice versa. In those procedures, the message or information signal of the FM-TV has been simply modeled by a dc voltage or a pure sinusoidal wave, to investigate the general case of an interfering environment. However, it is essential to define a complete model of a TV video signal in the time and spectral domains, for the further analysis of an overlay service.

In this section, the modeling procedures of an analog FM-TV video signal without preemphasis, and corresponding computer simulation results are explained first. Then, the same procedures are repeated with a preemphasis filter. Finally, an overlay service link analysis for C band is done to permit a performance analysis.

Precise modeling of a general TV video signal is almost impossible because the spectrum of a general TV signal is not known with any degree of certainty. The variety of images being shown gives a variety of spectral shapes. In addition, the FM TV signal is a wideband signal; in practice the entire overlay signal (chirp) will be contained within the bandwidth of a TV receiver [31]. Nevertheless, a realistic model of a TV video signal is required for analysis of the case of a TV signal overlaid with a chirp signal.

As a model for computer simulation, a typical TV video signal with NTSC 525 line format was selected. The usual TV signal contains synchronization pulses (vertical and horizontal), audio, color bars (in color TV only) or chrominance patterns, as well as the luminance signals. In horizontal line scanning, about 64 μs duration (63.55 μs exactly) of a single horizontal scan duration contains all the necessary information. Of the 64 μs duration, the first 11 μs is devoted to synchronization and the last 13 μs is used for color burst in a color TV. Therefore, the active video signal uses only 30 $\sim$ 40 μs duration in a single horizontal scanning period of 64 μs. The maximum video signal is 1.0 volt peak to peak amplitude.

3.3.1. Analog FM-TV signal modeling I -- Without preemphasis

A. Linear Step Staircase Function Model

Based on the typical model described above, a simple model in the time domain is illustrated in Fig. 10. The corresponding time domain expression can be written as a series of staircase functions as follows:

$$m(t) = A_1U(-t+\tau_1) + A_2U(-t+\tau_2) + ...A_7U(-t+\tau_7) + A_8U(-t+\tau_8) \quad (3.30)$$

or, in general form, it also can be written:

$$m(t) = \sum_{i=1}^{n} A_iU(-t+\tau_i):n = 1, ...m \quad (3.31)$$

where $m(t)$: analog FM-TV video signal in a single horizontal scanning period (64 μs).

A_i: incremental magnitude of unit step function in voltage, $0 \leq A_i \leq 1$

τ_i: time increment of luminance signal corresponding to magnitude A_i

m: desired number of luminance level.

As an extension of this model, the step size was increased to 200 later, as in Fig. 17.

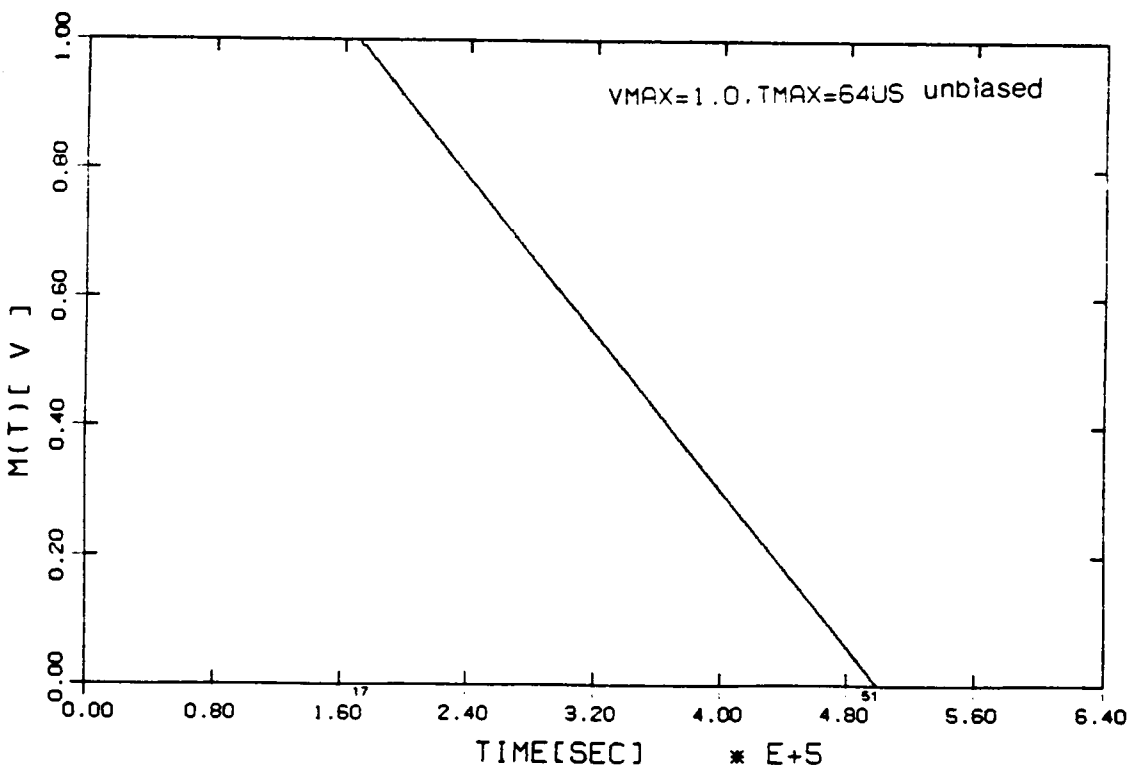

Figure 17. Time plot of simulated 200 step staircase function model for video signal

B. Random Step Staircase Function Model

The model of an analog TV video signal with a linear, 9 step or 200 step staircase function can be used to represent a typical video signal, even though it is simple. But this cannot be the worst case model which can be encountered in a real system. So another model was made which consisted of 256 steps of random amplitude. A uniform random number was generated with an arbitrary seed, in the range of 1 to 256. Incremental times between 17 μs to 50 μs were given random amplitudes which were generated by the random number generator. This gave a random amplitude step function. Because of the uniform distribution of the random step amplitude, the mean value was 0.5 Volt, as with the linear staircase function. Fig.18 shows this function.

3.3.2. Simulation of Wideband FM-TV Signal and Chirp I--No Preemphasis

As mentioned earlier, an analog FM TV signal is a wideband signal. In domestic satellite TV transmission, the baseband TV signal, with its video information bandwidth of approximately 4.2 MHz, is FM modulated so that its RF bandwidth fills an entire 36 MHz bandwidth of a satellite transponder [2].

In the overlay service, when a chirp signal is overlaid on an existing TV signal, the interference of the chirp signal into the TV signal is an all pass function because the chirp RF bandwidth is usually much narrower than that of the FM TV signal. But in the case when the chirp signal is interfered with by the TV signal, only a specific 5.0 MHz bandwidth of TV interference power is introduced in the chirp signal via the IF filter (if its bandwidth is set to 5.0 MHz).

For our study of mutual interference in an overlay system under the above conditions, the spectral shape of the TV signal is modeled by choosing a staircase or random video waveform. Computer simulation is an effective alternative to practical experiments, even though the final judgment on mutual interference is highly subjective and depends on the response of the human eye in the TV case. Because of the complexity of modeling RF signals, all the simulations were done in

baseband. By trial and error, we found that 2048 or more samples in the 64 μs horizontal scanning period guaranteed no aliasing effects. So 2048 samples were used for overall simulation, both in the time and frequency domains. The chirp signal used in the simulation was the positive (up) frequency swept signal with 10.0 MHz/26.0 μs sweep rate. By using 2048 samples, the maximum frequency span was -16 MHz to +16 MHz.

In spectral illustrations, the frequency i.d (or index) is the multiplier of incremental frequency (when N=2048, Δf = 0.015625 MHz), so, for example, the index number 100 means 1.5625 MHz. The the vertical axis of the graphs is the power density of the signal calculated with its minimum level set to -100dBW or -120dBW, assuming the maximum level of carrier amplitude is $\sqrt{2}$ for future convenience in power calculations.

For baseband simulation, the transmitted analog FM TV signal and chirp signal are defined as follows:

$$w(t) = \sqrt{2}\cos[\omega_c t + 2\pi f_d \int^t m(\alpha)d\alpha] \tag{3.32}$$

where $\omega_c = 0$ for baseband

f_d = 10.0 MHz/volt

$m(\alpha)$ = 200 step linear staircase function or 256 step random amplitude function

The transmitted chirp signal is written as

$$i(t) = \sqrt{2}\cos[\omega_c t + \frac{1}{2}\mu t^2] \tag{3.33}$$

where

ω_c = 0 for baseband simulation

μ = 10.0 MHz/26 μs

Simulation results in the time and frequency domains are illustrated in the following figures. Fig. 19 shows the transmitted analog FM-TV signal at baseband. The original message signal for TV

is the random function in Fig. 18 with 0.5 volt dc bias. Fig. 20 also illustrates the corresponding frequency spectrum (power spectral density) of the transmitted signal when the message signal is random. As another simulation model, the video is modeled by a 200 step linear staircase function; Fig. 21 shows the same form as Fig. 19 but with this linear step function as its message signal. Fig. 22 shows the corresponding spectrum. For the transmitted chirp signal, Fig. 23 shows the time waveform and Fig. 24 illustrates its spectrum.

The spectral plots, Fig. 20, Fig. 22, and Fig. 24 give the clues for an effective overlay service. Fig. 22 illustrates the transmitted FM-TV signal spectrum in baseband, with its message signal modeled as a 200 step linear decreasing staircase function, and Fig. 20 shows the same TV signal spectrum but with a 256 step random amplitude function as its video information. In both cases, the spectrum is nearly flat up to approximately 4.2 MHz. However, from 4.2 MHz to 16 MHz, the average level of the spectrum in the random video message case is much higher than that for the linear staircase function. Even though neither of these two cases is a real TV spectrum, they can be used as reference spectra for the design of a chirp overlay system. The spectrum depicted in Fig. 22 can be used as a general case of typical TV video spectrum, whereas that depicted in Fig. 20 can be considered a worst case spectrum. The fast decay of the energy in the spectrum in Fig. 22 (linear staircase message signal) above 4.2 MHz shows that this TV signal can be overlaid by a chirp signal if the relative power levels of the chirp and TV signals are set correctly in the transmission stage. The link analysis in the next section will provide the appropriate value of chirp signal suppression to prevent serious interference of the TV video reception, and also gives the specific value of compression gain required for chirp demodulation under the power limited situation of typical satellite links.

As mentioned before, the message signal (TV video signal) used in the simulation up to this point has not been processed by a preemphasis filter. Preemphasis increases the energy at higher frequencies in the FM-TV spectrum, which increases the interference into the chirp signal channel. The simulation was repeated with a preemphasis filter in the video channel to get results both in the time and frequency domains and to see the effect of preemphasis filtering.

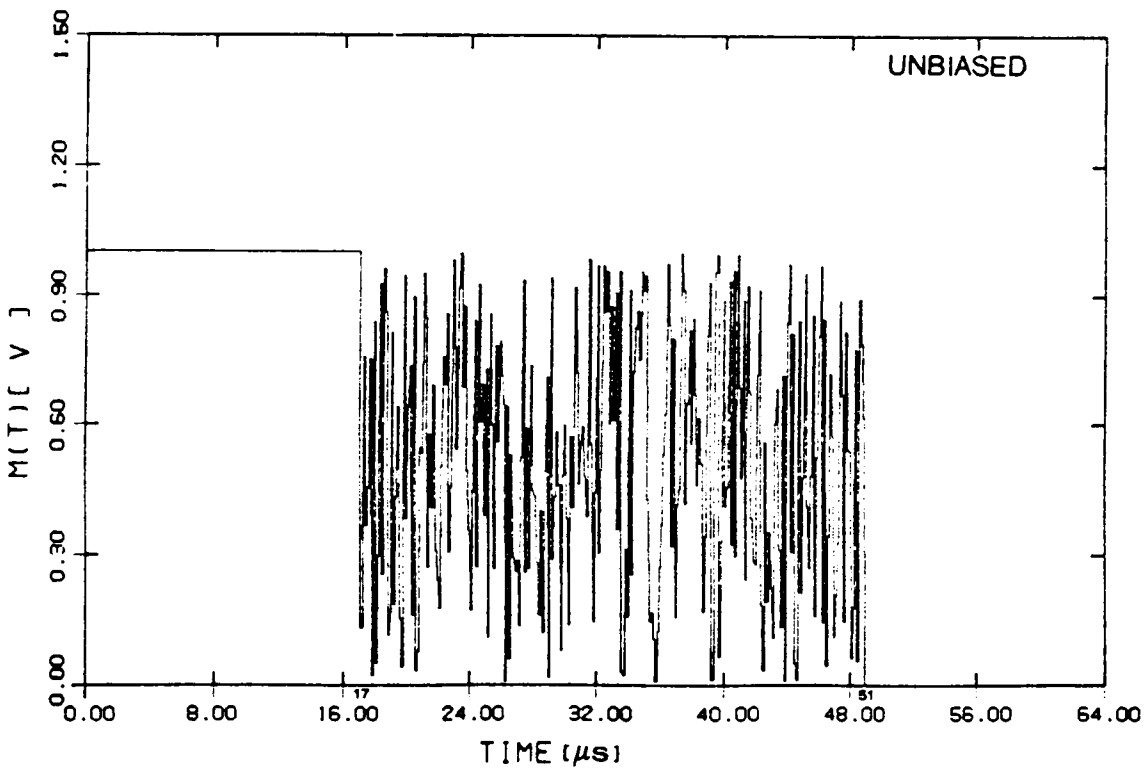

Figure 18. Time plot of simulated 256 step random amplitude model for video signal

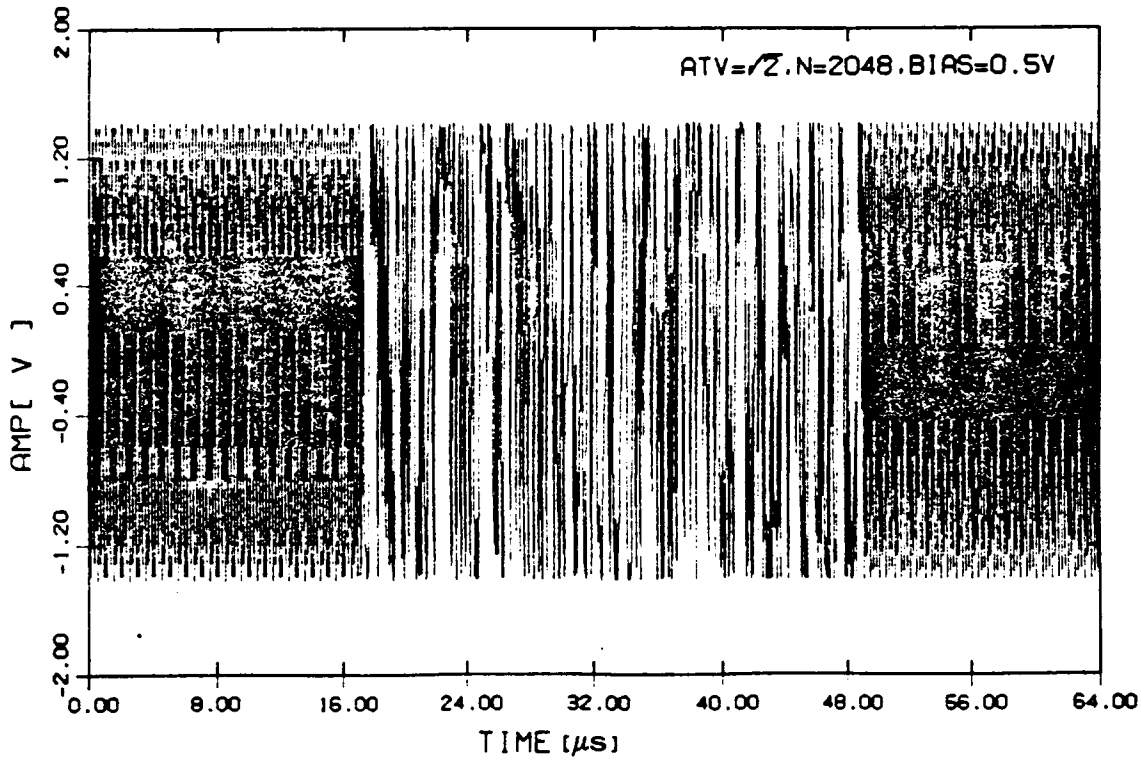

Figure 19. Transmitted FM-TV signal time plot (random)

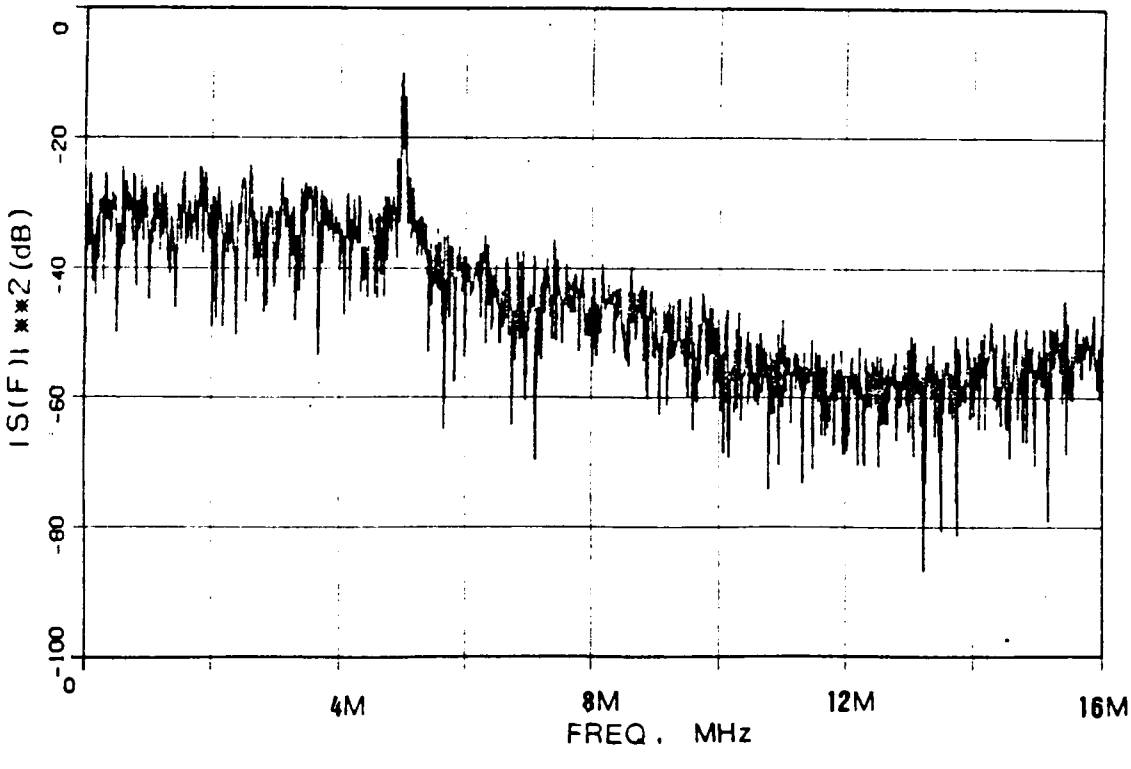

Figure 20. Frequency specttrum of Figure 19 (random)

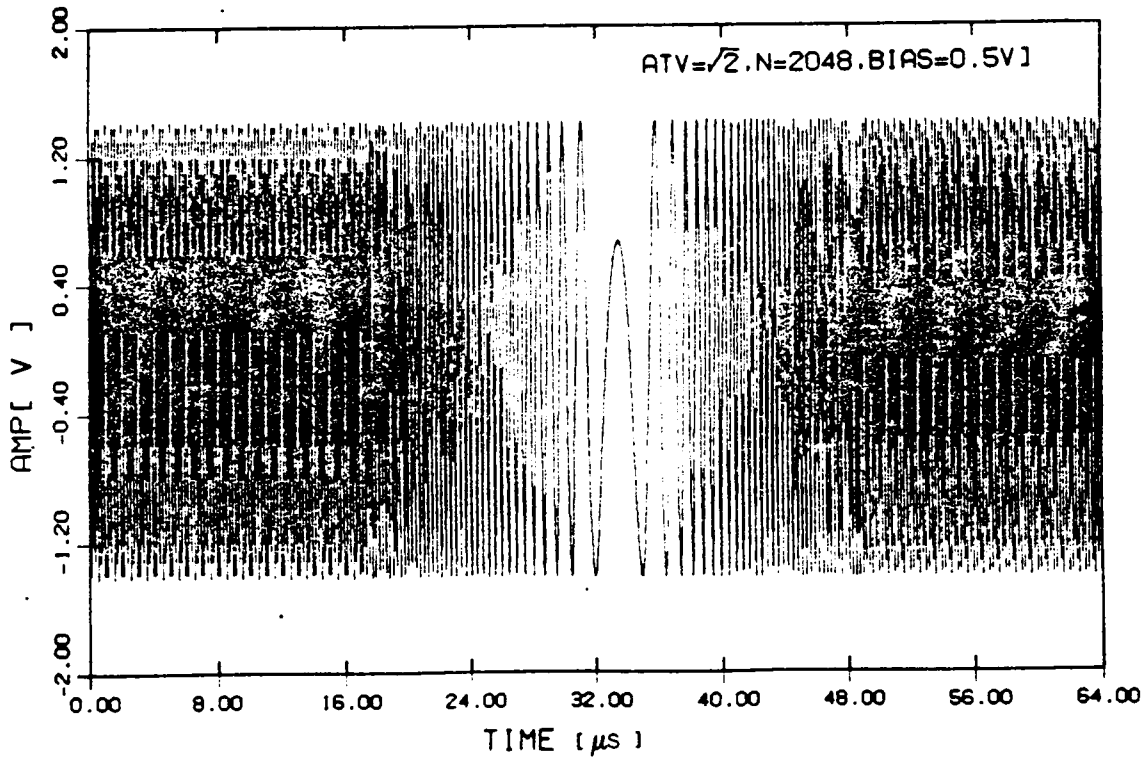

Figure 21. Transmitted FM-Tv signal time plot (linear)

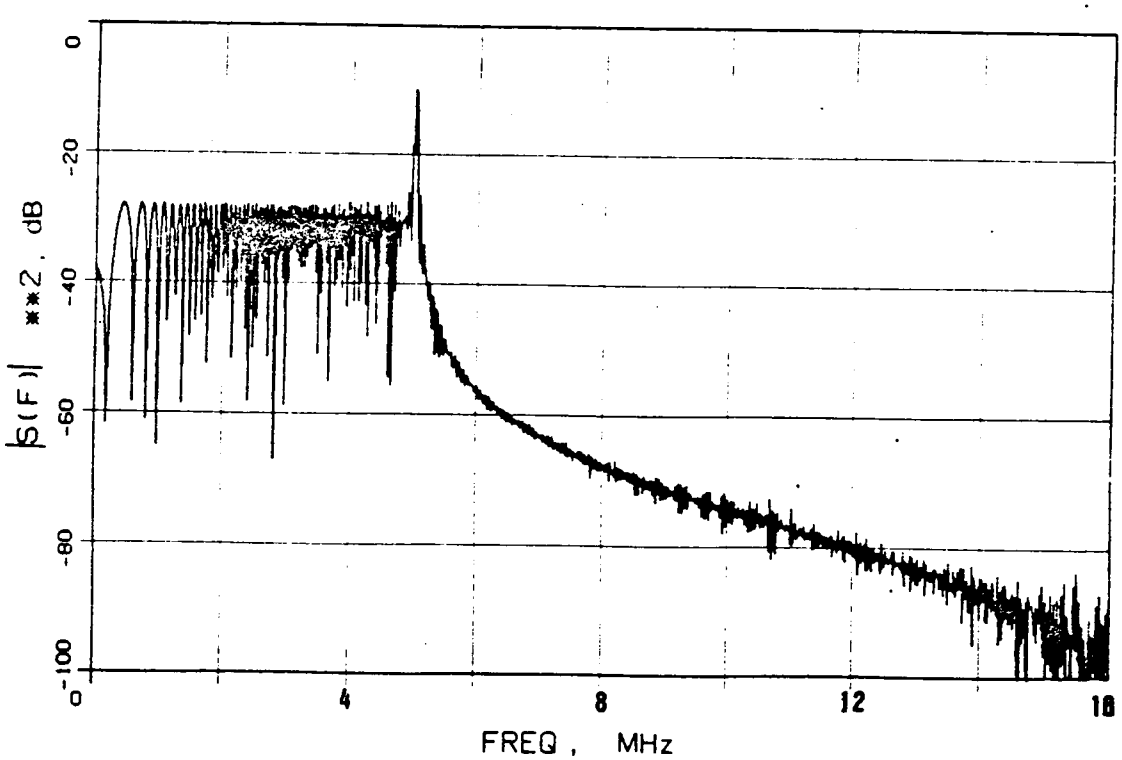

Figure 22. Frequency spectrum of figure 21 (linear)

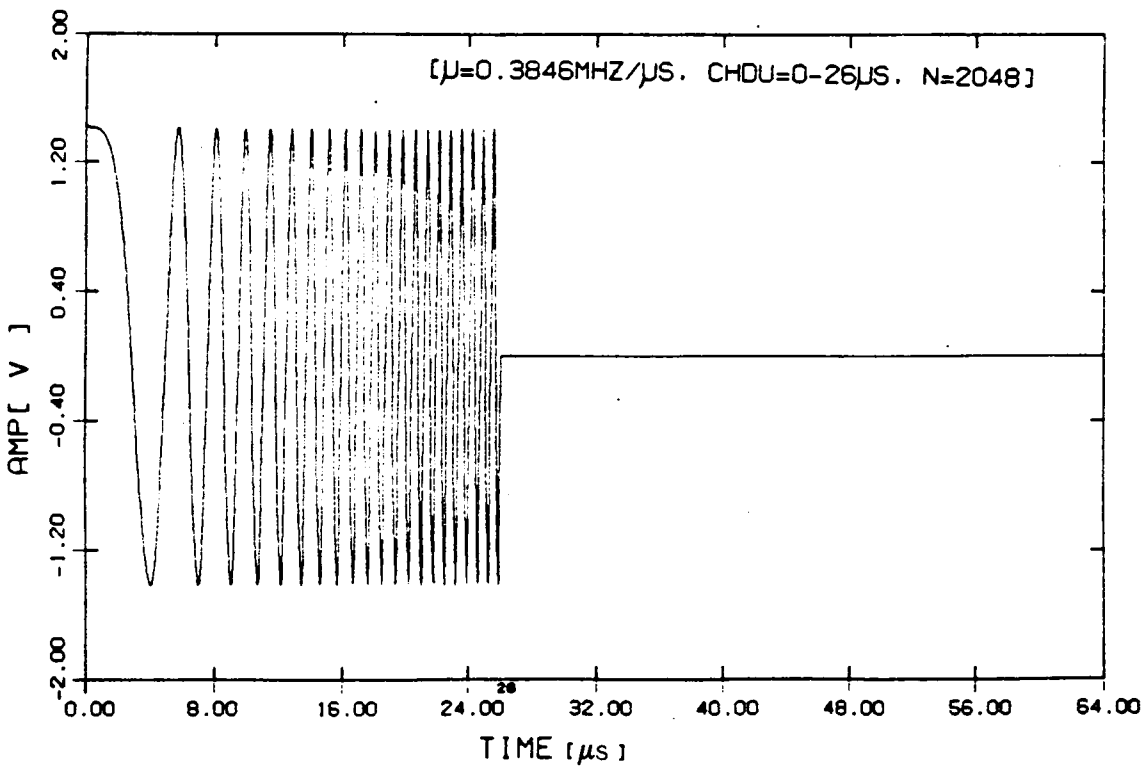

Figure 23. Transmitted chirp signal time plot

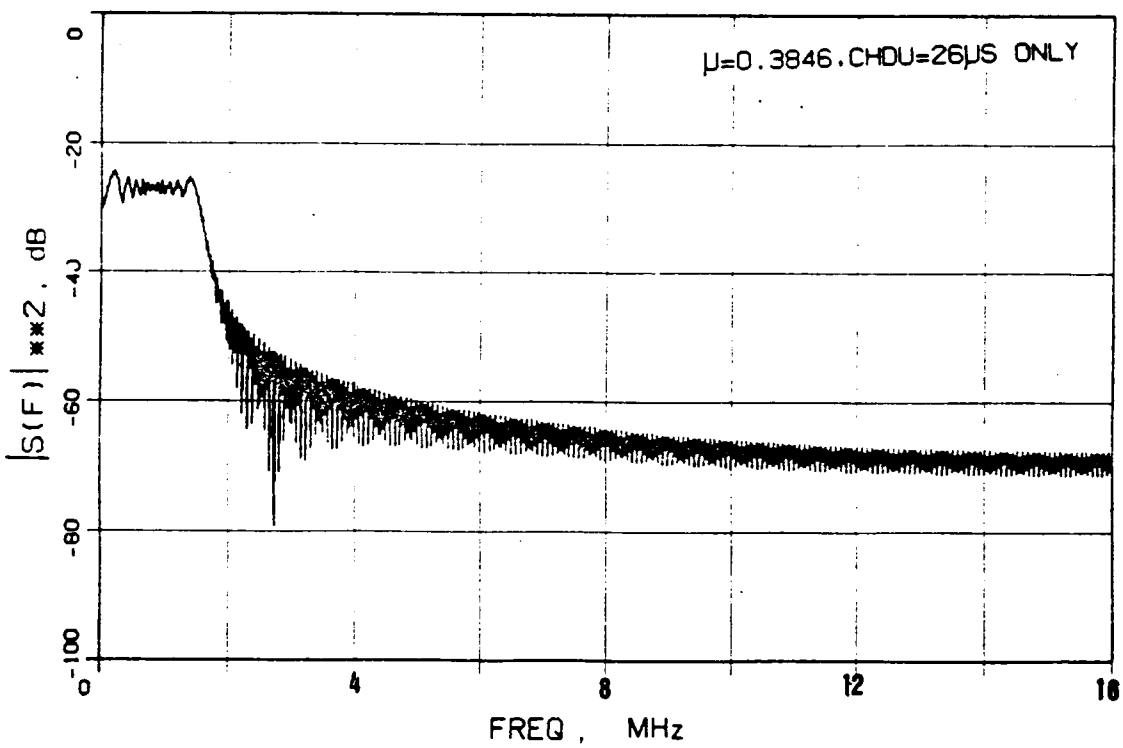

Figure 24. Frequency spectrum of Figure 23

3.3.3. Analog FM-TV signal modeling II -- With Preemphasis

In the previous analysis, the models used for the FM-TV video signal did not include preemphasis before modulation of the carrier. However, most practical FM systems employ preemphasis and deemphasis. Therefore, to get a more practical simulation result, preemphasis filtering of the analog FM TV signal is necessary. Theoretically, a deemphasis filter also must be included after the TV signal demodulation. But in the simulation performed here, especially the interference analysis at the input of the IF filter, it is not thought to be necessary, because deemphasis is achieved with a low pass filter which simply eliminates the residual interference spike after demodulation. The deemphasis filter can be eliminated from the simulation without losing validity of the simulation result. Fig. 25 illustrates an example of a NTSC FM TV modem block diagram which employs preemphasis and deemphasis, along with typical frequency response curves of each filter.

Preemphasis Characteristics - NTSC 525 line/simulation

The characteristics of typical preemphasis filters can be found in relevant references. Janskey and Jeruchim [33] describes the CCIR pre-emphasis technique in detail, and Freeman [31] presents the various preemphasis curves under CCIR Recommendation 405. For more detailed information, see CCIR Report 464 [34].

Fig. 26 illustrates the preemphasis characteristic curves for 405, 525, 625 and 819 line TV systems. Here, in the simulation, we have confined our analysis to the 525 line NTSC system. Fig. 27 shows the 525 line NTSC preemphasis curve which we used as a model for simulation. An algorithm was developed by trial and error variation of the parameters of the usual expression for preemphasis. Fig. 28 shows our simulated preemphasis characteristic curve. Although there are

some differences between Rec 405 and the simulated curve, the error is within $\pm$ 1dB over most of the frequency range.

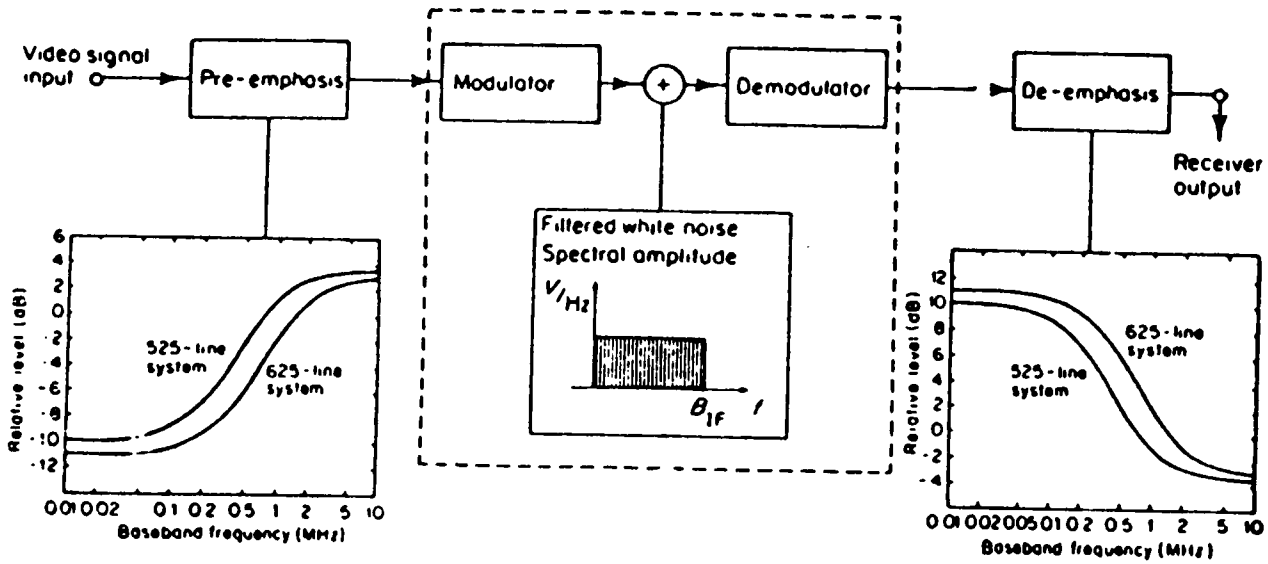

(Pre-emphasis characteristic CCIR Rec-405)

Figure 25. Typical NTSC modem structure with preemphesis/ deemphasis

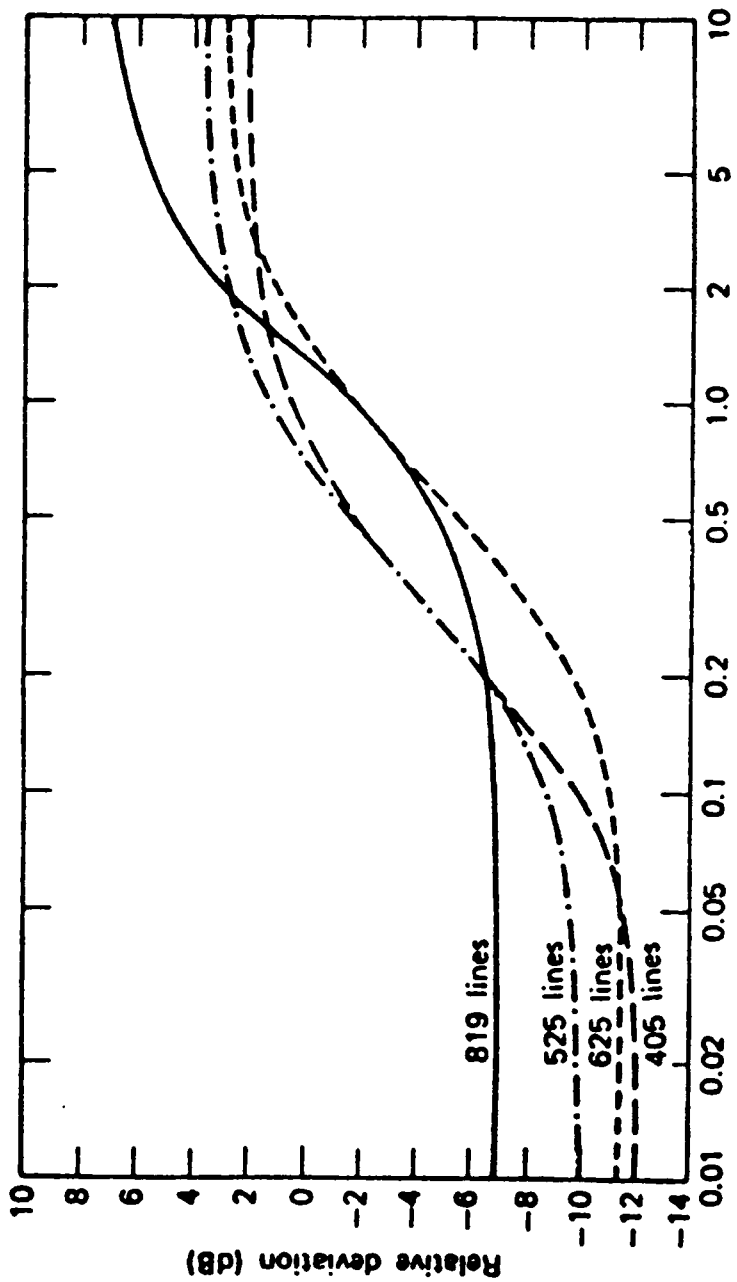

Figure 26. TV preemphasis characteristics(525, 625, 819 and 405 lines)

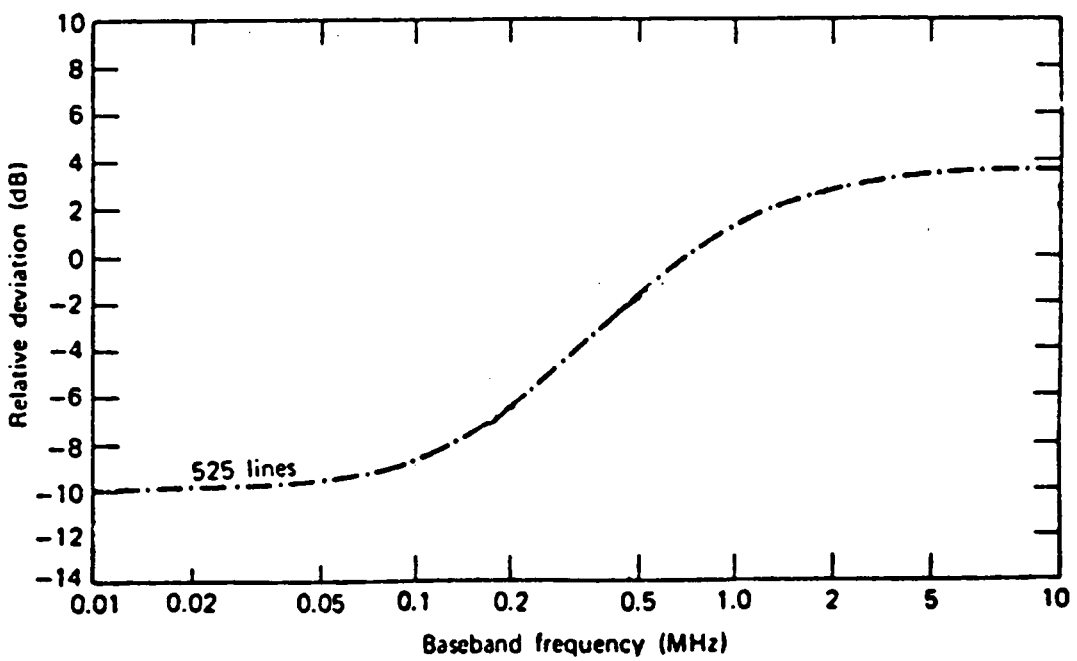

Figure 27. NTSC 525 line-CCIR Rec.405 preemphasis characteristic

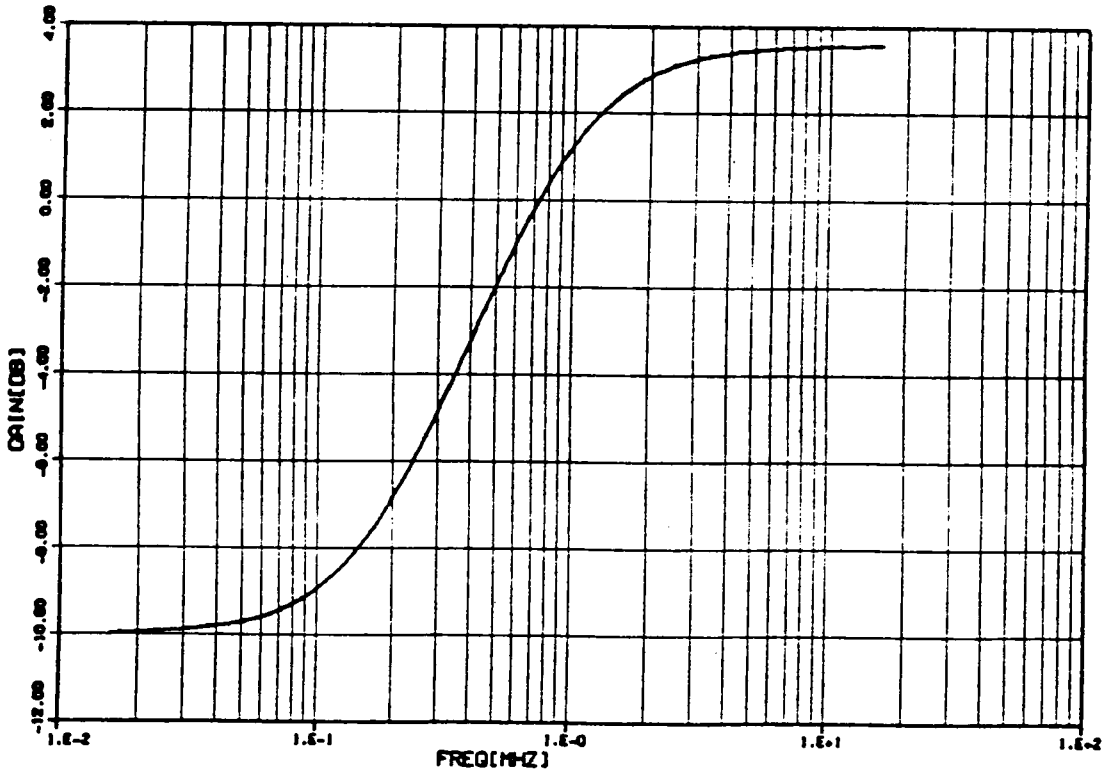

Figure 28. Simulated preemphasis filter for NTSC 525 line TV system

Modeling of FM-TV Video Signal - With Preemphasis

Basically, there cannot be any differences in the simulation models under the presence of preemphasis, because only a filtering operation has been added before frequency modulation of the wideband TV signal. But for the convenience of simulation, some changes are needed because of the complex valued form of signal used in the filter process. The active luminance signal duration was changed from 17 ~ 51 μs to 18 ~ 50 μs, which should not cause significant difference in the spectral domain. The other difference from the model used when there is no preemphasis in the random amplitude TV video was the number of random amplitude steps. It is necessary to keep the same number of time or frequency samples throughout the overall simulation procedure, and the filtering routine was made to accept data in this way. There are 2048 samples over the 64 μs duration of a single horizontal scanning line; a section lasting 32 μs (18 μs to 50 μs) which contained 1024 samples, was selected as having random amplitude. Therefore, instead of selecting and generating 256 random numbers, 1024 random numbers were generated in this simulation for the preemphasis version.

Fig. 29 shows the video signal with random amplitude before preemphasis, and Fig. 30 shows its preemphasized version. Because of the gain factor in the preemphasis filter at higher frequencies, the random portion has enhanced amplitude compared with the non-preemphasized case shown in Fig. 29. The other signal model was simulated by a staircase function. Fig. 31 illustrates the video message before preemphasis, and Fig. 32 shows the preemphasis version. In Fig. 32, a transient spike at 50μs is caused by the large level shift in the original message signal from -0.5V to 0.5V.

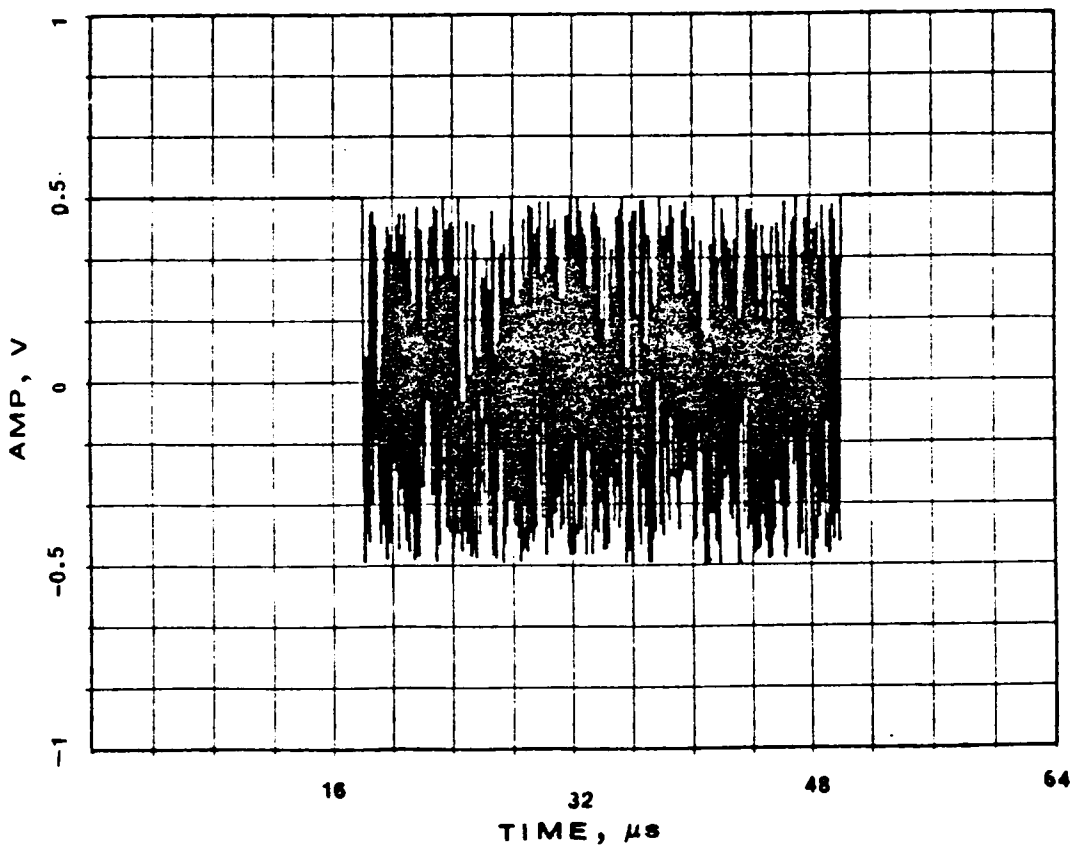

Figure 29. TV message m(t) before preemphasis(time plot) ;random amplitude

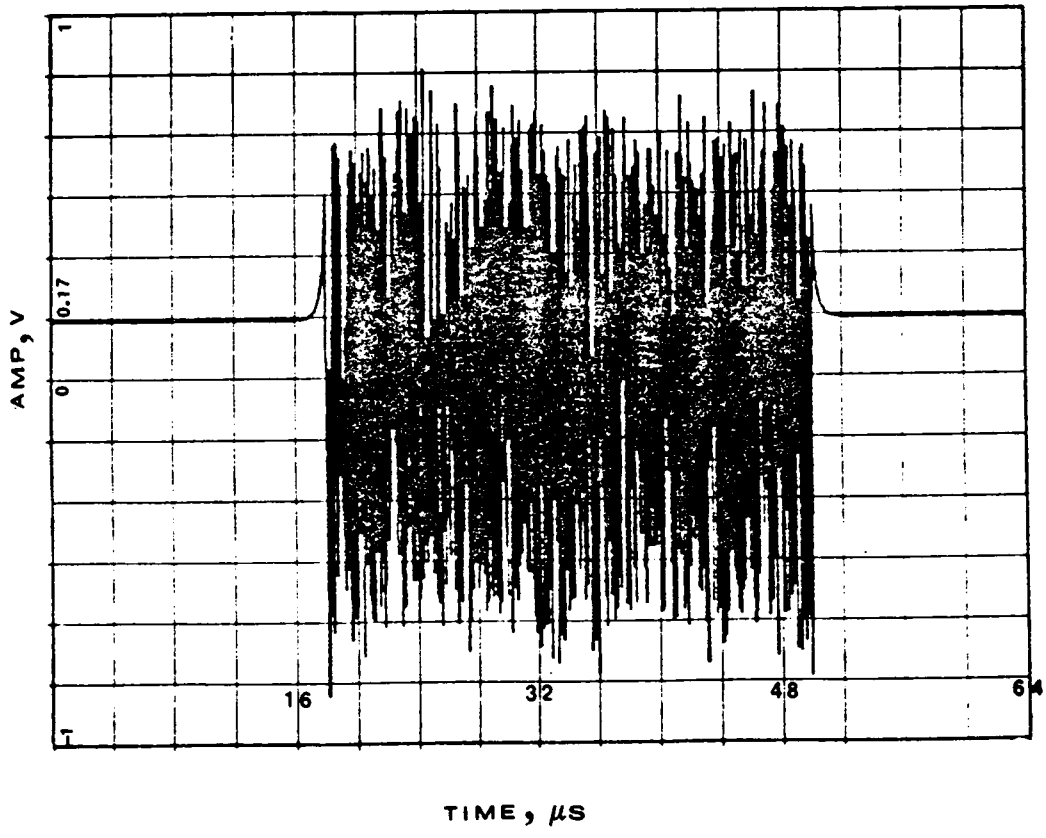

Figure 30. TV message m(t) after preemphasis(time plot) ;random amplitude

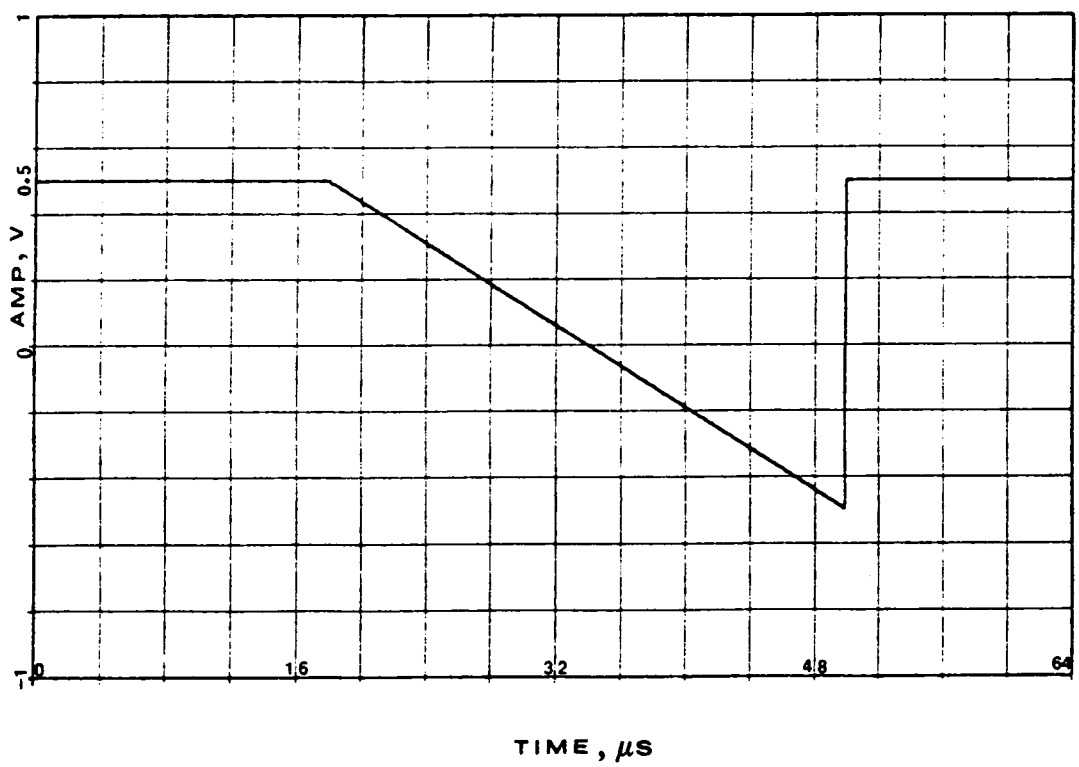

Figure 31. TV message m(t) before preemphasis(time plot); linear staircase function

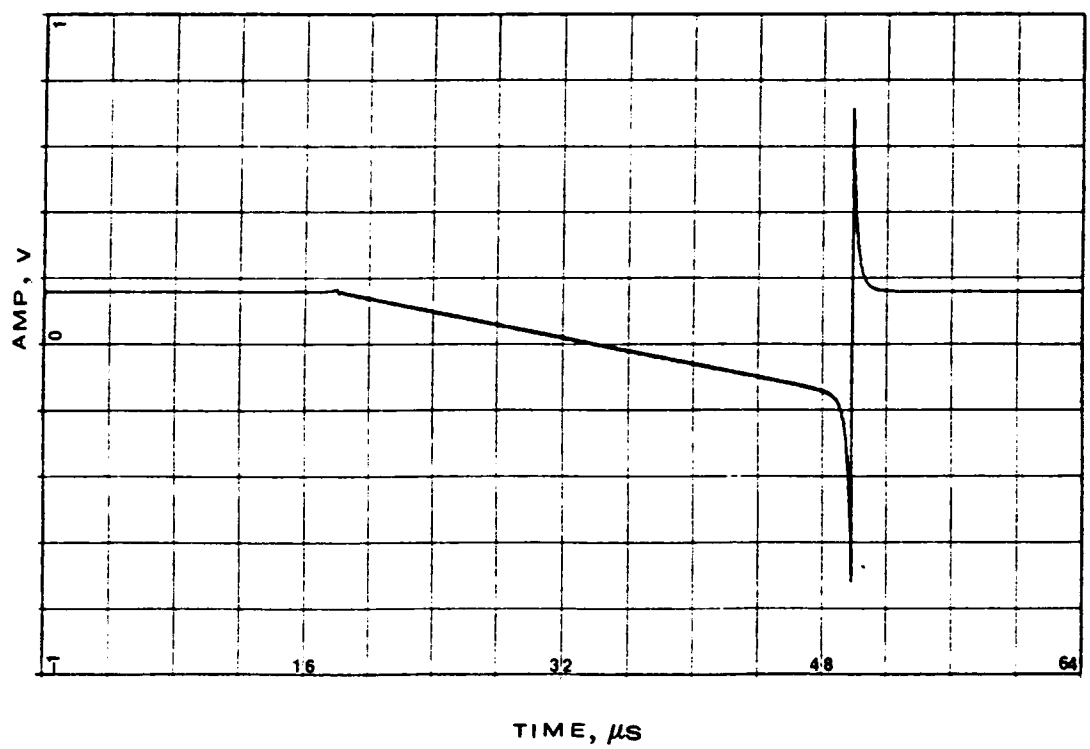

Figure 32. TV message m(t) after preemphasis(time plot); linear staircase function

3.3.4. Wideband FM TV Signal Simulation II-- With Preemphasis

Computer simulation was repeated using the same procedures as were described in Section 3.2, but with the preemphasized video information (message) signals depicted in Fig. 30 and Fig. 32 of the previous section. Fig. 34 shows the frequency spectrum of the transmitted FM-TV signal for baseband simulation when the video signal is a preemphasized 200 step staircase function. Fig. 33 illustrates the frequency spectrum of a transmitted FM-TV signal for baseband simulation when the video signal is a preemphasized 1024 step random amplitude function. When we compare the transmitted wideband FM TV spectra which were preemphasized (Fig. 33 and Fig. 34) with non-preemphasized ones (Fig. 20 and Fig. 22) (i.e., comparing Fig. 20 and Fig. 33 and comparing Fig. 22 and Fig. 34), we can observe that the average power density level at higher frequencies in the preemphasized spectra are raised relative to the non-preemphasis cases. The reason for this can be attributed to the gain factor in the preemphasis curve at the higher frequencies. However, the total average power is the same in all cases because the carrier amplitude of $\sqrt{2}$ is the same for all signals. In an FM signal, the transmitted power depends solely on the carrier amplitude, regardless of the modulating signal.

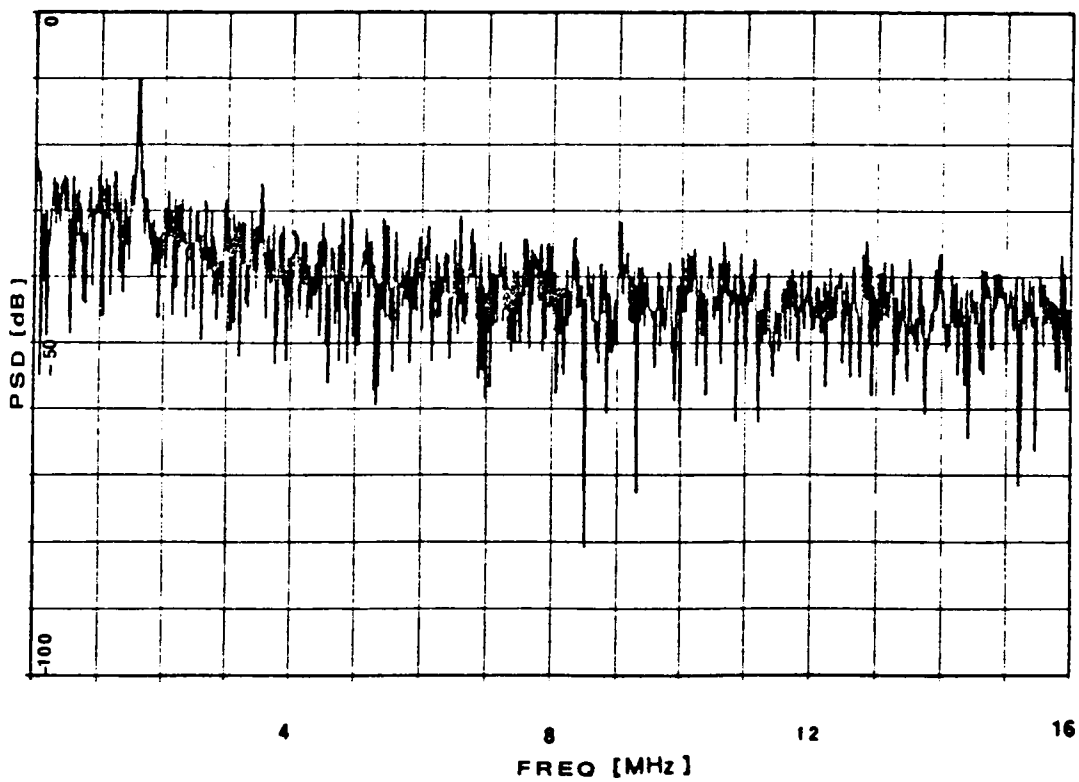

Figure 33. Transmitted FM-TV spectrum (m(t)= random, preemphasis version)

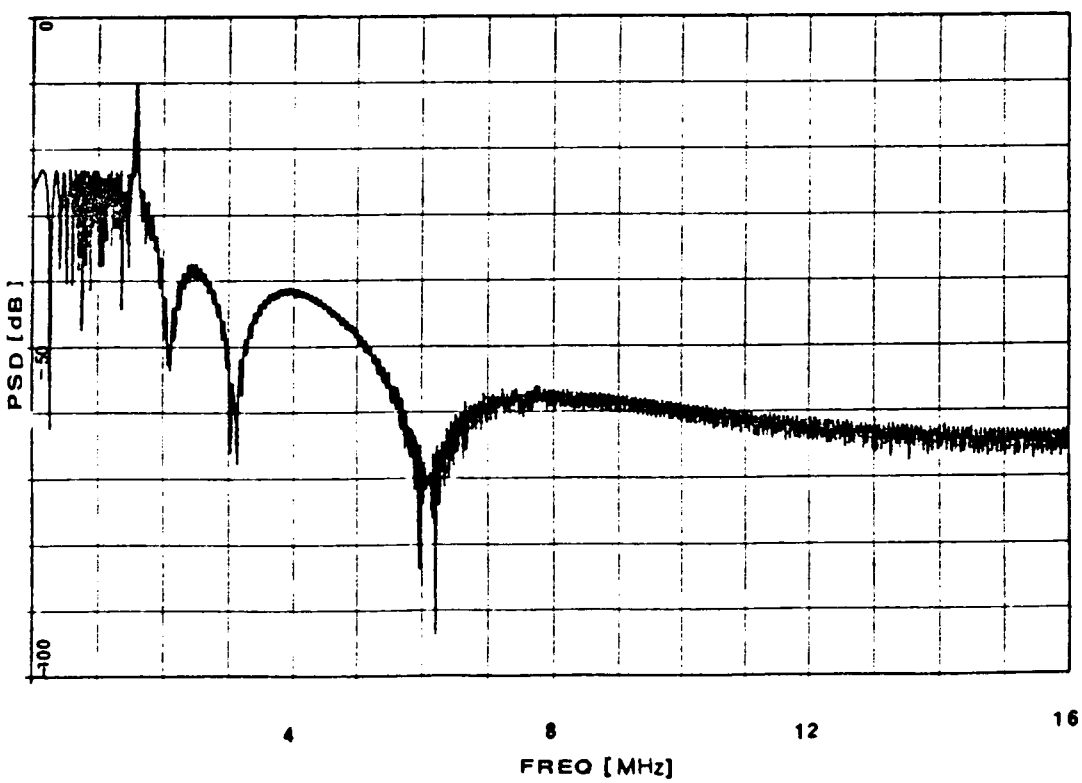

Figure 34. Transmitted FM-TV spectrum (m(t) = linear, preemphasis version)

3.3.5. Overlay System Link Analysis

In the previous section, we have simulated the transmitted TV signal and chirp signal at baseband, and found that a sufficient amount of suppression of the chirp signal permits the overlay of a chirp signal on top of a TV signal, and proper compression gain in the chirp demodulator can guarantee successful chirp demodulation. The determination of the parameters in a given system must be obtained through a link analysis.

The major difference between TV transmission and chirp via a satellite lies in the power limitation of the earth station in the case of the chirp signal because of the small antenna size and low transmitter power which are assumed for chirp transmission. The other major difference is the receiver bandwidth. Compared to the large IF bandwidth used for FM TV, a comparatively narrow IF bandwidth (about 5 MHz) is anticipated for chirp. From this point of view, appropriate selection of the chirp carrier frequency in the 36 MHz transponder bandwidth used for TV transmission plays an important role in deciding the carrier to interference ratios (C/I ratio). The final performance measure of the proposed coded multiple chirp s.s. system is the probability of bit (chip) error or word (code) miss probability. For the FM-TV service, the C/I ratio is a measure of degradation caused by chirp overlay.

In this analysis, a typical link using the Galaxy II satellite in C band was used as an example of overlay service. Some key parameter values of "Galaxy II" are listed below.

Galaxy II Parameters [Based on FM-TV Transmission with Chirp Overlay]

Satellite Transponder Parameters

EIRP	34 dBW
G/T	-3 to +3 dBK^{-1}

Bandwidth	36 MHz

Earth Station Parameters

Antenna Diameter	9.0 m or 2.4 m (for chirp only)
Aperture Efficiency	65 %
System Noise Temperature	100K (120K for chirp)
FM-TV Receiver IF BW	32 MHz (5.0 MHz for chirp)

Desired Performance

Analog FM-TV Down Link	C/N $\geq$ 10 dB
Chip Error Probability	$P_e \leq 10^{-4}$

The proposed overlay service depicted in Fig.35 is briefly explained here. The high power TV signal at 6 GHz is transmitted by a 9 meter antenna and is received by a smaller antenna (2.4 meter in diameter) via the 4 GHz downlink. At the same time, the chirp signal with relatively low power is transmitted through a 2.4 meter antenna and received by the 9 meter antenna. The next two tables shows the FM-TV and chirp spread spectrum system link analyses in C-band.

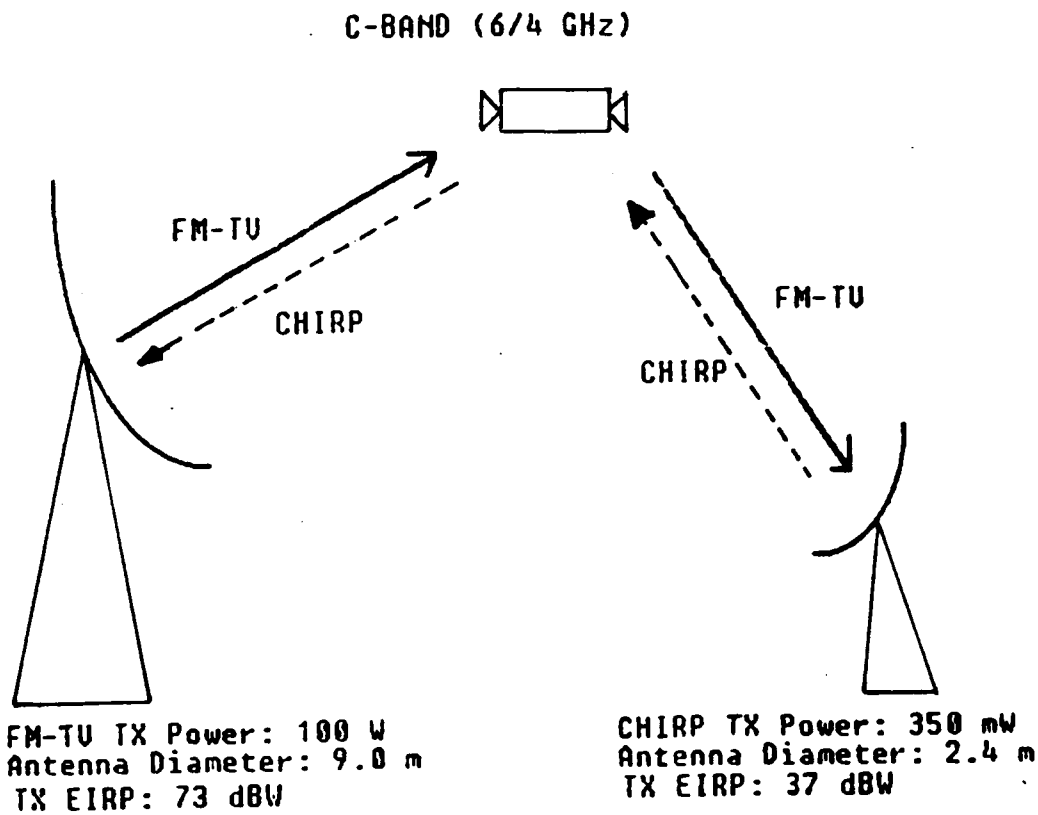

Figure 35. Spread spectrum overlay scheme between chirp and FM-TV signal in C-band

FM-TV Overlay Link Analysis

Based on the Galaxy II parameters and desired performance crieteria, the link analysis of FM-TV operating in C-band is listed in following Table 1.

Table 1. FM-TV Overlay Link -- C band

Uplink Parameters

Max Transmitter Power	20 dBW (100W)
Antenna Gain (9 m)	53.2 dB
EIRP	73.2 dBW
Path Loss (6 GHz, Clear Air)	200.2 dB
Rain Attenuation	Y dB

Satellite Parameters

Flux Density	-85.0 dBW/m^2
G/T	3.0 dBK^{-1}
C/N	(30.96- Y) dB

Downlink Parameters

EIRP	37.0 dBW
TWTA Output Backoff	3.0 dB
Path Loss (4 GHz, Clear Air)	196.3 dB
Rain Attenuation	X dB
Rx Antenna Gain (2.4 m)	38.18 dBK^{-1}
G/T	17.28 dBK^{-1}
C/N	(8.64- X) dB

Chirp Overlay Link Analysis

As the other phase, chirp spread spectrum overlay link was analyzed as in Table 2. Parameters in this table were found under the assumption that chirp's transmitted EIRP is lower than FM-TV uplink EIRP by 36 dB and the TV link parameter described in FM-TV link analysis.

Table 2. Chirp Overlay Link -- C band

Uplink Parameters

Max Transmitter Power	-4.52 dBW (350mW)
Antenna Gain (2.4 m)	41.7 dB
EIRP	37.2 dBW
Path Loss (6 GHz, Clear Air)	200.2 dB
Rain Attenuation	XX dB

Satellite Parameters

Flux Density	-121.0 dBW/m^2
G/T	3.0 dBK^{-1}
C/N (IF BW = 5.0 MHz)	(1.58 - XX) dB
C/N (IF BW = 40 KHz)	(22.6 - XX) dB

Downlink Parameters

EIRP	[1.0 + (X - XX)] dBW
TWTA Output Backoff	3.0 dB
Path Loss (4 GHz, Clear Air)	196.3 dB
Rain Attenuation	YY dB
G/T	29.66 dBK^{-1}
Chirp Carrier Power	[-148.6 + (X-XX)-YY] dBW
C/N (IF BW = 5.0 MHz)	-7.04 dB
C/N (IF BW = 40 KHz)	13.94 dB

Probability of Chip Error	1.76×10^{-6}

Note.

1. 36 dB attenuation is given under 36 dB compression gain of chirp
2. the probability of chip error is base on the Eq. (2.13).

3.4. Performance Analysis of Overlay Service I--Without Preemphasis

In the overlay link analysis in previous section, when the chirp signal EIRP is -36 dB below the FM-televison signal EIRP, the final chip error probability for the chirp system is around 1.0×10^{-6}, assuming 2400 bps(hence corresponding chip rate is around 40K chips/sec using 16 bit codewords). However, the link analysis done in previous section does not consider the interference factor when calculating C/N ratio; it cannot be a sufficient proof that the overlay service is safe from mutual interference. Calculation of the C/I ratio is needed, so that we can recalculate the final C/N ratio both in the FM-TV demodulator output and in the dechirper output, which will finally give the codeword error(miss) probability.

In the analysis procedure, the signal powers of the TV and chirp are calculated first at the earth station receivers. The FM-TV signal power and chirp signal power at the receiving earth station are calculated when each signal works as the interfering signal in the overlay service. Finally the C/I ratios for both cases are found and plotted for comparison. Because we dealt with two cases, the preemphasis case and the no-preemphasis case, the analyses will be done separately; then the final results will be compared.

3.4.1. Signal Power Calculation

A. FM-TV Power

FM-TV signal power was set to one watt watt and it can be calculated by

$$P_{tv} = \frac{1}{2}(A_{tv})^2 = \frac{1}{2}(\sqrt{2})^2 = 1.0 \text{ W} \tag{3.34}$$

when the transmitted FM-TV signal is expressed by

$$W(t) = \sqrt{2}\cos[\omega_c t + 2\pi f_d \int m(\alpha)d\alpha] \tag{3.35}$$

where $\omega_c = 0$ in the baseband, $f_d = 10$ MHz/Volt, $m(\alpha)$ is a staircase function or random amplitude function. In simulation, once the power spectral density of each data point is obtained, the total power for 2048 samples is the summation of the spectral density over all frequencies, i.e,

$$P_{tv} = \sum_{i=1}^{n=2048} |x(i)|^2 \tag{3.36}$$

where $|x(i)|^2$ is the power spectral density at the 'i'th sample(frequency) point.

The resulting FM-TV signal power calculated by summing spectral density values was:

case1; video signal is 256 step random amplitude function

$P_{tv} = 1.00537$ W

case2; video signal is 200 step staircase function

$P_{tv} = 0.97927$ W

When we compare the simulated FM-TV power with theoretical power, they are almost same (within 2.1 %).

B. Chirp Signal Power

Let the transmitted chirp signal be given by

$$i(t) = \sqrt{2}\cos[\omega_c t + \frac{1}{2}\mu t^2] \tag{3.37}$$

then theoretical power is set to one watt:

$$P_{chirp} = \frac{1}{2}(A_{chirp})^2 = 1.0W$$

By computer simulation, we get the simulated chirp power as

$$P_{chirp} = 0.42213W$$

The simulated chirp power is 3.7 dB lower than the theoretical value. But, this is expected because the chirp signal is applied only 26 μs of the 64μs scanning period. Thus, 26/64 = 0.406 W is the correct value. Because the simulated power is within 4 % error, it was assumed that the simulation was correct.

C. 36 dB Attenuated Chirp Power

In the link analysis, a chirp signal EIRP of -36 dB relative to FM-TV transmitted EIRP was assumed. Therefore, if we choose a simulated FM-TV power of 1.00537 watt in section A, -36 dB attenuated chirp power would be $1.00537 \times 10^{-3.6} = 0.0002528$ watt. Figure..36 illustrates this attenuated chirp spectrum; in this case, relative to the FM-TV signal of which the video signal is a 256 step random amplitude.[see Figure 24 for comparison.]

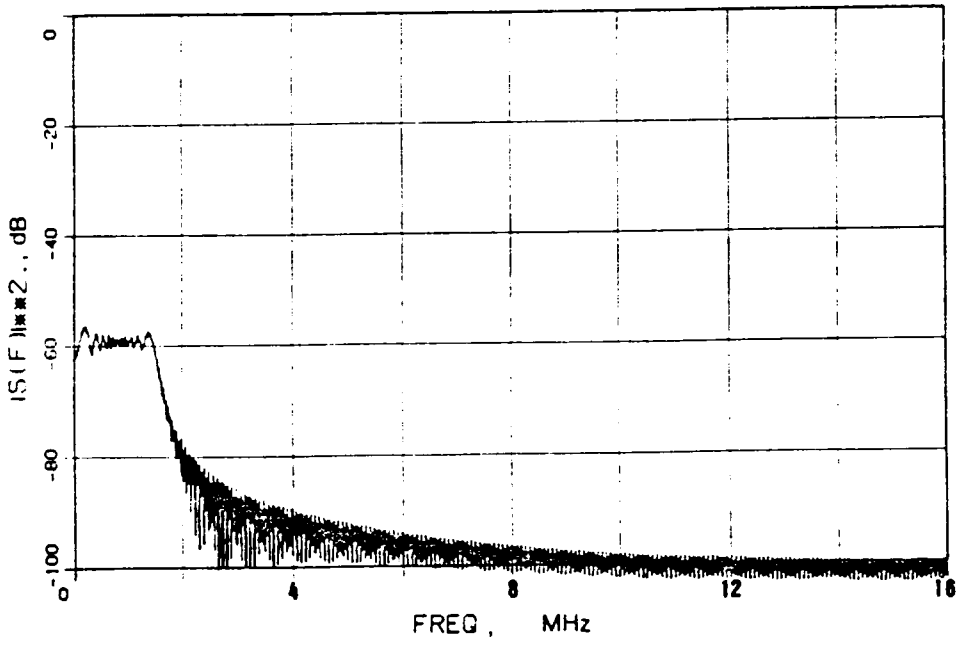

Figure 36. 36 dB attenuated chirp signal spectrum

3.4.2. Interference Power Calculation

In section 3.4.1, FM-TV signal power and chirp power at the earth station receiver were found both in theory and by computer simulation. As the second step, we calculated the mutual interference power I, and thus the C/I ratio, when we overlapped the chirp's attenuated spectrum onto the FM-TV signal transponder bandwidth and vice versa.

A. Chirp Interference to FM-TV

As mentioned earlier, FM-TV signals use the whole 36 MHz transponder bandwidth, but the overlaying signal, in this case the chirp signal, uses a relatively narrower bandwidth. We have already fixed the chirp signal bandwidth at 5.0 MHz in the overlay link analysis. However, because of a restriction of the FFT routine permitting only 2^n number of samples in frequency, a 32 MHz TV bandwidth was assumed. Because of this difference in bandwidth, to calculate the chirp interference into the FM-TV channel, it is necessary to find the power spectral density of chirp signals over a 5 MHz bandwidth. Fortunately the chirp spectrum has a relatively high level and a flat portion below 2.5 MHz. Therefore it is not required to move a 5.0 MHz bandwidth unit to and from the entire 32 MHz (two sided) bandwidth of the spectral plot. [Note: All the spectral plots are drawn only for positive frequency, and the maximum frequency in those plots is 16 MHz.]

We already know that the low power chirp signal has a power of 0.00025W relative to the FM-TV signal of one watt. When we calculated the single sided power of the chirp signal from 0 to 2.5 MHz bandwidth, we got 0.00012W. therefore the total power in a frequency bandwidth of -2.5 MHz to 2.5 MHz is almost the same as 0.00025W. We can conclude that at least 99 % of the power in the chirp signal is in the -2.5 MHz to 2.5 MHz range.

B. FM-TV C/I Ratio

From the result that almost all of chirp power is in the -2.5 MHz to +2.5 MHz band, with a total power of 0.00025W, there is no difference in C/I ratio if the chirp carrier frequency is located anywhere in the 32 MHz bandwidth used by the FM TV signal. In addition, chirp interference is an all pass signal in the wideband TV IF filter, so interference power from the chirp loses nothing. Therefore,

$$\frac{C}{I} = \frac{1.000537[W]}{0.00025[W]} = 36dB$$

C. Net C/N of FM-TV under chirp Interference.

By the result of section A, C/I is 36 dB. It is necessary to recalculate the C/N for the TV signal because the interference adds to thermal noise and affects the C/N. Because the chirp signal power is 36 dB attenuated relative to the TV signal, the interference power of the chirp signal is calculated as -163.12 dBW at the receiver, based on the FM-TV link analysis. If we regard the interference as another form of noise, the net noise power is -132.76 dBW. Therefore the net C/N under chirp interference is 8.636 dB. When we compare this C/N with the C/N defined in the link analysis, which does not consider the interference, there is almost no difference. Therefore we can conclude that the effect of interference on FM-TV is negligible.

D. FM-TV Interference on Chirp

As the reverse case of chirp interference, interference from FM-TV into the chirp channel, the high powered FM-TV signal is the interference into the chirp channel. Before starting the analysis, the following must be noted:

1. Compared to the wide bandwidth of FM-TV (32 MHz assumed), the chirp bandwidth is narrower at 5 MHz.

2. By (1), contrary to the previous case, only a 5.0 MHz bandwidth portion of the FM-TV power spectrum is interfering with the chirp signal.

3. By (2), there can be a large difference in interference level depending on the IF center frequency offset between the chirp and the TV signal center frequency, within the 32 MHz bandwidth.

E. Chirp C/I Ratio Calculation.

From the result that almost all of chirp power (36 dB attenuated) is located in the -2.5 MHz to 2.5 MHz range, we set the chirp power in a 5.0 MHz bandwidth as $C_{chirp} = 0.00025W$.

The C/I ratio for the chirp channel depends, in part, on the center frequency used for the chirp signal relative to the center frequency of the FM-TV signal. Figure 37 showing the spectrum of the FM-TV signal indicated that the TV signal has a much higher power spectral density close to the carrier than well away from it. To determine the C/I ratio as a function of frequency offset between the chirp and TV signal carrier frequencies, we shifted the center frequency for the chirp carrier across the 32 MHz band of the FM-TV signal in 0.5 MHz steps, and calculated the power from the TV signal in a 5 MHz bandwidth centered at the chirp carrier.

Table 3 lists all the necessary information when the FM-TV video signal is modeled by a 256 step random amplitude function and when the FM-TV video signal is modeled by a 200 step staircase function. As can be seen from Table 3, when the IF offset frequency approaches the positive maximum (or negative maximum) (far from the center frequency), the C/I ratio gets better. In addition, when the FM-TV signal is modeled by a staircase function, the C/I ratio is much better than that of the random amplitude function. This is expected because the spectrum of the FM-TV signal in this case (staircase function model) is decaying faster than that of the random amplitude case. Figure 37 and Figure 38 show the overlaid spectral plots of the FM-TV spectrum modeled by a staircase function (Figure 37)

and the FM-TV spectrum modeled by a random amplitude (Figure 38), with a 36 dB attenuated chirp spectrum. As a graphical representation, the C/I ratio vs IF offset frequency for both cases of FM-TV interference signal are drawn in Figure 39. Based on Table 3, when the chirp IF center frequency is located at 12.5 MHz from the center frequency of the FM-TV signal, the corresponding C/I ratio is -5.56 dB. The reason why the best C/I ratio is selected from Table 3, where the message signal (video) model is a random amplitude function, is that this should be a worst case analysis. Then the net C/N (E_b/N_o) recalculated for the existence of FM-TV interference, is -9.37 dB. When we compare this value with the C/N ratio in the earlier link analysis, about 1 dB degradation occurs because of the FM-TV interference. Finally, if we assume 23 dB compression gain, the C/N ratio after the compression filter will be +14dB, the corresponding probability of chip (bit) error will be around $5x10^{-6}$. In this case, the data rate is around 25 kbps.

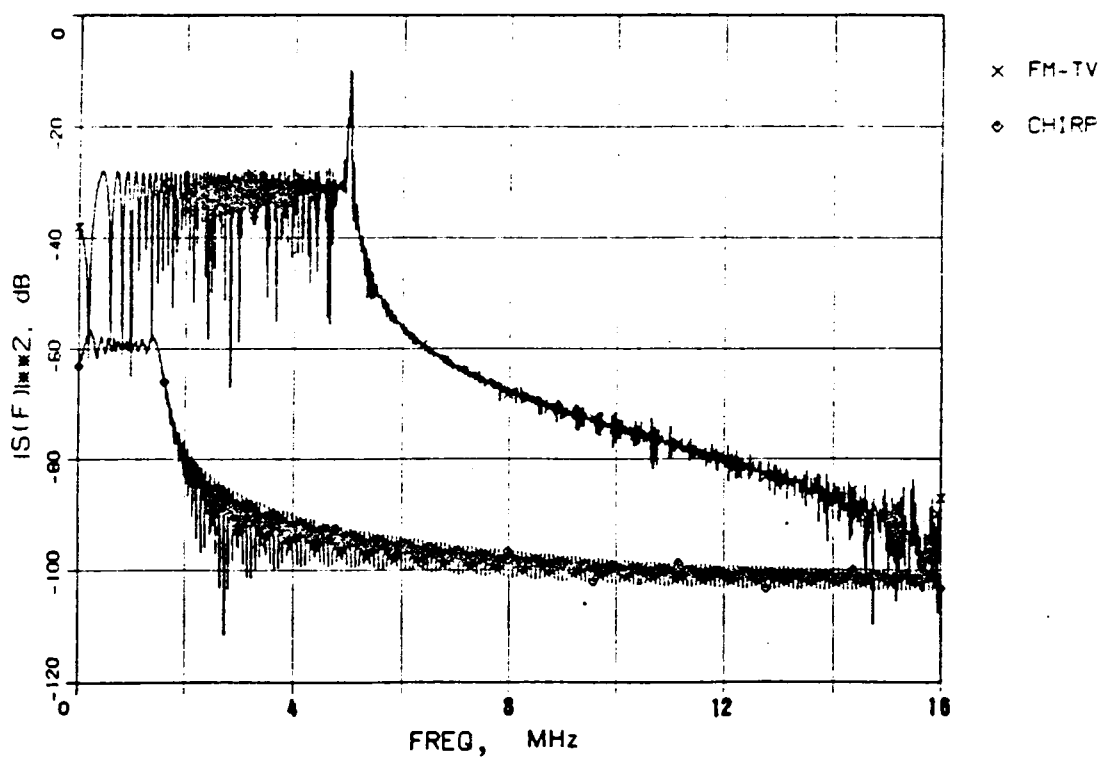

Figure 37. Overlapped spectrum of FM-TV (m(t) = linear stair) and 36 dB attenuated chirp

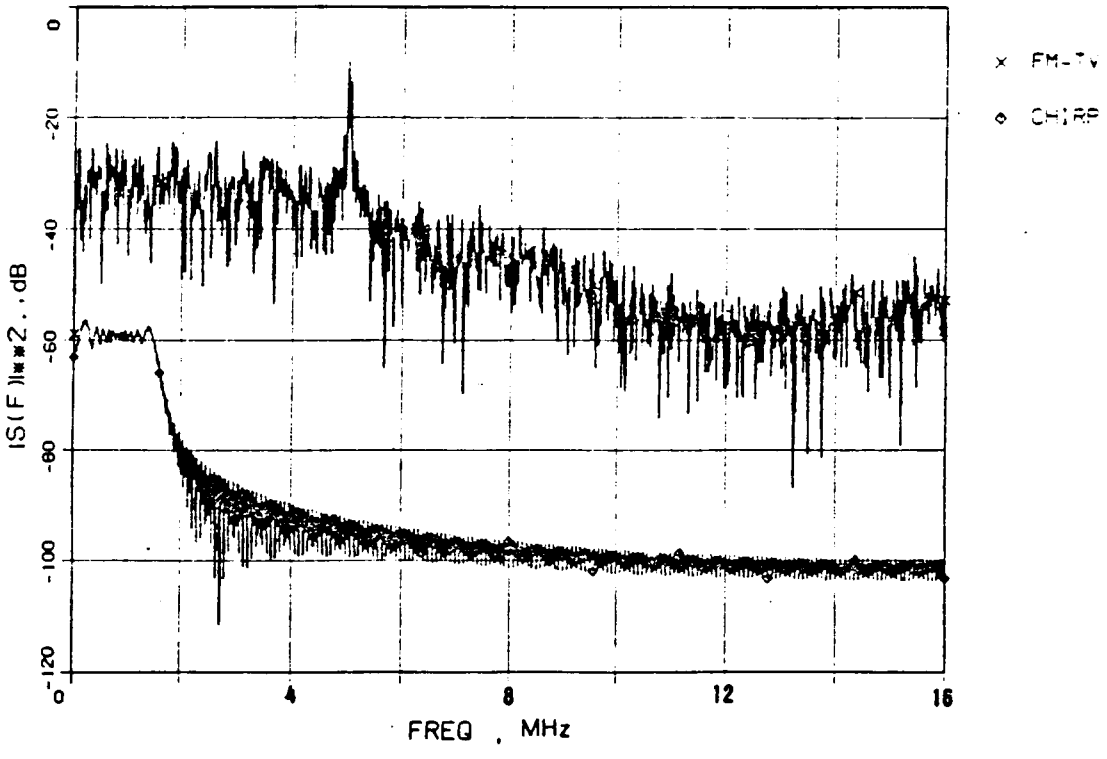

Figure 38. Overlapped spectrum of FM-TV (m(t) = random amplitude) and 36 dB attenuated chirp

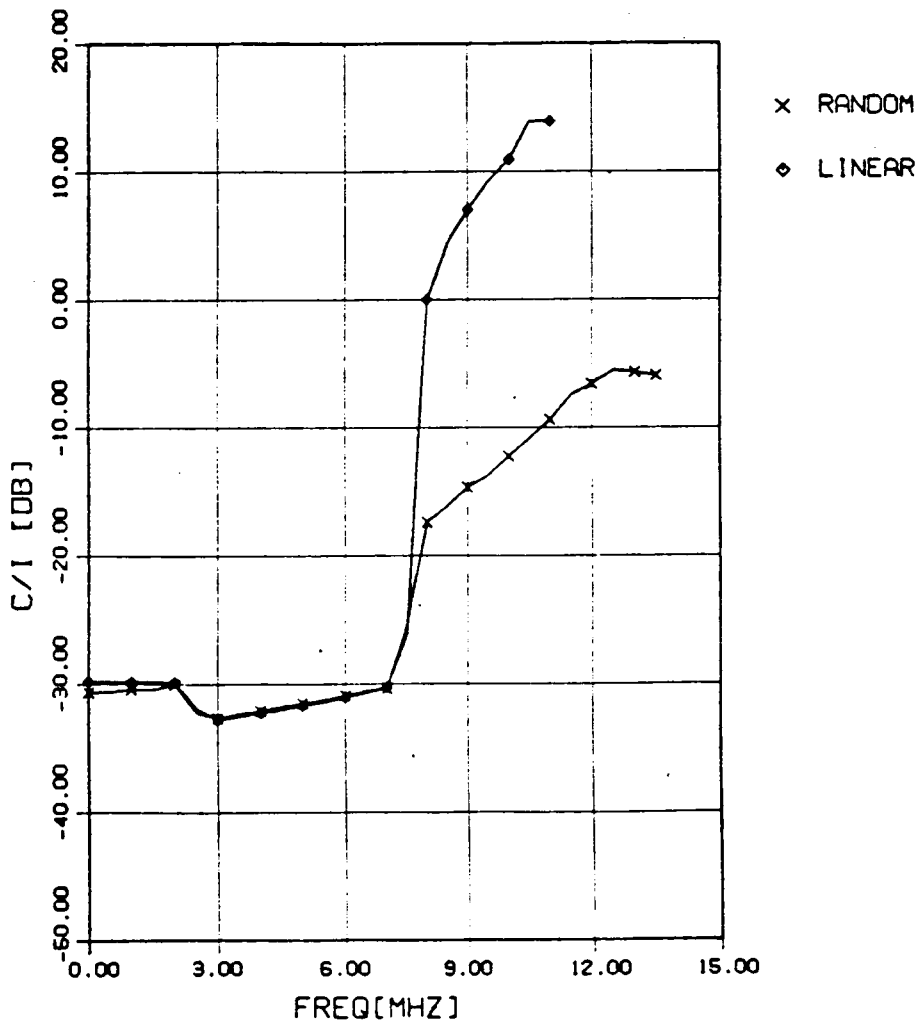

Figure 39. C/I ratio vs IF offset frequency (message are linear stair and random amplitude)

Table 3. C/I ratio vs IF offset for FM-TV spectrum [No preemphasis] [m(t): 256 step random function and 200 step linear step function]

			256 step random		200 step linear	
Leading freq [MHz]	Trailing freq [MHz]	Offset freq [MHz]	5 MHz BW Tv POWER [W]	C/I [dB]	5 MHz BW Tv POWER [W]	C/I [dB]
2.5	-2.5	0.0	0.289	-30.6	0.240	-29.8
3.0	-2.0	0.5	0.287	-30.6	0.239	-29.8
3.5	-1.5	1.0	0.274	-30.3	0.238	-29.8
4.0	-1.0	1.5	0.275	-30.4	0.238	-29.8
4.5	-0.5	2.0	0.253	-30.0	0.242	-29.8
5.0	0.0	2.5	0.414	-32.2	0.387	-31.9
5.5	0.5	3.0	0.459	-32.6	0.471	-32.8
6.0	1.0	3.5	0.426	-32.3	0.449	-32.5
6.5	1.5	4.0	0.407	-32.1	0.422	-32.2
7.0	2.0	4.5	0.375	-31.8	0.396	-32.0
7.5	2.5	5.0	0.353	-31.5	0.369	-31.7
8.0	3.0	5.5	0.332	-31.2	0.344	-31.4
8.5	3.5	6.0	0.307	-30.9	0.318	-31.0
9.0	4.0	6.5	0.285	-30.5	0.292	-30.6
9.5	4.5	7.0	0.272	-30.4	0.266	-30.3
10.0	5.0	7.5	0.086	-25.4	0.103	-26.1
10.5	5.5	8.0	0.013	-17.4	0.000	0.0
11.0	6.0	8.5	0.010	-16.1	0.0002	4.4
11.5	6.5	9.0	0.007	-14.6	0.0001	6.9
12.0	7.0	9.5	0.005	-13.7	---	---
12.5	7.5	10.0	0.004	-12.2	---	---
13.0	8.0	10.5	0.003	-10.8	---	---
13.5	8.5	11.0	0.002	-9.4	---	---

14.0	9.0	11.5	0.001	-7.4	---	---
14.5	9.5	12.0	0.001	-6.6	---	---
15.0	10.0	12.5	0.001	-5.6	---	---
15.5	10.5	13.0	0.001	-5.7	---	---
16.0	11.0	13.5	0.001	-5.9	---	---

3.5. *Performance Analysis of Overlay Service II- With Preemphasis*

In Section 3.4, we have analyzed the interference effects in an overlay service, but without preemphasis filtering at the input video signal to the FM-TV modulator. In this Section, the same procedures as in Section 4 are repeated for the case when preemphasis is considered. Based on the spectrum and time plots of the transmitted wideband signal in Section 3.4, the chirp signal is also attenuated by 36 dB relative to the FM-TV signal spectrum. Figure 40 and Figure 41 show the overlapped spectra of chirp and FM-TV signals. For simplicity and to avoid repetitive explanation, only the result of the calculations are described here.

3.5.1. Signal Power

1. FM-TV signal power (by simulation)
   - <Case 1> when video signal is modeled by random amplitude, the TV power is 1.00507 W
   - <Case 2> when video signal is modeled by staircase function, the TV power is 1.02763 W
2. Chirp signal power is same as before because preemphasis is not applied to the chirp signal. However after 36 dB attenuation, it turn out to be 0.00025 W. Because the simulated TV power is within 1 % error from the theoretical value of 1.0W, we need no normalization of the FM-TV spectrum. In addition, the 36 dB attenuated chirp power can be used as before.

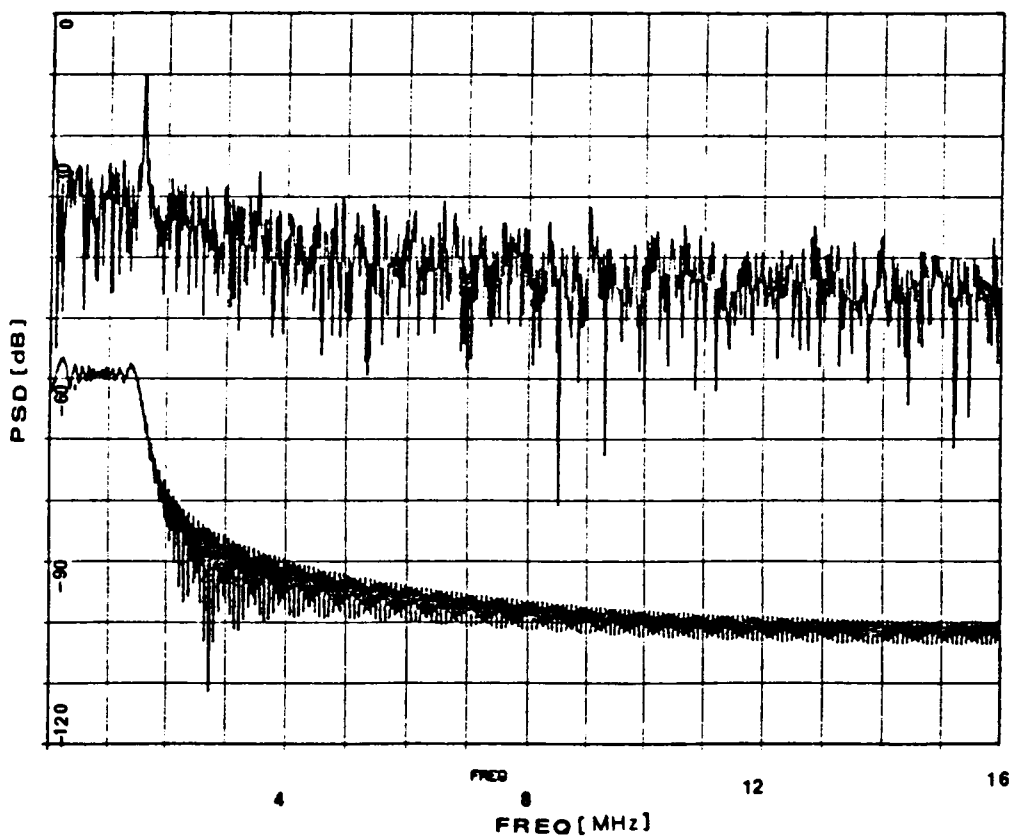

Figure 40. Overlapped spectrum of FM-TV (preemphasis) and 36 dB attenuated chirp(random)

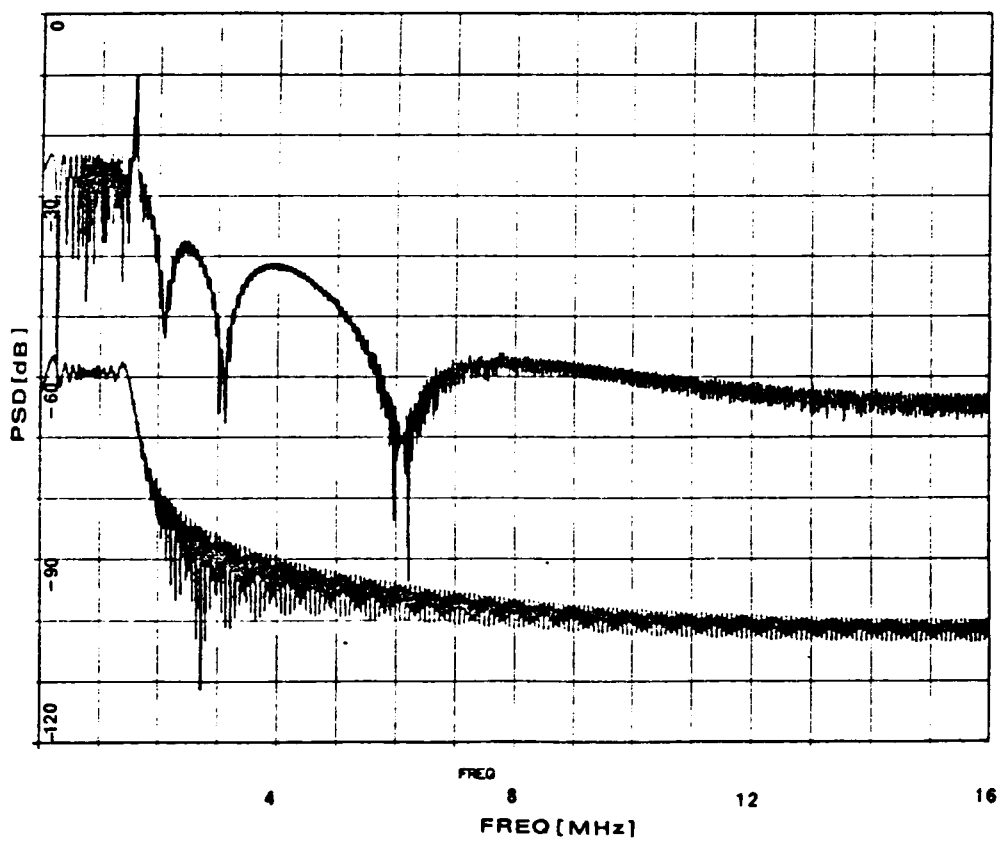

Figure 41. Overlapped spectrum of FM-TV (preempehsis) and 36 dB attenuated chirp(linear stair)

3.5.2. Interference of Chirp to FM-TV

By using the same procedures in Section 3.4.2.A, almost all the chirp power is in the -2.5 MHz to 2.5 MHz bandwidth. Therefore, I=0.00025 W and C=1.00537 W,and the C/I ratio will be 36 dB. In addition, the net C/N ratio of FM-TV under chirp interference is the same as before because the C/I ratio is the same as before.

3.5.3. Interference of FM-TV into chirp channel.

By following the same procedure as in Section 3.4, Table 4 can be obtained for the case when the FM-TV video signal is modeled by random amplitude function and the FM-TV video signal is modeled by the staircase function, respectively. Figure 42 illustrates the C/I ratios versus IF offset frequencies for the different video signal models. Figure 43 depicts the four cases of C/I ratio vs IF offset frequencies. One pair is for the cases when preemphasis is used and the other pair is for the cases when no preemphasis is used. In Figure 43, the C/I ratio still maintains the trend that C/I ratio gets better as the TV carrier frequency goes away from the chirp IF center frequency. In Figure 43, we can observe the effect of preemphasis. The use of preemphasis in the FM-TV video signal, regardless of the modulation applied, degrades the C/I ratio approximately 15-20 dB in general. Figure 44 shows the calculated chip error rate when the C/N of the chirp signal is found for the case of FM-TV signal interference. From the result for FM-TV interference, the final C/N ratio of the chirp signal is found to be -20 dB before compression. If 23 dB compression gain is provided, the probability of chip error is around 10^{-1} . When this is compared to the case for no preemphasis in Section 3.4, about 10^{5} times more error can occur in the preemphasis case. However, the compression gain can be arbitrarily increased up to 10000 using recent advanced technology, although the cost may be a critical factor. Around 5-10 dB increase in processing gain can be used to compensate for this degradation caused by preemphasis filtering.

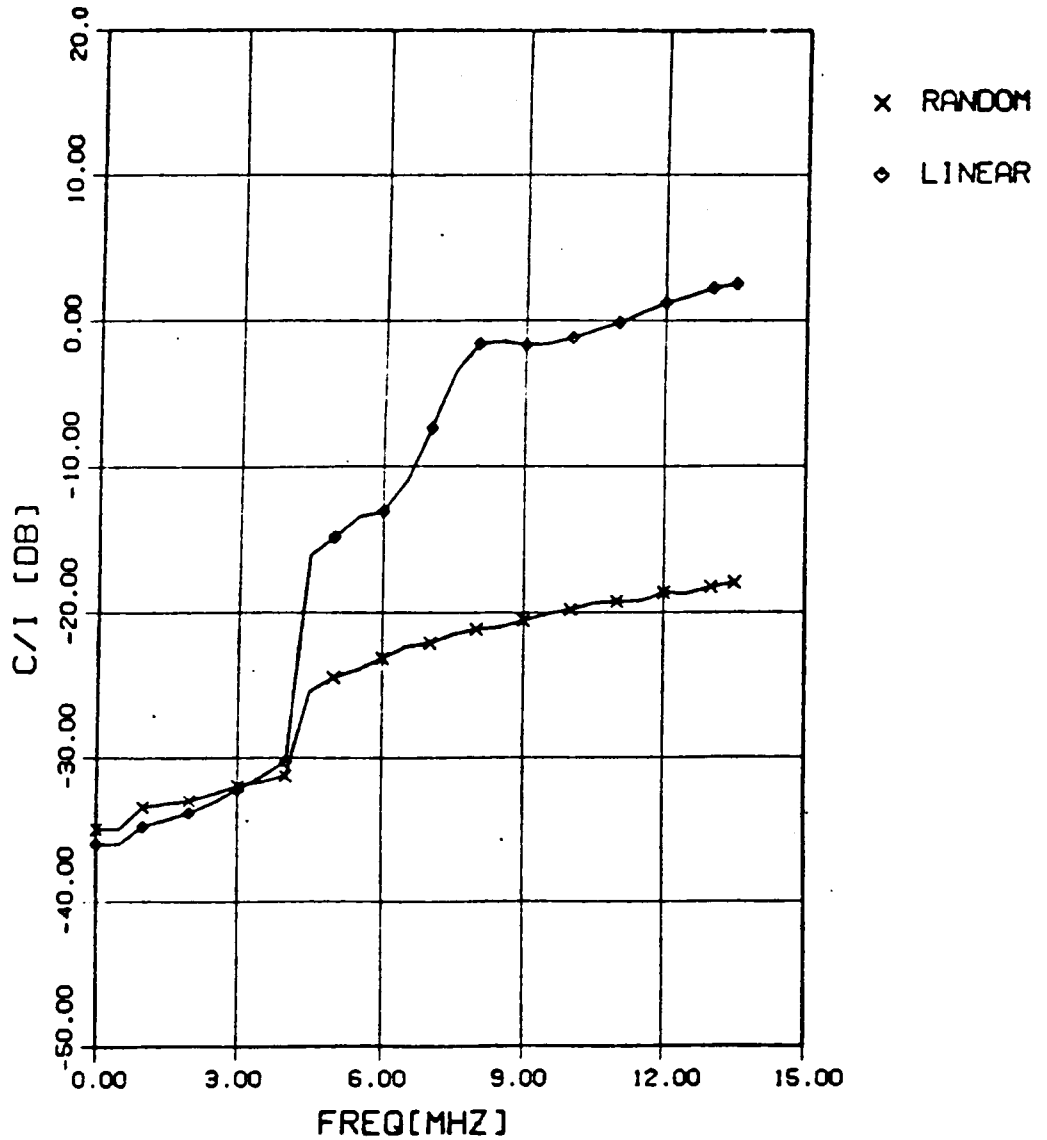

Figure 42. C/I ratio vs IF offset frequency(preemphasis case)

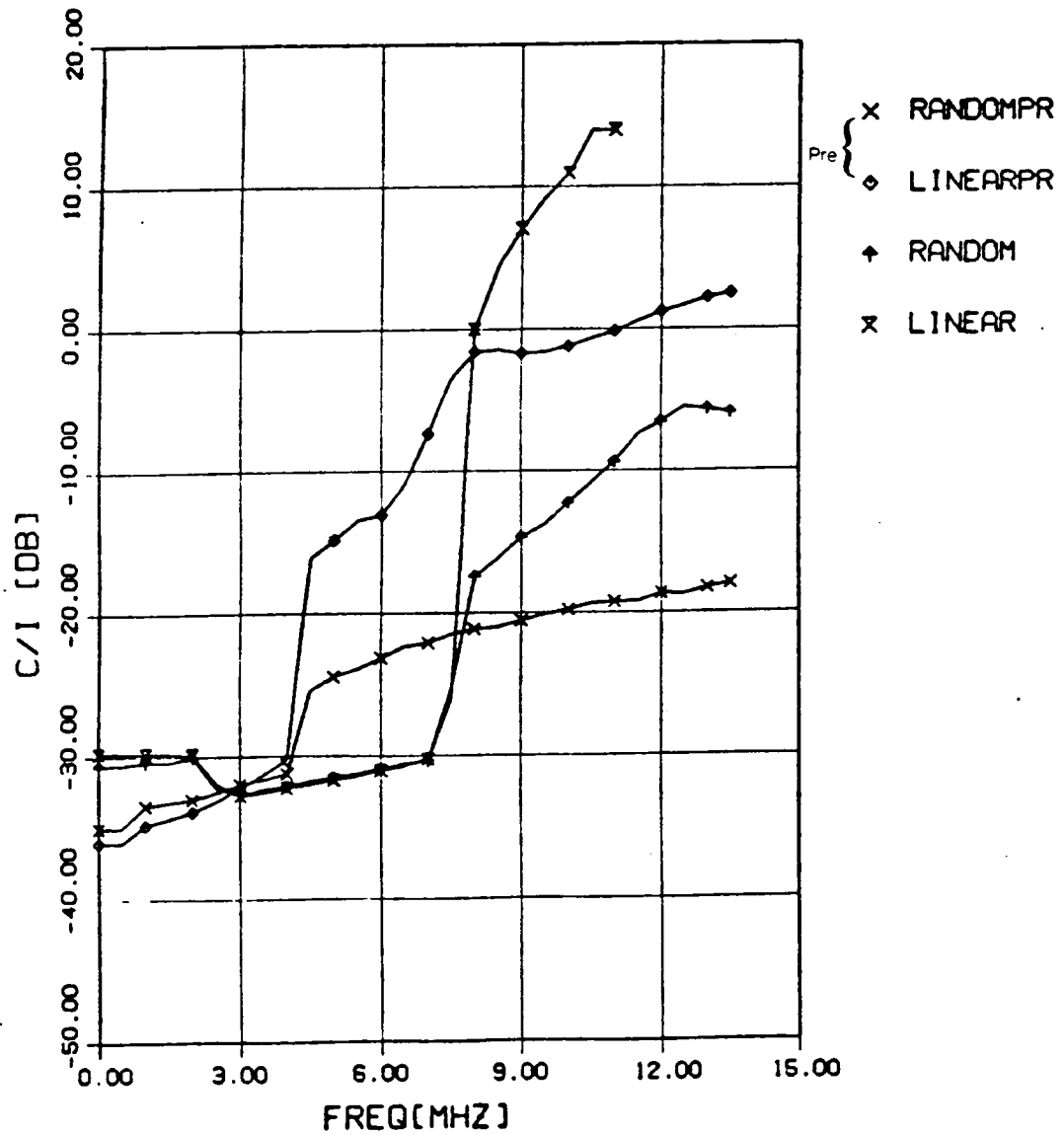

Figure 43. C/I ratio vs IF offset frequency(preemphasis case and no preemphasis case)

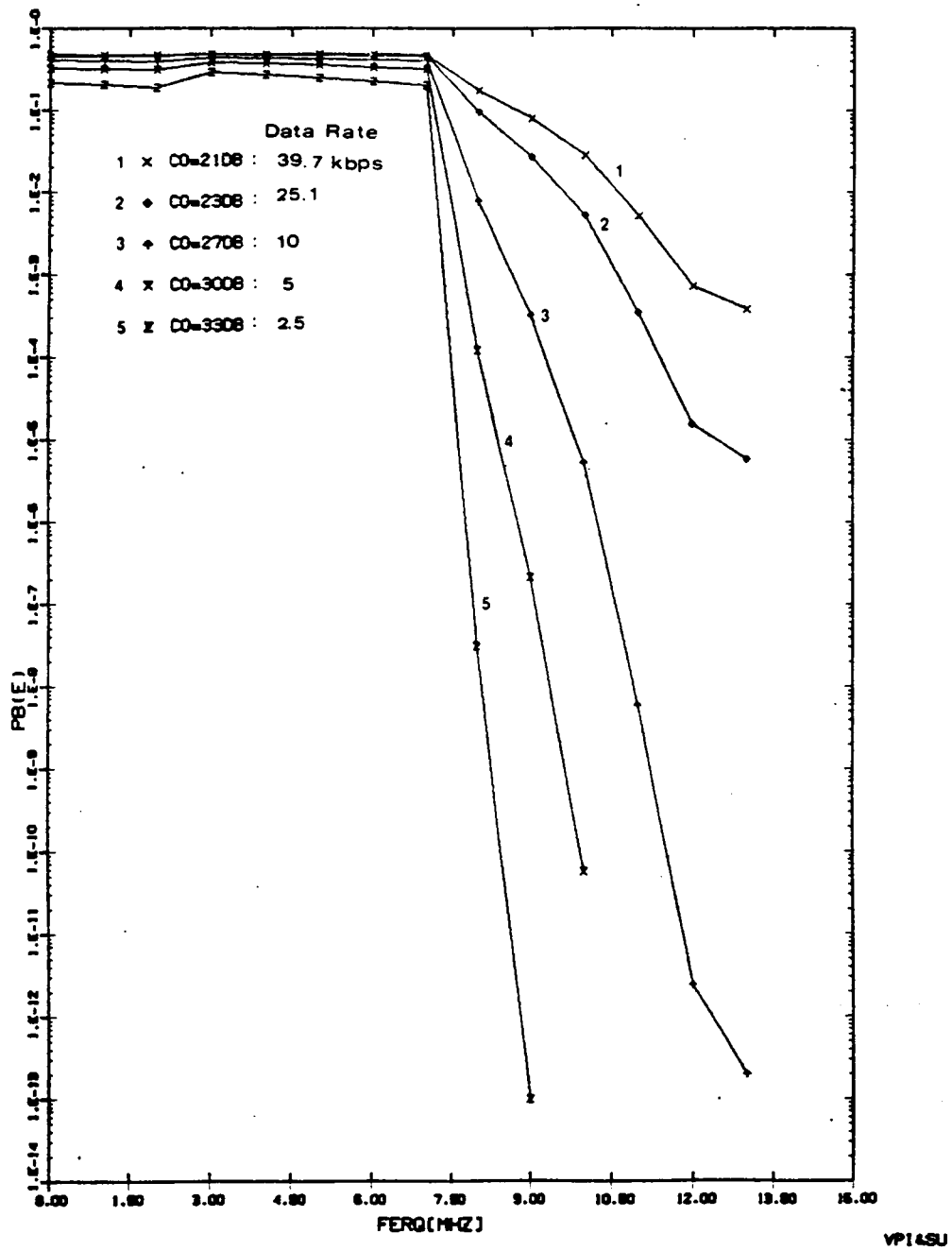

Figure 44. Offset(IF) frequency vs chip error rate for some compression gains

Table 4. C/I ratio vs IF offset for FM-TV spectrum[With Preemphasis] [m(t): 256 step random function and 200 step linear step function]

			256 step random		200 step linear	
Leading freq [MHz]	Trailing freq [MHz]	Offset freq [MHz]	5 MHz BW TV POWER [W]	C/I [dB]	5 MHz BW TV POWER [W]	C/I [dB]
2.5	-2.5	0.0	0.788	-34.5	1.001	-36.1
3.0	-2.0	0.5	0.788	-34.5	1.001	-36.1
3.5	-1.5	1.0	0.551	-33.4	0.752	-34.8
4.0	-1.0	1.5	0.523	-33.2	0.682	-34.4
4.5	-0.5	2.0	0.497	-33.0	0.605	-33.8
5.0	0.0	2.5	0.442	-32.5	0.511	-33.1
5.5	0.5	3.0	0.393	-32.0	0.417	-32.2
6.0	1.0	3.5	0.365	-31.6	0.339	-31.1
6.5	1.5	4.0	0.332	-31.2	0.266	-30.3
7.0	2.0	4.5	0.087	-25.4	0.011	-16.1
7.5	2.5	5.0	0.069	-24.5	0.007	-14.8
8.0	3.0	5.5	0.061	-23.9	0.005	-13.4
8.5	3.5	6.0	0.052	-23.1	0.005	-13.0
9.0	4.0	6.5	0.043	-22.3	0.003	-11.0
9.5	4.5	7.0	0.041	-22.1	0.001	-7.4
10.0	5.0	7.5	0.035	-21.5	0.0005	-3.5
10.5	5.5	8.0	0.033	-21.1	0.0003	-1.5
11.0	6.0	8.5	0.031	-20.9	0.0003	-1.5
11.5	6.5	9.0	0.028	-20.5	0.0004	-1.7
12.0	7.0	9.5	0.025	-20.1	0.0004	-1.7
12.5	7.5	10.0	0.024	-19.8	0.0003	-1.2
13.0	8.0	10.5	0.022	-19.4	0.0003	-1.2
13.5	8.5	11.0	0.021	-19.2	0.0002	-0.1

14.0	9.0	11.5	0.020	-19.2	0.0002	0.5
14.5	9.5	12.0	0.018	-18.6	----	----
15.0	10.0	12.5	0.018	-18.7	----	----
15.5	10.5	13.0	0.017	-18.2	----	----
16.0	11.0	13.5	0.015	-17.9	----	----

3.6. Summary

With the proposed coded multiple chirp spread spectrum system, the spread spectrum overlay service is studied. The FM-TV signal is selected as the overlaied signal because of its vulnerability to the chirp signal from the nature of FM demodulation process. From the analytic result for mutual interference between the chirp signal and FM-TV signal, it turns out that spread spectrum overlay is possible without causing any harmful interference if the chirp IF center frequency is properly offset from the FM-TV carrier. If this overlay scheme is applied to a VSAT network using C band satellites, data transmission of 2.5 kbps is possible with 300 mW transmitter when a 2.4 meter antenna is used.

IV. Review of Digital Modulation in LMSS Channels

4.1. Introduction

The proper selection of spectrally efficient modulation and fade resistant coding schemes has been an active area of research for the past few years in the Mobile Satellite Experiment (MSAT-X), the first phase of NASA's technology development program for LMSS. However, no final decision has been made about this selection even though there have been many proposals and much experimental data.

The reasons that account for this uncertainty are clear. Because this selection requires a knowledge of the LMSS channel characteristics, particularly propagation effects - without a thorough analysis of fading statistics and other propagation impairments, it is not easy to decide which digital modulation technique is most suitable for the LMSS channel. In addition, most of the fading statistics used in past studies were from artificial fades generated by analytic models that frequently did not account for the effects of vegetative shadowing, which is the most important but difficult to analyze factor in an LMSS channel. Hence, most of the results were valid only for special environmental conditions, or were unlike the practical implementation, and thus the process could not be generalized to find the most suitable digital modulation technique or effective coding scheme.

However, the study of modulation techniques can be improved and made more realistic if we use fading statistics obtained from an empirical data base rather than from artificial fade data. Among the recent trials to process empirical fading data, the propagation simulator developed in Virginia Tech [77] can furnish a reliable data base. With this powerful tool, it is now possible to get closer to the correct decision about modulation and coding schemes for an LMSS channel under fading conditions.

As was mentioned earlier in the Introduction, a tremendous amount of work has already been done to verify the causes and effects of fading in an LMSS channel because of its relative importance in MSAT-X. However, if we set the goal of the research as the performance evaluation of an LMSS channel through software simulation of an end to end test using digital modulation and coding, it is natural to be more concerned with the application of results obtained from propagation simulations, rather than with propagation effects. Therefore, a detailed discussion of propagation effects and their modeling was intentionally excluded from this thesis.

Based on this point of view, this chapter is devoted solely to the survey and review of possible candidates for a spectrally efficient digital modulation technique for the LMSS channel, where fading is the dominant factor in performance degradation. A brief explanation of the basic propagation mechanism of an LMSS signal under fading is included at the beginning. Coherent and noncoherent digital modulations are discussed initially, followed by an investigation of modulation and detection schemes for four modulation techniques: QPSK, MSK, DGMSK, and TCM 8-DPSK. In addition, some efficient coding techniques (channel encoding, differential encoding, and block interleaving) for a fading channel are also discussed, including the newly developed trellis code [92].

4.2. Land Mobile Satellite System under Fading

There are three major approaches to long distance digital communications: land line, satellite, and terrestrial radio. The last two methods transmit signals via a channel which exhibits time and/or frequency dependent variations in signal amplitude and phase. Such a channel is usually referred to as a "fading channel" [79].

The Land Mobile Satellite System using a geosynchronous satellite for voice and data transmission inevitably experiences fading effects in the satellite channel, which result in amplitude and phase distortion at the receiver. The inherent nature of a fading channel, in addition to its time varying characteristics, makes it more difficult to use conventional digital modulations and coding techniques that are usually suitable for stationary channels, simply because recovering the transmitted signal sometimes requires a totally different detection schemes.

It is well known from extensive studies [79] that, however complex and elaborate a digital modulation technique is, it will not achieve the minimum error probability without the use of a proper error correction code. Therefore trials to separate these two techniques and optimize each one never guarantees optimal performance of the system. The best way to determine the optimum digital signalling and coding under fading is simultaneous evaluation of the possible schemes, both in modulation and coding, under fading conditions. This might be the final goal of our research.

However, prior to the evaluation of possible modulation and coding, it is necessary to understand the propagation mechanisms and signal characteristics of a fading channel where our LMSS simulator is to operate. By doing this, we can get closer to the right decision criteria with a solid understanding of functional models under fading.

The major causes of fading can usually be classified into three categories: multipath, environmental changes, and relative motion. The most common cause is multipath. In multipath, the transmitted signal arrives at the receiver via more than one propagation path with relative differences in phase that are time or frequency varying. However, the receiver cannot discriminate between the

different signals and it adds them all up. Then the resultant signal is a modified version of the transmitted one with varying amplitude and phase. For the severe case of a large number of paths, the received signal frequently takes on a random variation.

Another cause of fading is due to ionosphere layer height and thickness variation [80]. As is usual in radio communication, sometimes the length of the transmission path varies depending on environmental conditions, and thus induces a variation of received signal amplitude and phase. The worst fact is that this effect usually occurs simultaneously with multipath.

The last common cause of fading is relative motion between the transmitter and the receiver. The relative motion causes misalignment of the vehicle antenna and thus results in a loss of antenna gain. It also induces Doppler shift. This effect sometimes causes the phase to change rather than causing envelope fluctuations of the signal.

Fading is relatively common in radio communication systems, not just in satellite channels. But here we will confine the discussion of fading effects and relevant topics to the the LMSS channel. A brief discussion of the composition of received signals in a mobile system is given first, followed by an explanation of the major parameters that may be necessary to evaluate the performance of a simulated system in the future, even though only the results from the fading (propagation) simulator are used in this research.

The propagation charecteristics of land mobile satellite systems are unique. Compared with other satellite systems and terrestrial mobile radio systems, the dominant cause of fading is shadowing, especially vegetative shadowing, rather than multipath and blockage effects even though multipath and blocking cannot be ignored [80].

Fig.45 shows the propagation environment of an LMSS channel for the unshadowed case with three major signal components. The mobile receiver is equipped with a smaller, less directive, low gain antenna compared with the large, directive high gain antenna in a fixed satellite earth station.

The electromagnetic rays collected by the mobile antenna can be classified into three components: a direct wave R_{dir}, a specularly ground reflected wave R_{spec}, and a diffusely reflected

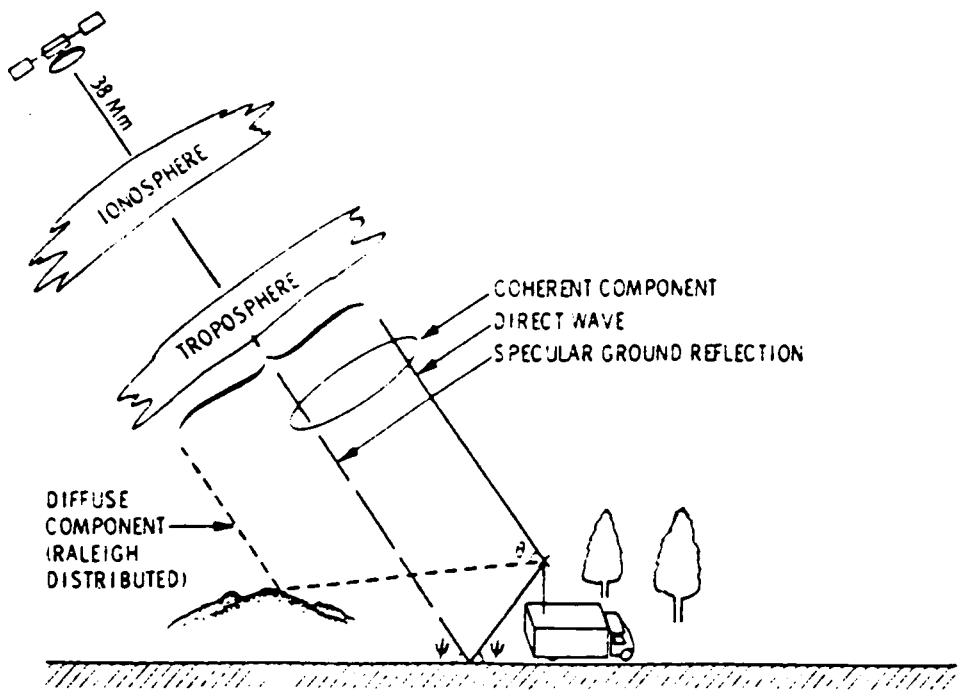

Figure 45. A physical representation of the LMSS channel showing the Direct(LOS), Specular, and Diffuse components for the unshadowed propagation case. From Vogel and Smith [112]

wave R_{diff}. In contrast to LMSS, conventional fixed satellite earth stations equipped with high gain antennas can completely reject the last two components and collect only the direct wave [75]. Before discussing the total received LMSS signal in various environmental conditions, it is necessary to examine these three individual components.

The direct wave is the line-of-sight (LOS) signal from the satellite and is mainly affected by shadowing obstacles on the terrain such as vegetation or man-made overpasses. Ionospheric and tropospheric effects have been found to be negligible at 1.5 GHz, although tropospheric absorption losses tend to be more severe with increasing frequency [81]. Therefore, shadowing is the major factor of significant attenuation, especially when LMSS is used in rural areas. Among the major causes of shadowing of the LOS, overpasses are not the object of this research, because of the complete loss of the LOS. However, the significant but partial loss of LOS under vegetative shadowing is not easy to analyze and is not yet completely verified and understood [80].

The specular component is a phase coherent ground reflected wave. It may cause deep fades in the received signal envelope if its amplitude is comparable to that of the direct component and its phase is reversed. This component is the result of radiation from points in the elliptically shaped first Fresnel zone of the scattering surface surrounding the mobile receiver. Because of the use of circularly polarized waves in LMSS, specular reflected waves tend to be elliptically polarized. Details of the magnitude and related antenna discrimination for specular waves can be found in [82],[83]. Based on the analysis by Butterworth [46], which included antenna effects, fade depths caused by specular components should be negligibly small in LMSS links with elevation angles above 20 degrees.

The diffuse component is a phase incoherent reflected wave representing the sum of all the scattered waves from the terrain around the mobile. Its magnitude is assumed to be Rayleigh distributed while its phase is uniformly distributed [80]. Interference of this component with the direct component causes rapid fading in the received signal. The degree of influence on the received signal mainly depends on the antenna pattern. When the antenna gain is rolled off below the horizon, the

contribution from this component can be small compared with the direct component. However, it cannot be ignored because of its Rayleigh distribution in magnitude.

With these three components, the input signal to the mobile receiver, R_{tot} , can be modeled as the vector sum of the two coherent components (direct wave and ground reflected specular wave) and incoherent diffuse component

$$\vec{R}_{tot} = \vec{R}_{dir} + \vec{R}_{spec} + \vec{R}_{diff} \tag{4.1}$$

However, the total input signal expressed in Eq.(4.1) can be simplified depending on the environmental conditions, such as unshadowed or vegetatively shadowed cases. The case of shadowing due to terrain blockage or man-made obstacles can be excluded from the consideration because of total loss of LOS, and this case is well understood already.

In the case of propagation for an unshadowed mobile, depicted in Fig.45, the input signal consists of the three components previously mentioned, and Eq.(4.1) can be used directly. There is no fading of the direct wave due to obstacles in this case, and atmospheric effects are negligible. In addition, the specular components can also be ignored as discussed before; then the total signal can be written as

$$\vec{R}_{tot} \simeq \vec{R}_{dir} + \vec{R}_{diff} \tag{4.2}$$

The total received signal at the mobile in the unshadowed case has a Rician distribution because the direct component is essentially constant relative to the fast varying diffuse component and the diffuse component is Rayleigh distributed in amplitude and uniformly distributed in phase [80],[81].

The scenario for vegetative shadowed mobile propagation is shown in Fig.46. Even though there is no final model for the vegetatively shadowed signal and study is still underway by JPL with field experiments [80], the method of vector summation used in the unshadowed case can still be applied.

The specular component and atmospheric effects on the direct wave are still negligible. However, there is fading of the direct wave due to the vegetation in the propagation path. Then the total signal is the same as in Eq.(4.2). In this case, the diffuse component has Rayleigh distributed [81] magnitude and uniformly distributed [81] phase as before. However, the direct component cannot be assumed to be constant. Instead, it is assumed to be lognormally distributed [81].

The distribution of the total received signal in this shadowed case is called a VS (vegetatively shadowed) distribution and details can be found in [84]. This total signal is the combination of a Rayleigh distributed diffuse component and the lognormally distributed direct component.

Until now, we have reviewed the basic propagation mechanisms of an LMSS signal under two typical environmental conditions, the unshadowed case and the shadowed case, and seen that the total input signal in these two cases takes different distributions in its amplitude and phase.

The major parts of the propagation study for LMSS have been developed in two steps. The first step was the verification and modeling of LMSS signal statistics under fading, called the 'primary statistics', in which the probability density function and cumulative distribution function of amplitude and phase of the received signal were found. Finding the 'secondary statistics' was the next step. These secondary statistics describe the dynamic, time varying characteristics of the received signal. The average fade duration (AFD) and interfade interval or level crossing rate (LCR) are important parameters. These parameters depend on the shadowing conditions, the mobile's speed, the relative direction of the source, and the antenna pattern.

The level crossing rate is the number of times the received signal envelope crosses the threshold with a positive slope in a given time period. An example of this is illustrated in Fig.47. In this example, there are three positive crossing (at points 1,2, and 3) in T seconds. In this case, the LCR, N(R) for the threshold level R is defined as

$$N(R) = \frac{3}{T} \tag{4.3}$$

The average fade duration is the average length of a fade for a given threshold. For the example in Fig.47, the AFD is the average D(R) of the three fades (T_1,T_2, and T_3).

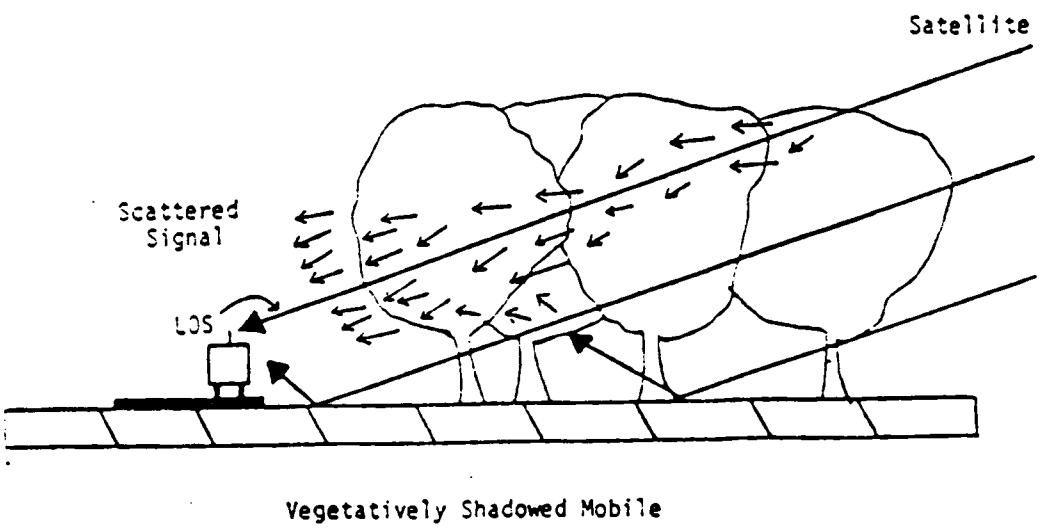

Figure 46. A physical representation of LMSS channel showing the Direct(LOS), Specular, and Diffuse components for vegetatively shadowed propagation case. From Smith [81].

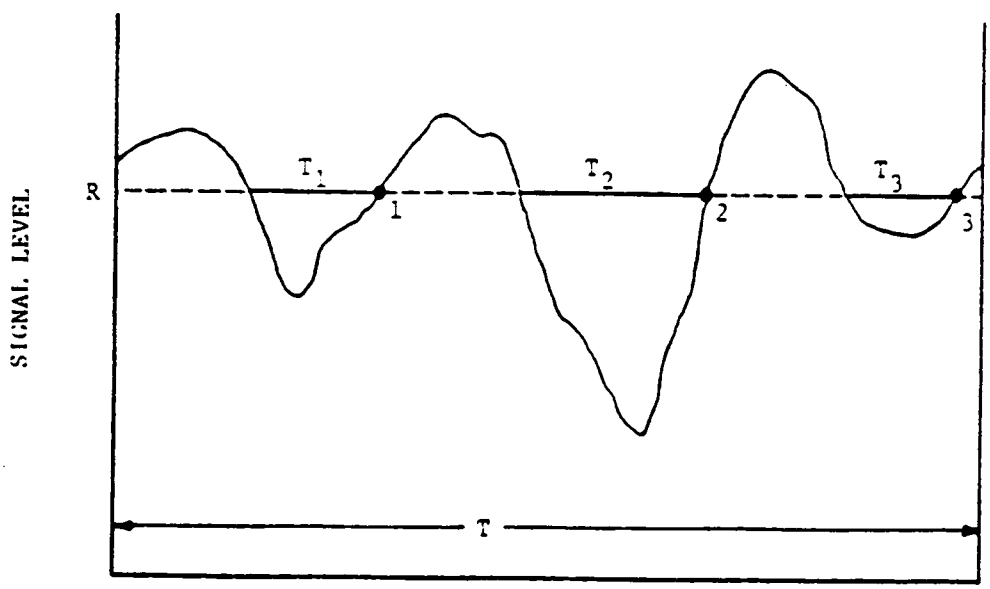

Figure 47. Definition of average fade duration(AFD) and level crossing rate(LCR). From Bradley and Stutzman [113]

$$D(R) = \frac{T_1 + T_2 + T_3}{3} \tag{4.4}$$

Thus far, we have briefly reviewed the fading mechanisms of the received signal and the major parameters in an LMSS channel. All of them were the results of propagation studies and modeling of received signal by experiments or simulation. As mentioned earlier, the Virgina Tech propagation simulator can simulate and generate the fading signal depending on the desired environmental conditions, based on an empirical data base. Therefore, we can use the output of this simulator for the LMSS channel simulation to find the best feasible digital modulation and coding schemes by performance evaluation in terms of error rate. We need to use the diverse fading statistics that can represent various mobile conditions, along with key parameters such as AFD or LCR. Once these data are given to the channel simulator, it is possible to investigate link performance using different modulation techniques and coding schemes, and thereby determine which modulation and coding schemes are most suitable for different fading conditions.

4.3. Digital Modulations in LMSS

4.3.1. General Requirements for Digital Modulations

Of many digital modulation techniques, only a handful are desirable for satellite communications, mainly because nonlinearity in the satellite TWTA requires a constant envelope, bandwidth efficient modulation. The desire to facilitate speech communication as well as high-speed data transmission using the land mobile system, where fading is the dominant factor of performance

degradation rather than nonlinearity, imposes other requirements such as resistance to multipath fading and adjacent channel protection. Even though there are some variations depending on whether data transmission or digital voice transmission is required, the general requirements for digital modulation in an LMSS can be written as follows: [85],[86]

1. Compact output power spectrum. (The output power spectrum must be severely restricted to suppress the out-of-band radiation power below 60 to 80 dB in an adjacent channel.)

2. Constant envelope. (To avoid periodic burst errors caused by deep fades in the envelope and fast phase transitions in a fading channel, a class C linear high power amplifier is usually employed. Modem schemes must be suitable for this amplifier.)

3. Good error performance. (Under inferior conditions of noise, interference, and fading, reasonable bit/symbol error rates must be maintained.)

4. Simple implementation. (To maintain low cost of the mobile terminal, and small size for portability.)

Among these particular requirements, priority must be given to the first two items in selecting digital modulation techniques, because of their relative importance to the others. In addition, the last two requirements are obvious from the engineering aspects.

4.3.2. General Investigation of Some Candidate Modulations

As a first step to finding the best modulation schemes, several kinds of bandwidth efficient modulation with constant envelope were investigated. However, a little caution must be taken in selecting suitable ones. Because the use of LMSS also includes digital voice transmission, not just

data transmission, the selected modem must be compatible with any modem used only for data transmission, and should be able to provide highly secure voice transmission simultaneously.

From this point of view, narrow-band digital FM (NBFM) signaling such as Tamed FM (TFM) and Gaussian baseband filtered Minimum Shift Keying (DGMSK) have recently been reported to be applicable to LMSS [87]. This type of digital FM has exactly the same features as the general requirements. However, the digital modulations traditionally used like Quaternary Phase Shift Keying (QPSK) and Minimum Shift Keying (MSK) were strong candidates in the preliminary tests performed by JPL [75] and are still widely used in satellite communications because of their constant envelope and spectral efficiency. In addition to these techniques, attempts to combine modulation and coding has revealed that the so called trellis coded modulation (TCM) with 8 or 16 PSK can also be a good choice for a LMSS channel. Most of the recent work in the 1980's on digital modulations in LMSS have been concentrated on those techniques mentioned above [88],[89]. In this section, the advantages and disadvantages of these techniques are investigated with a brief discussion of their signaling schemes.

Modulation techniques that have discontinuous phase such as Binary Phase Shift Keying (BPSK) and Quarternary PSK (QPSK) (compared with the continuous phase schemes such as MSK) have been widely used and still are used in satellite communications because of their constant envelope property and spectral efficiency. However, these techniques have the common disadvantages of abrupt phase transitions between bits or symbols, compared with the continuous phase type modulations. Especially in a fading channel like the LMSS channel, the time varying phase distortion of the signal as well as envelope fluctuation makes it difficult to detect signal phase when conventional detection schemes are used.

To avoid the abrupt phase changes in QPSK and BPSK, the class of digital FM techniques known as continuous phase frequency shift keying (CPFSK) has been studied and considered for use in LMSS. The special case of CPFSK with a frequency deviation $f_d = 0.5$ is called MSK. Although MSK

is not the most bandwidth efficient of its class (or compared with QPSK), the constant envelope characteristics and continuous phase property can be traded off with its excess bandwidth property. However, the desire to achieve more spectrally compact modulation property of MSK, while keeping the constant envelope and continuous phase, has led to the appearance of generalized MSK type signaling such as TFM and Gaussian MSK.

In generalized MSK, initial trials have been done to replace the half sinusoidal pulse shaping ($\cos\frac{\pi}{T_s}t$) function of MSK with a more generalized function of the form ($\cos(\frac{\pi}{T_s}t)\,g(t)$) that can be controlled to get a sharper and narrower spectrum. By proper choice of the function, it was shown that a so called 'MSK type signal' that met all the desired requirements could be generated [90],[91]. However, this method was not easy to implement and complex optimization procedures are needed to get parameter values for g(t) [90].

As an alternative approach in generalized MSK, phase smoothing techniques such as premodulation lowpass filtering or postmodulation PLL (Phase Locked Loop) circuits were also proposed to reduce spectral occupancy [90]. One of the results was TFM. In TFM, the premodulation lowpass filter coefficients were optimized using specific functions such as a Nyquist filter or a Gaussian filter. However, these techniques need relatively complicated adjustment of filter parameters (usually transversal filters) which depend on the system design.

Gaussian MSK (DGMSK) is the another version of this class of modulation, in which spectral shaping is done by a simple Gaussian lowpass filter that has the same performance as the delay line filters used in TFM. However, implementation of DGMSK is much simpler than TFM and performance is known to be better than TFM in a fading environment. In DGMSK, phase information is obtained from the convolution integral of the input NRZ data stream and a Gaussian impulse response. Compared with conventional MSK, the weighting function used in waveform shaping in DGMSK to produce a compact spectrum is no longer a constant. (Note. In MSK, g(t) in the waveform function is 1, while g(t) is a Marcum Q function in DGMSK) Even though the addition of a Gaussian filter is required in DGMSK, the spectral shape of DGMSK can be narrower and decays faster than in conventional MSK. This spectral shape can be adjusted more easily than in TFM [88], [89].

Trellis Coded Modulation (TCM), invented by Ungerboeck [92] in 1976, is unique and totally different from previously discussed digital modulation techniques in that this scheme does not separate modulation and coding. Additional coding gain can be directly obtained from the set partitioning and signal phase mapping in PSK applications if an optimized trellis code is used [92]. Modulation schemes that are optimal in given conditions are usually selected independently, without considering the coding schemes. A repetitive process of optimization is needed to find the best combination of modulation and coding, and this approach frequently deviates from the most satisfactory result in practical conditions. From this point of view, TCM is revolutionary. Even though much effort and analysis are needed for selection of an optimal trellis code, this method can achieve additional performance gain over conventional modulation techniques without bandwidth expansion. (In conventional systems using coding, bandwidth is expanded as many times as the reciprocal of the code rate.) Details of this topic will follow in the next section.

Apart from the classification of modulation schemes depending on the signaling method used, modulation schemes can be implemented in different ways depending on the environmental conditions by using coherent or noncoherent detection. In conventional digital communication, to achieve good power efficiency in terms of error rate performance, coherent detection has been preferred, especially when detection schemes are relatively simple as in QPSK or in conventional MSK. In this case, carrier recovery is essential and the performance of the system frequently depends on the performance of this function. However, in land mobile communication operating in the VHF band, UHF band, or in L band, signal levels at the input of the receiver can fluctuate significantly due to the rapidly varying Rayleigh multipath fading. Fast acquisition of the reference carrier is very difficult because of phase ambiguity, especially when a Costas loop or squaring device is used to provide the carrier reference phase, as is usual in coherent detection schemes [86].

In order to circumvent the difficulties associated with carrier recovery, noncoherent detection is frequently used. Although its static bit error rate performance in nonfading or quasi-static fading conditions is inferior to that of coherent detection because of inter-symbol interference (ISI) effects,

the dynamic behavior in fast varying multipath fading conditions is superior to that of coherent detection [86],[88].

Two kinds of noncoherent detection schemes can be used, differential detection and frequency discrimination. Differential detection is the preferred technique, in which the reference carrier can be recovered by using simple delay lines. Frequency discrimination is normally used in the detection of TFM signals only.

Among the two noncoherent detection schemes, only the differential detection scheme is considered appropriate for our objectives of computer simulation. The other method is more suitable for hardware implementation because of its complexity. In addition, frequency discrimination is not generally useful for other than TFM signals.

Thus far, some possible candidates for the selection of digital modulation schemes have been briefly investigated, based on their signaling methods and detection schemes. Almost all of the possible modulation techniques presented in relevant papers were considered. However, it is still not easy to decide which one is most suitable because we should consider the possibility of trade-offs in every aspect of engineering. There can be many other factors that affects this decision. However, based on the general trend available in relevant papers and the investigation we have done, the following intermediate conculsions can be drawn.

- Trellis coded modulation with 8-PSK is regarded as the most suitable digital modulation scheme in a land mobile satellite channel because of its compactness of implementation by combining modulation and coding.

- Gaussian MSK (DGMSK) is also a good candidate because of its relative flexibility in adjusting spectral occupancy of the signal.

- QPSK and MSK are also candidates because of easy implementation and compatibility with existing satellite facilities.

- Noncoherent detection is preferred to coherent detection in continuous phase modulation schemes.

Four modulation techniques were selected for computer modeling and simulation based on the above intermediate conclusions. For coherent modulation, QPSK and MSK were selected because of QPSK's dominant use in satellite communication, as well as its spectral efficiency in a band limited channel, and MSK's typical continuous phase property.

For noncoherent detection, TCM 8-PSK with one-bit differential detection was chosen because of its promising performance in a fading channel, as well as being the first practical implementation of the idea of combining modulation and coding. As the second candidate of a noncoherent scheme, DGMSK with one-bit differential detection was also considered because of its unique use of a spectral shaping function such as a Gaussian lowpass filter.

In the next few sections, these modulation and demodulation schemes are briefly reviewed, with an explanation of conventional differential detection.

4.3.3. Coherent Modulations : QPSK and MSK

As the first trial to find suitable digital modulations using coherent detection, QPSK and MSK were selected. QPSK and MSK are frequently used in satellite communication because of their relatively simple structure and reasonable error performance. The two schemes have the common property of constant envelope and good spectral efficiency, even though MSK is a little inferior to QPSK because of its wider spectral occupancy. However, contrary to the abrupt phase changes of QPSK between the four possible symbols, MSK maintains phase continuity even in symbol transitions.

Although there have been some trials to implement QPSK and MSK with noncoherent detection [93], especially MSK, QPSK and MSK are mostly used with coherent detection these days. In this section, two coherent modem schemes are briefly reviewed based on their block diagrams.

QPSK (Quaternary Phase Shift Keying)

QPSK is a digital phase modulation technique where the information of the digital signal is transmitted in the phase of the modulated carrier. The phase of the carrier can take on one of four possible values during each signaling interval. The modulated QPSK signal is represented by

$$S_{QPSK}(t) = A\ \cos(\omega_c t + \phi_k)\ ,\quad 0 < t < T_s\ , \tag{4.5}$$

where

A: carrier amplitude

ω_c: carrier radian frequency

ϕ_k: $= k\pi/4$ for $k = 1, 3, 5, 7$

T_s: symbol duration.

If we expand Eq.(4.5) using trigonometric identities, we can get another form of QPSK signal represented by

$$\begin{aligned} S_{QPSK}(t) &= (A\ \cos\phi_k)\ \cos\omega_c t - (A\ \sin\phi_k)\ \sin\omega_c t \\ &= \pm\frac{A}{\sqrt{2}}\cos\omega_c t \pm \frac{A}{\sqrt{2}}\sin\omega_c t\ ,\quad 0 < t < T_s\ . \end{aligned} \tag{4.6}$$

In Eq.(4.6), the first and the second terms are both BPSK signals. The first term is a BPSK signal in phase with the carrier, whereas the second term is a BPSK signal in quadrature with the carrier. Therefore, if we combine two BPSK signals in phase quadrature, a QPSK signal can be generated. For notational convenience, we call the first term the I (in-phase) channel and the second the Q (quadrature phase) channel. When the binary symbol 1 (or +1 in NRZ form) represents $\frac{+1}{\sqrt{2}}$ volt and the binary symbol 0 (or -1 in NRZ form) represents $\frac{-1}{\sqrt{2}}$ volt, we can say that the unique dibits(pairs of bits) (1,0), (0,0), (0,1) and (1,1) generate the four possible QPSK phases $\frac{\pi}{4}$, $\frac{3\pi}{4}$, $\frac{5\pi}{4}$, and $\frac{7\pi}{4}$ respectively.

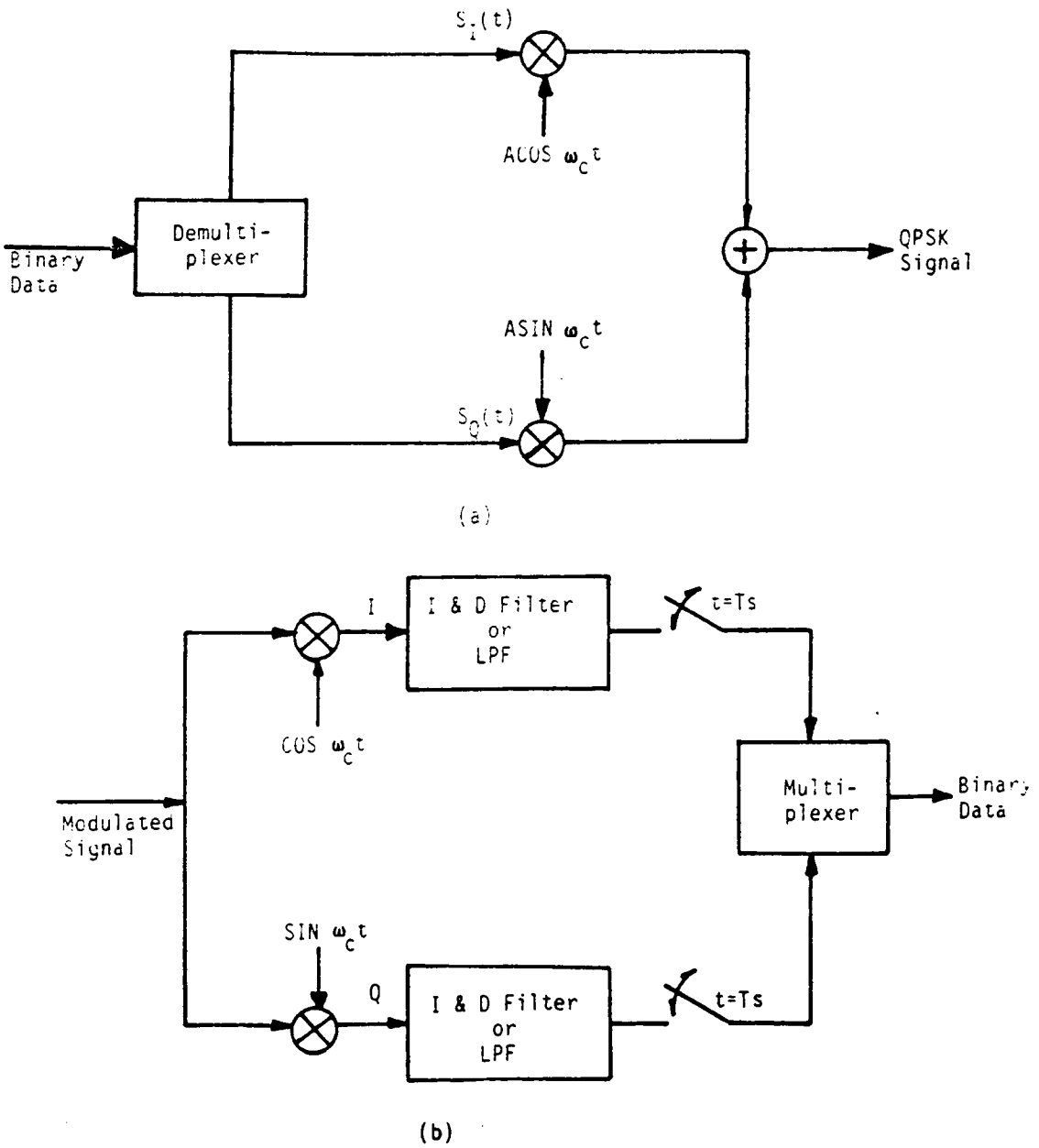

Figure 48. QPSK (a) modulator (b) demodulator

QPSK Modulator

Fig.48 (a) shows the block diagram of a QPSK modulator, which consists of a demultiplexer (also called a serial to parallel converter), a pair of carrier multipliers or mixers, and a summer. When the incoming NRZ data stream with bit rate R_b bits per second (bps) is applied to the modulator, the demultiplexer divides the incoming data stream into an odd bits stream and an even bits stream. Usually the odd bits stream is represented as $S_I(t)$ and the even bits stream is represented as $S_Q(t)$.

To achieve the bandwidth efficiency of 2 bps/Hz, the signaling interval (also called symbol duration T_s) is made twice as long as the bit duration T_b of the incoming data stream. Then the odd bit stream modulates the in phase carrier generating the I-channel BPSK signal and the even bit stream modulates the 90 degree phase shifted carrier, thus generating the Q-channel BPSK signal. Finally I-channel and Q-channel signals are summed to form the QPSK signal. Because the two input data streams are synchronously aligned such that their transitions coincide, the phase shift in QPSK will occur after one symbol duration,T_s.

In QPSK, a phase shift occurs only when one or both bit streams change bits in one symbol duration. Therefore, if both channel data streams change their data, a 180 degree phase shift occurs, whereas a 90 degree phase shift occurs when only one channel data stream changes its data. When there are no changes in both channel data streams, no phase shift occurs. The sign of the phase change depends on which channel has changed its data in one symbol duration compared with the previous state.

QPSK Demodulator

In general, a QPSK signal can be demodulated using a coherent demodulation technique if a phase reference is available. Because the QPSK signal is the sum of two BPSK signals in phase quadrature, the typical QPSK demodulator contains two BPSK demodulators. Fig.48.(b) shows the QPSK demodulator, which consists of two binary correlators connected in parallel, a pair of samplers,

and a multiplexer. The correlator itself consists of a carrier multiplier or mixer and an integrate-and-dump (I & D) circuit. The symbol timing recovery and carrier recovery parts are excluded from the diagram because we have assumed perfect symbol timing and carrier recovery in the simulation for simplicity. The in-phase correlator computes the cosine of the carrier phase, while the quadrature correlator computes the sine of the carrier phase. Under noise-free conditions, the input signal m(t) to the QPSK demodulator is represented by

$$m(t) = A\ \cos(\omega_c t + \phi_k)\ . \tag{4.7}$$

After carrier multiplication, the I-channel component can be expressed as

$$\begin{aligned} m_{I1}(t) &= A\ \cos(\omega_c t + \phi_k)\ \cos(\omega_c t) \\ &= \frac{A}{2}\left[\cos\phi_k + \cos(2\omega_c t + \phi_k)\right] \end{aligned} \tag{4.8}$$

and the Q-channel component is written as

$$\begin{aligned} m_{Q1}(t) &= A\ \cos(\omega_c t + \phi_k)\ \sin(\omega_c t) \\ &= \frac{A}{2}\left[-\sin\phi_k + \sin(2\omega_c t + \phi_k)\right] \end{aligned} \tag{4.9}$$

These two components are passed through the I&D filters which eliminate the second harmonics, and then are sampled at the symbol rate R_s. Immediately after sampling, the integrators are instantaneously discharged. The signs of the time sampled integrator outputs uniquely decide which phase angle was transmitted. The integrators are usually replaced by lowpass filters (LPF) in high speed modems (modulator and demodulator) where the input bit rate is more than 10 Mbps. The filtered I-channel signal and the filtered Q-channel signal are the baseband signals. The two baseband signals are then passed through threshold detectors. For each channel, if the signal is positive, a binary symbol 1 is assumed to have been transmitted, whereas a binary symbol 0 is assumed to have been transmitted if the detected signal is negative. Finally, these two binary sequences from the I and the Q channels are combined in a multiplexer to restore the originally transmitted binary input data sequence.

MSK (Minimum Shift Keying)

The desire to achieve maximum spectral efficiency in digital modulation for wideband satellite channels inevitably leads to the modulation scheme which maximizes the bandwidth efficiency and minimizes the spectral components which fall outside the Nyquist bandwidth. In QPSK, the theoretical bandwidth efficiency is 2 bps/Hz and the power spectral density falls off with a rate proportional to the square of frequency. In CPFSK (Continuous Phase Frequency Shift Keying) where the phase of the FSK signal is used to decrease the out of band spectral components, the power spectral density falls off at a rate proportional to the fourth power of frequency. By proper control of phase, CPFSK maintains the same bandwidth efficiency as QPSK [94].

The typical form of a CPFSK signal is

$$S(t) = A\ \cos[\omega_c t + \phi(t)]\ , \tag{4.10}$$

where $\phi(t)$ is no longer constant as in QPSK. Let the radian frequencies ω_1 , and ω_2 represent the binary symbol 0 and 1 respectively, and the carrier radian frequency ω_c is chosen to be $\frac{\omega_1 + \omega_2}{2}$. In addition, if the radian frequency deviation $\Delta\omega$ is chosen to be $\frac{\omega_2 - \omega_1}{2}$, then the phase function $\phi(t)$ with respect to carrier frequency in one bit interval can be expressed as

$$\phi(t) = \pm \Delta\omega\, t + \phi(0)\ ,\quad 0 < t < T\ , \tag{4.11}$$

where $\phi(0)$ is the initial phase needed to maintain the phase continuity and depends on the past history of the modulation process. To achieve orthogonal frequency shift keying, the frequency separation in the bit interval $(0\ ,\ T_b)$ must be chosen to satisfy the condition $2\Delta\omega T_b = n\pi$. Therefore the minimum frequency separation requires $n = 1$, hence

$$\Delta\omega = \frac{\pi}{2T_b}\ . \tag{4.12}$$

This particular choice of CPFSK is called MSK (Minimum Shift Keying). Thus MSK is CPFSK with a frequency separation equal to the one half of the bit rate. Therefore the expression of the phase function in Eq.(4.11) can be written as

$$\phi(t) = \pm \frac{\pi}{2T_b} t + \phi(0) \ , \quad 0 < t < T_b \ . \tag{4.13}$$

The phase function $\phi(t)$ in Eq.(4.13) is confined to one bit interval T_b. To see the phase variation with time t over one bit interval, let's assume $\phi(0) = 0$. Then it can easily be seen that $\phi(t)$ takes only the two values $\frac{\pm \pi}{2}$ at odd multiples of T_b, and only the two values 0, π at even multiples of T_b. Therefore the phase variation over each bit duration is $\frac{\pm \pi}{2}$. By defining b_k as a binary switching function taking the value of ± 1 only for k = 1,2,.. and ϕ_k ($= \phi[(k-1)T_b]$) as excess phase at the beginning of k th bit interval to maintain a continuous waveform, we can write the phase function $\phi(t)$ over more than one bit duration as

$$\phi(t) = b_k \frac{\pi t}{2T_b} + \phi_k \ . \tag{4.14}$$

In addition, from the fact that $\phi(t)$ varies only $\frac{\pm \pi}{2}$ in one bit interval, the recursive phase constraint can be obtained as

$$\phi_k = \phi_{k-1} + b_k \frac{\pi}{2} \ . \tag{4.15}$$

Therefore, substituting Eq.(4.14) into Eq.(4.10) yields the MSK signal in CPFSK form over more than one bit interval

$$S_{MSK}(t) = A \cos[\omega_c t + b_k \frac{\pi}{2T_b} t + \phi_k] \ . \tag{4.16}$$

If we expand Eq.(4.16) using trigonometric identities, it can be expressed in terms of in-phase and quadrature components as

$$S_{MSK}(t) = A\left[\cos\left(\frac{\pi t}{2T_b} b_k + \phi_k\right)\cos(\omega_c t) - \sin\left(\frac{\pi t}{2T_b} b_k + \phi_k\right)\sin(\omega_c t)\right]. \quad (4.17)$$

If we assign even numbered data pairs of the input binary data stream to the in-phase components and odd numbered data pairs to the quadrature components, the excess phase ϕ_k will always increase by 0 or π (modulo 2π) for the successive values of input data, and the phase difference between components will be $\frac{\pm\pi}{2}$ by the phase constraint in Eq.(4.15). This phase difference can be taken care of by applying a relative time delay of T_b between the in-phase and quadrature components as is used in staggered QPSK [95]. If Eq.(4.17) is expanded further using trigonometric identities and the fact that $\sin\phi_k = 0$ for both the in-phase and the quadrature components, we get

$$S_{MSK}(t) = A\left[\cos\phi_k \cos\frac{\pi t}{2T_b} \cos\omega_c t - b_k \cos\phi_k \sin\frac{\pi t}{2T_b} \sin\omega_c t\right]. \quad (4.18)$$

The term $\cos\phi_k$ and $b_k\cos\phi_k$ in Eq.(4.18) can be considered as two quadrature data channels of staggered QPSK. Then we can finally express the MSK signal obtained from staggered QPSK as

$$S_{MSK}(t) = A\left[S_I(t) \cos\frac{\pi t}{2T_b} \cos\omega_c t - S_Q(t) \sin\frac{\pi t}{2T_b} \sin\omega_c t\right]. \quad (4.19)$$

where $S_I(t)$ and $S_Q(t)$ represent the I channel or Q channel bit streams respectively. Therefore we can conclude that MSK is either a special case of staggered QPSK with cosine pulse shaping or a special case of CPFSK with the frequency separation of half of the incoming bit rate.

MSK Modulator

The fact that MSK can be regarded either as a special case of staggered QPSK with a half sinusoidal pulse shape rather than rectangular pulse shape or as a particular case of CPFSK with a frequency spacing equal to the one half of the bit rate provides two different modulation schemes. Fig.49.(a) represents the MSK modulator considered as staggered QPSK with half sinusoidal pulse

shaping. The MSK modulator is analogous to that of QPSK except for the offset delay and the cosine pulse shaper. Therefore, by demultiplexing the input data stream, the odd bit stream and the even bit stream are generated. Then, the odd bit stream $S_I(t)$ is multiplied with a half-sinusoidal pulse $\cos(\frac{\pi t}{2T_b})$ while the even bit stream $S_Q(t)$ is delayed by one bit and multiplied by a half-sinusoidal pulse $\sin(\frac{\pi t}{2T_b})$. These sinusoidally shaped bit streams are then multiplied by the orthogonal carriers and the resulting signals of the I-channel and the Q-channel are subtracted to yield the MSK siganal expressed in Eq.(4.19).

MSK Demodulator

Fig.49 (b) shows the MSK demodulator. The matched receiver for a distortionless channel consists of two correlators followed by an integrator. Assuming no noise and no ISI (Inter-Symbol Interference) , the input MSK signal is

$$Y(t) = S_I(t)\ \cos\frac{\pi t}{2T_b}\ \cos\omega_c t - S_Q(t)\ \sin\frac{\pi t}{2T_b}\ \sin\omega_c t\ . \tag{4.20}$$

Then after the integration operation, the integrator output is

$$Y_I(t) = \int_{(2k-1)T_b}^{(2k+1)T_b} Y(t)\ \cos\frac{\pi t}{2T_b}\ \cos\omega_c t\, dt\ . \tag{4.21}$$

$$Y_Q(t) = \int_{(2k)T_b}^{(2k+2)T_b} Y(t)\ \sin\frac{\pi t}{2T_b}\ \sin\omega_c t\, dt\ . \tag{4.22}$$

When these outputs are sampled at even or odd integer of a bit duration, the sign of the sampler output decides the binary state of $S_I(t)$ or $S_Q(t)$. Then, by passing the sampler output through a decision threshold device and multiplexing, the desired transmitted data stream can be obtained.

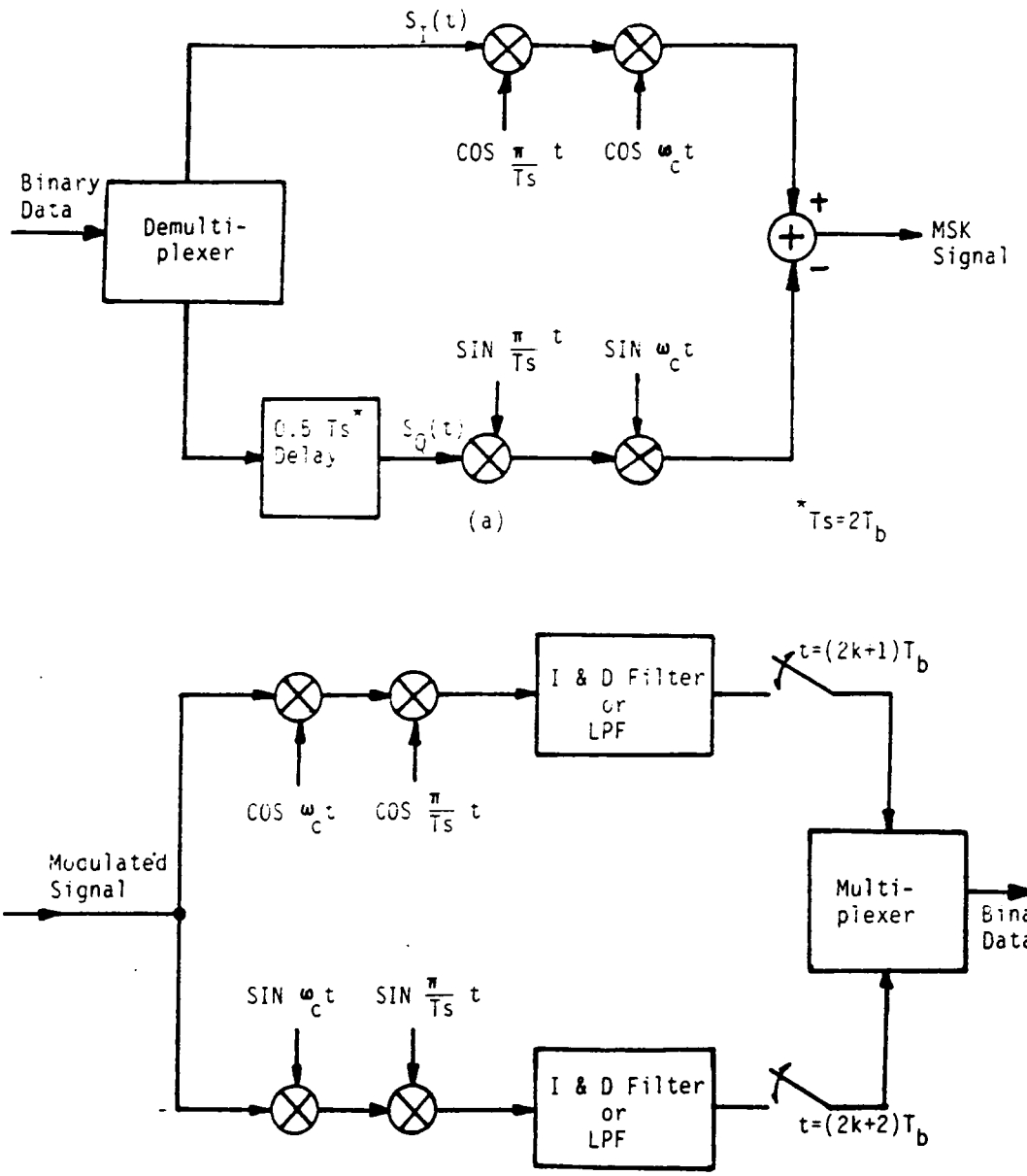

Figure 49. Coherent MSK (a) Modulator (b) demodulator

4.3.4. Principle of Differential Encoding/Decoding

The implementation of noncoherent detection in digital modulations is frequently achieved by using the method of differential detection, because of its simplicity. In this section, the principle of this scheme is briefly reviewed.

Differential encoding and decoding is simple in principle. Assume that there is a serial bit stream to transmit. In the encoder, each bit in the encoded sequence is obtained by comparing the present input bit and the previous encoded bit depending on the given encoding rule. This rule can be set arbitrarily for convenience. However, for binary data encoding, Mod-2 addition (or exclusive OR) is used. In this rule, a binary 0 is assigned as the encoder output if the present input bit and the previous encoded bit are of opposite state, and a binary 1 is assigned if these states are the same. A beginning reference bit (either 0 or 1) is needed for initial encoder output. At the decoder, the encoded data is decoded by comparing the state of adjacent bits using the same rule used in the encoder. The same reference bit must be used for decoding for correct recovery of the original data.

Although this principle of differential encoding and decoding is generally kept, there are some variations depending on the practical form of transmission.

Practical Implementation of Differential Encoder/Decoder

The usual implementation of a differential encoder and decoder is by using delay lines or corresponding logic. The number of delay elements used is denoted by mT (where T is the bit duration). In general, 'm' denotes the the number of delay units in the differential detector rather than in the encoder. This is because when m delay units are used in the detector, m-1 delay elements are needed in the encoder [89],[96].

The number 'm' has a more complicated meaning than just the number of delay units. 'm' also means the number of bits used for the decision of the received state. Therefore, if m = 1, the decision

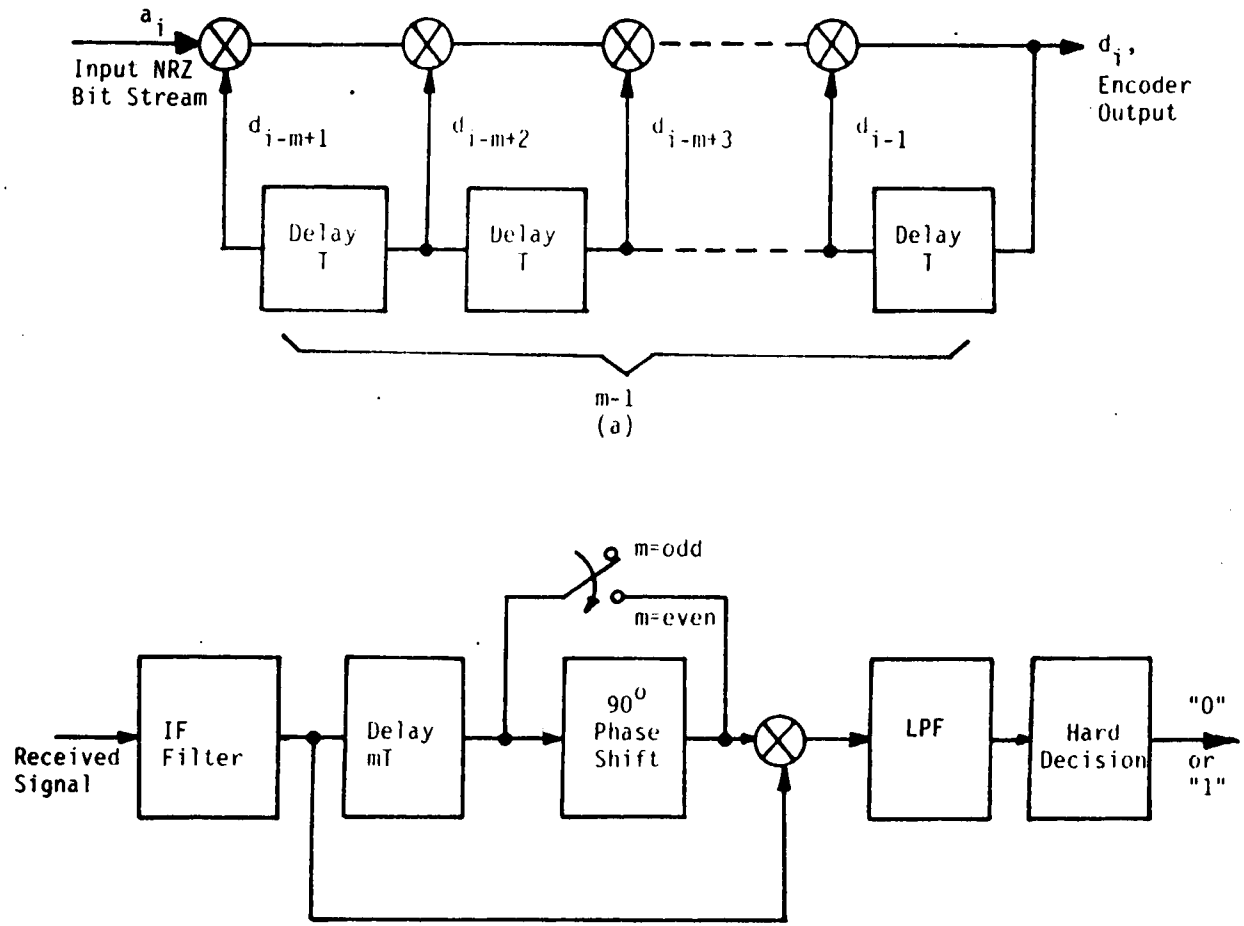

Figure 50. General form of m-bit differential (a) encoder and (b) decoder

of received bit is made based on one bit duration. Therefore, as 'm' increases, the detection capability gets enhanced because of the longer observation time of received data. However, $m > 2$ is not usually used because of system complexity and difficulties in error detection.

Fig.50 shows the general form of a m-bit differential encoder and decoder. As was stated before, the differential encoding operation is needed only for the case $m > 1$ in order to make a hard decision on the m-bit differential detector output. Therefore, for 1-bit differential detection, the effective transmitted bit stream received at the decoder and encoder output is the actual input bit stream itself. In the decoder of Fig.50, it is shown that for m odd, the 90 degree phase shifter is required in the delayed arm whereas, for m even, it is not. In effect, this is equivalent to saying that, for m even, the multiplier output represents the cosine of the change of the received signal over m bit periods while for m odd, this same output represents the sine of this phase change as was the case for $m = 1$. Detailed mathematical verification can be found in [88],[102].

As was mentioned earlier in this section, there are some variants in differential detection techniques depending upon the application. In the case of M-ary PSK, differential encoding and decoding (or detection) are usually done for each symbol, not for each bit.

Hence, in M-ary PSK (MPSK) modulation, a given data symbol phase is sent as the difference of the two adjacent symbol phases. If X(k) represents the symbol to be transmitted at time k (before differential encoding), and $X_T(k)$ represents the symbol actually transmitted at time k, then the differential encoding process for M-ary PSK can be represented as $X_T(k) = (X(k) + X_T(k-1)) \bmod M$. In the detection process, the phase difference between two adjacent symbols is recovered by using the same method. In this case, the previous phase is always used as the phase reference. Detailed procedures and explanation will be presented in the section about modeling of 8-DPSK in the next chapter.

4.3.5. Noncoherent Modulations : DGMSK and TCM 8-DPSK

As the second trial to find a suitable modulation scheme in a LMSS, noncoherent versions of Gaussian MSK and Trellis Coded Modulation 8-PSK using differential detection were selected for investigation. These two schemes were already under consideration in the current MSAT-X system [75],[88]. In this section, the basic configuration of these two promising schemes is briefly investigated, based on the previously discussed differential encoding/decoding principle.

Differential GMSK (Gaussian Minimum Shift Keying)

Gaussian MSK and Tamed FM(TFM) have drawn considerable attention recently because they satisfy the stringent out-of-band radiated power requirements of a mobile radio application. However, Gaussian MSK has been thought easier to implement, because simple addition of a Gaussian filter prior to the MSK modulator can easily shape the transmitted RF spectrum as desired. Although coherent and differentially coherent detection schemes have been described in the open literature, we have confined our investigation to the latter detection schemes because of simplicity. Even though 2-bit differential detection schemes have been proposed [102], most of the current applications concentrate on the 1-bit case. Therefore, our discussion is also confined to the 1-bit case as much as possible. For notational convenience, we denotes this modulation scheme as DGMSK.

The transmitter and receiver of DGMSK with 1-bit and 2-bit differential detection is depicted in Fig.51. The transmission part consists of a 1-bit differential encoder (exists only when 2-bit differential detection scheme is employed in the receiver), a Gaussian premodulation baseband filter (lowpass filter), and a conventional FM modulator with modulation index 0.5 [88]. The Gaussian filter is used to shape the spectrum of the incoming binary NRZ pulses so as to a produce constant envelope RF output and to suppress the out-of-band spurious power.

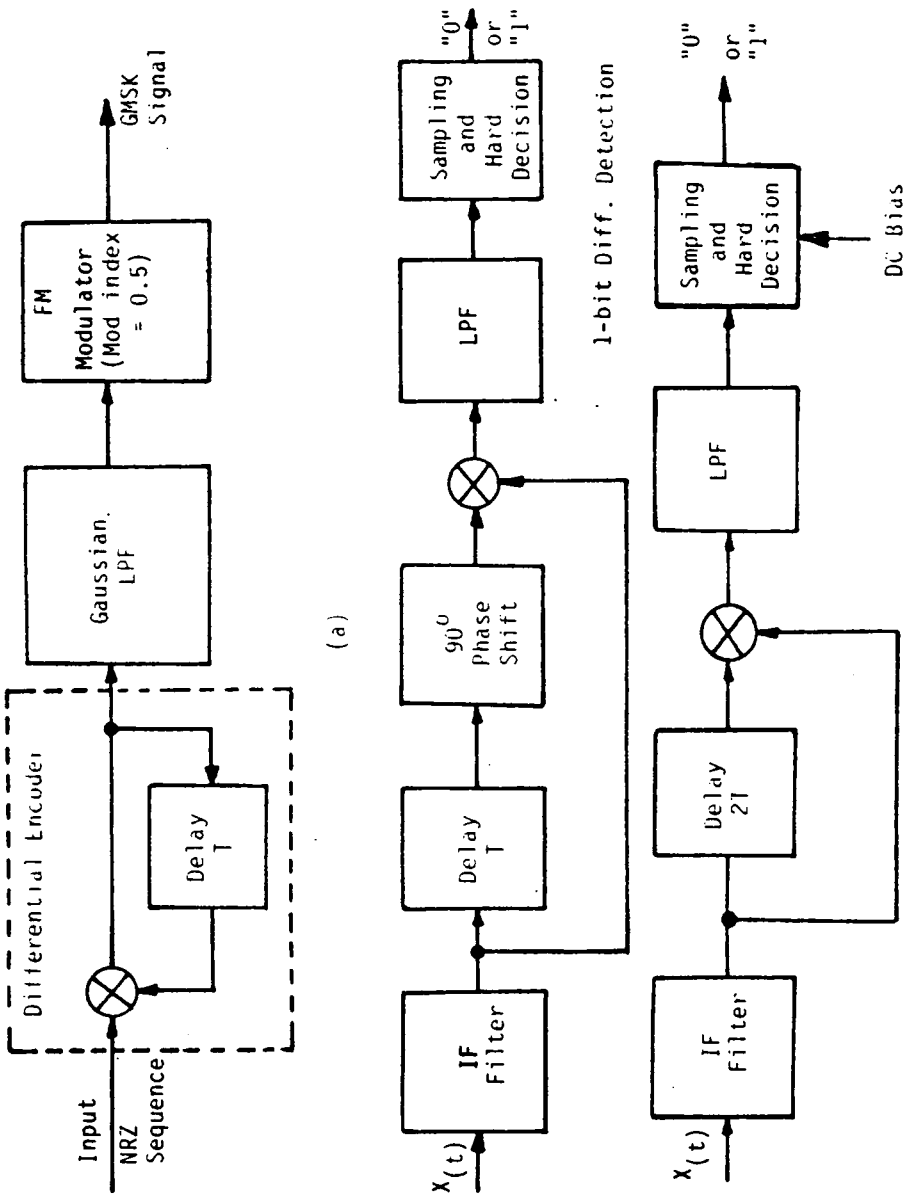

Figure 51. 1-bit and 2-bit Differential DGMSK (a) transmitter and (b) receiver. From Simon and Wang [89]

The input binary NRZ data stream is differentially encoded (2-bit case) or directly provided to the following Gaussian baseband filter for spectral shaping. After shaping, this lowpass filtered signal is frequency-modulated and transmitted. The transmitted signal can be denoted as [88]

$$x(t) = \sqrt{2S}\ \cos[\omega_0 t + \theta(t)] + \hat{n}(t)\ . \tag{4.23}$$

In Eq.(4.23), S is the signal power, ω_0 is the radian IF frequency, and $\hat{n}(t)$ is the AWGN noise with one sided power spectral density N_o. $\theta(t)$ is the phase of the transmit-filtered data after frequency modulation that is the result of convolution integral of the Gaussian lowpass filter response $h_t(t)$ and input binary NRZ data sequence d(t) expressed by

$$\theta(t) = \frac{\pi}{2T} \int [d(t) * h_t(t)]\, dt\ . \tag{4.24}$$

In Eq.(4.24), the multiplication factor $\frac{\pi}{2T}$ is the phase constraint conventionally given to the MSK type signal and T is the symbol duration. In addition, the premodulation Gaussian filter is characterized by the following equations where k is the transmission coefficient relating the 3 dB bandwidth B_t to the noise equivalent bandwidth B_{tn}.

$$\begin{aligned} h_t(t) &= \frac{1}{\sqrt{\pi}}\ \alpha_t\ \exp[-(\alpha_t t)^2] \\ \alpha_t &= 2\sqrt{2\pi}\ B_{tn} = 2\sqrt{2\pi}\ kB_t \\ k &= \frac{1}{2}\sqrt{\frac{\pi}{\ln 2}} = 1.0645\ . \end{aligned} \tag{4.25}$$

In the receiver, the input signal represented by Eq.(4.23) is band limited and thus results in a time varying envelope and distorted phase. The signal dependent noise term n(t) can be expressed in following manner:

$$x_{IF}(t) = \sqrt{2S}\ a(t)\ \cos[\omega_0 t + \phi(t)] + n(t)\ . \tag{4.26}$$

If we set $n_c(t)$ and $n_s(t)$ as independent lowpass zero mean Gaussian random processes with variance

$$\sigma^2 = N_0 \int_{-\infty}^{\infty} |H_r(f)|^2 df = N_0 B_{rn} \ , \tag{4.27}$$

where B_{rn} is the two-sided noise bandwidth of the equivalent lowpass filter $H_r(f)$ (the IF filter), then the noise voltage n(t) can be written in its narrow-band form

$$n(t) = n_c(t)\ \cos[\omega_0 t + \phi(t)] - n_s(t)\ \sin[\omega_0 t + \phi(t)] \ . \tag{4.28}$$

If we substitute noise in Eq.(4.26) with Eq.(4.28), the IF filtered output signal is written as

$$x_{IF}(t) = R(t)\ \cos[\omega_0 t + \phi(t) + \eta(t)] \ , \tag{4.29}$$

where

$$\begin{aligned} R(t) &= \sqrt{(\sqrt{2S}\ a(t) + n_c(t))^2 + n_s^2(t)} \\ \eta(t) &= -\tan^{-1} \frac{n_s(t)}{\sqrt{2S}\ a(t) + n_c(t)} \ . \end{aligned} \tag{4.30}$$

When this signal is given to the differential decoder, it is delayed by one symbol duration and 90 degree phase shifted. Then this delayed and phase shifted input is multiplied with the original received signal expressed in Eq.(4.29) in case of 1-bit differential detection. Then the output of the 1-bit differential decoder is expressed as

$$y(t) = \frac{R(t)\,R(t-T)}{2}\ \sin[\omega_0 T + \Delta\Phi(T)] \ , \tag{4.31}$$

where $\Delta\Phi(t)$ is defined by

$$\Delta\Phi(T) \equiv \phi(t) - \phi(t-T) + \eta(t) - \eta(t-T) \ , \tag{4.32}$$

$\Delta\Phi(T)$ denotes the phase difference during the single symbol duration caused by the distorted signal phase and the phase change due to AWGN noise. If we set the carrier frequency as an integer multiple of $\frac{2\pi}{T}$, the 1-bit differential decoder output in Eq.(4.31) can be simplified as

$$y(t) = \frac{R(t)\,R(-T)}{2} \sin \Delta\Phi(T) \ . \tag{4.33}$$

Then a hard decision can be made on the basis that if $y(t) > 0$, it is assumed a data "1" was sent, and vice versa. In the 2-bit case, the argument T in Eq.(4.31) to Eq.(4.33) should be changed to 2T and 'sine[ ]' in Eq.(4.31) and its simplified form Eq.(4.33) should be changed to 'cosine[ ]' because there is no phase shift in the 2-bit differential decoder and there is a two symbol unit delay instead of the one symbol delay used in the 1-bit differential detection. However, the decision rule for the 2-bit case is not so simple as in the 1-bit case. Details can be found in Simon and Wang [88].

Trellis Coded Modulation 8- differential PSK

Introduction

In the past, coding and modulation were treated as separate operations in the overall system design. However, after Massy [97] showed that considerable performance improvement could be obtained by treating them as a single entity, Ungerboeck [92] proposed and proved that optimally designed rate n/(n + 1) trellis codes suitably mapped into conventional 2^{n+1} point signal sets can provide significant coding gain without bandwidth expansion when compared with uncoded conventional 2^n signal sets. In this section, the basic algorithm and structure of trellis coded modulation is briefly investigated based on the practical approach of a 8-PSK case study. Because the process of differential encoding has already been described, an explanation of differential detection in trellis coded 8- differential PSK is omitted in this section. For notational convenience, TCM is used for Trellis Coded Modulation in this section.

Basic Concepts

TCM schemes use redundant nonbinary modulation in combination with a finite-state encoder which governs the selection of modulation signals to generate the coded signal sequence at the transmitter. At the receiver, the noisy signals are decoded by a soft decision maximum-likelihood sequence decoder to enhance link performance. In general, signal waveforms representing information sequences are most impervious to noise-induced detection error if they are very different from each other, i.e., each signal sequence should have a large Euclidean distance from all the others [92].

The essential concept of TCM which provides improvement compared to conventional uncoded modulations is the use of a signal-set expansion to provide redundancy for coding, and the joint design of coding and signal mapping functions so as to maximize the minimum Euclidean distance (ED) or free distance between coded signal sequences. This allows the construction of modulation codes whose free distance significantly exceeds the minimum distance between uncoded modulation signals at the same information rate, bandwidth, and signal power [92]. The name 'trellis' is used here because a similar state transition diagram to a binary convolutional code is used to represent the branches labeled with redundant nonbinary modulation signals.

In conventional multilevel modulation, the modulator maps m binary bits into one of $M(=2^n)$ possible signals during each signaling interval, and the transmitted m bits are recovered at the receiver by making an independent M-ary nearest-neighbor decision. In a convolutional code with a rate of k/n, where k is the number of information bits and n is the code length, n-k redundant bits are used for parity checking in general. In this case, the decoder decides the received state by examining of the discrete code symbols only; this decision process is usually called 'hard decision'. Thus the measure in hard decision is the 'Hamming distance', d_{free}. However, in certain circumstances, if a system works at low signal to noise ratios, so called rate loss occurs. The rate loss is defined : the loss of transmission rate when extra bits are added to the transmitted data for the error-correcting purpose, hence long time delay occurs than is needed to decode these extra bits. Only two ways exist to compensate this loss. One is to increase the modulation rate by expanding channel bandwidth, and

the other is the expansion of the signal set if the channel is band-limited. The latter change leads to the use of nonbinary modulations ($M > 2$).

One other effective way to compensate for this loss is to use soft decision decoding. In this case, the decoder makes the decision directly from the unquantized output sample of the channel. The measure is then the Euclidean distance, which is a function of the energy per signal set. However, independent use of this decision process cannot fully compensate the rate loss. This can only be achieved by doubling the channel signal set as was proven in the case of QPSK and 8-PSK in Ungerboeck's models. Simply speaking, the use of 'maximum likelihood soft decision Viterbi decoding' and 'signal set expansion by a factor of 2' can effectively compensate the irreversible loss. However, to realize this concept, some complicated procedures are necessary. Now, let us look at the design procedure of TCM scheme briefly.

The TCM scheme should be interpreted in terms of convolutional codes with special signal mapping, and this mapping should be based on grouping signals into subsets with large distances between the subset signals. Because of its nature, a general TCM scheme which generates trellis code with redundancy and performs signal mapping requires a conventional binary convolutional encoder followed by a signal mapper as depicted in Fig.52.

Based on this approach, TCM signals are generated as follows; if m bits are transmitted for one symbol duration, $\tilde{m} \leq m$ bits are expanded by a rate $\tilde{m}/(\tilde{m}+1)$ binary convolutional encoder into $\tilde{m}+1$ coded bits per symbol. These bits are used to select one of $2^{\tilde{m}+1}$ subsets of a redundant 2^{m+1}-ary signal set. The remaining $m-\tilde{m}$ uncoded bits determine which of the $2^{m-\tilde{m}}$ signals in this subset is to be transmitted.

In this general TCM scheme, the output of uncoded $m-\tilde{m}$ bits appears to become associated with $2^{m-\tilde{m}}$ parallel transitions. In this case, the free Euclidean distance is expressed as [92]

$$d_{free} = \min[\Delta_{\tilde{m}+1},\ d_{free}(\tilde{m})] \ , \tag{4.34}$$

where $\Delta_{\tilde{m}+1}$ denotes the minimum distance between parallel transition and d_{free} denotes the minimum distance between non-parallel paths in the trellis diagram depicted Fig.52. In another way of saying,

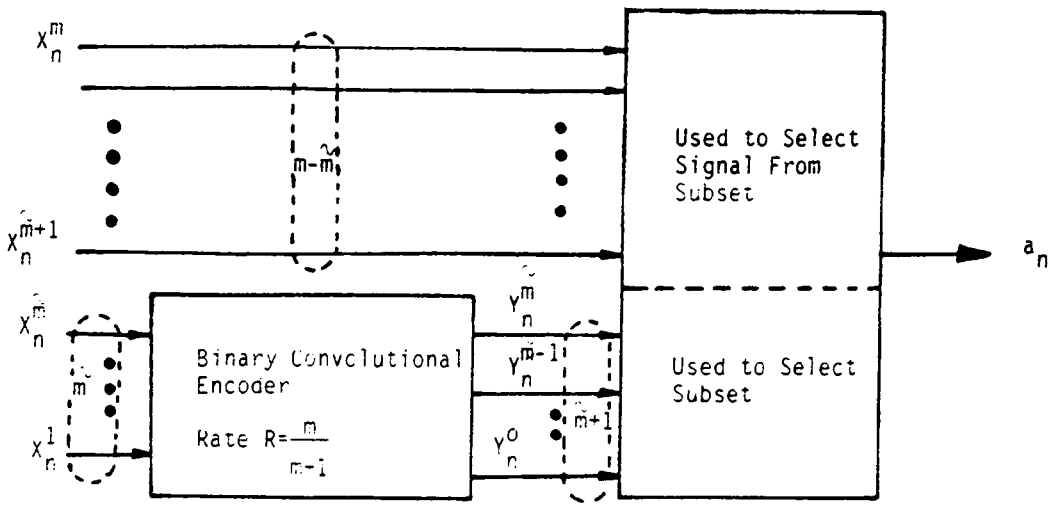

where

m; Original number of bits to the TCM encoder

$\tilde{m}$; Number of bits/symbol needed for uncoded $\tilde{m}$-ary PSK

$\hat{m}$+1; Number of expanded bits/symbol after signal set expansion

m-$\tilde{m}$; Number of uncoded bits from original stream

a_n; Mapped signal sequence

〈 Example of Parallel Transition or Non-parallel Transition 〉

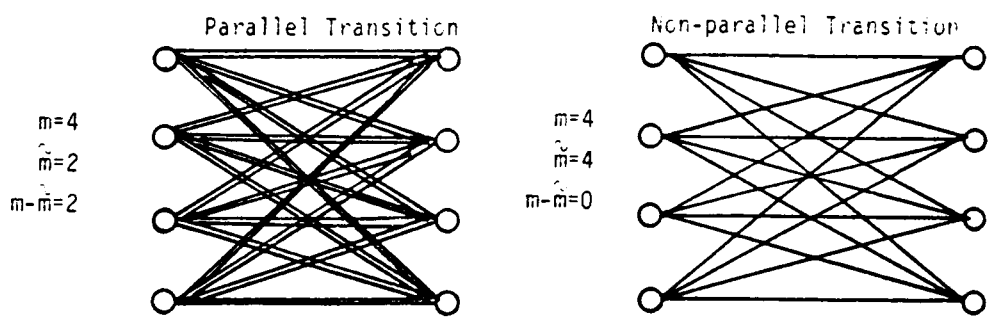

Parallel transition occurs only when m > $\tilde{m}$, if m = $\tilde{m}$, no parallel transition occurs.

Figure 52. General TCM scheme with examples of Trellis code state transition diagrams

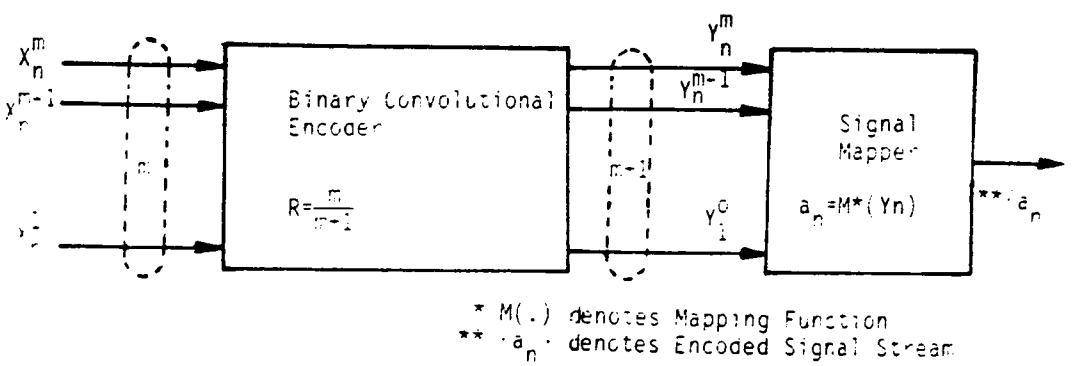

Notes:

1. In this special case, $\tilde{m}=m$. Hence signal subset is composed of 1 signal only.

2. By the above property 1, there is no need to select signals from the subset. It is impossible to do so because there are no redundant bits (i.e., only the exact number of bits from the original stream is provided, hence $m-\tilde{m}=0$).

3. Because of the nature 1.2 above, only the non-parallel transitions between states are occured (see example of Figure 52).

Figure 53. Special case of general TCM scheme

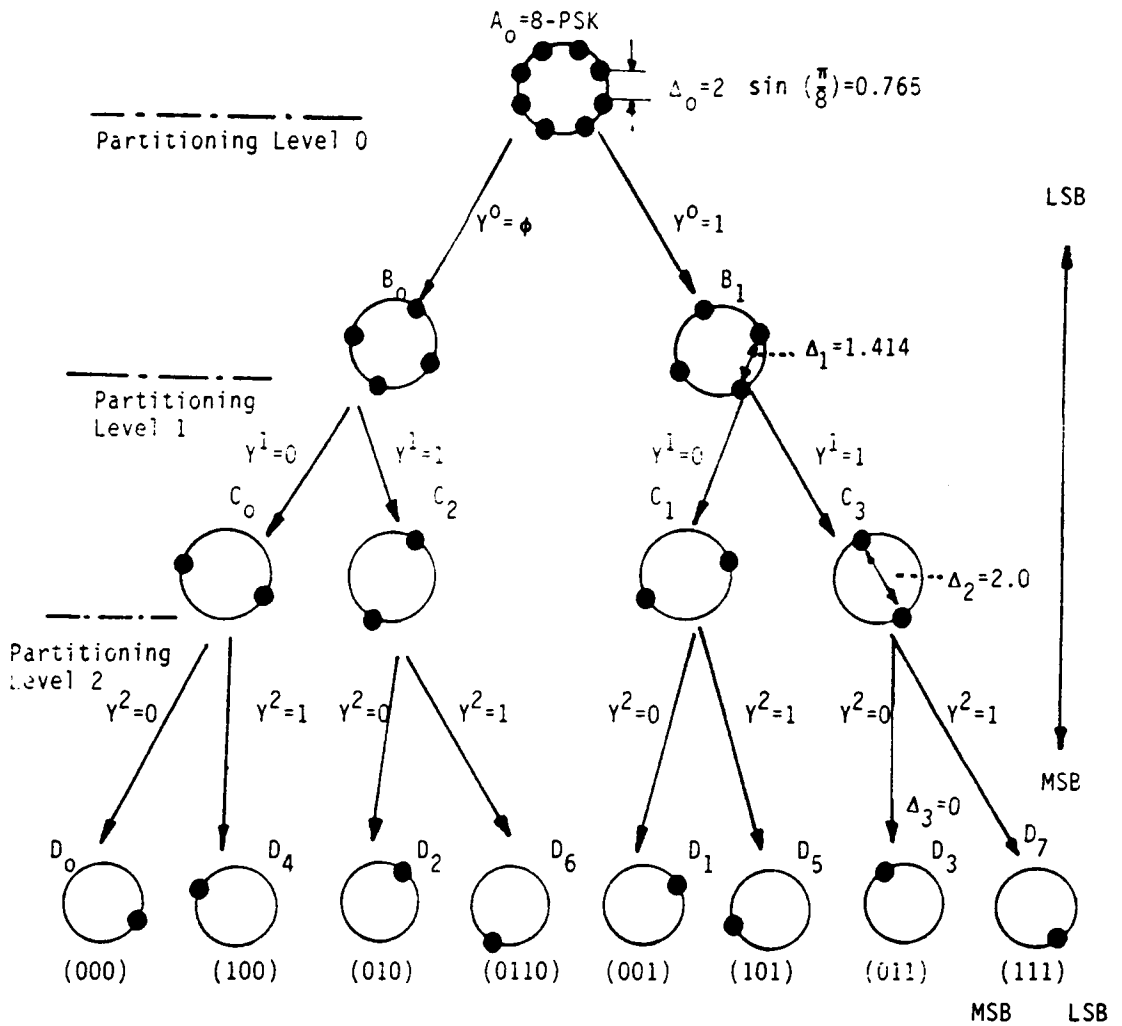

Note

1. A_0, B_0, B_1, $C_0 \sim C_3$, $D_0 \sim D_7$ are all subsets.
2. Δ_i=Euclidian Distance (Ed), i=0, 1.2 for $\tilde{m}$=2.

Figure 54. Example of Set Partitioning in TCM scheme

the free Eucildean distance is defined as the minimum intra set distance or the minimum distance between signals in the subset, whichever is smaller depending on the existance of uncoded bits. In addition, parallel transition means that both the origniating and terminating of state transition can occurs at the same node, whereas non-parallel transition means either originating or terminating of state transition occurs.

As a special case of the above general TCM scheme, let us look at the case of $m = \tilde{m}$. This case can be used to create a modulation that gives a 2 bits/sec/Hz rate. This case is simple because only $\tilde{m}$ is substituted with m in the general TCM scheme. Expansion of the binary data sequence with a rate $R = m/(m + 1)$ convolutional encoder is done first, followed by mapping of groups of $m + 1$ bits into the larger set of signals. In this case, the Euclidean distance must be maximized between all pairs of signal sequences that the encoder produces. Fig.53 shows this special case.

Once a trellis code is generated with a specific encoding rule, the next important procedure is the signal mapping by set partitioning that can be illustrated as in Fig.54. This mapping follows from successive partitioning of signal sets into subsets with increasing intra-set distance $\Delta_0 < \Delta_1 < \Delta_2$ .... between the signals of these subsets, i.e., each partition is two way. The partitioning is repeated $\tilde{m} + 1$ times until $\Delta_{\tilde{m}+1}$ is equal to or greater than the desired free distance. Fig.54 shows the example of set partitioning of 8-PSK channel signals into subsets with increasing minimum subset distance. In this case, the signal constellation is symmetric. The minimum free distance is always the Euclidean distance. As can be seen from the footnotes, Δ_i gets increased by additional partitioning. In this case, a special case of $\tilde{m} = m = 2$, the partitioning level is repeated up to y^0, y^1, y^2 because $\tilde{m} + 1$ is 3.

Only the basic concepts of generation of TCM code and signal mapping have been described thus far. Many other relevant ideas could not be fully discussed here. The modeling procedures for TCM- 8 DPSK in Chapter 5 will clarify some of them. Further discussion can also be found in Ungerboeck's papers [92],[99].

4.4. Efficient Channel Encoding in LMSS Channels.

The purpose of channel encoding is to convert the source code to a form that will allow the receiver to reduce the number of errors at its output due to channel noise. The distinction between channel encoding and source encoding must be clear. Source encoding transforms the source output into a sequence of binary digits called the information sequence, whereas channel encoding transforms the information sequence generated by the source encoding into a discrete encoded sequence called a code word [100],[103]. We will confine the discussion to channel encoding in this section. As the counterpart of channel encoding, the process of channel decoding transforms the received sequence into a binary sequence called the estimated sequence. The decoding strategy is based on the rules of encoding and the noise characteristics of the channel. Ideally, the estimated sequence will be a replica of the information sequence although the noise may cause some decoding errors.

The above description is expressed diagramatically in Fig.55. In this diagram, the symbol U denotes the information sequence(uncoded), and V denotes the (channel) encoded sequence, r represents the received sequence corrupted by channel noise and $\hat{U}$ denoted the estimated sequence. The decoder must produce an estimate $\hat{U}$ of the information sequence U based on the received sequence r. Equivalently, because of the one-to-one correspondence between the information sequence U and the code word V, the decoder can produce an estimate $\hat{V}$ of code word V. Clearly, $\hat{U} = U$ if and only if $\hat{V} = V$. A decoding rule is a method used to choose an estimated code word $\hat{V}$ for each possible received sequence r [100].

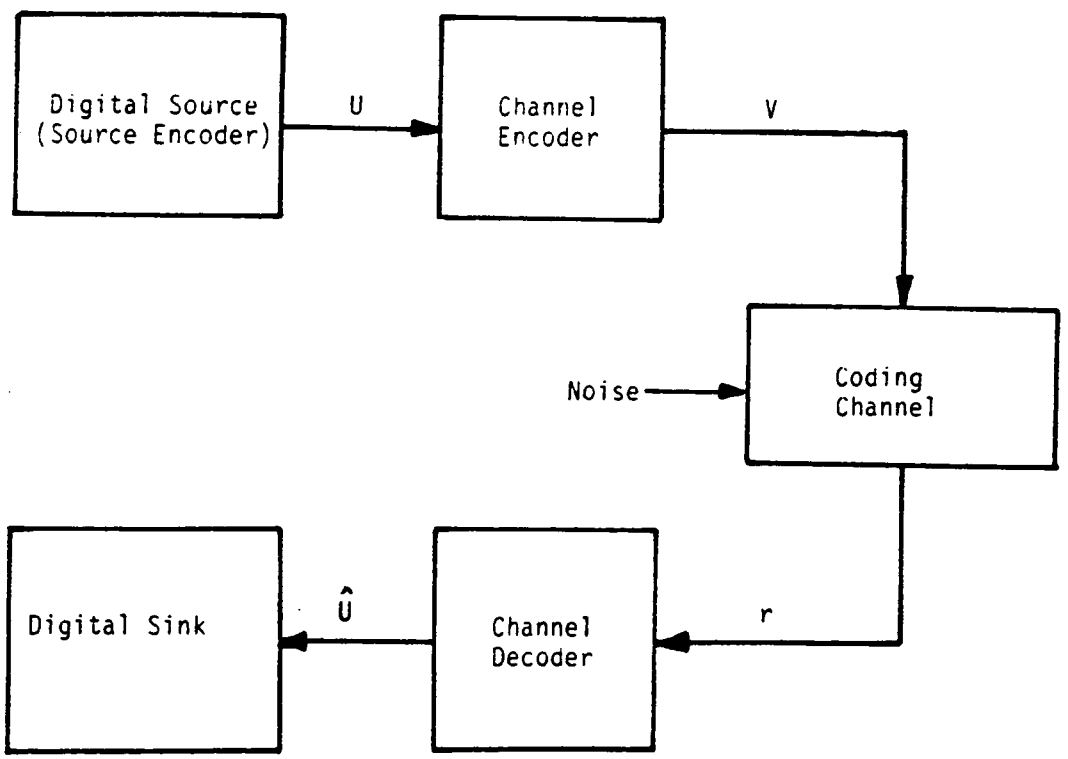

Figure 55. Typical Coding System

Thus far, the principle of channel encoding has been described. However, the reason for channel encoding may not be clear at this moment. In general, the reason is that by channel encoding, system performance can be improved relative to the case of no coding. If we define coding gain as the ratio of required energy per bit transmission under coding to the no coding case, we can expect to realize this gain by using the overhead of a coding scheme. However coding gain varies with the channel characteristics. In an AWGN channel, denoted by BSC(binary symmetric channel), coding gain is higher if the symbols are independent, i.e., the channel is memoryless.

However, in a fading channel, under severe Rayleigh fading, successive symbols are not statistically independent. Thus the degree of independence between transmitted signals is reduced. Therefore, conventional coding schemes designed to operate on memoryless channels will result in poor performance.

To circumvent this performance degradation, numerous proposals and experiments have been done. Many of them tested the design of special coding schemes that resist the burst errors. These codes are called burst-error-correcting codes. Cyclic codes such as the Fire code was reported as being effective for a fading channel, for single error correction [100]. Some convolutional codes were also used for burst error correction as well as for random error correction, such as Berlekamp-Preparata codes. However, regardless of code type, it is not easy to generate and find a code with the desired properties even by using a computer. In addition, burst error protecting codes are generally complicated to use.

Interleaving and deinterleaving is an appropriate technique that does not use this kind of special coding. Instead, it is possible to use a conventional code even in a channel which has memory. This method is usually preferred over special error protection codes in practical applications, especially in mobile radio communication. In the next section, the method of interleaving and deinterleaving will be described briefly.

Note:

X_i: Encoded symbol of Codeword (length N).

I: Number of rows (Column size)

n: Number of columns (row size)

Ixn: Total number of symbols to be transmitted and received

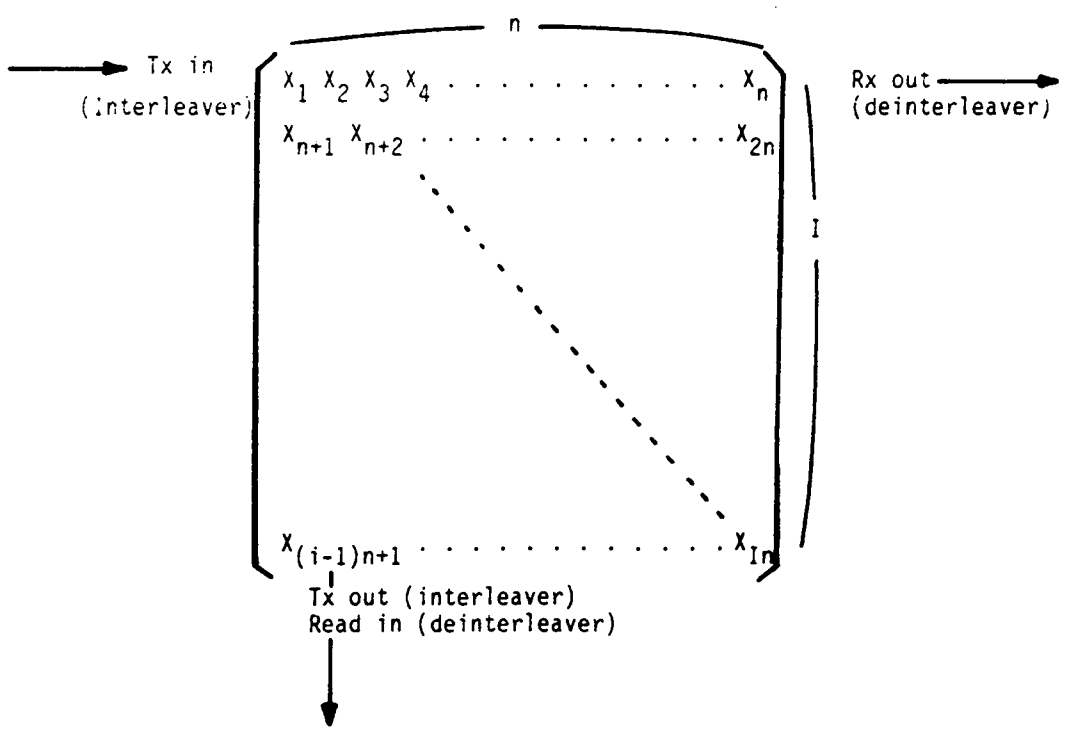

Figure 56. Method of Interleaving and Deinterleaving

Method of Interleaving and Deinterleaving

There can be an abundant number of methods for practical implementation of interleaving and deinterleaving. However, the most frequently used one is rectangular array implementation. In this method, the array has dimensions of I rows and n columns; thus it constitutes an I x n matrix. The encoded data are written into the array by rows and transmitted by columns.

Each element of the array is used to store one code symbol. Usually, the size of the row n is the block length of the code, called the span length, so that the row contains one codeword. The vertical dimension of the array I is called the interleaving depth, or degree. It is common to refer to the entire array as an interleaving frame. It can be seen that an error burst spanning L < I code symbols produces at most a single error in L consecutive codewords. Therefore, selection of I depends on the expected error-burst length [100]. Deinterleaving is the reverse procedure of interleaving. Data are read into an Ixn array by columns and out by rows. Although bursts of channel errors are spread among successive codewords, it is important to note that periodic disturbances can produce many errors in a single word.

Fig.56 depicts the idea of interleaving and deinterleaving based on the above rectangular array structure. The major factor that decides the dimensions of the array is the fade duration or the average burst length. However, it is almost impossible to adjust the array dimensions to match the varying fade characteristics. Therefore, an estimated dimension based on known fade statistics must be used. If a fade lasts longer than the interleaving depth, effective burst error protection is impossible. However, there is no way to protect the data in this case, except by the use of an infinite dimension in the interleaver. Therefore, accurate prediction of fade duration is the most important factor in determining the performance of interleaving [101].

4.5. Summary

An investigation to find a suitable digital modulation scheme and coding techniques for an LMSS channel was performed. The fading conditions of a LMSS channel were briefly discussed first. We found that vegetative shadowing was the most difficult case to analyze, and it was not understood well. With this basic knowledge, candidates of suitable modulations were compared for system complexity and anticipated performance in an LMSS channel. Based on this preliminary survey, four digital modulations were selected for more detailed study.

These were QPSK, MSK, DGMDK, and TCM 8-DPSK. The first two were investigated using coherent detection schemes, while the latter two were investigated using the noncoherent detection. Finally, interleaving and deinterleaving were discussed as an efficient channel encoding technique for burst error protection in a fading channel when a conventional coding scheme is used for the LMSS signal. All of these surveys were described as an introduction to modeling of LMSS components to be described in the next chapter.

V. LMSS Channel Simulator Modeling

5.1. Modeling Overview

With the brief review of digital modulation schemes and the relevant techniques in a Land Mobile Satellite System under fading described in the previous chapter, it is now possible to start modeling the LMSS channel simulator. In this chapter, detailed modeling procedures are described based on the system block diagrams as well as on the component block diagrams, followed by a brief introduction of the modeling methodology used in the simulation process.

For proper and efficient modeling, we can divide the necessary procedures into two steps : system level modeling and component level modeling, depending on the sequence of work. In the first step, system level modeling, decisions about basic methodologies must be made. These tasks can be classified into the following stages :

1. How to constitute the LMSS link in fading conditions
2. What kind of simulation method is used
3. What kinds of modulation schemes will be simulated

4. How to analyze the result

Once these methodologies are determined, system level modeling can proceed in the form of system specifications or modeling specifications along with system block diagrams. For convenience of description, we are dealing with the methodologies described above in this section, and system level modeling will be explained in the next section based on the system block diagram.

Based on system model, component level modeling can be started. In this step, with the system block diagram and modeling specifications set up, functional components must be modeled in a flexible manner for easy interconnection and modification. A modular structure for each component is desirable. The component modeling procedures will be described in detail after the system level modeling description.

A brief introduction to the methodologies that were used in the overall simulation processes follows.

1. Simulation Method : One of the most important decisions is the method used for simulation. Software simulation with a computer program was selected rather than hardware simulation, because of the flexibility this permits.

   Even though hardware simulation is avoided, much effort has been devoted to making the system model as close as possible to practical devices. The results of these efforts can be seen in the process used for simulation of fading effect, as well as in the use of practical filters in the system.

2. Modulation Schemes : In our simulation, four digital modulation schemes were initially selected. Those are QPSK, MSK, DGMSK, and TCM 8-PSK. The former two are modeled with coherent detection, whereas the latter two are modeled with noncoherent detection using coherent differential detection. However, some of them may not be used for the final comparison of performance if simulation results are not satisfactory.

3. Signal Processing : The way in which data in the communication link simulation are processed is also important, because the efficiency of the simulation frequently depends on the proper selection of this method. The terminology 'signal processing' in this simulation means the way in which the transmitted data were processed in the various functional models to get the proper forms for performance evaluation.

   The chief signal processing function is filtering. For baseband simulation, the complex envelope of the bandpass signal is used for simplicity. The use of the complex envelope of a bandpass signal is the dominant methodology in communication channel simulation because of its efficiency and ease of implementation [103]. All the bandpass filters in the simulation process are changed into their lowpass equivalents. Details of the complex envelope, baseband simulation, and lowpass equivalent filtering can be found in [29], [103] [104].

4. Fading Effects : The inclusion of fading effects is the key factor in the LMSS channel simulation. However, in this simulation where the performance evaluation of a fading channel is the main subject, simulation of the fading effects are avoided. Instead, results from a propagation simulator that can furnish various fading data are inserted in the simulation.

   These data, as well as the noise in the down-link of the LMSS channel, will provide the test conditions for the evaluation of error performance. For a more thorough analysis, various cases for fading data, such as no fading, partially vegetative shadowed, terrain obstacles, etc., will be inserted.

5. Nonlinearity : In an LMSS channel, a linear high power amplifier is assumed in the satellite transponder. The nonlinearity inherent in a conventional TWTA is not considered. However, this nonlinearity can be included in the modeling of the channel simulator. Only a helix-type TWTA without memory is used for modeling of the dominant AM/AM and AM/PM conversion effects.

6. Performance Evaluation : Among the many effective methodologies for performance evaluation of satellite communication channels, the most frequently used is analytic calculation of performance measures such as average bit error rate as a function of bit energy to noise power

spectral density or as a function of carrier to noise power ratio. The second methodology is the method of Monte-Carlo simulation. In this method, a huge amount of data is processed to get reliable statistics for the performance measure. the results are comparable with those from analytic calculations.

Comparing the two methodologies, the former is simple and thus easy to use ; the latter is time-consuming and expensive. However, the former analytic method cannot be used in some cases of simulation especially when a non-mathematical model is used or some effects exist that cannot easily be modeled analytically. In the case of an LMSS channel where fading is the dominant factor for performance degradation, the latter methodology is thought to be effective.

In our simulation, both methodologies are employed. For coherent modulation schemes, the method of analytic calculation of error rate is used, whereas the method of Monte-Carlo simulation is employed for noncoherent schemes. Because most of the current performance evaluations for LMSS channels use the former method, it is thought to be valuable to use the latter method as an alternative.

For the calculation of error rate under noise and fading effects, the nature of these disturbances is much more important than the method of calculation. The noise and fading effects in our simulation are down-link oriented, i.e, we are dealing with the noise and fading effects that can be encountered in the down-link only. In some cases, only the up-link noise is the issue of the simulation. This assumption is based on the fact that the down-link is generally more critical than the up-link in typical power and band-limited channels.

Because two different methodologies are used for error rate calculations, there are some differences in the way noise is treated. In coherent schemes, only the signal power is calculated from the sampled values of the received signal; then a pre-determined noise power at a fixed carrier to noise ratio is provided for the final bit error rate calculation.

However, in the noncoherent schemes, the number of symbol errors and bit errors are calculated by comparison of the decoded data with the originally transmitted data. Noise is generated in the simulator and directly added to the transmitted data. A huge number of symbols

must be generated and processed to obtain a reliable estimate of error rate in various environmental conditions, when the error rate is small.

With the methodologies listed above, and the concurrent requirements of the MSAT-X experiments conducted by NASA JPL, the following specifications were prepared. These specifications apply to the overall simulation process regardless of the modulation scheme, or the coding technique.

Modeling Specifications

1. Modulation Schemes.
   - Trellis Coded Modulation (TCM) 8-PSK with differential detection
   - Gaussian MSK with differential detection
   - QPSK with coherent detection
   - MSK with coherent detection
2. Transmission Speed.
   - Symbol rate : 2.4 K symbols/sec (or 1.2 K)
   - Bit rate (before coding) : 4.8 K bits/sec (or 2.4 K)
   - Bit rate (after coding) : 7.2 K bits/sec (coding case only)
   - Bits per symbol(before and after coding) : 2 bits/symbol
   - Bits per symbol(after coding) : 3 bits/symbol
3. Bandwidth and Transmission Frequency.
   - Channel bandwidth : 5.0 KHz RF bandwidth
   - Transmission frequency : UHF, and L band (850 MHz or 1542 MHz)
4. Detection schemes.
   - Coherent detection using carrier synchronization in QPSK and MSK
   - Differential phase mapping and recovery at symbol unit in TCM 8-DPSK
   - 1-bit differential detection in DGMSK
5. Channel Encoding/decoding scheme.
   - Rate 2/3(=k/n) Trellis code with 2-bit delayed nonsystematic encoding and Viterbi MLD (Maximum Likelihood Decoding) with hard decision for TCM 8-PSK.
   - Rate 2/3 convolutional encoding (n, k, m =3, 2, 4) and Viterbi MLD decoding with hard decision for DGMSK
   - No channel encoding in coherent QPSK and MSK
6. Burst Error Protection Scheme.

- Rectangular array block interleaving/deinterleaving
- Interleaving frame size : 128 symbols/block (384 bits per block)
- Interleaving Depth : 16 symbol
- Interleaving span length : 8 symbol
- Interleaving element format : 3-bit binary data/symbol

7. Simulation methodology
   - Baseband simulation
   - Filtering and Sampling specifications (based on 4.8 Kbps bit rate)
     - Baseband simulation with Lowpass Equivalent filter for all bandpass filter
     - Frequency domain filter with linear phase assumption
     - FFT and IDFT are interchangeably used for time and frequency domain conversion
     - Nyquist frequency :1.2KHz (for square root raised cosine Nyquist filters)
     - Roll-off Factor : 0.2 --1.0 (for square root raised cosine Nyquist filters)
     - BT product for Gaussian pre-modulation baseband filter : 0.2---1.0
     - Number of time and frequency samples/symbol : 16
     - Total number of symbol/simulation path : 128 (256 bits before coding)
     - Total number of time/frequency samples : 2048
     - Time sampling interval : 0.026402 ms
     - Frequency sampling interval : 18.75 Hz
     - Total time(real) for 128 symbol transmission : 53.33 ms
   - Nonlinearity.(TWTA in satellite transponder only)
     - TWTA model: helix type (no-memory type)
     - AM/AM and AM/PM nonlinear conversion model
   - Fading Effects.
     - Direct use of built-in propagation simulator output in UHF and L band (850 MHz and 1.5GHz)
     - Self-generated fade from empirical fade data base
   - Performance Evaluation.

- Coherent Schemes (QPSK and MSK)
  - ▲ Analytical calculation of noise power based on the fixed C/N ratio
  - ▲ Signal power(bit power) calculation based on the sampled value
  - ▲ Indirect calculation of average BER(Bit Error Rate) and bit/bit error rate calculation by using error function
- Noncoherent Schemes(TCM 8-DPSK and DGMSK with Differential Detection)
  - ▲ Direct noise insertion after fading with fixed C/N ratios
  - ▲ Direct symbol error rate counting based on the decoder output comparison
  - ▲ Direct bit error rate calculation by Monte-Carlo simulation

5.2. System Level Modeling

As the first step in the practical modeling of a LMSS channel simulator, system models were designed. In these modeling procedure, two basic differences were used as the guide lines in classifying the system level models, depending on the coding techniques and detection schemes used in the transmitter and receiver.

For the case of QPSK and MSK, we already decided to use coherent detection, whereas nonconerent detection by differential detection is employed for DGMSK and TCM 8-PSK. In addition, no coding is assumed in the coherent schemes because better performance is generally expected in the coherent schemes than in the noncoherent cases. System level modeling is done separately for the coherent schemes and the noncoherent schemes.

In this section, two different system level models are described, based on their block diagrams. Note that these system level models are furnished based on the previously described simulation methodologies and modeling specifications in Sec.5.1.

Before we look into the LMSS channel simulation model under fading, it is helpful to understand conventional satellite communications. Fig.57 shows a typical single satellite communication link in which fixed earth stations communicate via a satellite.

At the transmission side, information is generated in the appropriate format, such as an NRZ pulse stream and is modulated with a sinusoidal carrier, in general. The modulated carrier that contains the information in the form of carrier amplitude or phase passes through the spectral shaping filter and high power amplifier for transmission to the satellite in the sky.

At the satellite transponder, the input signal is band-limited for effective up-link noise rejection by the input filter. This signal is amplified by the TWTA in a nonlinear way, and thus the output amplitude and the phase are distorted. This distorted but amplified signal is spectrally shaped by the transponder output filter to prevent interference into adjacent channels, before retransmission to the receive-side earth station.

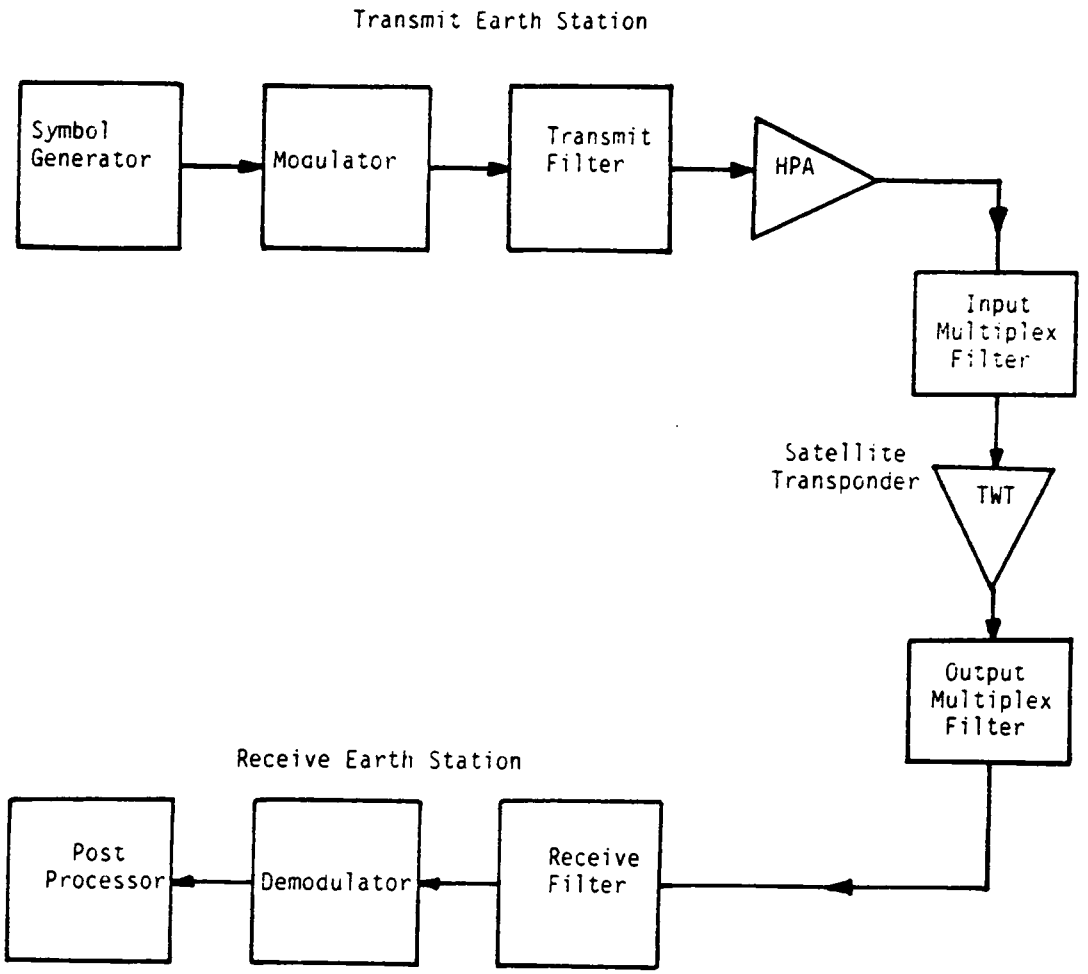

Figure 57. Typical fixed single satellite communication link.

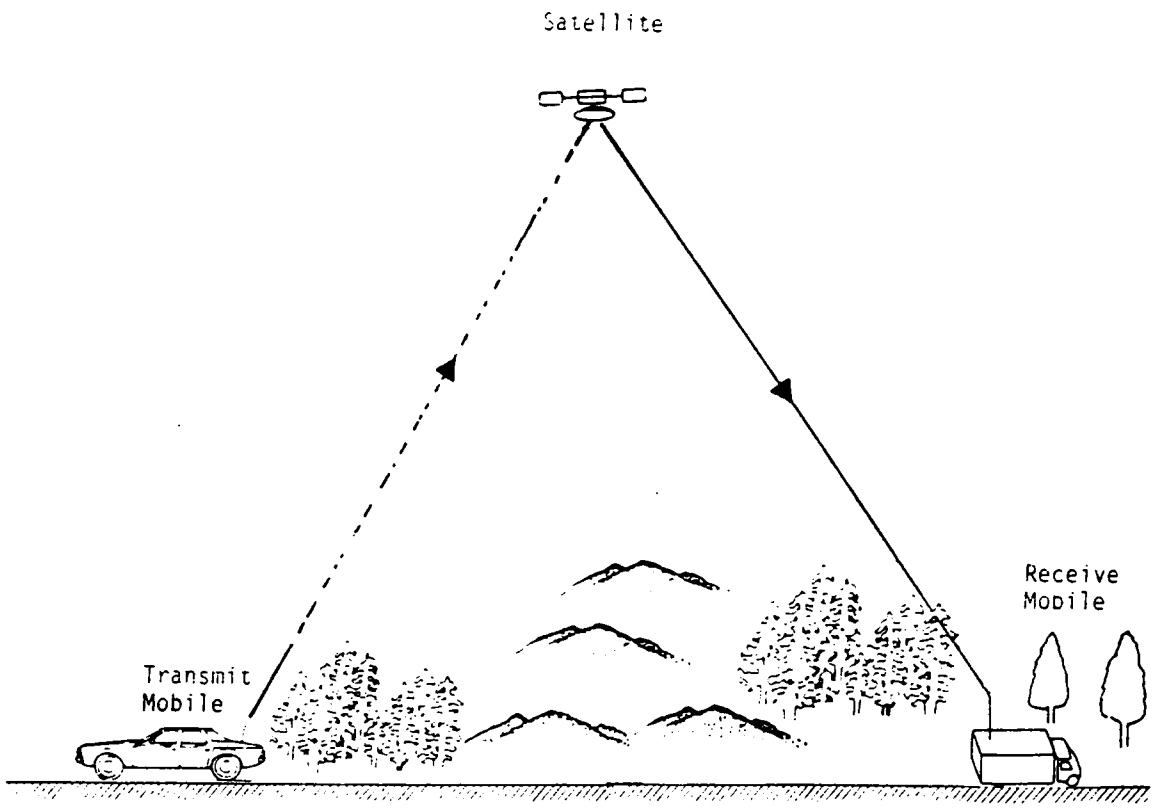

Figure 58. Example of Land Mobile Satellite System environment.

At the receive side, the input filter provides additional spectral shaping to reduce ISI (Inter-Symbol Interference) and down-link noise. This filtered signal is processed by the demodulator and decoder (if any) to recover the originally transmitted information.

Compared with the typical satellite communication link depicted in Fig.57, the communication link in a Land Mobile Satellite System is basically the same as for fixed earth stations, except for some features. The first feature of LMSS is the location of the transmitter and the receiver. In the land mobile case, both sides can be moving vehicles, or at least one side may be a moving vehicle. This situation makes for great differences in the design and performance of the communication link compared with the fixed earth station case.

The second feature directly results from the first one. Because at least one side, either the transmitter or the receiver, is moving, the propagation path length varies with their relative location and speed, especially when there is shadowing. In addition, contrary to the fixed earth station, a moving vehicle has the restrictions of smaller antenna and limited transmission power. Fig.58 shows an example of the LMSS environment when both sides are moving vehicles.

5.2.1. Coherent Systems : QPSK and MSK

The system level model for the coherent QPSK and coherent MSK is depicted in Fig.59 with the major functional blocks. This system level model is designed based on the description of the QPSK and MSK modem in Chapter 4. For the description of the system level model, a block diagram in which each block represents the functional component to be modeled is used here. This is because most of the channel modeling programs developed for the performance evaluation of communications satellites allow the channel to be modeled from a block diagram base.

To model and simulate the channel, it is fundamental to perform four major steps regardless of the modulation scheme used : signal generation, filtering, linear or nonlinear amplification, and demodulation. The system model designed consists of four major parts : the pseudo random signal

generator, the modulator and demodulator, the filter, and the optional nonlinear TWTA. These functional blocks can be located at the transmit(Tx) side, satellite transponder, or receive(Rx) side. In addition, extra modules such as a BER calculator can also be included for the analysis of results. Even though two modulation schemes, QPSK and MSK, are used, most of the elements can be used in common because they both use coherent detection schemes and no coding is employed for simplicity.

For convenience of description, the system model is divided into three parts : the transmit side, the satellite transponder, and the receive side.

At the transmit side, the first step in modeling is signal generation. In our model, a pseudo randomly generated NRZ pulse sequence is applied to the QPSK/MSK modulator, where even and odd bit streams respectively modulate the two orthogonal carriers and sinusoidal pulse weighting is done for the MSK case. These modulated carriers are then added and passed through the Tx filter. Before filtering, amplitude equalizing with a specific function depending on QPSK or MSK is performed (pre-filtering).

In filtering, the fast Fourier transform (FFT) of time samples from the modulated signal is multiplied by the specific filter frequency response. All filters' phase responses are assumed to be zero for simplicity. The time waveform of the filtered signal is obtained by returning the above frequency domain signal into the time domain using an inverse discrete Fourier transform (IDFT). In this step, to get the phase and amplitude information easily for the filtered signal, filters are modeled with their lowpass equivalent, and all the inputs and outputs of filter are expressed as complex envelopes. By using the complex envelope notation, it is possible to do the simulation at baseband, regardless of the carrier frequency used. From the complex envelope of the filtered output, the amplitude and the phase are easily obtained. This procedure is needed especially when the amplitude and phase model is used for TWTA modeling.

Based on an assumption of linear high power amplification at the transmit side, the filtered signal is linearly amplified and transmitted to the satellite transponder.

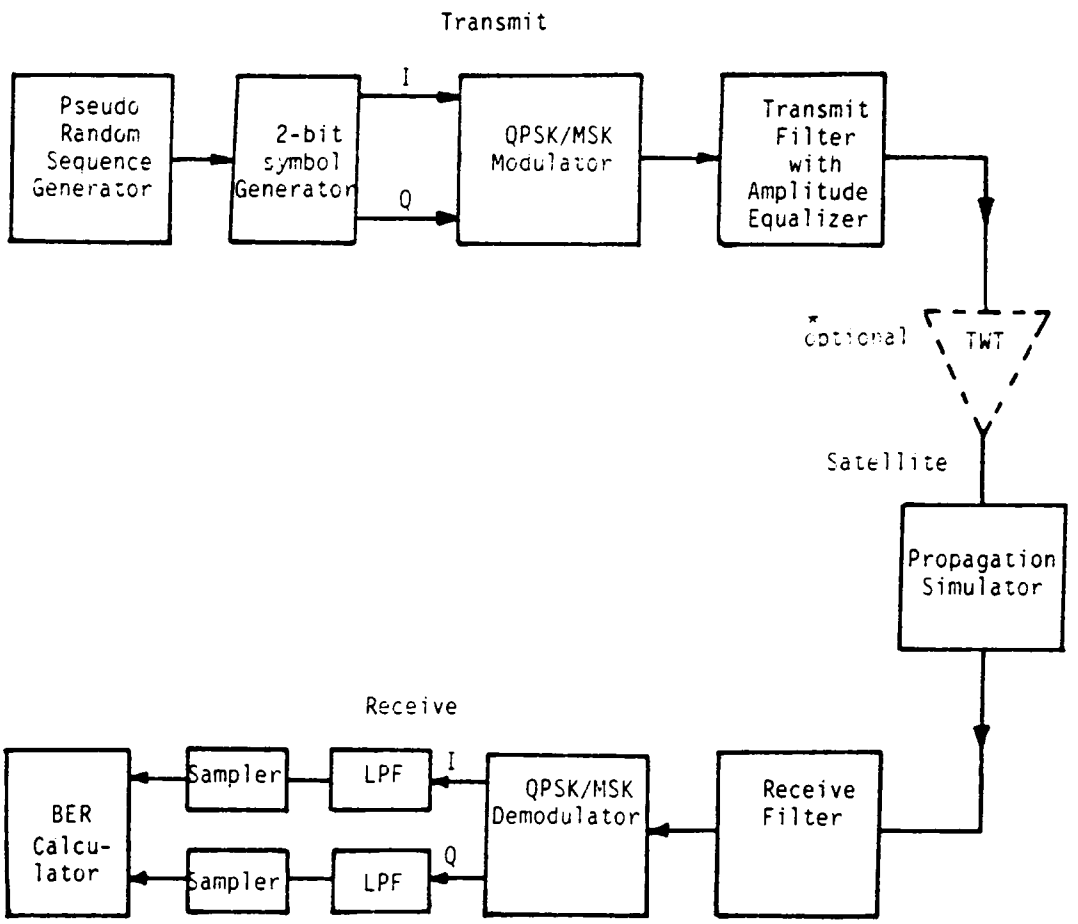

Figure 59. Coherent QPSK and MSK systems simulation block diagram

In the satellite transponder, the uplink noise is assumed to be smaller than the downlink noise. Therefore, only the downlink noise is considered. Because the bandwidth of the input/output multiplexer filters is normally larger than that of the signal, they are excluded in the single link simulation at first. But the addition of these filters in the future can be done easily by inserting one command line in the program. The signal is amplified either by a nonlinear TWTA that is represented by an amplitude and phase model (will be described in detail later in this chapter) or by a class B linear amplifier. Then this signal is corrupted with noise (AWGN is assumed, but not really added at this step) and fades. To simulate the fading effect, a propagation simulator output that consists of faded amplitude and distorted phase at a specific wavelength interval is inserted in complex form, to be matched with the sampled complex envelope of the retransmitted signal.

The retransmitted signal from the satellite passes through the Rx filter in the receive side. This Rx filter shapes the spectral components of the received signal, which is then demodulated by carrier multiplication, and sinusoidally pulse shaped for MSK. The baseband signal is then lowpass filtered and time sampled by the sampler. In the extra module used for performance evaluation, bit error rate (BER) is calculated.

For the BER calculation, the signal power is calculated at the input of the Rx filter first, then for the desired value of carrier to noise ratio (CNR), the noise power must be calculated. To do this, instead of direct addition of noise (downlink thermal noise) at the input of the Rx filter, analytically calculated noise power is added in the simulation and an average BER, as a function of $\frac{E_b}{N_o}$ (bit energy to noise power spectral density), is found.

Throughout the modeling procedure, the signal that is generated and processed is real-valued, even if it takes complex form in some cases for transformations. At the signal generation stage, the real-valued signal is time sampled with a rate of 16 samples for one bit duration. Therefore the discrete power spectra at the modulator would span 8 times the bit rate in one (+ or -) direction of frequency. These time sampled signal data are converted to frequency sampled data in the filtering process by an FFT. After multiplying with the filter frequency response, the filtered result is converted

to the time domain by the IDFT. This procedure for filtering is the same for every filter used in the simulation. The signal used in the TWTA is real-valued in the time domain. Using the same transformation procedure as for the transmit case, the demodulated and time sampled value is the real-valued signal. In sampling at the demodulator, samples should be taken at the sampling point within each symbol where decision metrics are derived. Sometimes this procedure requires linear polynomial interpolation between samples.

5.2.2. Noncoherent Systems : TCM 8-DPSK and DGMSK

Unlike the system level model for coherent systems previously described, the noncoherent system model consists of some unique functional blocks related to the channel encoding and differential detection scheme. Because of this complexity, the system block diagram is divided into four sections: transmit parts A and B, and receive parts A and B. The description of nonlinearlity in the TWTA and the fading effects are basically the same as for coherent systems, and will not be repeated here.

All explanations are based on the corresponding block diagrams, as before. Although the two digital modulation schemes are basically different, most of the functional blocks are designed to be used in common so far as is possible. Therefore, the system models for TCM 8-DPSK and DGMSK will be explained together unless a separate description is needed.

Transmit Part A (Fig.60)

Part A of the transmit part of the TCM 8-DPSK and DGMSK systms with coherently differential detection is depicted in Fig.60. The major functional blocks in this part are the random symbol generator, the trellis encoder or the convolutional encoder, and the block interleaver. The convolutional encoder uses the same code rate R=2/3 (k/n) as the TCM encoder for simplicity.

For symbol generation, a number of binary (not necessarily NRZ) data bits are randomly generated by a PN(Pseudo Noise) sequence generator. As was mentioned before in the modeling specifications, 256 bits (before encoding) are normally generated to meet the block size of the block interleaver. The conversion of binary (0 or 1) data to NRZ data is temporarily postponed until this format is needed in the DGMSK case. Therefore, a serial bit stream is provided to the serial to parallel (S/P) converter to constitute the 2-bit symbol stream for channel encoding. Therefore, in a given symbol duration T_s, one 2-bit symbol is fed to the channel encoder.

The trellis encoder used for TCM 8-PSK is a special case of a general TCM encoder in which all the input bits are used for encoding (see Fig.53). Therefore no redundant bits are used for set partitioning in our case. This decision is based on the recommendation of NASA JPL's initial design [100]. In this case, the TCM encoder is the same as the conventional convolutional encoder. By doing this, it is possible to use the same encoder for DGMSK if the code rate R is kept the same.

In the TCM encoder (or non-systematic convolutional encoder) of code rate R=2/3, which has constraint length m =4, (hence n, k, m = 3, 2, 4), the 2-bit input symbol is converted into a 3-bit symbol (i.e, code length=3) at the encoder output. Therefore the original 2-bit symbol is changed to a 3-bit symbol by channel encoding. However, the symbol rate is kept as before. For the case of an original bit rate 4.8 kbps, the encoder output bit rate is changed to 7.2 Kbps because of the coding rate 2/3. However, the symbol rate is still 2.4 ksps because only the number of bits per symbol is changed.

The encoded symbols are fed to the following interleaver in parallel format because the interleaving element is written as a binary 3-bit symbol unit. However, the serial format also can be used for the case when integer values (0 to 7) are needed for future use.

At the interleaver, the 2-dimensional array of 128 3-bit symbols is sequentially stored in row by row for interleaving. The dimension 128 comes from the two major parameters, span length and interleaving depth, that must be determined from the fade duration statistics. In our case, a depth of 16 and span length of 8 is used yielding an 8 X 16 array. Because the interleaving elements are 3-bit symbols, we can store 384 bits of encoded data at a single interleaving cycle. The expansion of the block size of the interleaver is restricted by the transmission delay, because interleaving is usually

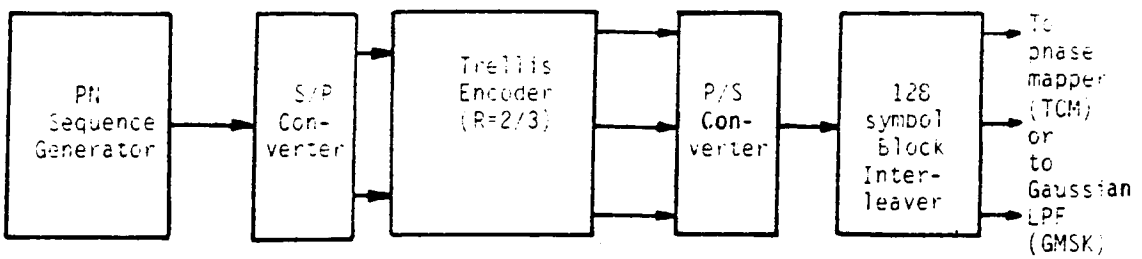

Figure 60. Noncoherent TCM 8-DPSK and DGMSK system model block diagram : Transmit Part A.

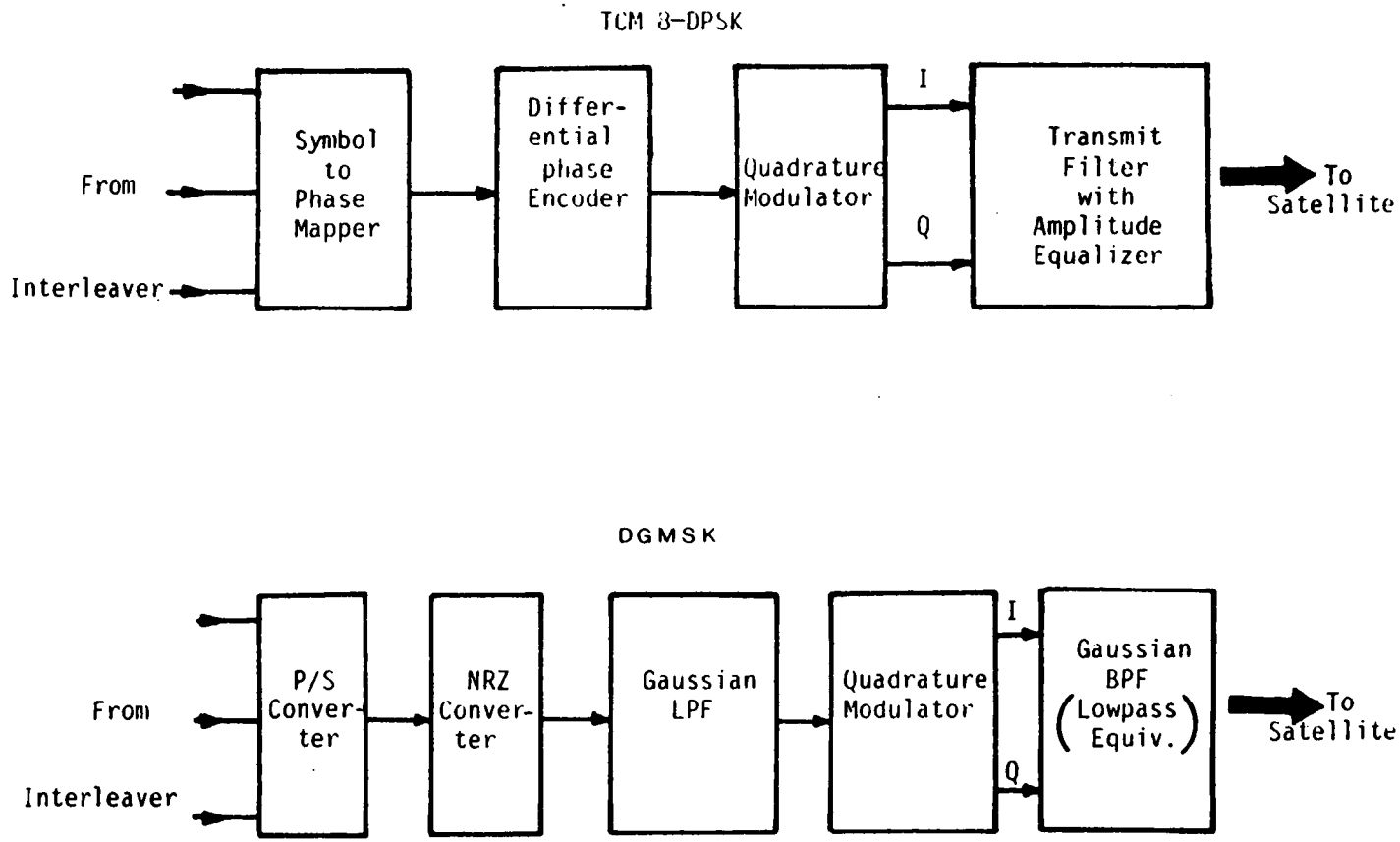

Figure 61. Noncoherent TCM 8-DPSK and DGMSK system model block diagram : Transmit Part B.

possible only after a whole block is filled to a predetermined size. Once the writing or storing procedure is finished, stored symbols are provided to the following functional blocks such as the 8-phase signal mapper in the TCM 8-PSK case, or the binary to NRZ converter in the DGMSK case.

Transmit Part B (Fig.61)

This part of the system model performs the differential encoding or differential phase mapping, Gaussian pre-modulation, carrier (IF) modulation, and filtering. Fig.61 shows the functional modules for this part.

The interleaved symbol stream with 3-bit binary data is directly provided to the 8-phase mapper in the TCM 8-PSK case, or passes through the binary to NRZ converter in the DGMSK case for differential encoding. In the TCM case, the optimally partitioned signal set previously depicted in Fig.53 in Chapter 4 is individually assigned to 1 of 8 phases in a circular symmetric signal constellation with $\frac{\pi}{8}$ phase spacing. Therefore, 1 of 8 symbol phases is assigned to the input symbol for each symbol duration.

Once phase mapping is finished for the whole 128 symbols, differential phase mapping starts. In this procedure, an initial dummy phase is added to the first symbol phase, and the second phase is added to the previous differential phase mapper output phase and the same operation is repeated until 128 symbols are differentially encoded.

The differentially encoded phase is changed into complex envelope form with a predetermined carrier amplitude in the quadrature modulator and provided to the transmission filter for waveform shaping to reduce the out-of-band spectrum. In the TCM case, a square root raised cosine Nyquist filter with roll-off factor 1.0 and Nyquist frequency of 1.2 KHz (half of the symbol rate) is used for this purpose. The spectrally shaped TCM- 8PSK signal with differentially encoded phases is finally transmitted to the satellite.

In DGMSK, the procedures for differential encoding, modulation, and filtering are a little different from those of TCM 8-DPSK. The interleaved symbol stream is changed into serial form at first for differential encoding. In differential encoding, as was noted in Chapter 4, it is not necessary to encode the input data stream when a 1-bit differential detection scheme is assumed. (Note that we already assumed 1-bit detection only.) Therefore, the serial output symbol stream is directly provided to the Gaussian baseband filter for spectral shaping while maintaining the phase continuity as is typical in the MSK type signal.

However, prior to Gaussian filtering, the process of converting binary data into NRZ data is required, and a binary/NRZ (B/N) converter in the block diagram performs this function. Once the NRZ converted bit stream is given to the Gaussian filter represented by Eq.(4.25), the output yields the time convolution of the filter function and input bit stream, and this turns out to be the phase of the transmitted signal if a phase constraint of $\frac{\pi}{T_s}$ is included in the process.

This continuous phased signal is modulated by the quadrature modulator as in the TCM case, and the output of this modulator is changed into its complex envelope for baseband simulation. This premodulated DGMSK signal is provided to the transmission filter. This filter is no longer the Nyquist filter in DGMSK. A Gaussian bandpass filter is normally used for the final spectral shaping before transmission to the satellite. In our modeling, this filter is modeled by its lowpass equivalent filter, as was mentioned earlier in this chapter.

Receive Part A (Fig.62)

The first part of the receive side depicted in Fig.62 consists of the receive (Rx) bandpass filter, a differential phase decoder for TCM 8-DPSK or a 1-bit differential detector for DGMSK.

In TCM 8-DPSK, the transmitted signal which was faded and corrupted by the down-link noise, is bandpass filtered with its lowpass equivalent to reduce the channel noise. A matched filter implemented by a square root raised cosine filter (as used in the transmitter, with the same filter parameters but without equalization), is used for this purpose.

This filtered signal is forwarded to the differential phase decoder for phase retrieval. In this phase decoding step, exactly the reverse operation of differential phase encoding is performed to find the original phase. In this method, the received signal in complex envelope form is used to get the initial phases from the sampled values. From the real part and imaginary part of the sample of the filtered signal, the phase of this sample is found by taking the inverse tangential value. This process is repeated for the whole 2048 time samples to get the phase trajectory.

To get the original phase, the dummy phase (which is the same as was used in the encoding process) is also used. The initial TCM phase trajectory is delayed by one symbol duration, corresponding to 16 time samples, then the dummy phase is used to fill the first symbol sample position (amount to 16 samples phases). The dummy phase symbol is subtracted from the the original phase trajectory. The result is the original transmitted phase trajectory, expanded in its sampled version.

The optimum sampler finds the most stable phase for every 16 sample phases, from 2048 phase samples, to get the estimated phase for each symbol transmitted. Once estimated phases are found, the corresponding signal set(3-bit symbol) is assigned for the phase of the 128 symbols. The decision criteria for this will be explained in detail at the component modeling level. However, the recovered symbols from the process of differential phase decoding are not the original symbols, but the interleaved version of them. So they are forwarded to the deinterleaver for recovery.

In DGMSK with 1-bit differential detection, the input signal is band-limited by the receive(Rx) filter and thus has a time varying envelope and phase. The IF filter, implemented by its lowpass equivalent, is modeled as a Gaussian bandpass filter as in Eq.(4.25) and Eq.(4.27). This filtered signal is then forwarded to the 1-bit differential detector, the subsequent lowpass filter, and hard decision logic.

Once this filtered signal is given to the 1-bit differential detector in DGMSK, the signal is processed in two ways as was depicted in Fig.51. For the path where there is no delay element, the input signal to the differential detector is directly applied to the multiplier without any further processing. For the delayed-arm path, the input signal is one bit delayed and shifted 90 degrees. By

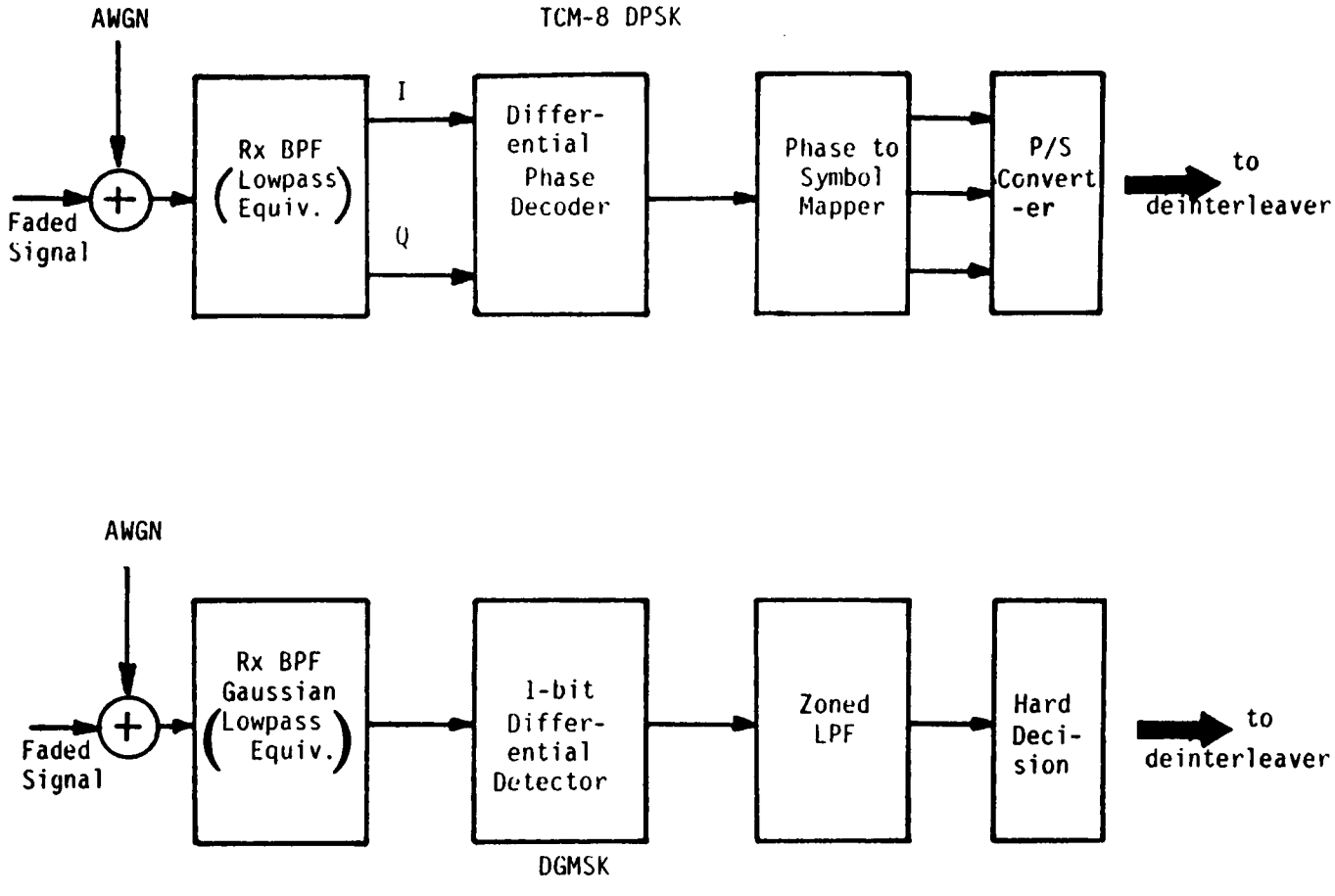

Figure 62. Noncoherent TCM 8-DPSK and DGMSK system model block diagram : Receive Part A.

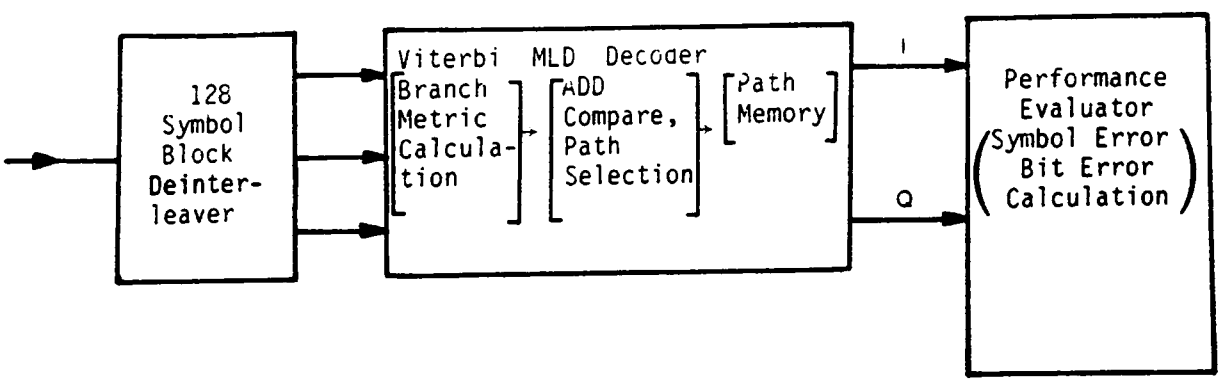

Figure 63. Noncoherent TCM 8-DPSK and DGMSK system model block diagram : Receive Part B.

multiplying these two signals, we can get the decision variable for the hard decision(decide binary 1 or 0) as expressed in Eq.(4.31) or in Eq.(4.33).

Before hard decision, the differential decoded or detected value in analog form is smoothed by the lowpass filter to get a stable analog amplitude. By sampling this amplitude at the center of the bit interval T_b for every bit duration, positive or negative values can be found. If we assign the positive value as binary 1 and binary 0 for the negative, a hard decision can be made for every transmitted bit. Note that the decision is no longer made with the symbol duration in DGMSK. Because of this nature, the output from the differential detector in DGMSK is usually in serial format. This serially formatted bit stream is directly connected to the following deinterleaver.

Receive Part B (Fig.63)

The final step for system modeling in noncoherent DGMSK and TCM 8-PSK is the receive part B depicted in Fig.63. This part consists of a block deinterleaver for 128 symbols, a TCM decoder for TCM 8-DPSK and a Viterbi MLD (Maximum Likelihood Decision) decoder for the convolutional decoder, and a performance evaluator.

The differentially decoded serial bit stream of DGMSK data, or the parallel symbol stream (3-bit symbol in TCM) is forwarded to the 128 symbol block deinterleaver. Because the block interleaver/deinterleaver are designed to accept a serial input only, the parallel input in the TCM case is changed into a serial form by using a parallel to serial (P/S) converter first.

This serial input bit stream corresponding to 128 encoded symbols is stored in the deinterleaver column by column at the write-in process. Once the write-in process is finished, deinterleaving starts. Because interleaving and deinterleaving are complementary operations, the read-out procedure in the deinterleaver is the same as the write-in procedure in the interleaver, i.e, the stored symbols are read out row by row.

After deinterleaving, the TCM encoded 3-bit symbols, or the Gaussian MSK 3-bit symbols, are now arranged in their original sequence. The only thing left for information recovery is the decoding process. Because basically the same encoder with the same code rate was used in the channel encoding process, decoding can be described together for the DGMSK and TCM 8-DPSK cases.

The trellis decoder in our case, for the special case of a general TCM encoder, is the same as the convolutional decoder using the Vitebi algorithm, if a hard decision metric is used. If soft decision is used for TCM only, a special decoder must be designed for this purpose, and it is impossible to use the same decoder both for TCM 8-DPSK and DGMSK. Because of this, an effort was made to simplify the design process of the complex decoder. Although soft-decision is mainly used in TCM schemes, hard decision also works well, and it is not necessary to make the system complicated. So the same decoding algorithm was used here for two cases of digital modulation.

The decoding process starts from the branch metric calculation in the trellis diagram or trellis table. For a given input symbol, all the possible paths or branches are searched by calculating the anticipated branch metric for all possible input symbols. The metric used is the Hamming distance, and this is the difference between the current symbol and the previous or the next symbol. Depending on the subsequent symbol, metrics are calculated again at the branches to find the largest branch metric path. This path, called the survival path, is kept for each transition of the symbol. This processes of calculating branch metrics, comparing the path metric at every transition and determining the optimal path is called the " Viterbi algorithm using MLD " [97],[105].

By finding the survival path and the comparing path metric in the code trellis, the original transmitted 2-bit symbols are found. For this recovery, the decoder must store the encoder state transition diagram or table to find which 2-bit input was encoded into any specific 3-bit encoder output that was provided from the deinterleaver. Therefore, in a practical implementation, a large amount of memory is allocated for this purpose. In our model, a large table of multi-dimensional arrays was assigned to store these data.

From the recovered 2-bit symbol stream, we can find the symbol error rate or the bit error rate by comparing all the transmitted bits and the recovered bits. Because of noise and fade in the

down-link, some bits may be incorrectly decoded and thus cause errors. This phenomenon gets severe as the noise power is increased or the fading effects become severe.

Contrary to the analytic calculation of error rate used previously, the method of error counting, based on the transmission of a large number of symbols, is used here. It takes a long time and is expensive to get reliable error performance, comparable to the results found in the analytic calculation. There also exists a risk that the whole result may not be valid depending on the interpretation of the result. However, this simulation model has unique advantages with which other methods cannot compete. The system model and simulation methodology are no longer theoretical, rather, they are more practical than any other simulations ever implemented.

5.3. Component Level Modeling

As the second step in modeling, functional components are modeled based on the system level block diagram. The principle of a modular structure was generally kept in component modeling to minimize the effects of modifications, and the inclusion or exclusion of specific functional components.

By using a modular structure in component modeling, modules in the system block diagram coincide with subroutines in the simulation program. Therefore, without changing the main stream of simulation, various tests are possible and system flexibility is enhanced.

Even though the principle of a modular structured design was kept in the component modeling process, the description is done based on the functions of the modules, i.e, similar functional components are explained together to avoid repetition or confusion. The component models in the system block diagrams for the four modulation schemes, the coherent QPSK and MSK, and the differential versions of TCM 8-DPSK and DGMSK, are classified into the following functional groups for convenience of description.

1. Random symbol generation
2. Coherent QPSK/MSK modulators and demodulators
3. Transmit and receive filtering
4. Satellite transponder nonlinearity
5. Trellis encoding and decoding
6. Differential encoding and decoding
7. TCM 8-DPSK/DGMSK modulators and demodulators
8. Interleaver and deinterleaver
9. Method of fading effect insertion
10. Performance evaluator

Based on this classification, functional component modeling procedures are described in detail. However, repetition of a basic principle or algorithm that had already been described earlier has been avoided whereever possible.

5.3.1. Random Symbol Generation

Symbol generation is the first step in channel simulation regardless of modulation type used. To generate the required symbols, a pseudo random number generation is required. The random generator must exhibit good randomness to get valid statistics.

Two slightly different types of pseudo random number generators were used for QPSK/MSK and for TCM 8-DPSK/DGMSK. However, the required processes from random number generation to symbol generation are the same, so the description given here can be applied to any 2-bit symbol generation case.

In coherent QPSK and MSK, the algorithm of a uniform pseudo random number generator routine 'GGUBS' of IMSL was used to generate the random binary input sequence for the simulator. With the externally provided 'dseed' and 'number of desired numbers', random binary numbers 0 or 1 are generated with a uniform distribution. For the NRZ data stream, the randomly generated 0s are assigned as -1s while keeping all the 1s as +1s.

With the generated random binary or NRZ sequence in serial format, the desired symbols are generated by a process of demultiplexing or serial to parallel (S/P) conversion. In Fig.64 (a), blocks for the pseudo random number generator and the symbol generator are shown, along with the QPSK/MSK modulator. By S/P conversion, the even ordered bits and the odd ordered bits are serially collected to constitute the two separate serial bit streams. For notational convenience, the even ordered bit stream is called the I channel and the odd ordered bit stream is called the Q channel. This separation is especially useful for quadrature modulation, as was used in QPSK/MSK in our simulator.

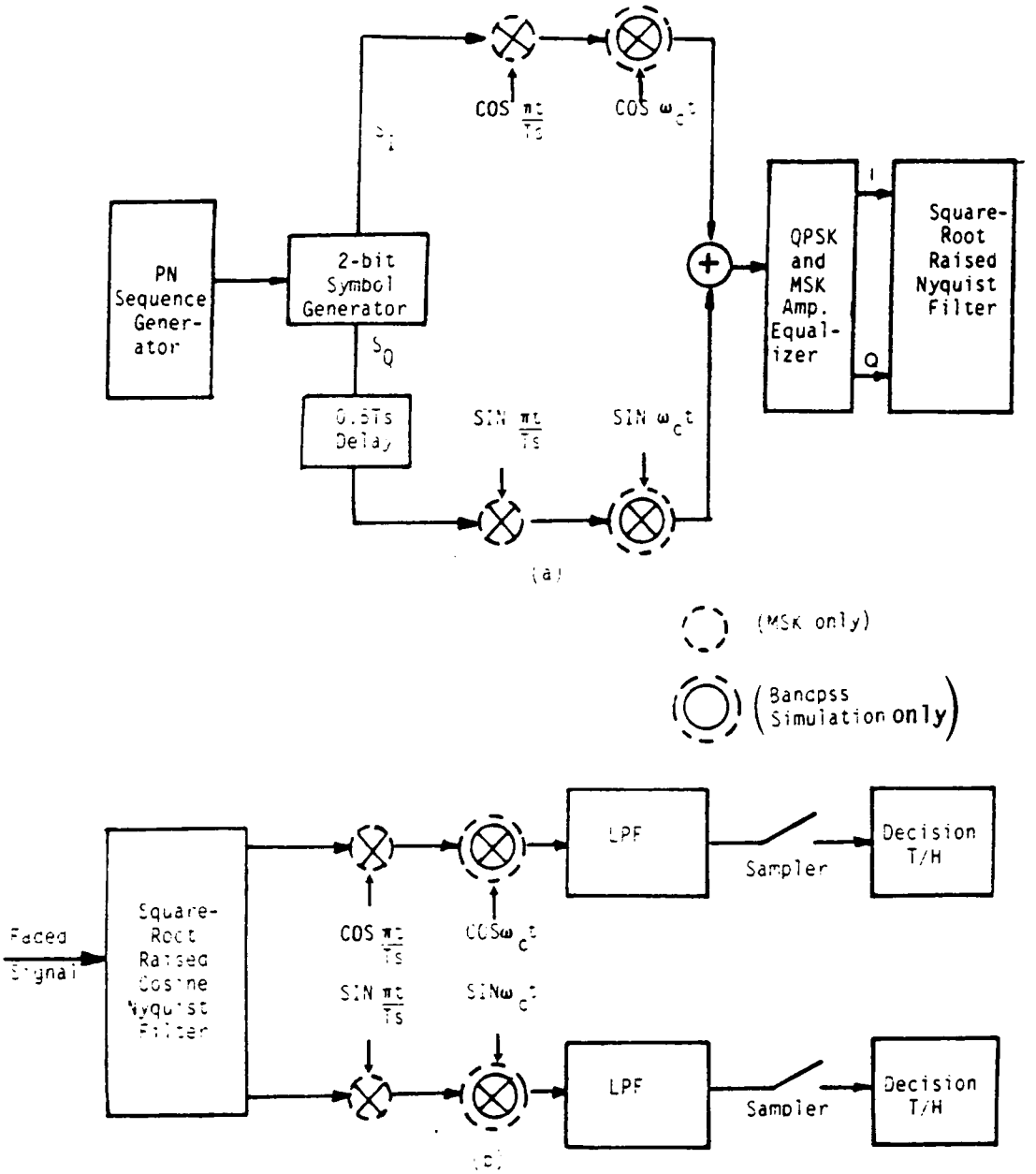

Figure 64. Block diagrams of coherent QPSK/MSK (a)Modulator with symbol generator and Tx filter (b) Demodulator with lowpass filter and decision circuit.

From these two separate serial bit streams, 2-bit symbols are generated by taking one bit from each channel. The bits are synchronously time aligned, except in MSK. The 2-bit pair or di-bit is the defined (original) symbol in our simulation. Remember that all the digital modulation schemes we are dealing with have a rate of 2 bit/Hz before channel encoding.

In MSK, the symbol generation is different because of the required relative 1-bit delay between the quadrature data sequence I channel and the Q channel. To give a relative delay, the I channel data stream is made to advance by one bit interval rather than delaying the Q channel data stream. Therefore, synchronously aligned I channel and Q channel data are provided to the quadrature modulator in QPSK, while 1-bit skewed I and Q channels data streams are applied to the MSK modulator.

In TCM 8-DPSK and DGMSK, symbols are generated in the same manner as in the QPSK case. However, a more advanced uniform random number generator was used to enhance the randomness and to generate a large amount of random data with an automatic seed change. A portable uniform random number generator 'RAN 0' [106] was selected with minor modification for our purpose. The generated 2-bit symbols are forwarded to the channel encoder in parallel format to be encoded into 3-bit symbols when a code rate of 2/3 is used.

5.3.2. Coherent QPSK/MSK Modulators and Demodulators

Based on the review of coherent QPSK and coherent MSK in Chapter 4, the modulators and demodulators for the two schemes are basically the same. MSK needs additional sinusoidal pulse shaping, and the bit streams used in MSK are skewed by 1 bit duration. Because the skewing is already done in the symbol generation procedure, only the pulse shaping is needed in the MSK signal generation and demodulation module.

The even and the odd bit streams are applied to the modulator with half of the original incoming bit rate, and modulate the in-phase and quadrature phase components of the carrier. After carrier

multiplication, these two orthogonal components are added. When the input data stream is applied to the modulator, it is necessary to make the carrier and shaping function (MSK only) into a time sampled form to get time sampled data for the modulated carrier. Therefore the modulated signal can be expressed as the sum of two quadrature components :

$$X(t)_{QPSK} = S_I(t)\ \cos\omega_c t + S_Q(t)\ \sin\omega_c t \tag{5.1}$$

$$X(t)_{MSK} = S_I(t)\ \cos\frac{\pi t}{T_s}\ \cos\omega_c t + S_Q(t)\ \frac{\pi t}{T_s}\ \sin\omega_c t\ , \tag{5.2}$$

where $S_I(t)$ and $S_Q(t)$ respectively denote the I channel and Q channel data streams. The two terms in Eq.(5.1) represent the two BPSK signals which can be detected independently due to the orthogonality of the carrier. In the simulation model, the above QPSK modulator output is expressed in the following compact form, instead of Eq.(5.1).

$$X(t)_{QPSK} = \sqrt{2}\ \cos[\omega_c t - \theta(t)]\ , \tag{5.3}$$

where $\theta(t) = \tan^{-1}(\frac{S_Q(t)}{S_I(t)})$ and $\theta(t)$ takes the values of 45, 135, 225, and 315 degrees, depending on the combination of I channel input and Q channel input. The dibit forms are (1, 1), (-1,1), (-1,-1), (1,-1). In MSK, the above Eq.(5.2) can be simplified by using a trigonometric function and the fact that I and Q channel data are always $\pm$ 1, then

$$X(t)_{MSK} = \sqrt{2}\ \cos[\omega_c t + b_k(t)\ \frac{\pi t}{T_s} + \phi_k]\ , \tag{5.4}$$

where b_k is 1 when the I-channel and Q-channel data have opposite sign and -1 otherwise, and ϕ_k is 0 or π when the I-channel data is +1 or -1.

Fig.64 (a) shows the combined modulator for the coherent QPSK and MSK along with symbol generation and transmit filters. In this diagram, the dotted circled parts illustrate the sinusoidal shaping function necessary for MSK only.

The QPSK/MSK demodulator models are depicted in Fig.64 (b) along with the lowpass filters, samplers, and decision logic. As can be seen from the model, demodulation is the exact reciprocal of the modulation process.

The nonlinearly amplified and band-limited signal from the satellite transponder is corrupted by downlink noise and ISI. In addition, this signal experiences fading. At the input bandpass (IF) filter, modeled with its lowpass equivalent, the received signal in time sampled form is converted to the frequency domain by the FFT routine and multiplied with the discrete frequency components of the receiving bandpass filter, then converted to the time domain by the IDFT, as in the Tx filter case.

In the demodulator, this filtered signal is multiplied by the locally generated carrier. However, in baseband simulation, the processes of carrier generation and multiplication are not needed. Therefore, the complex-envelope received and filtered signal is directly forwarded to the following I&D (Integrated and Dump) circuit, or lowpass filter(ideal brick-wall filter) in the QPSK case. In MSK, sinusoidal pulse shaping is needed before lowpass filtering.

In this step, after IF filtering, the input signal in complex form is separated into its real part and imaginary part for the reconstruction of I and Q channel signals, for the convenience of hard decision based on the sampled values of the two orthogonal channels.

In principle, the demodulated signal passes through the integrator,where integration is carried out for one symbol duration. Carrier multiplication and integration in a linear noise-free system constitute the optimum correlation receiver for an infinite bandwidth signal. But for the band-limited signal in a practical situation, the integrator is replaced with a conventional lowpass filter. Therefore, instead of an I&D circuit, an ideal brick-wall type low pass filter(not the lowpass equivalent) with a cutoff frequency of $\frac{R_s}{2}$ (where R_s is the symbol rate) is used in modeling.

For this final lowpass filtering, the separated I and Q channel signals are converted into their complex form again by creating an imaginary part with all 0s, and all filtering processes are performed separately on the two parts. This demodulated and smoothed signal in two orthogonal channels is then doubled to recover the estimated QPSK and MSK signal amplitude before sampling and hard decision (see Eq.(4.4)). Time sampling is performed on this signal with the correct sampling

rate. The sampling instants must be determined from the signals. It is necessary to find the optimal sampling time empirically to ensure minimum bit error.

For the hard decision case, a decision threshold of 0 volt is used in QPSK/MSK. If the sampled value is positive, a binary 1 is assumed to have been transmitted and vice versa. In the hard decision case, two orthogonal binary or NRZ data streams for the I and Q channels are made. To recover the original transmitted serial bit stream, a parallel to serial (P/S) converter is used. However, the sampled values are kept for final performance evaluation.

5.3.3. Transmit(Tx) and Receive(Rx) Filtering

In channel simulation, where digital modulation schemes dominate, the design and selection of the channel filters plays an important role in deciding final system performance. The prevention or rejection of ISI(Inter-Symbol Interference) and adjacent channel interference are critical factors in performance degradation, as well as fading in the radio link.

ISI is the direct result of bandwidth limitation when a sequence of pulses is transmitted in a band-limited channel, as in satellite communication. Interference between consecutive bits causes amplitude fluctuations in the synchronously sampled signals. If we classify the filters used in the channel simulation into transmit filters and the receive filters, the major role of the transmit filter is the spectral shaping of the bit stream to minimize ISI.

Adjacent channel interference is the result of channel nonlinearity in the TWTA. The amplitude nonlinearity in a TWTA causes spectrum spreading ; the filtered sidebands of the carrier tend to resume their original levels after passing through a nonlinear amplifier, and this causes adjacent channel interference. Even though a linear high power amplifier is assumed in LMSS, and only a single channel is assumed in our simulation, it is often necessary to consider the effect of adjacent channel interference in a band-limited channel. In addition, the effect of fading must be considered because of its nonlinear effect on the retransmitted amplitude and phase. From this point of view, the

major role of the receive filter and the optional output multiplexer filter at the satellite transponder should be the rejection of down-link noise and adjacent channel interference.

In this section, the process of designing and modeling filters to minimize ISI and possible adjacent channel interference is described. Because most of the background information and design procedures are already well defined in the relevant literature, only the main ideas of modeling will be described here, with a brief introduction to filter characteristics. The basic assumptions used in the filter design are :

1. All filters are real-valued frequency domain filters, and thus they have zero phase response for simplicity and no phase delay in the filter is assumed.
2. For baseband simulation, all the bandpass filters required in the simulation process are modeled with their lowpass equivalents.
3. All the input and output signals to and from filters are expressed in their complex envelope form for baseband simulation.
4. For time and frequency domain conversion, a 2048 (or 4096) point FFT (Fast Fourier Transform) and an IDFT (Inverse Discrete Fourier Transform), based on the Cooly-Tukey Algorithm [107], are used interchangeably.

The process of baseband filtering with a complex enveloped input signal and a lowpass equivalent filter response can be briefly described as follows :

To simulate filtering in general, it is necessary to have time-sampled values of the input signal and the filter function expressed in the time or frequency domain. If x(t) is the input and h(t) is the filter impulse response, the filtered output y(t) can be expressed in the time domain as,

$$y(t) = x(t) * h(t) \ , \tag{5.5}$$

and its Fourier transform is written as

$$Y(f) = X(f)\, H(f) \ , \tag{5.6}$$

Because the modulator output can be expressed in complex envelope form as

$$z(t) = x_r(t) + j\, x_i(t) \ , \tag{5.7}$$

the corresponding Fourier transform of the complex envelope of the filter output will be

$$\hat{Y}(f) = X_r(f)\, \hat{H}(f) + j\, X_i(f)\, \hat{H}(f) \ , \tag{5.8}$$

where $\hat{Y}(f)$ and $\hat{H}(f)$ are the Fourier transforms of the complex envelope of the filter output and the filter impulse response respectively.

Filtering starts from the transformation of the time-sampled values of the input signal into frequency domain values by an FFT. Because the FFT and IDFT routines are programmed to accept and output complex values, if a real-valued signal is to be processed, it must be expressed in complex form first by substituting zero in its imaginary part. Multiplying the two frequency responses and using the IDFT yield the desired filtered output in a time domain expression. Because of the inherent property of the FFT and IDFT routines used here, the output of the IDFT has the same number of time samples as before filtering. The simulated filters are lowpass equivalents of the bandpass filters. The response of the filter was assumed to be zero phase, so the equivalent filter's frequency response is symmetrical contrary to the more generally used nonsymmetric form of the equivalent lowpass filter.

The complex envelope of the baseband signal is input to the desired filter. This baseband complex envelope without a carrier component is multiplied by the frequency response of the lowpass equivalent filter corresponding to the desired bandpass filter, which makes the filtering process much simpler and easier to manipulate. The carrier contribution can easily be included at any desired point in the simulation. This is the baseband simulation, and is preferred because of its simplicity compared to the much less efficient bandpass simulation.

Five kinds of analog bandpass filter are simulated with their lowpass equivalent frequency response, and two lowpass filters are modeled. These are the raised-cosine Nyquist filter, square root

raised-cosine Nyquist filter, Butterworth filter, Chebyshev filter, Gaussian filter, and Gaussian pre-modulation lowpass filter and conventional lowpass(brick-wall) filter.

Because of the relative importance of the Nyquist type filters, the modeling procedure for the first two filters is described in detail, as well as the required amplitude equalizer in this section. For the other filters, except the Gaussian type filters, the characteristics can easily be found in the relevant literature, so individual descriptions are not included here.

The raised cosine Nyquist filter is the closest practical approximation of the Nyquist minimum bandwidth theorem [29] for ISI-free transmission. Eq.(5.9) shows the corresponding frequency response used in modeling this filter under the constant zero phase response assumption.

$$H(f) = \begin{cases} 1 & 0 < f < f_n - f_x \\ \frac{1}{2}\left[1 - \sin\frac{\pi}{2r}\{f/f_n - (1-r)\}\right] & f_n - f_x < f < f_n + f_x \\ 0 & f_n + f_x < f \end{cases} \tag{5.9}$$

In this equation, f_x is a frequency determined by the roll-off factor, r, and f_n is the Nyquist frequency. The roll-off factor r is the ratio of the occupied bandwidth to the minimum bandwidth required for ISI-free transmission. This minimum required bandwidth is defined as half the maximum symbol rate by the Nyquist theorem mentioned above.

For the effective reduction of possible ISI, matched filters are frequently used in which the frequency response of the two filters (one in the transmit side and the other in the receive side, for example) must be complex conjugate. The square-root raised cosine Nyquist filter meets this condition if it is modeled so that the combined frequency response of two identical filters equals the response of a raised cosine Nyquist filter, while keeping the condition of zero phase. Therefore, by making each filter have the squared root magnitude of Eq.(5.9), a practical model of a matched filter can be realized.

However, the Nyquist-type filters approximated above produces zero ISI only for impulse transmission. Neither the rectangular pulses used in QPSK, nor the sinusoidal pulses used in MSK are impulses. To meet the generalized Nyquist theorem [29], in which the input signal must be an

impulse, transformation, such as pre-filtering, is needed with the non-impulse type signals before filtering. Amplitude equalization is used in our case when zero phase response is assumed.

In the generalized Nyquist theorem, the transmission of arbitrary pulses (other than impulses) requires pre-filtering in which the spectrum of the input signal is made constant over the occupied bandwidth. This is necessary to keep the frequency response of the channel the same as for impulse excitation [29]. Therefore, for the rectangular type inputs such as QPSK or TCM 8-DPSK, an $\frac{X}{\sin X}$ type equalizer with $X = \frac{2\pi f T_s}{2}$ is needed. Eq.(5.10) shows this function with radian frequency ω and bit rate R_b

$$\frac{X}{\sin X} = \frac{\omega/R_b}{\sin(\omega/R_b)} \quad . \tag{5.10}$$

In the case of MSK-type signals such as MSK or DGMSK, the excitation is neither an impulse nor a rectangular pulse. Because the pulse shaping function in MSK-type modulation is a half wave sinusoid such as $\cos(\frac{\pi}{T_s}t)$, the Fourier transform of this function as in Eq.(5.11) should be found for correct amplitude equalization.

$$F\left[\cos\frac{\pi t}{T_s}\right] = \frac{2T_s}{\pi}\frac{\cos(\pi f T_s)}{1-2fT_s} \quad , \quad -\frac{T_s}{2} < f < \frac{T_s}{2} \quad . \tag{5.11}$$

The required amplitude equalization or the pre-filtering for a flat frequency response must be the inverse of the above transform

$$X(f) = \frac{1-(2fT_s)^2}{\cos(\pi f T_s)} \quad . \tag{5.12}$$

Gaussian filters are frequently used for practical implementation of spectrally efficient modulations such as DGMSK, generalized MSK, or TFM (Tamed FM). A premodulation lowpass Gaussian filter is usually employed to control the binary or NRZ input data spectrum before modulation, while a Gaussian bandpass filter is usually used for noise and channel induced ISI

reduction. For the practical implementation of this filter, the following frequency response function is used in modeling.

$$H(f) = \sqrt{\pi}\ e^{-(\pi f/\alpha)^2}\ , \tag{5.13}$$

where α is a parameter related to the 3 dB bandwidth of the filter defined by Eq.(4.25). However, for most applications, the parameter time-bandwidth (BT) product is used. From the bit rate used, the signal interval can be found first, and then for a fixed BT product, α can be found from the relation denoted in Eq.(4.25). By adjusting BT, α in Eq.(5.13) can be controlled.

In simulation programs based on these models, various parameters must be chosen for proper filtering. These are the optional parameter for the modulation scheme selected (QPSK and MSK case only), the desired filter type, the mode which indicates the filter is used in the Tx or the Rx part of the system, the optional parameter that indicates the inclusion of an amplitude equalizer, and the basic filter parameters such as roll-off value, Nyquist frequency, number of poles, ripple value, 3 dB frequency for a lowpass filter or time-bandwidth product.

5.3.4. Satellite Transponder Nonlinearity

In a LMSS, linear high power amplification in the satellite transponder has been assumed thus far. Nonlinear effects can occur in the satellite output, caused by the nonlinear TWTA. Modeling of this nonlinearity is indispensable in conventional satellite link simulation, and this modeling has itself been the major subject of many researchers. In this section, modeling procedures for the nonlinearity in a TWTA are described. In modeling the TWTA, only the helix-type TWTA that does not contain memory is used.

The TWTA exhibits two types of nonlinearities: AM/AM conversion effects and AM/PM conversion effects. These occur when a time varying bandpass signal is input to the TWTA. The envelope fluctuation in the input signal caused by bandpass filtering is converted into nonlinear

variations in the output amplitude and a phase shift. Of the many models for this nonlinearities [108],[109],[76], Saleh's [76] simple two parameter formula for the amplitude and phase is the best.

In his model, the output of the TWTA is expressed as

$$y(t) = A[r(t)]\ \cos\{\omega_c t + \psi(t) + \phi[r(t)]\}\ , \tag{5.14}$$

where A(r) represents the AM/AM conversion function, and $\phi(r)$ represents the AM/PM conversion function. These two function can be found from the following two formulas [76],

$$A(r) = \frac{\alpha_a r}{(1 + \beta_a r^2)} \tag{5.15}$$

$$\phi(r) = \frac{\alpha_\phi r^2}{(1 + \beta_\phi r^2)} \tag{5.16}$$

Therefore, to get the output in Eq.(5.14), we must find the value of A(r) and $\phi(r)$ first. Curve fitting procedures with measured data from specific TWTA curves are generally used for this purpose.

Now let us explain the practical modeling procedures. The modeling procedure can be divided into 3 major steps : input signal modeling, AM/AM and AM/PM nonlinear function modeling, and normalization/back-off adjustments.

The input signal applied to a TWTA is always a bandpass signal. This signal has phase and envelope different from the modulated signal because it has passed through a bandpass filter. If a channel filter exists, the result is only the cascading of filter functions. In baseband simulations, the modulator output expressed in its complex envelope form passes through the lowpass equivalent of the desired bandpass filter, and the filtered output can be expressed as a complex envelope. The usual expression for the input signal to the TWTA is

$$x(t) = r(t)\ \cos[\omega_c t + \psi(t)]\ . \tag{5.17}$$

In complex envelope notation, this input is expressed by

$$z_1(t) = r(t)\, e^{j\phi(t)} \quad . \tag{5.18}$$

When the input bandpass signal $z_1(t)$ passes through the nonlinear TWTA, the output will be expressed in Eq.(5.14), and its complex envelope is written as

$$z_2(t) = A[r(t)]\, e^{j\phi(t)}\, e^{j\phi[r(t)]} \quad . \tag{5.19}$$

Therefore, the amplified amplitude is expressed as A[r(t)] and the phase will be denoted as $\theta(T) = \psi(t) + \phi[r(t)]$. The AM/AM nonlinear function A[r(t)] and the AM/PM nonlinear function are the same as Eq.(5.15) and Eq.(5.16). But to get the practical output for a specific TWTA, the four parameters that represent the relations of time varying input and the nonlinear amplitude function and nonlinear phase function, α_a, α_ϕ, β_a, and β_ϕ must be dectermined. Fig.65 shows the results of minimum mean-square error curve fitting procedures giving phase and amplitude values from the experimental amplitude and phase characteristic curves shown (15 point measurements).

Once the nonlinear modeling is finished, it is necessary to normalize the input envelope voltage (or power) to the saturation level. Many papers use different scales for the axis of these nonlinear curve such as dBm, volts(rms or peak). If we use volts as the scale, the unit of the input and output will be the volt. Usually the saturation level is arbitrarily set to 0 dB.

Depending upon the system requirement, it is frequently necessary to move the TWTA operating point from saturation to the desired point to improve the bit error rate. This is called back-off. Input back-off is usually given in dB. For example, an IBOF(input back-off) of 3 dB means the input level is reduced to one half of the input power for saturation of the TWTA output. Similarly, an OBOF (output back-off) of 3 dB means the output power is reduced to half of the output power level at satutation, i.e, the voltage is reduced to 0.707 times the saturated output operating voltage level.

Therefore, for the general case, X dB IBOF leads to the calculation of the new input operating point given by

$$r(t)_{IBOF} = 10^{-x/20} \quad . \tag{5.20}$$

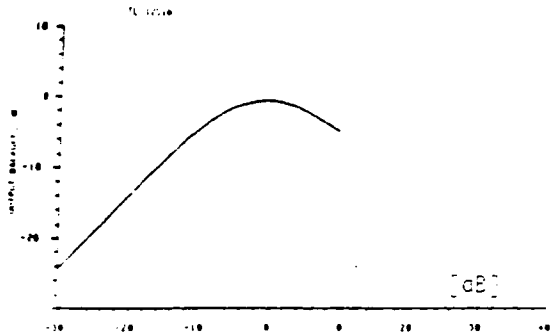

Amplitude

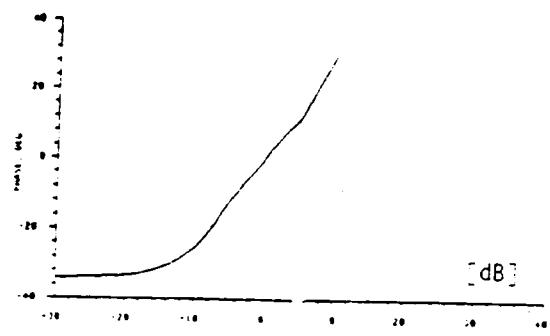

Phase

MEASURED AMPLITUDE AND PHASE DATA FROM CURVES ABOVE

SAMPLE POINTS	INPUT NORMALIZED VOLTAGE	DB	OUTPUT AMPLITUDE DB	VOLTAGE	OUTPUT PHASE DEGREE (RADIAN)
1	0.2	-14.0	-8.0	0.398	5(0.08)
2	0.4	-7.95	-3.0	0.708	14(0.244)
3	0.6	-4.44	-1.0	0.891	24(0.419)
4	0.8	-1.94	-0.3	0.966	31(0.541)
5	1.0	0.0	0.0	1.000	35(0.611)
6	1.2	1.58	-0.2	0.977	40(0.698)
7	1.4	2.92	-0.3	0.966	42(0.733)
8	1.6	4.08	-0.9	0.901	45(0.785)
9	1.8	5.10	-1.7	0.832	46(0.803)
10	2.0	6.02	-2.5	0.750	49(0.864)
11	2.2	6.85	-3.0	0.707	53(0.925)
12	2.4	7.60	-3.3	0.684	57(0.995)
13	2.6	8.30	-3.5	0.668	59(1.030)
14	2.8	8.94	-4.0	0.631	61(1.065)
15	3.0	9.54	-4.5	0.596	62(1.082)

OPTIMUM VALUES OF 4 AM/AM and AM/PM PARAMETERS

	14 POINTS	15 POINTS
α_a	1.98361	2.56074
β_a	1.01415	1.24726
α_ϕ	1.29179	1.58746
β_ϕ	1.12379	1.44647

Figure 65. Results of 15 point curve fitting from the TWTA characeristic amplitude and phase curves to obtain the 4 parameter values. (see 4 parameter values at the righit table)

Therefore the input back-off A[r(t)] and $\phi[r(t)]$ are easily found by replacing the argument r(t) with $r(t)_{IBOF}$. For X dB OBOF, the corresponding input level (voltage) r(t) is derived from the amplitude and phase model's nonlinear function as

$$A(r)_{OBOF} = 10^{-x/20} \quad . \tag{5.21}$$

When we substitute r in Eq(5.15) with r_{OBOF}, we get the second order relation

$$A(r)_{OBOF}(1 + \beta_a r_{OBOF}^2) = \alpha_a r_{OBOF} \quad , \tag{5.22}$$

By solving this 2nd order equation for r and taking the smaller root, the desired output back-off is given as

$$r_{OBOF} = \alpha_a - \frac{\sqrt{\alpha_a^2 - 4 A^2[r] \beta_a}}{2 A[r] \beta_a} \quad . \tag{5.23}$$

5.3.5. Trellis Encoding and Decoding

After symbol generation, channel encoding is assumed in the case of TCM 8-DPSK and DGMSK. In this section, the process of channel encoding by trellis code or convolutional code is described. As was mentioned earlier, we wanted to use the same coding scheme for TCM 8-DPSK or DGMSK. Trellis code using a special TCM scheme (see Chapter 4) with code rate 2/3 can be used for both TCM 8-DPSK and DGMSK. In reality, the TCM code used here is generated by a conventional convolutional encoder. Therefore, the explanation of the coding and decoding schemes used in these two digital modulation schemes is done here for both schemes. In the description, most of the terminologies used are for TCM.

The modeling procedure for trellis encoding can be divided into five steps based on the sequence of preparation of the encoder output. These steps are the selection of the generation structure, set partitioning, code search, encoder design, and signal to phase mapping(only for the TCM 8- DPSK case).

Before the selection of a generation structure, it should be remembered that TCM is a combination of coding and modulation. The generation structure must be the integration of the coding part and the subsequent signal mapping. This idea is well depicted in the general structure of an encoder/modulator for TCM in Fig.52 (Chapter 4).

There are two choices in the selection of a generation structure : a general structure and the special case of this general structure which was depicted and explained in Fig.52 and Fig.53 in Section 4.5. The decision factor in this selection is the trade-off between system complexity and the achievable coding gain from the increased free distance between the signal sets.

In practice, this decision turn out to be the selection of the number of redundant bits used in signal selection from the subset. If redundant bits (number of input symbol bits - number of bits used for convolutional encoding in the encoder) are permitted, as in the general TCM scheme, there can be more choices for signal selection per subset, and a relatively large distanced signal set can be

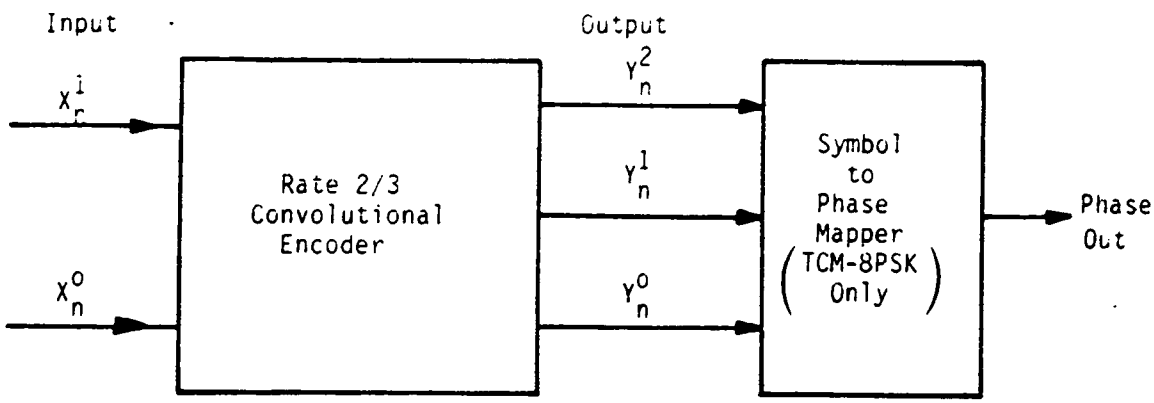

Figure 66. Selected special case of the general TCM generation scheme for TCM 8-DPSK and DGMSK code generation.

selected. In the special case, all the inputs bits are used for encoding. Therefore, no redundant bits are left for additional signal selection, because the subset contains a single signal to be transmitted, i.e, the number of subsets is the same as the number of signals.

For example, in the case of a general structure, if 3 bits from 5 parallel input bits are used for TCM encoding with a code rate 3/4, we have a 64-ary(2^5) signal set and 16 (2^4) subsets. In this case, the encoded 4 bits from each group of 3 input bits are uses to select one of the 16 subsets of the 64-ary signal set, while 2 uncoded bits (5 input bits - 3 bits for rate 3/4 encoding) are used to determine which of the 4 signals in this subset is transmitted. On the other hand, in the special case, all the 5 parallel input bits are used for encoding at a different code rate such as 5/6, and we have 64 subsets. Each of these subset has only one signal.

After comparing the two structures, we decided to use the special case because of its relative simplicity of implementation. Fig.66 shows this scheme for the Trellis coded 8-ary PSK used in our simulation model. Note that this structure is also used for convolutional code generation for DGMSK because of the identity of rate $m/m+1$ encoders. Eight different phases (signals) are needed at the encoder output from the 2-bit parallel input symbol defined by the symbol generation, so a code rate of 2/3 ($k=2$, $n=3$) is used in TCM 8-DPSK.

With the fixed special case TCM structure, the set partitioning must be done to find the optimal code that can achieve the maximum coding gain compared with the uncoded digital modulation scheme. Based on the procedure by Ungerboeck's [98] and the explanation in Sec.4.4, set partitioning is repeated up to 3 levels, as can be seen in Fig.67. The distance between signal sets, (subset in this case), is increased as the level goes up. At the bottom of the set partitioning diagram, assigned 3-bit binary symbols can be found. However, this assignment need not be unique if the relative distance between signals at the specific level is maintained.

Once the generation scheme is decided and set partitioning completed, the process of finding an optimal code search follows. Because the encoder is rate a 2/3 convolutional encoder, the parity

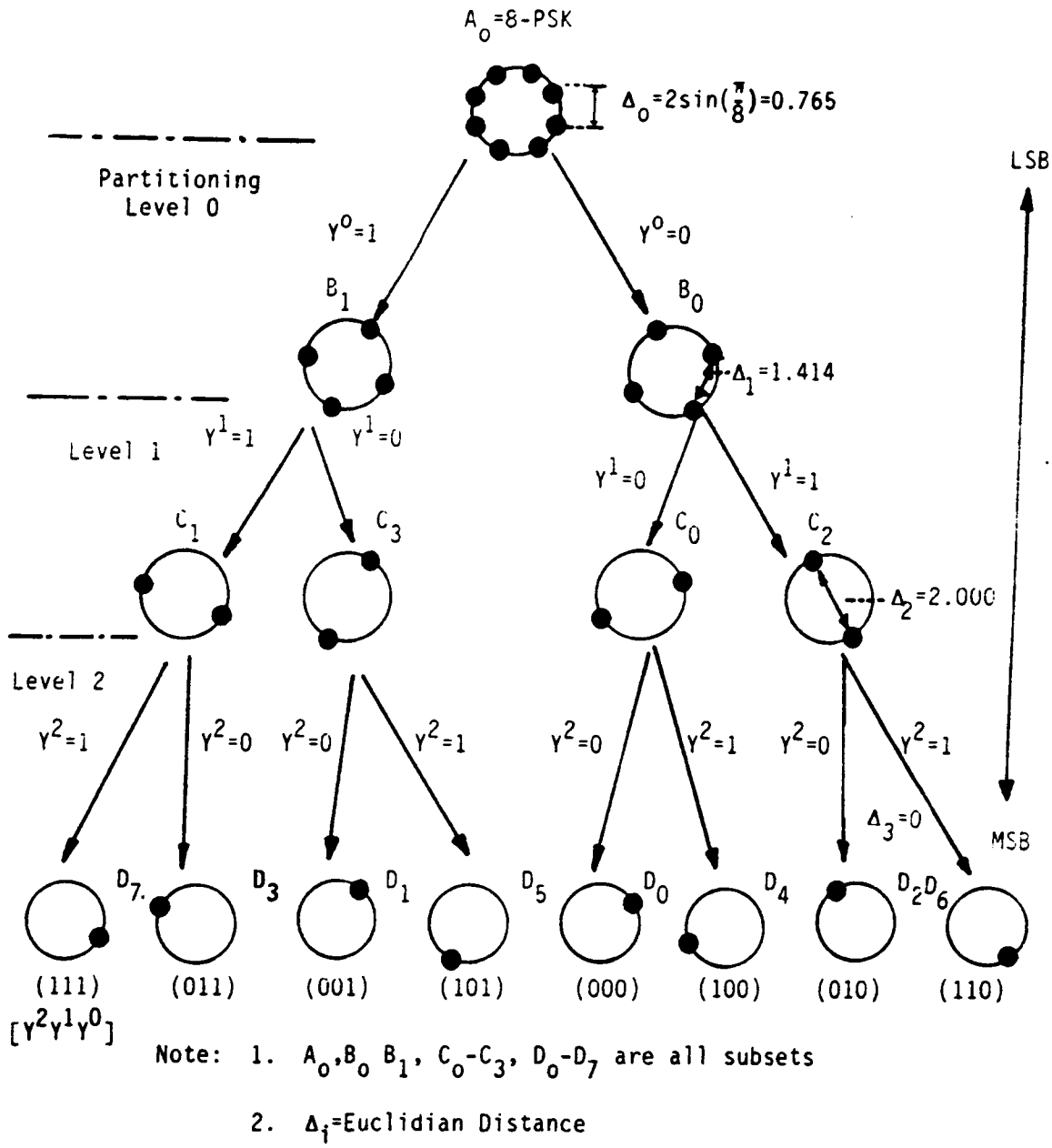

Figure 67. Set Partitioning of TCM 8-DPSK signal (this code is also used for the convolutional code for DGMSK).

check equation of a convolutional code is generally used to find the optimal trellis code. In the parity check equation, the constraint length ν is the key parameter for the code search. The object of this search is to find the code sequence that has maximum free distance between codes when the constraint length is varied. If the constraint length ν is increased for the same code rate R, coding gain is increased, as well as the number of state transitions. However, increased state transitions need more delays or storage elements, and thus system complexity is increased. Therefore, there must be some trade-off between code performance and system complexity.

This process is important, because the design of the encoder and decoder depends greatly on the constraint length and the maximum free distance found. In addition, coefficients for the parity check equation are decided in this process, and these coefficients as well as the constraint length ν decide the encoder structure. However, code search for a constraint length greater than 3 is usually done by computer because of the complexity involved. In our simulation, the code with constraint length $\nu = 4$ found by NASA JPL was used. This result is realized in the following encoder design.

Once the optimal code for the specific constraint length has been found, it is possible to design an encoder with predetermined code rate R. However, the code and its parity check equation define only the code sequence, not the input and output relations of the encoder. Therefore, there is no unique encoder for the code found, because the same code can be generated with a different type of encoder. Thus, the encoder design process can be regarded as an independent step from all the previous steps.

Two types of encoder scheme are usually used for code implementation. One is the systematic encoder with feedback, in which the input bits appear unchanged at the output. The other is the feedback-free or non-systematic encoder. Fig.68 shows the two possible encoder structures for our application, when the code rate is 2/3 and the constraint length ν is 4. The constraint length ν in the code is realized as the number of delay elements T or D in diagram, where T or D denotes a 1-bit delay. In the hardware implementation, this delay is frequently represented as the shift register length. If we use one of these encoders, we have 16 state transitions because there are 4 delay elements (2^4).

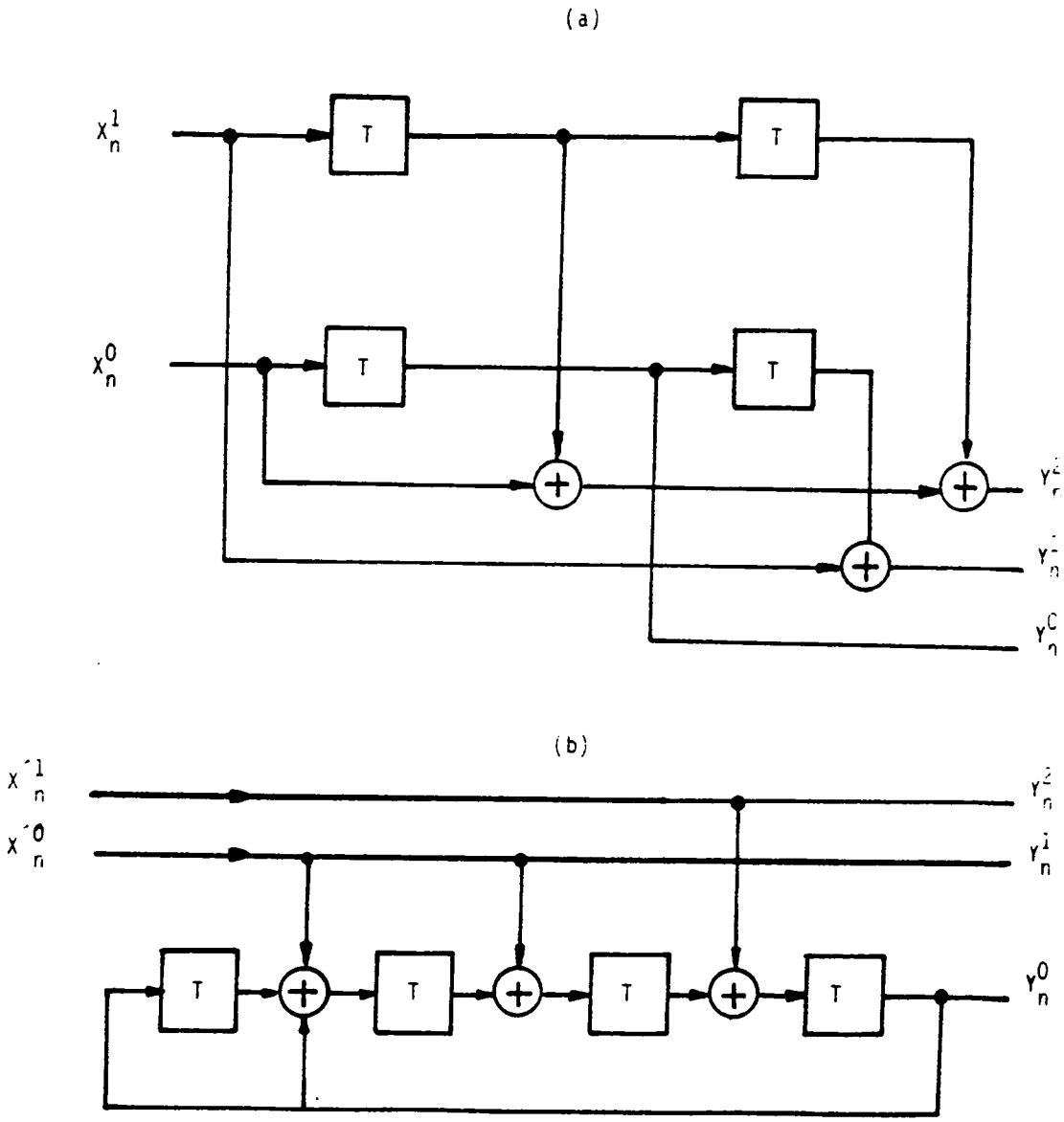

Figure 68. Two possible encoder for TCM 8-DPSK and DGMSK with code rate R = 2/3, and constraint length = 4. (a) Feedback-Free Encoder (b) Feedback (Systematic) Encoder.

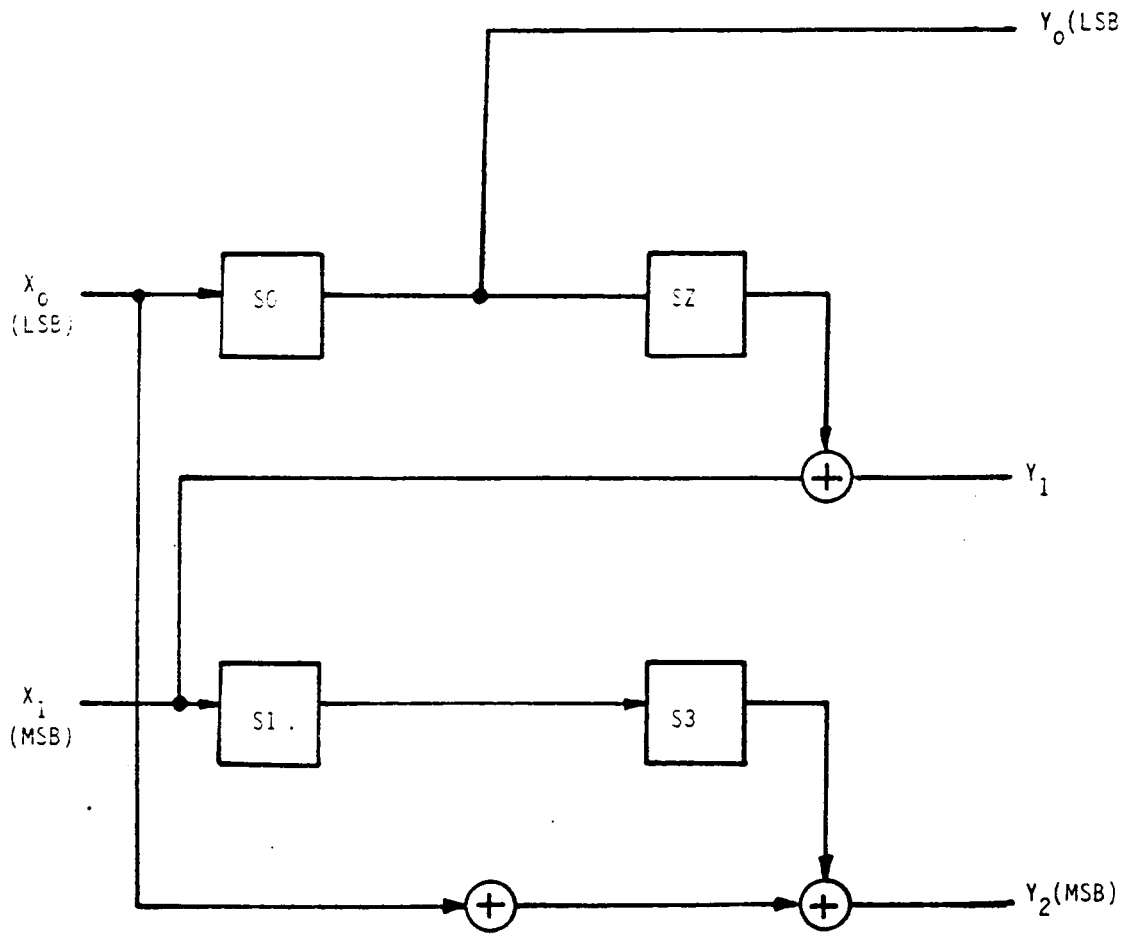

Figure 69. The TCM(and Convolutional) Encoder for TCM 8-DPSK and DGMSK redrawn from Fig.67 (a) for the (3,2,4) code generation.

These two encoders are minimal in the sense that they are realized with the same constraint length. However, to use the systematic encoder, the parity check equation must be found whenever the code rate is changed. In addition, the input to the encoder must be scrambled from the original input sequence, and this will be an additional overhead in the design process. From this point of view, the feedback-free(or feed-forward) non-systematic encoder in Fig.68 (a) was selected as the TCM and convolutional encoder in our simulation.

Fig.69 shows the encoder in Fig.68 (a), redrawn for the convenience of analysis. Our encoder has 4 delay elements (S0,S1,S1, and S3), 2 input bits (X_0 (LSB) and X_1 (MSB)), and 3 output bits (Y_0 (LSB), Y_1, and Y_2 (MSB)). Therefore, the 2 parallel input bits (or 2-bit symbol) are encoded into 3 parallel bits (or 3-bit symbol) output. Because of the constraint length 4, this code can be represented by conventional notation as a (n, k, m) = (3, 2, 4) convolutional code.

The encoding process of this encoder for single bit duration can be expressed by the following equations :

$$\begin{aligned} y_0 &= D X_0 \\ y_1 &= D^2 X_0 + X_1 \\ y_2 &= X_0 + D^2 X_1 \end{aligned} \tag{5.24}$$

In turn, these equation can be written in matrix form as

$$[X_0 \; X_1] \begin{bmatrix} D & D^2 & 1 \\ 0 & 1 & D + D^2 \end{bmatrix} = \begin{bmatrix} y_0 \\ y_1 \\ y_2 \end{bmatrix}, \tag{5.25}$$

where the middle 2 by 3 matrix is the generator matrix corresponding to our encoder. Because there are 8 possible combinations from the 3-bit output, 8 different phases can be assigned to the 3-bit symbols from 000 to 111. This phase assignment will be described in the phase mapping section. From this encoder output, we can construct the state transition diagram or trellis diagram of Fig.70, and the state transition table as in Table 5.1.

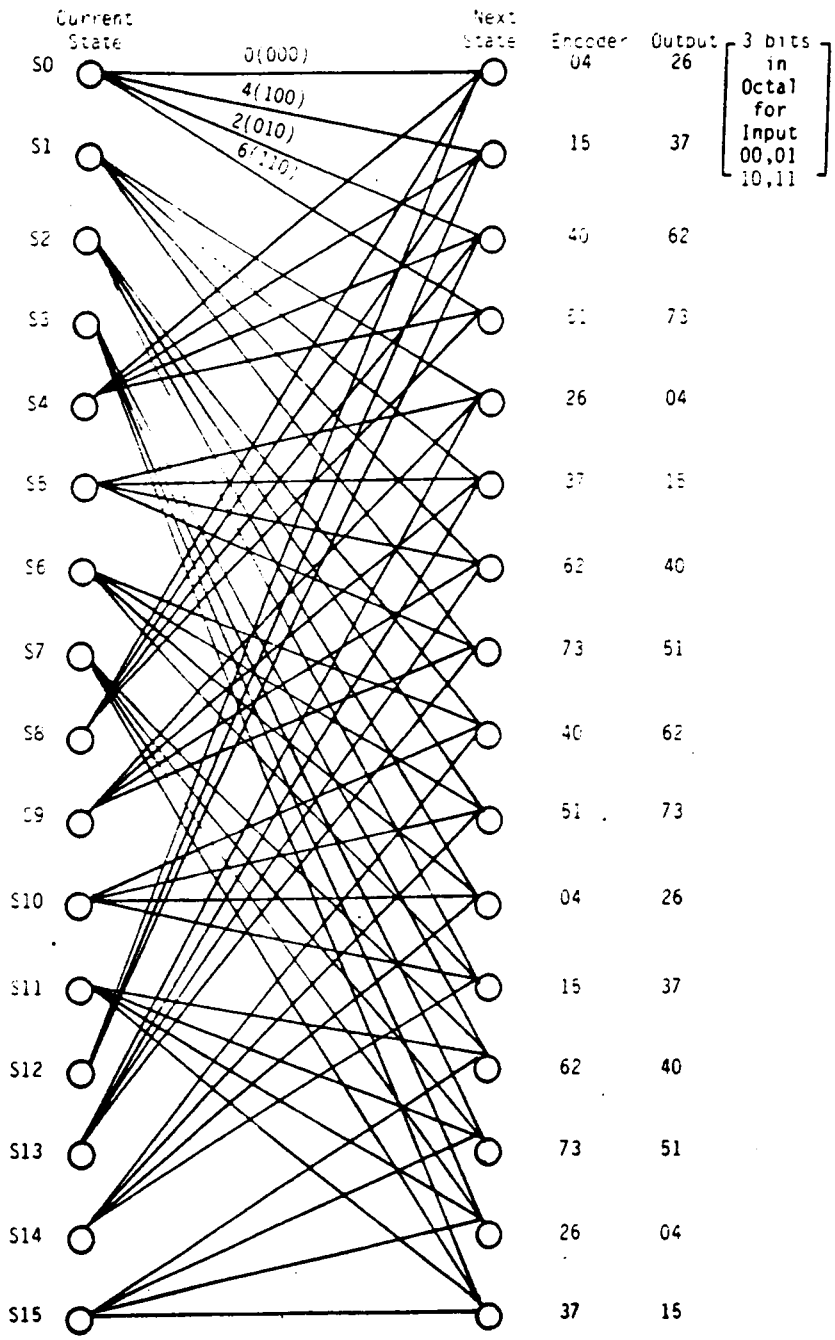

Figure 70. State transition diagram (or Trellis Diagram for the encoder of Fig.69)

Current State	Input x_1x_0 / S_3~S_0	00	01	10	11
S0	0000	S0 0	S1 4	S2 2	S3 6
S1	0001	S4 1	S5 5	S6 3	S7 7
S2	0010	S8 4	S9 0	S10 6	S11 2
S3	0011	S12 5	S13 1	S14 7	S15 3
S4	0100	S0 2	S1 6	S2 0	S3 4
S5	0101	S4 3	S5 7	S6 1	S7 5
S6	0110	S8 6	S9 2	S10 4	S11 0
S7	0111	S12 7	S13 3	S14 5	S15 1
S8	1000	S0 4	S1 0	S2 6	S3 2
S9	1001	S4 5	S5 1	S6 7	S7 3
S10	1010	S8 0	S9 4	S10 2	S11 6
S11	1011	S12 1	S13 5	S14 3	S15 7
S12	1100	S0 6	S1 2	S2 4	S3 0
S13	1101	S4 7	S5 3	S6 5	S7 1
S14	1110	S8 2	S9 6	S10 0	S11 4
S15	1111	S12 3	S13 7	S14 1	S15 5

Encoder Output in Octal Form (000=0 ~ 111=7)

Next State / Encoder Output

Table 5.1. State transition of Figure 70.

The diagram and table are basically the same because they use the same finite state machine, in which data are latched and output whenever clocking occurs. In this case, the encoder is the corresponding finite state machine, because after 4 transitions from a specific input, the contents of the 4 delay elements (S0 to S3) are all cleared and filled with new input bits. Table 5.1 shows the possible transitions from the current state to the next state that is defined by the contents of the 4 delay elements. We define the 16 possible states and number them from S_0 to S_{15} , based on the contents of the 4 delays from 0000 to 1111. Because two bits are input simultaneously, we have 4 possible combinations such as 00, 01, 10, and 11. At a specific current state, 4 different input combinations induce 4 possible transitions, and thus 4 different encoder outputs are denoted as 0 to 7 in the table and diagram (labeled on the branch and left side of the diagram). We have 16 possible states, and 4 transitions are possible from each node(or current state), so we can have a total of 64 possible transitions at a specific time interval. For a 128 input symbol frame (parallel 2-bit input/symbol), these transitions are repeated 128 times, because there are 128 clock pulses input to the finite state machine (the encoder). These numbers become larger as the constraint length ν and the input bits used for encoding are increased. Even in the 16 state case used here, it is not easy to follow the transitions by hand.

For the 8 possible encoder outputs (000 to 111 (MSB -LSB) in binary 3-bit form, or 0 to 7 in octal form), phase mapping is required in TCM 8-DPSK. In the case of DGMSK, this phase mapping is not needed. Instead encoder outputs are directly forwarded to the Gaussian lowpass filter for spectral shaping before modulation.

In TCM phase mapping, the symbol phase mapping from the set partitioning process depicted in Fig.67 is used. Compared with the symbol mapping included in the set partitioning example in Fig.54, the symbol mapping is different here. Because the symbol 000 does not start from the natural position in Fig.54, symbol assignment is changed from this mapping by using a different set partitioning from Fig.54. Fig.71 shows the symbol phase mapping constellation as well as the

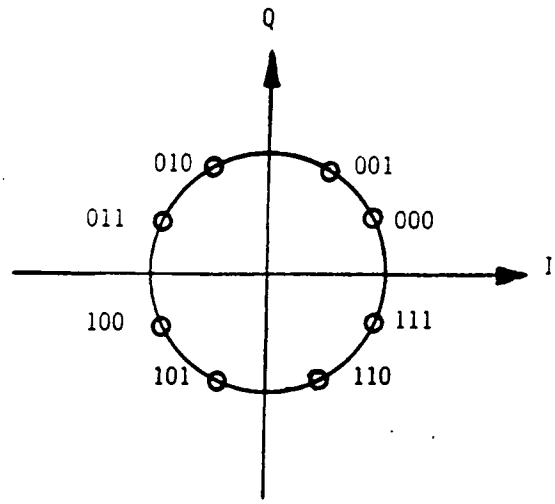

Y_2(MSB)	Symbol Y_1	Y_0(LSB)	Mapped Phase (Radian)
0	0	0	$\pi/8$
0	0	1	$3\pi/8$
0	1	0	$5\pi/8$
0	1	1	$7\pi/8$
1	0	0	$9\pi/8$
1	0	1	$11\pi/8$
1	1	0	$13\pi/8$
1	1	1	$15\pi/8$

Figure 71. TCM 8-DPSK symbol to Phase Mapping.

corresponding map table. As was mentioned earlier, once the relative Euclidian distances between symbols determined in the set partitioning are known, it is possible to change the symbol assignment.

The TCM decoding process is the same for conventional convolutional decoding because we have assumed hard decision rather than soft decision. This decision makes it possible to use the same encoder and decoder for the two different digital modulation schemes, TCM-8 DPSK and DGMSK in its differential version, even though some possible coding gain from the use of soft decision detection may be lost.

For hard decision decoding, the transition table listed in Table 5.1 or the code trellis diagram depicted in Fig.70 must be maintained in the program. Because the performance of the decoding scheme depends greatly on the length of the previous path in the trellis diagram, the previous path for 128 symbols is stored in the simulation program. The effects of a previous input in the decision of a current output may be an advantage or a disadvantage in the decoding process ; that is a characteristic of convolutional codes (remember that TCM code is generated by the convolutional encoder and decoded by the Viterbi algorithm).

For the specific input to the decoder, in this case a 3-bit symbol in parallel format, the decoder starts finding possible 2-bit inputs in the code trellis. For all possible branches, the decoder has the predetermined metric table that should be updated at each transition. When the next 3-bit symbol is input, the decoder searches for the optimal path that has maximum Hamming distance between codes, based on the previous 2 input symbols. In this step, the metric calculated before is recalculated based on the updated input sequence. As the input sequence is increased, these calculations get complicated. At the same time, the path metric is compared between every path from the specific transition. By repetitive metric calculation, path selection, metric comparison, and re-selection of the path and re-calculation of the path metric, the optimal path from the 1st symbol to the last (in our case 128th) symbol is found. Once this path is found, the corresponding original 2-bit symbol stream can be reconstructed.

5.3.6. Differential Encoding and Decoding

For the simulation of noncoherent detection in TCM 8-DPSK and DGMSK, differential detection was selected. Differential detection can be achieved through the process of differential encoding in the transmit side and differential decoding in the receive side as is usual in channel encoding. However, depending on the modulation scheme used, there can be many variants in the practical implementation. In our case, two different methods were used for TCM 8-DPSK and DGMSK respectively. The major reason for this difference comes from the detection method used in the receiver. In TCM 8-DPSK, we have assumed that detection is done on a symbol basis, because phases are mapped on a symbol by symbol basis, whereas detection is done on a bit by bit basis because phase is continuously changed in DGMSK. We call the detection technique for the differential version of TCM 8-DPSK as "differential phase detection", and call the technique for DGMSK "1-bit differential detection". Because the 1-bit differential detection scheme has already been described in detail in Sec.4.3.5, emphasis is given to the explanation of differential phase detection in TCM 8-DPSK in this section.

For the differential phase encoding at the transmit side of TCM 8-DPSK, 1 of 8 phases depicted in Fig.71 is assigned to the 3-bit output symbol of the TCM encoder. This symbol to phase mapping is repeated for the whole 128 symbols (capacity of interleaver). Then, an initial dummy phase corresponding to a dummy symbol is selected. In our simulation, a symbol 111 (7 in octal form) and corresponding phase of $\frac{15\pi}{8}$ are used for the dummy parameters. These dummy parameters are needed for encoding and decoding because the first encoder output and decoder input is not available before starting differential encoding and decoding.

With the dummy phase and the 128 mapped phases for 128 symbols, differential encoding starts. In this scheme, the first differential phase output is made by the addition of the dummy phase and the first symbol's phase. Even though a dummy phase is selected as the initial phase of the differential

phase encoder, this phase is not transmitted and it is selected only for convenience, so the first real differential phase encoder output is the sum of the dummy phase and the first symbol's phase.

The second differential phase encoder output is the sum of the first encoder output phase and the phase of the second symbol from the TCM encoder. This addition is repeated for all 128 symbols to be transmitted. As a result, we have a stream of differentially encoded phases for 128 symbols. The upper part of Table 5.2 illustrates this process with an example of 4 symbols.

The addition of phases between the previous encoded symbol phase and the current symbol's phase is the same as the multiplication (or modulo-8 addition for a 3-bit symbol) in a usual differential encoding process. The multiplication is translated into phase addition of the complex phasors of the current symbol and the previous encoder output [89], [110]. The practical implementation of this encoded phase output will be explained in the TCM-8PSK and DGMSK modulator and demodulator section.

Differential phase decoding in TCM 8-DPSK is exactly the reverse operation of encoding. The received symbol phases are first delayed by one symbol duration and the first received phase is then shifted to the second symbol position and so on. This delaying operation is repeated for all 128 symbols. Then the first vacant phase is filled with the dummy phase that was used in the differential phase encoding process. Therefore, we have 129 symbol phases in which the first phase is a dummy and the phases from the second to 129th are the real received symbol phase. The resulting stream of symbol phases corresponds exactly to the originally transmitted phases.

This phase decoding process is the reverse operation of the corresponding phase addition operation at the transmit side. In reality, this process is the subtraction of the phase of the current received symbol from the previous decoder output. This phase decoding process is also illustrated in the lower part of Table 5.2. By using the same principle as in the transmit side, this operation can be translated into a subtraction of complex phasors. From this point of view, the delay process can be interpreted as a step of complex conjugation. The practical implementation of this process will also be explained in the TCM modem section following.

1) Let the input symbols be:	1φφ	1φ1	φφ1	1φφ
2) The corresponding mapped phase are: (by Table 5.4)	$\frac{9\pi}{8}$	$\frac{11\pi}{8}$	$\frac{3\pi}{8}$	$\frac{9\pi}{8}$
3) Corresponding differential phase encoder outputs are: (Assuming initial dummy symbol of '111' and its phase $\frac{15\pi}{8}$)				
Diff. encoder input:	$\frac{9\pi}{8}$	$\frac{11\pi}{8}$	$\frac{3\pi}{8}$	$\frac{9\pi}{8}$
Diff. encoder output:	*$\frac{15\pi}{8}$	$\frac{24\pi}{8}$	$\frac{35\pi}{8}$	$\frac{38\pi}{8}$	$\frac{47\pi}{8}$

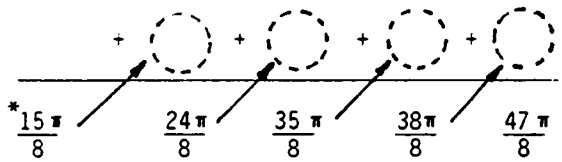

* Not Transmitted

4) Received phases are differentially phase decoded as following.					
a) Diff. decoder input:	$\frac{15\pi}{8}$	$\frac{24\pi}{8}$	$\frac{35\pi}{8}$	$\frac{38\pi}{8}$	$\frac{47\pi}{8}$
b) 1 Ts delayed input:		$\frac{15\pi}{8}$	$\frac{24\pi}{8}$	$\frac{35\pi}{8}$	$\frac{38\pi}{8}$	$\frac{47\pi}{8}$
Decoded phase = (a-b):		$\frac{9\pi}{8}$	$\frac{11\pi}{8}$	$\frac{3\pi}{8}$	$\frac{9\pi}{8}$	
Recovered symbol:		1φφ	1φ1	φφ1	1φφ	

Table 5.2. TCM 8-DPSK differential phase encoding and decoding example with 4 symbols.

One thing must be mentioned about the received phase used in the decoding process above. The received phase cannot be directly obtained from the received signal. Because the received signal takes the complex envelope form with real and imaginary parts, and these data are in time sampled form (2048 time samples), phase information must be obtained from these sampled data. Under noise-free conditions, the phase retrieval is simple because the transmitted phase is relatively stable among 16 time samples of each single symbol duration. However, under noise and fading, this process is not so easy and making a decision of the received phase may need some additional processing, such as analysis of the received phase trajectory, that will be explained later.

In DGMSK, 1-bit differential detection was assumed. This scheme is relatively simple in implementation, under the assumption of a hard decision based on the differential detector output. Even though the 2-bit differential detection scheme is reported to have better performance, this scheme needs a complicated decision threshold that must be decided by trial and error. As was noted before, most of the detection procedures have already been described in detail in Sec.4.3.5. Therefore, only the key ideas of modeling are briefly described here.

One of the best advantages of 1-bit differential detection in DGMSK is the absence of any encoding in the transmitter. The interleaved symbols are converted into serial format for Gaussian lowpass filtering and the filtered signal is modulated and transmitted without any modification. Fig.51 in Sec.4.3 was used for modeling of this 1-bit differential detection.

At the 1-bit differential detector, the input received signals in complex envelope form are provided to the detector as time samples. For differential detection, we need this stream of time samples and a 90 degree phase shifted and 1-bit delayed version of the originally received time sampled data stream. At the decoder, the original received stream and the 1-bit delayed and 90 degree phase shifted version of the original received stream are multiplied.

To give the 1-bit delay, time samples corresponding to the 1/7.2Kbps duration are shifted first. After 1-bit delay, the delayed 2048 time samples are complex conjugated to give the effect of a 90 degree phase shift. In the multiplication, the 1-bit delayed and 90 degree phase shifted time samples are multiplied with the original time sampled stream, sample by sample. The resulting time sampled

version of the 1-bit differential decoder output, in complex envelope form is forwarded to the lowpass filter for smoothing.

After lowpass filtering, the decoder output in complex form is converted into the frequency domain by an FFT operation, and this input is multiplied by the lowpass filter response in which the cutoff frequency is half of the bit rate of 7.2 Kbps. The filtered and converted time samples (by using an IDFT) are used to find the the differential phase between the original received phase and 1-bit delayed and 90 degree shifted phase. Finally, the decoded output including the differential phase $\Delta\Phi(T)$ in Eq.(4.32) is used for the decision of binary 1 or binary 0. However, the decoded and filtered output are still in time sampled form. Therefore, an additional sampling procedure is needed to pick up the stable output from the lowpass filter output.

For the decision of binary state 0 or 1, the polarity of y(t) in Eq. (4.33) is used. If this is positive, we assume a binary 1 was transmitted and a binary 0 is assumed to have been transmitted when y(t) is negative. These decisions are repeated for a total of 384 bits (the original 256 bits of 128 symbols for a single frame are converted to 384 bits by the result of rate 2/3 encoding). The estimated 384 bits from the decision process are serially forwarded to the deinterleaver.

5.3.7. TCM 8-DPSK/DGMSK Modulators and Demodulators

After the differential phase encoding in TCM 8-DPSK or the Gaussian lowpass filtering in DGMSK, functional blocks for modulation and filtering follow in the transmit side. In the receive side, the received signals are bandpass filtered (with a lowpass equivalent filter) and forwarded to the differential phase decoder in TCM 8-DPSK, or differentially decoded by a 1-bit detector in DGMSK, and lowpass filtered prior to a hard decision detector.

In this section, the modulation and demodulation processes in TCM 8-DPSK and DGMSK are explained. Because most of the other functional blocks have already been described, emphasis is given here to the interconnection between the previously described modules and the modems of these two schemes.

In TCM 8-DPSK, the encoder output symbols are interleaved for burst error protection before they are forwarded to the symbol to phase mapper. After phase mapping, differential phase encoding is performed for each 128 symbol unit. This differentially phase encoded data stream is the input to the TCM 8-DPSK modulator. Because of the uniqueness of the TCM scheme, the modulation process is described separately in this section for the convenience of functional description.

Fig.72 shows the quadrature modulator model used for TCM 8-DPSK, with the other functional blocks connected to the modulator. The main function of this modulator is the generation of a time sampled complex envelope of differential input phases. Because this is a baseband simulation, the carrier frequency is not needed in this procedure. The input phases for 128 symbols (differentially encoded phases) are used to generate the I and Q channels signals by taking cosine and sine of those phases. With these I and Q channel signals, time sampling is done at the rate of 16 samples per symbol duration. Therefore, 2048 time samples are generated from each of the 128 symbols in each channel. After multiplying each sample in the I and Q channel by $\sqrt{2}$ (dummy carrier amplitude), I channel samples are used to constitute the real part of the complex envelope and Q channel samples

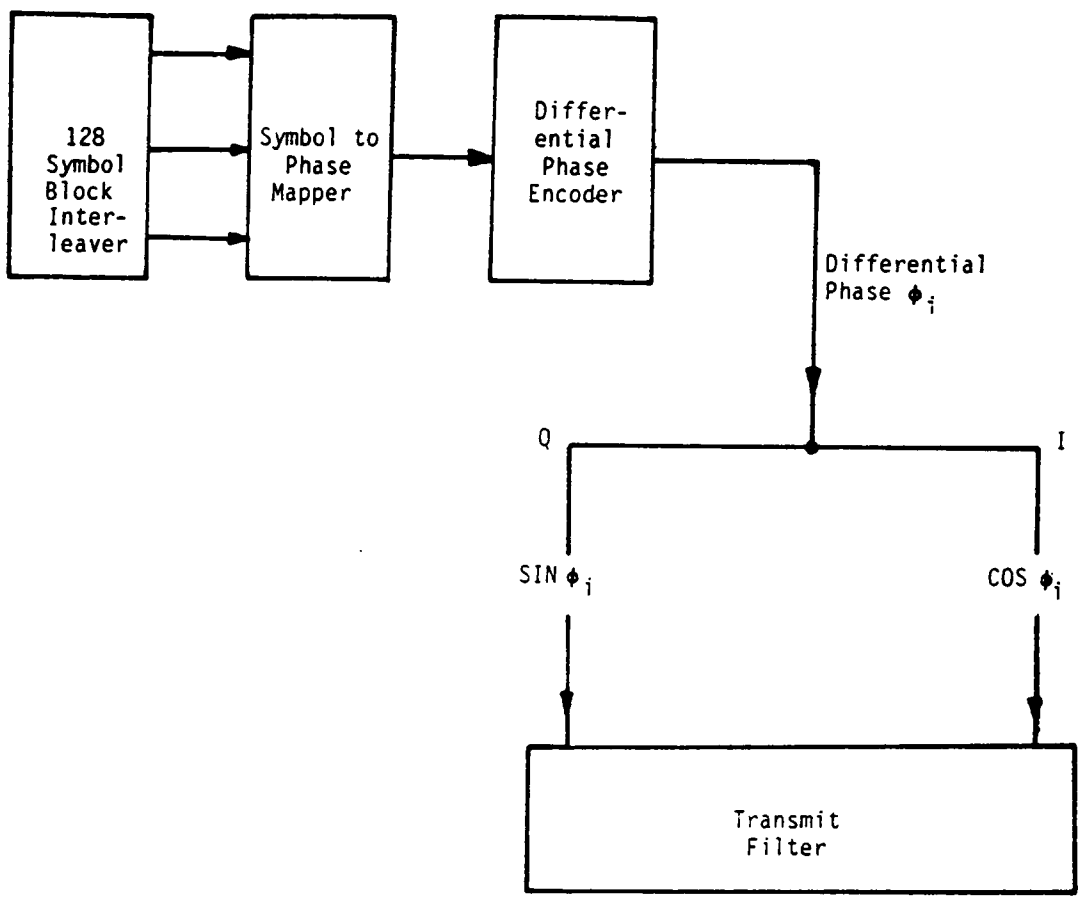

Figure 72. TCM 8-DPSK quadrature modulator block diagram with surrounding functional components.

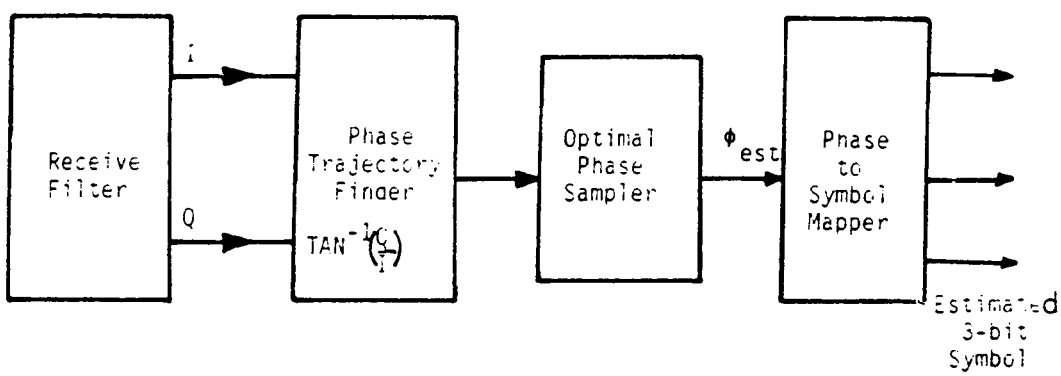

Figure 73. TCM 8-DPSK demodulation block diagram including estimated phase to symbol mapper.

are used to constitute the imaginary part of the complex envelope. The result is that we have 2048 complex time samples for final spectral shaping and transmission to the satellite channel.

The demodulation process of TCM 8-DPSK cannot be explained without the differential phase decoder and phase to symbol mapper, as can be seen in the TCM 8-DPSK demodulation block diagram depicted in Fig.73. In Table 5.2, we have seen an example of differential phase decoding. However, in practice, this phase recovery needs more explanation because the true input to the differential phase decoder is the complex phasor in time sampled form, not the phase itself.

In the process of differential phase decoding, the original received signal in complex form consists of 2048 time samples, shifted by 16 samples to give the effect of a one symbol delay. The vacant first 16 sample positions are filled with a complex phasor of dummy phase $\frac{15\pi}{8}$. To give the effect of phase subtraction as the reverse operation of phase addition in the phase encoding stage, this one symbol delayed complex phasor stream is first complex conjugated. Then it is multiplied with the original received complex phasor stream. As a result of complex multiplication with the delayed and complex conjugated pair, phase subtraction is accomplished.

The next step is the detection of the differentially decoded phase. We must find the true phase of the interleaved 128 symbols. The estimated phases are found by taking tangential values for each sample, such as $\tan^{-1}(\frac{Q}{I})$, where I and Q denotes the real part of the sample and the imaginary part of the sample, respectively. However, the sign of the I and Q channel samples must be accounted for in this step because 'tan (x)' is defined only for the angles from $\frac{-\pi}{2}$ to $\frac{\pi}{2}$. By repeating this procedure, we get the trajectory of the estimated phase for the phase to symbol mapping procedure that flollows immediately. Table 5.3. illustrates an example of this procedure.

The final step in TCM 8-DPSK demodulation is phase to symbol mapping. For this purpose, the data stream is sampled to find the most stable phase from the 2048 estimated phase trajectories. Because 16 samples are assumed per symbol duration, the mid-point of every 16 samples of phase trajectories is selected as the symbol phase for each of the 128 symbols.

Under noise-free conditions, the disturbances that affect this decision are due solely to filtering effects, such as ISI. However, these effects are minimal when mid-point sampling is performed. Under

1)	Input symbols and mapped phase are:	$\phi\phi\phi$	$\phi\phi\phi$	$\phi\phi\phi$	$\phi\phi\phi$
		$\frac{\pi}{8}$	$\frac{\pi}{8}$	$\frac{\pi}{8}$	$\frac{\pi}{8}$
2)	Diff. phase encoder outputs are (by the method in Table 5-2) [dummy symbol ='111', dummy phase $=\frac{15\pi}{8}$] :				
	Output phase:	$\frac{16\pi}{8}$	$\frac{17\pi}{8}$	$\frac{18\pi}{8}$	$\frac{19\pi}{8}$
	Complex phasor:	$e^{\frac{16\pi}{8}}$	$e^{\frac{17\pi}{8}}$	$e^{\frac{18\pi}{8}}$	$e^{\frac{19\pi}{8}}$
	Modulator Output:	(1, 0)	(0.92, 0.38)	(0.707, 0.707)	(0.38, 0.92)
3)	Received and 1 Ts delayed inputs (with dummy) after complex conjugation:	(0.92, 0.38)	(1, 0)	(0.92, -0.38)	(0.707, -0.707)
4)	By multiplication of original received signal and result of (3) yields:	(0.92, 0.38)	(0.92, 0.38)	(0.92, 0.38)	(0.92, 0.38)
5)	By the phase decision and phase to symbol mapping (Table 5.4) recovered phases and symbols are :	$\frac{\pi}{8}$	$\frac{\pi}{8}$	$\frac{\pi}{8}$	$\frac{\pi}{8}$
		$\phi\phi\phi$	$\phi\phi\phi$	$\phi\phi\phi$	$\phi\phi\phi$

Table 5.3. An example of differential phase decoding for a complex phasor.

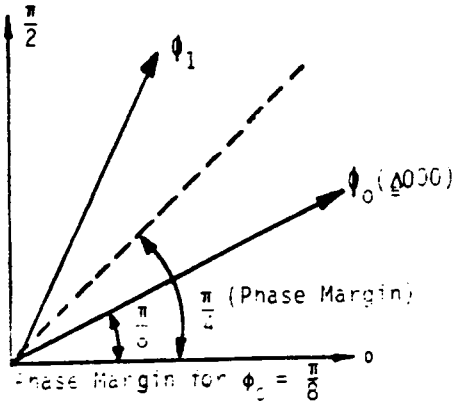

Sign of Channel Signal		Estimated Phase; ϕ_{est}
$S_I(t)$	$S_Q(t)$	
+	+	ϕ_p*
-	+	$\phi_p + \pi$
-	-	$\phi_p + \pi$
-	-	ϕ_p

* $\phi_p \triangleq \text{TAN}^{-1}\left(\frac{S_Q(t)}{S_I(t)}\right)$

Estimatec Phase ϕest Range	Assigned Phase	Mapped Symbol (MSB)		(LSB)
$0 \leq \phi est < \frac{\pi}{4}$	$\frac{\pi}{8}$	0	0	0
$\frac{\pi}{4} \leq \phi est < \frac{\pi}{2}$	$\frac{3\pi}{8}$	0	0	1
$\frac{\pi}{2} \leq \phi est < \frac{3\pi}{4}$	$\frac{5\pi}{8}$	0	1	0
$\frac{3\pi}{4} \leq \phi est < \pi$	$\frac{7\pi}{8}$	0	1	1
$\pi \leq \phi est < \frac{5\pi}{4}$	$\frac{9\pi}{8}$	1	0	0
$\frac{5\pi}{4} \leq \phi est < \frac{3\pi}{2}$	$\frac{11\pi}{8}$	1	0	1
$\frac{3\pi}{2} \leq \phi est < \frac{7\pi}{4}$	$\frac{13\pi}{8}$	1	1	0
$\frac{7\pi}{4} \leq \phi est < 2\pi$	$\frac{15\pi}{8}$	1	1	1

Table 5.4. Decision criteria of estimated phase to symbol mapping in TCM 8-DPSK demodulation.

conditions of noise and fading, there must be some phase margin in order to assign the correct symbol, because noise and fading will affect the received sample value nonlinearly. By trial and error, a phase margin of $\frac{\pi}{4}$ was found. Table 5.4 shows the decision criteria used for estimated phase to symbol mapping, as well as the decision criteria for estimating phase from the tangential operation mentioned earlier. Once estimated symbols are found, these symbols are formatted serially and forwarded to the block deinterleaver.

In DGMSK, the same type of quadrature modulator can be used for DGMSK signal modulation as in the TCM 8-DPSK case. However, the input to this modulator is a Gaussian lowpass filtered output which is already in complex envelope form. In addition, because this filter output is derived from bit by bit transitions rather than symbols, the phases provided to the following quadrature modulator are different from those of the TCM 8-DPSK case.

Fig.74 shows a quadrature type DGMSK modulator along with a Gaussian lowpass filter and Gaussian bandpass filter (lowpass equivalent), at the transmit side. As was mentioned earlier in the filtering section, by multiplying the phase constraint of $\frac{\pi}{T_s}$ (where $T_s = 3T_b$ in DGMSK because of rate 2/3 encoding) with the result of Gaussian lowpass filtering, we obtain the instantaneous phases for 384 bits (the original 256 bit are converted to 384 bits by rate 2/3 encoding) in time sampled complex envelope form. The Gaussian filtering block illustrates this process.

Quadrature moduation is performed on this instantaneous phase stream in the same fashion as in the TCM case. The resulting modulator output in sampled form is spectrally shaped with a Gaussian shaping filter for final transmission.

The demodulation process and the differential detection scheme have already been described in detail in Sec.4.3.5 and Sec.5.3.5 respectively. The model for the DGMSK demodulator was selected as the one depicted in Fig.51 (a). However, it should be remembered that the input to the 1-bit differential detector is always a complex valued time sample. Therefore, the procedures of a one bit time delay, 90 degree phase shift, and multiplication with the original complex valued stream must

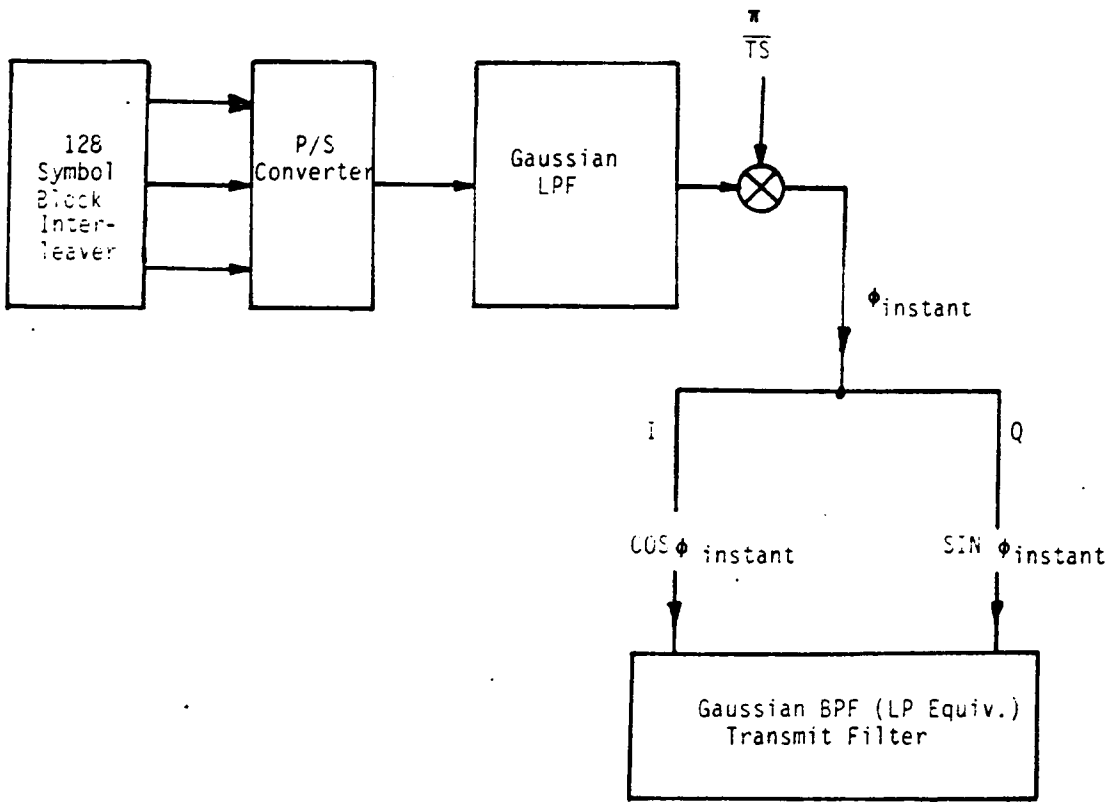

Figure 74. Quadrature modulator for DGMSK and surrounding Gaussian lowpass and bandpass(lowpass equivalent) filters.

be done on a sample by sample basis. That principle must be retained for the following lowpass filtering. After filtering, sampling must be performed to recover the estimated 384 bits in binary form from the filter output.

5.3.8. Block Interleaver/Deinterleaver

The necessity of block interleaving of the symbols to be transmitted, and block deinterleaving of the received symbols has already been explained. However, block interleaving and deinterleaving is needed only when the Viterbi algorithm is used for decoding, because of propagation effects in the convolutional code. Therefore, if a code other than a convolutional-type code is used for encoding/decoding, such as a block code, these techniques are not needed.

The block interleaver and deinterleaver are simultaneously modeled in our simulation by using a 16 by 8, 3-dimensional matrix because we have assumed that a single element of this matrix is basically a 3-bit symbol. Converting this 3-bit symbol into octal form is achieved by changing the array dimensions.

Fig.75 shows a model of a rectangular type interleaver/deinterleaver, as well as an example of interleaving and deinterleaving when 128 symbols are used as the block size. In the interleaving stage, the 3-bit or octal symbols are provided to the interleaver. These symbols are stored (or are written) row by row until 16 rows are filled with 128 symbols. In our case, there are 8 columns and 16 rows. A row is called the interleaving depth, while a column is called the span length. As a result of the writing process, symbols are written in a zig-zag fashion from the 1st to 128th symbol.

For interleaving, the reverse operation is performed. The written symbols are read out column by column. Therefore, the original sequence of symbols is separated by the interleaving depth, as can be seen in the example in Fig.75. These interleaved symbols are forwarded to the following phase mapper in the TCM case and forwarded to the Gaussian lowpass filter in DGMSK.

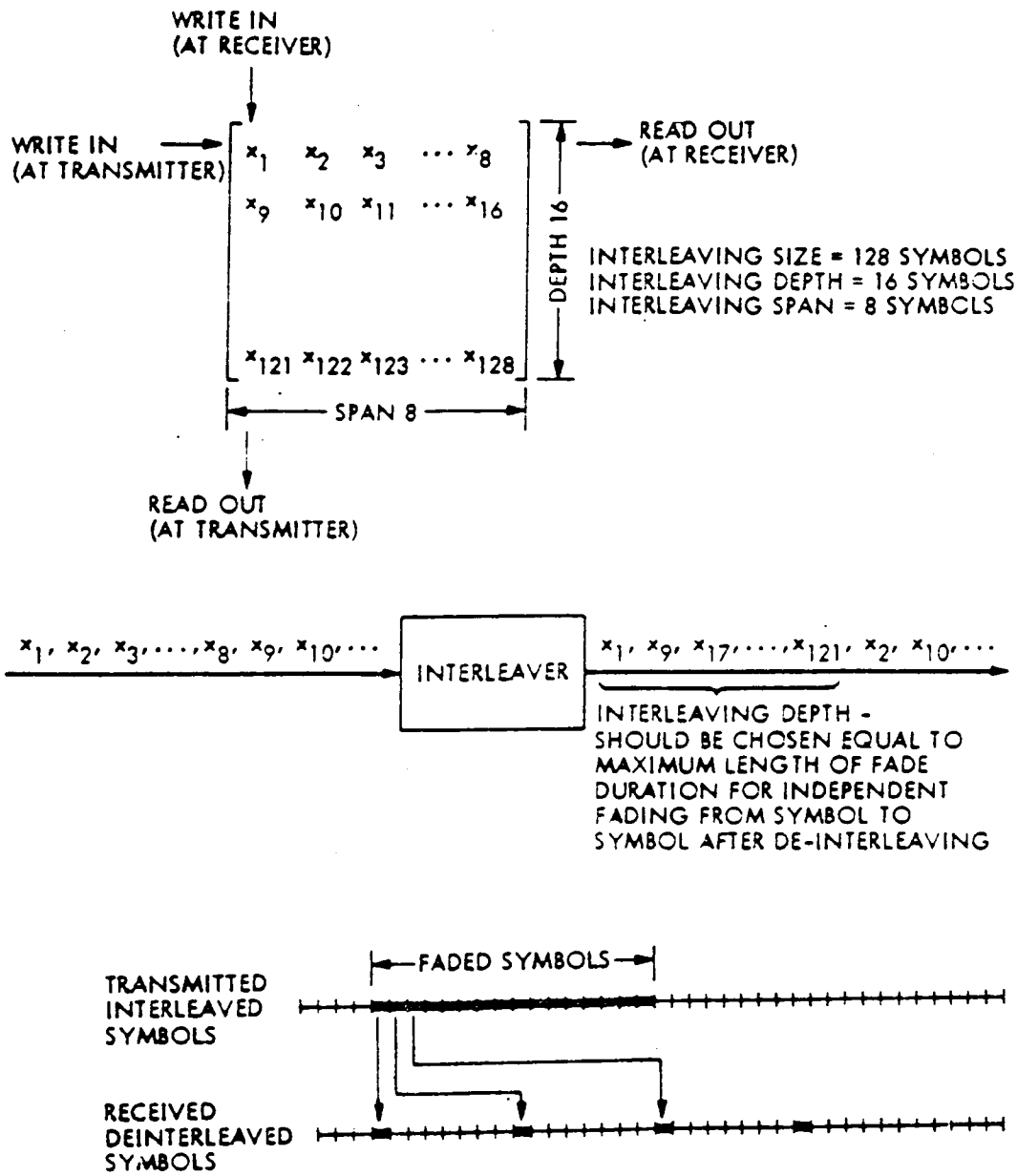

Figure 75. 128 symbol block interleaver/deinterleaver in 16x8 matrix model with the example of interleaving and deinterleaving. From NASA JPL [100]

At the deinterleaver in the receiving side, the input signal is a stream of 3-bit binary or octal symbols, as in the interleaver. These symbols are written in column by column and read out in row by row. As a result, the original transmitted symbols are recovered sequentially. This output is forwarded to the convolutional decoder for final conversion to the original 2-bit symbols.

In this model, the key parameters such as interleaving depth, span length, and block size are borrowed from preliminary results obtained by NASA JPL [100].

5.3.9. Method of Fading Effects Insertion

For the simulation of fading effects, we have assumed that only the results of the propagation simulator [80] are used to fade the down-link signal. In this section, the way in which these fading data are used in the simulation is explained.

The propagation or fading data, provided to the channel simulator from the propagation simulator, usually consists of amplitude and phase samples of the received signal, with a specific wavelength interval, usually 0.1λ. For convenience of baseband simulation, these data can be changed into complex form. In addition to these measured and pre-processed data, the speed of the moving vehicle, and the transmission frequency of the measured data are also provided.

The first step is the calculation of the time required to transmit the original block of 128 symbols (or 256 original bits, or 384 encoded bits) at the given bit or symbol rate. This time is important, because the time calculated above is the only key to link to the propagation data provided. Once we have the transmission time, the next step is the calculation of the time for the vehicle to move 0.1λ, because we have the data at this wavelength interval. This time can be calculated using the relationship of vehicle speed and transmission frequency.

With the required simulation time for transmission of a block of 128 symbols, and the time for 0.1 wavelength movement of the vehicle at the specific transmission frequency (either UHF or L band), we can calculate the maximum number of wavelengths that can be simulated in a single 128 symbol transmission cycle by dividing the simulation time by the 0.1 wavelength moving time.

The next step is the one to one matching of the signal to be faded with the fading data provided by the propagation simulator. This can be achieved in a simple way. From the calculated maximum wavelength, we know how many data points are provided to the channel simulator. If this number is X, and if we use 2048 time samples, the result of dividing 2048/X is the required factor for the duplication of the given fading data. Unless the time to move 0.1λ is unusually long, interpolation is not necessary, since the time to move 0.1 λ is usually on the order of milliseconds.

Each 0.1 wavelength fading value is duplicated to make the number of fading values the same as that of the time samples of the signal to be faded. Multiplication of the two data streams, sample by sample, for all 2048 (or 4096) time samples that are expressed in complex form gives the required fading effect. These faded data are then provided to the stage of noise addition.

5.3.10. Performance Evaluator

When modeling of all the functional blocks had been completed, and tests of transmission and reception finished, a method for performance evaluation was needed. However, this decision frequently depends on the method of noise insertion, or the calculation of signal power to be compared with noise power.

Based on the modeling specifications and system level modeling, we decided to use two different methods of error rate calculation, depending on the method of noise insertion. For coherent QPSK/MSK, the so called hybrid simulation method [103] is used, in which analytically calculated noise is inserted into the process of average bit error rate (or bit error probability) calculation. Direct (or Monte-Carlo) simulation is used for the noncoherent TCM 8-DPSK/DGMSK case in which noise is directly added to the signal at the receiver front-end. In this section, the detailed procedure used for each of these two method is described.

Theoretically, thermal noise should be added at the input of the receive bandpass filter, and this signal should be demodulated and sampled. Then the sampled result is compared with the known Tx

symbols, so that errors are counted to obtain average error rate. This is called a direct simulation method and usually is used when there is the a nonlinear element in the detection or modulation process. This method is time consuming and inefficient, because errors must be counted for all the symbols transmitted. When low error rates, such as 10^{-4} or 10^{-5} are to be calculated, hundreds of thousands of symbols must be sent to obtain a reliable result. In hybrid simulation for coherent QPSK/MSK, noise (thermal noise) is neglected at first, and the same steps of demodulation and sampling are performed. After getting the detected value, an analytically calculated noise power is used to calculate the BER (Bit Error Rate) for a fixed carrier to noise ratio (CNR) using the complementary error function.

To express the noise power spectral density N_o, the equivalent noise bandwidth of the receive filter is needed. In satellite communications, where digital transmission rather than analog transmission is used, the carrier to average noise power ratio, C/N, is used instead of a S/N ratio. In M-ary PSK, all the performance measures are based on the bit or symbol. Therefore the required bit energy E_b to noise density N_o ratio, $\frac{E_b}{N_o}$ is frequently used. The relationship of $\frac{E_b}{N_o}$ to C/N ratio can be written as

$$\frac{E_b}{N_o} = \frac{C}{N}\frac{B_n}{R_b} \quad , \tag{5.26}$$

where B_n is the receiver noise equivalent bandwidth, and R_b is the bit rate. The error performance can be expressed as the probability of bit error (usually called Bit Error Rate(BER)). For the QPSK and MSK cases, the probability of bit error is expressed as follows.

$$P_{e,\ BPSK} = P_{e,\ QPSK} = P_{e,\ MSK} \simeq \frac{1}{2}\,\mathrm{erfc}\sqrt{\frac{E_b}{N_0}} \quad , \tag{5.27}$$

where

$$\text{erfc}(x) = \frac{2}{\sqrt{\pi}} \int_x^{\infty} e^{-y^2} dy \ , \quad x > 0$$

$$E_b = C\,T_b \tag{5.28}$$

C: received signal power

T_b:bit duration $(= 1/R_b)$.

To use the above formula for the calculation of the average BER, the received signal power C and the noise density N_o must be calculated first. Normalization of the received signal (noise-free) to an average signal level C of 1 watt gives a convenient reference level. To get N_o at the same level for a given $\frac{E_b}{N_o}$ ratio, Eq.(5.26) and the relationship of $N = N_o B_n$ (where N is noise power) can be used. For a fixed $\frac{E_b}{N_o}$ ratio, N_o can be found easily if C is set to unity and B_n is designed to be the the bit rate. Once N_o is found for a specific C/N ratio, the average BER can be found from the bit power E_b in the sampled symbol, and from the relationship $E_b = CT_b$ [26].

In a fading channel, the probability of error for each individual bit, rather than the average BER calculated above, is more meaningful because of rapid fading. For this calculation, the same method described above can be used, but the bit energy E_b for each specific bit is calculated for a fixed C/N ratio, instead of averaging. By comparing individual bit error probabilities, it is possible to find the effects of fading in a shorter time.

In the simulation of QPSK and MSK, only one channel, either the I or Q channel, is needed for the BER calculation, based on the fact that both in-phase and quadrature channels exhibit the same performance, because each channel is a BPSK signal and the probability of error for BPSK and QPSK is identical.

In the direct simulation for noncoherent TCM 8-DPSK and DGMSK, thermal noise(AWGN) is added directly to the faded signal in complex form. For noise generation in this case, a a portable Gaussian random number generator [106] is used. Uniformly distributed random numbers are converted to random noise phases by multiplying π. Then, Gaussian distributed random numbers are generated to be used as the random amplitude of the noise phasor. Real and imaginary part are generated by taking the cosine and sine of the random phase.

Before Gaussian random number generation, a generation parameter, noise variance σ , is found from the given C/N ratio. Signal power can be calculated from the complex envelope of the signal, and noise power N corresponding to a specific C/N ratio (in dB usually) is calculated first. This power is the theoretical noise power and must be equal to the noise power from the randomly generated complex noise. To achieve this, the calculated σ is multiplied by the magnitude of the Gaussian random numbers. For confirmation of the correctness of noise generation, the complex noise power for a specific C/N ratio, adjusted with σ, is calculated from the true noise samples. Generated and power-adjusted noise are added to the input signal only when the theoretically calculated noise power for a given C/N ratio is equal to the practically calculated noise power from the generated complex samples. The signal with added noise is forwarded to the receive input filter.

Once the simulation results are obtained in the form of the originally transmitted data sequence, counting the number of error is essential in direction simulation. The objective of error counting is to find the number of symbols or bits that are different from the transmitted ones. In this counting step, as many symbols as possible should be simulated to obtain a reliable error rate. However, there is no finite guide line about this decision at this moment; there must be a compromise between the desired error rate from the simulated data and the number of symbols to be simulated.

5.4. Summary

For effective performance evaluation, four digital modulation schemes (coherent QPSK/MSK and noncoherent TCM 8-DPSK/DGMSK) were selected for system level modeling and component level modeling.

In system level modeling, general methodologies for software simulation were discussed first. Based on this discussion, modeling specifications, as well as system level block diagrams, which include all the functional components to be modeled at the components level, were prepared.

In component level modeling, functional modules were constructed for symbol generation, coherent QPSK/MSK modem, trellis(or convolutional) encoding and decoding, differential encoding

and decoding, transmit and receive filtering, optional satellite transponder nonlinearity, a TCM 8-DPSK/DGMSK modem, block interleaving/deinterleaving, fading effect insertion, and performance evaluation. These are all modeled in a modular structure for easy modification if needed.

VI. Performance Analysis of LMSS Channel under Fading

6.1. Simulation Overview

Based on the components models and system block diagrams, three separate simulation programs were made to evaluate the effect of fading on system performance in a LMSS channel. Because of the major differences in detection schemes and coding, the first program was made to simulate coherent schemes, QPSK and MSK, without coding, while the second and the third programs were made to simulate the the noncoherent schemes using differential detection, TCM 8-DPSK and DGMSK, with coding.

In this chapter, a brief introduction to each simulation package is given first. In the introduction, descriptions of the simulation procedures related to the system or component level modeling are avoided. Instead, emphasis is placed on the explanation of the differences between the three programs which were developed. After a brief description of the modem back to back test, and the fading channel test, simulation results are analyzed for performance evaluation of QPSK and MSK.

For the convenience of description, the coherent schemes and the noncoherent schemes are discussed separately.

All three programs were written using the following four principles:

1. Baseband simulation.
2. Frequency domain filtering with zero phase assumption.
3. Direct use of propagation simulator output for fading effect insertion.
4. Direct (Monte-Carlo) simulation for noncoherent TCM 8-DPSK/DGMSK and indirect (Hybrid) simulation for coherent QPSK/MSK.

While keeping to the above principles, the three programs are slightly different from each other, depending on the modulation scheme used or the existence of coding.

The first program, 'LANSIM 1' simulates the LMSS channel using the two coherent digital modulation schemes, QPSK and MSK. Because the two schemes are almost identical except for sinusoidal pulse shaping in MSK modulation, most of the functional components are common to both programs. Therefore, by changing the modulation type in the system parameters, both schemes can be simulated easily. Nonlinearity of a TWTA can be inserted optionally. For performance evaluation based on average BER, indirect simulation is used. Therefore, only a small number (compared with the direct simulation case) of symbols are needed. Insertion of fading is directly follows to the transmit filter output in this program, assuming no TWTA nonlinearity. No coding is employed in this program for simplicity. However, interleaving and deinterleaving is used to see the effect of interleaving on the bit by bit BER, because the process of interleaving can spread the effect of fading over a portion of the transmitted data.

The second program, 'LANSIM 2' is for TCM 8-DPSK with differential detection. In this program, trellis encoding/decoding, block interleaving/deinterleaving, and differential phase encoding techniques are employed. The optional TWTA nonlinearity used in 'LANSIM 1' can be inserted if needed. Direct simulation is used for performance evaluation. A large number of symbols must be

generated to get a reliable BER (or symbol error rate), because the counting of the number of bit or symbol errors is the only way to get the performance measure.

The third program, 'LANSIM 3' is for the DGMSK only. Even though almost all the functional blocks in 'LANSIM 2' are used by both programs, a separate program was written because of the basic differences between DGMSK and TCM 8-DPSK, and to avoid possible difficulties in modification once they were combined into one program. Although differential detection is assumed in TCM 8-DPSK, bit by bit differential encoding is used in DGMSK, contrary to the symbol by symbol phase encoding in TCM 8-DPSK. In addition, DGMSK uniquely uses a Gaussian lowpass filter before modulation while maintaining phase continuity, contrary to the abrupt phase change between symbols in TCM 8-DPSK. The same direct simulation as in 'LANSIM 2' is used for performance evaluation.

6.2. Performance of Coherent QPSK and MSK

Several tests were performed to evaluate performance using the developed simulation programs 'LANSIM 1'. The first test was a modem back to back test to get a reference for further tests. Once this modem back to back test was done, tests with fading data followed to see the effect of fading. By comparing the results of the two tests, the effects of fading on LMSS link performance can be analyzed.

In a modem back to back test, the results are expressed as the average BER, whereas results from the tests under fading can be expressed either in average BER or in bit by bit error probability (simply, bit error probability). However, bit error probability can be used more effectively to analyze the fading effect, because the effect of mild or deep fades can be directly reflected in the individual bit error probability. Simulation with the nonlinearity caused by a TWTA was not performed here. It was assumed that a linear high power amplifier was used in the practical system. Results of nonlinear tests with a TWTA can be found in Junghwan Kim' M.S thesis [111].

6.2.1. Modem Back to Back Test

This test is needed to establish a reference for comparison with the results of further tests. No fading effects are included in this test. Instead, the output of the transmit filter is applied directly to the receive filter input, as depicted in Fig.76.

The following conditions were used in this test: an incoming bit rate of 2.4 Kbps, hence 1.2 Ksps symbol rate (2bits/symbol), square root raised cosine Nyquist filters with a roll-off factor of 0.5, and Nyquist frequency of 1.2 KHz for the transmit and receive filter to constitute matched filters. In the simulation of QPSK, an x/sinx type amplitude equalizer is used after the transmit filter for spectral compensation of the rectangular pulse input. A sinusoidal amplitude equalizer is used for MSK signal shaping in the transmit filter.

Fig.77 shows the results of the modem back to back test, and the theoretical performance for coherent QPSK and MSK expressed as average BER versus E_b/N_o . As can be seen from these curves, the results of the QPSK modem back to back test lie within 0.2 dB of the theoretical performance in the BER range of 10^{-2} to 10^{-9}. However, MSK deviates a little more from the theoretical performance, by about 0.4 to 0.5 dB for the same BER range, and MSK requires an additional 0.2 to 0.3 dB to achieve the same BER as QPSK. However, it is too early to say that MSK is inferior to QPSK based on this result. Use of the same filters with the same bandwidth for both QPSK and MSK may result in loss of signal power in MSK, because the main lobe of the MSK spectrum is approximately 1.5 times wider than for QPSK.

Although the results of the modem back to back test for QPSK and MSK deviate slightly from the theoretical performance, these deviations can be attributed to the effect of quantitization noise that is inherent in any computer simulation, and the results of the modem back to back test can be used with confidence as a reference for further tests under fading conditions.

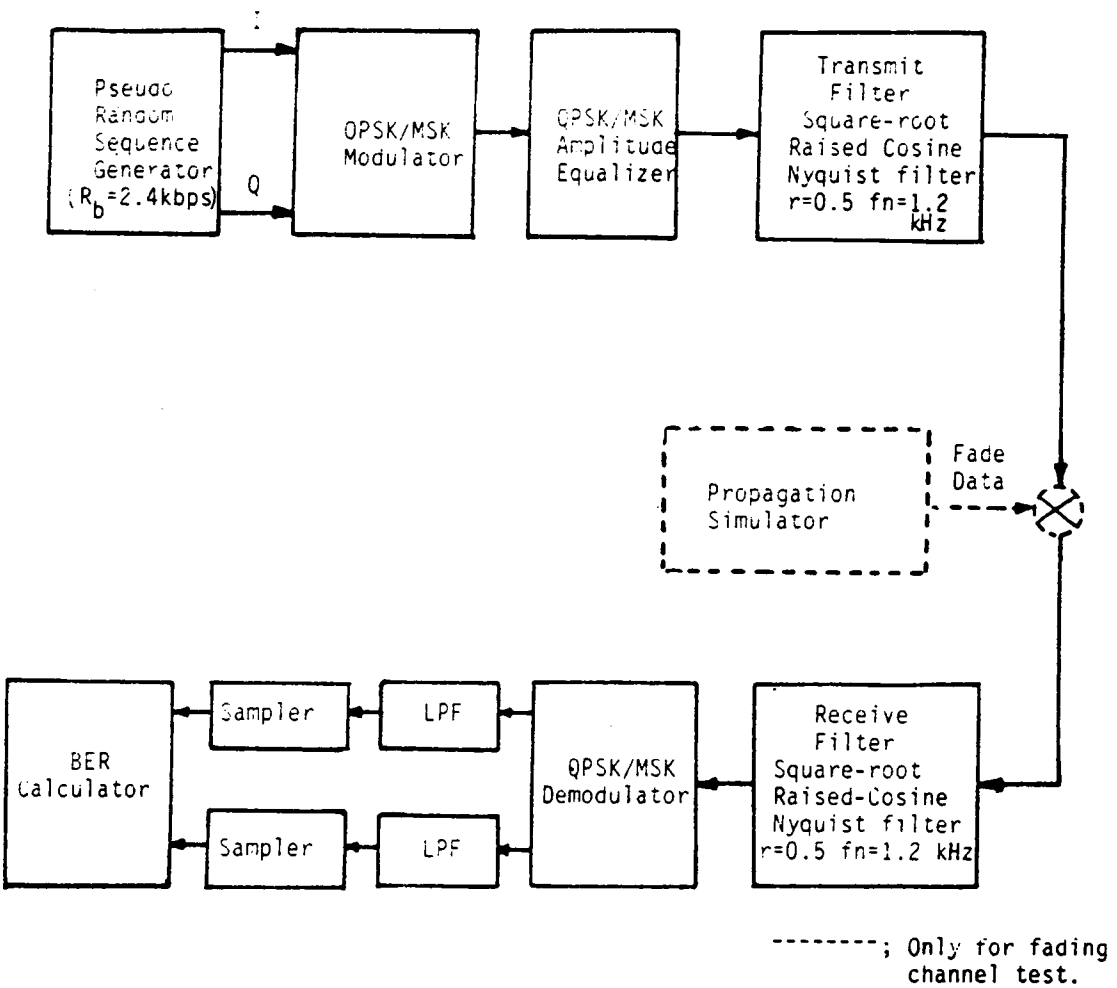

Figure 76. Coherent QPSK/MSK modem back to back test system block diagram.

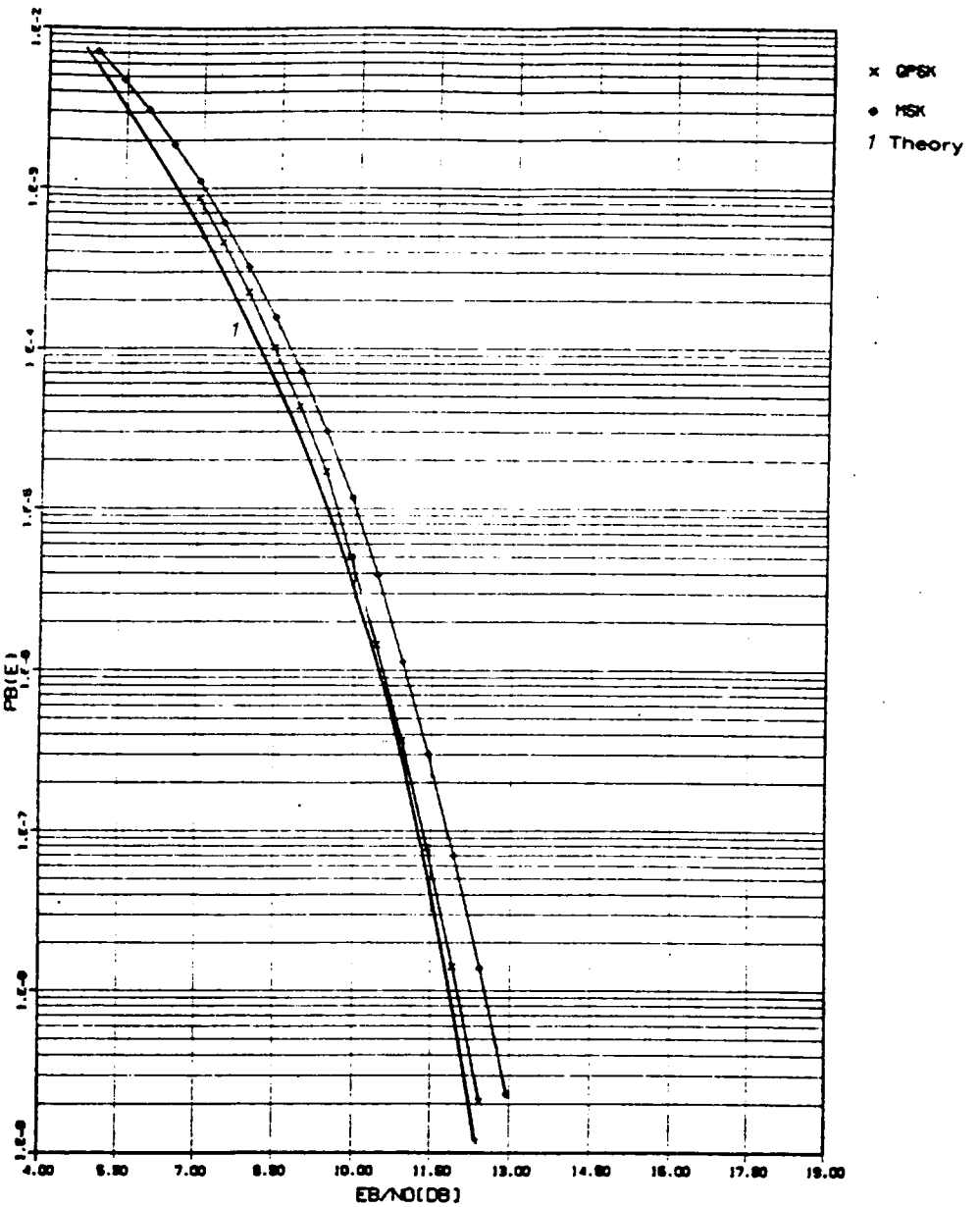

Figure 77. Coherent QPSK/MSK modem back to back test results and theoretical performance.

6.2.2. Fading Channel Test

The previous modem back to back test provided the reference case for comparison with the test results that will include fading effects. In the fading channel test, the output of the transmit filter is faded before it is applied to the receive filter input, as depicted in Fig.76, by including the optional propagation simulator denoted by the dotted block.

In the simulation, the fading data provided by the propagation simulator [80] are a processed version of W. Vogel's empirical data [50] and are characterized by amplitudes and phases recorded at 0.1 λ wavelength intervals. However, the amplitudes and phases of the fading data are converted into their complex form before they are provided to the transmit filter output, because the filter output/input in our simulation must be in complex form.

The fade data were originally made by measurement of the received signal level at a receiver when a signal was transmitted from a 1.5 GHz transmitter and received by a vehicle that was moving with a speed of 55 mph (24.59m/sec). The total length of available fade data used in this test was 204.7 wavelength intervals. Fig.78 shows the amplitude characteristic of the fade data, on a dB amplitude scale in amplitude versus wavelengths (λ) travelled by the receiving vehicle. The fade amplitude, or fade depth, characteristic curve of Fig.78 shows the combination of a LOS signal, and a faded signal. The portion from 0.0 to 100.0 λ can be regarded as a LOS signal, while the portion from 100.0 to 204.7 λ can be interpreted as the faded signal. The faded portion also can be classified into a milder fade portion and a severe fade portion. Fig.79 shows the phase (in radian) of the received faded signal, corresponding to the amplitude characteristic in Fig.78.

Preprocessing of the faded data is required to give the fading effects to the transmitted signal, i.e, to the transmit filter output in this case. For the simulation of 256 bits at 2.4 kbps, the required time is 106.7 mS, and the required time for the the vehicle to move a distance of 1 λ is approximately 8.13 ms, assuming a constant 55 mph vehicle speed (for 1.5GHz, $\lambda \simeq 0.2$m, and 55mph = 24.59 m/sec). Therefore, it takes 0.83 mS for the vehicle to travel 0.1 λ distance. For the simulation of a 106.7 ms data transmission (128 symbols or 256 bits), approximately 13.2 λ of fading data are needed. If the total

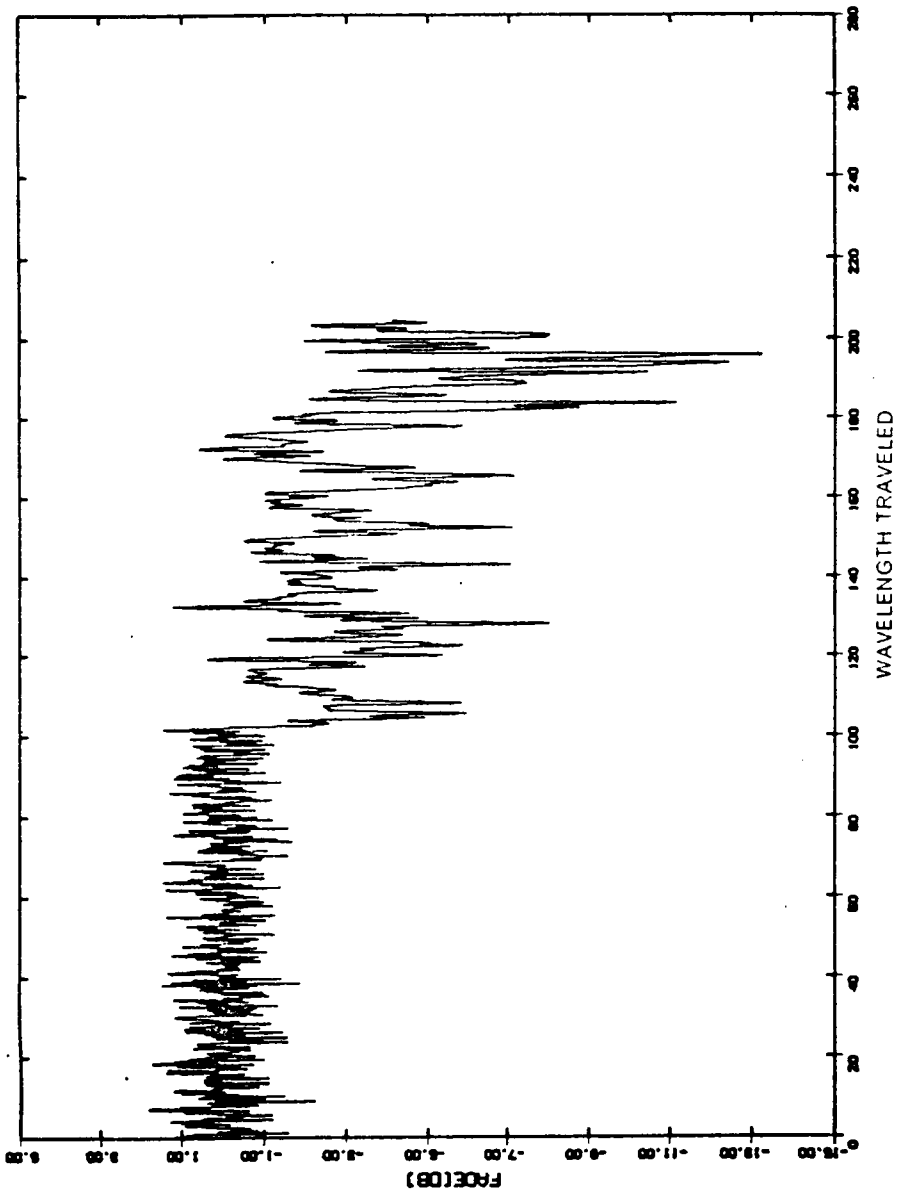

Figure 78. Amplitude (or fade depth) of 204.7 λ length fade data that were used in QPSK and MSK fading channel test.

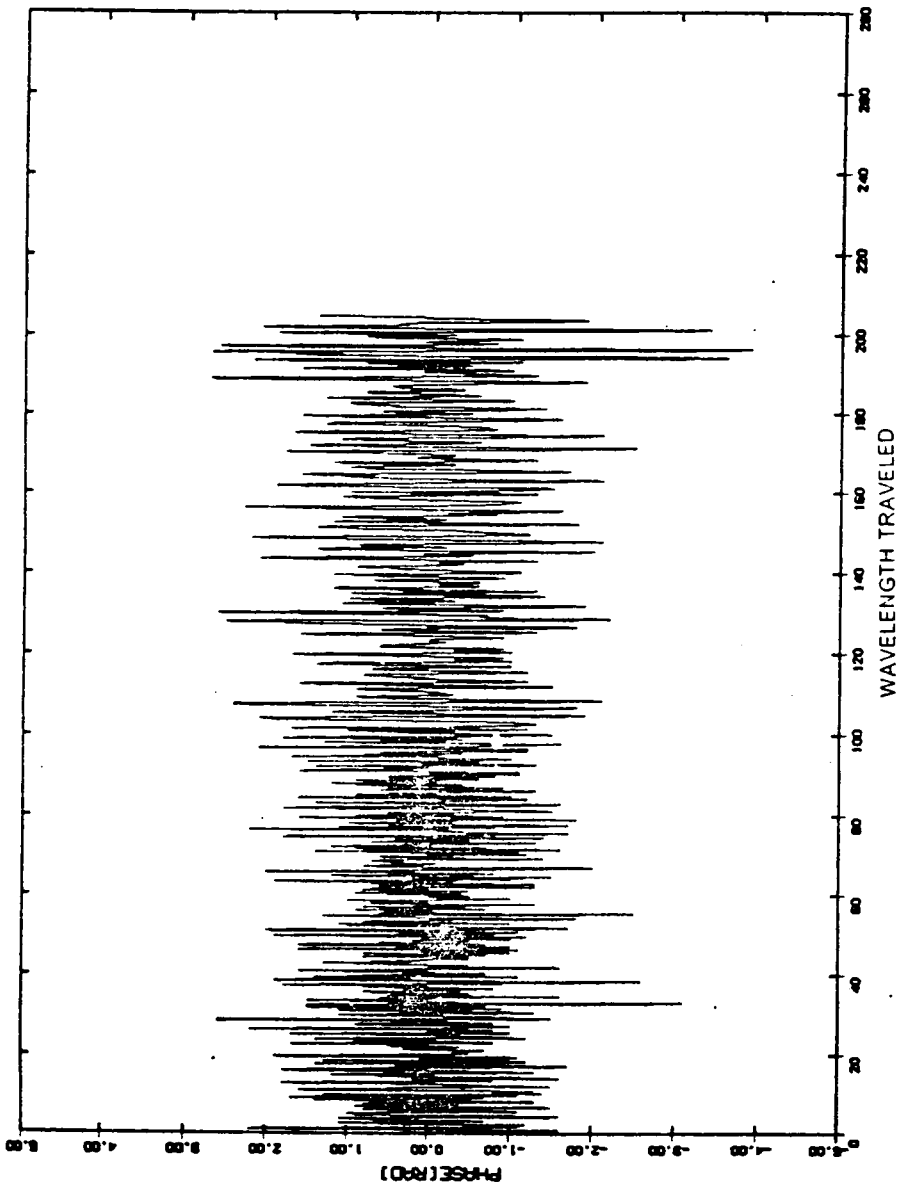

Figure 79. Phase (radian) characteristics of the signal whose amplitude was displayed in Figure 78.

204.7 λ interval fade data are processed, a total simulation time of 1956.9 ms is needed, and this time corresponds to 15.5 simulation cycles of 128 symbol blocks.

Any portion of the fade data corresponding to a 13.2 λ interval can be selected to provide 132 fading data points.

However, the 13.2 λ fade data (in practice, 132 fade data points) cannot be used directly. Although the sampling interval used in the simulation (assuming 2048 samples) is much shorter than the 0.1 λ travel time, the current fade data from the propagation simulator cannot provided data at less than a 0.1 λ interval. Therefore 2048 fade data point are generated from the selected 132 data points by a duplication factor of 15.5 (approximately, $2048/132 = 15.5$). Although the use of linear or nonlinear interpolation might enhance the accuracy, the method of simply duplicating the fade data is used here because the corresponding time to travel 0.1 λ is so short an interval that no significant change in the fade depth and phase is expected during this time interval.

Based on the preprocessing described above, several portions of 13.2 λ length were selected and applied to the transmit filter output. In simulation, the complex data for the signal and the fade are multiplied sample by sample to get the faded signal samples. Fig.80 to Fig.84 show the selected five 13.2 λ length interval of fade data used for the fading channel simulation. The original 13.2 λ portions from Fig.78 have been expanded in Fig.80 through Fig.84.

Fig.80 shows the fade data from 40.0 λ to 53.2 λ. This portion is selected because of its relatively small variations in fade depth compared with other portions. This portion represents the LOS signal. Fig.81 shows fade depth for the 95.0 λ to 108.2 λ portion. Compared with the fade of Fig.80, this portion shows the mixed characteristics of the LOS signal and a milder fade.

Contrary to Fig.80 and Fig.81, Fig.82 to Fig.84 shows the case of relatively severe fades. Among these three portions, fade depth in Fig.84 (portion of 190.0 λ to 203.2 λ) exhibits the most dramatic and rapidly varying characteristics in a short time interval. Compared with the fade of Fig.84, Fig.82 (portion of 118.0 λ to 131.2 λ) does not shows any significant change. The portion for the time interval 175.0 λ to 188.2 λ depicted in Fig.83 shows the start of changes in fade depth compared with Fig.82.

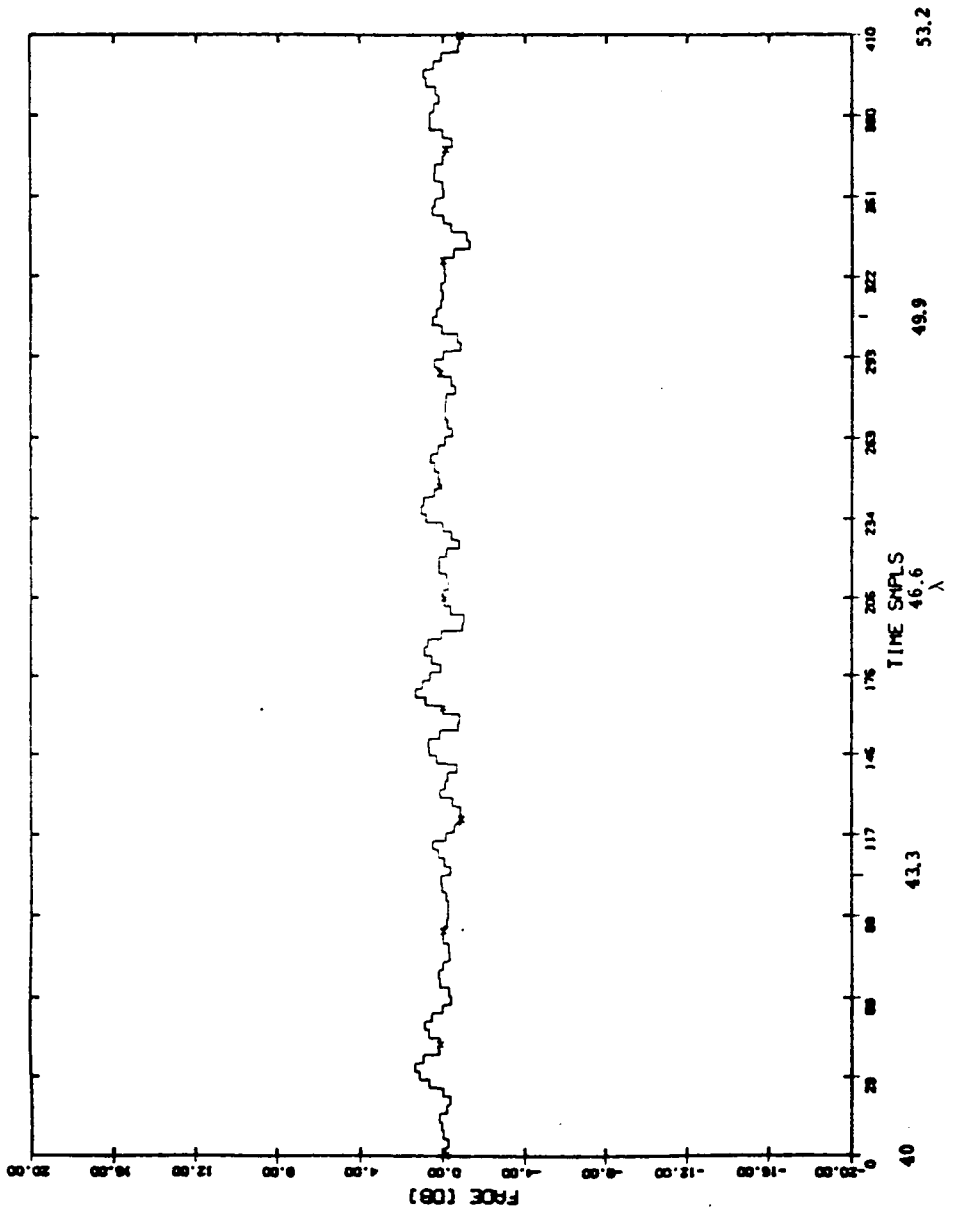

Figure 80. Expanded time scale showing fade depth for Fig 78 for 40 λ to 53.2 λ portion.

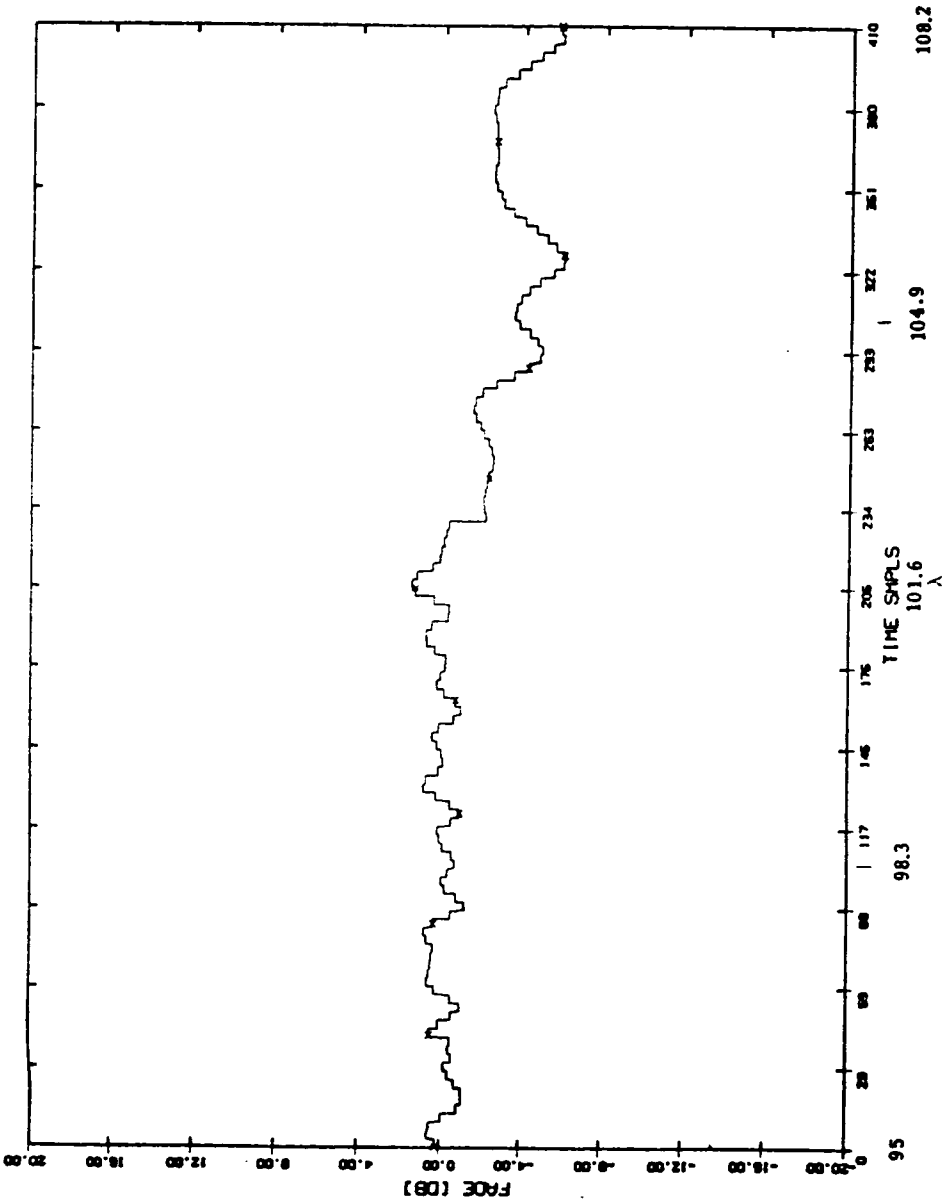

Figure 81. Expanded time scale showing fade depth for Fig.78 for 95.0 λ to 108.2 λ portion.

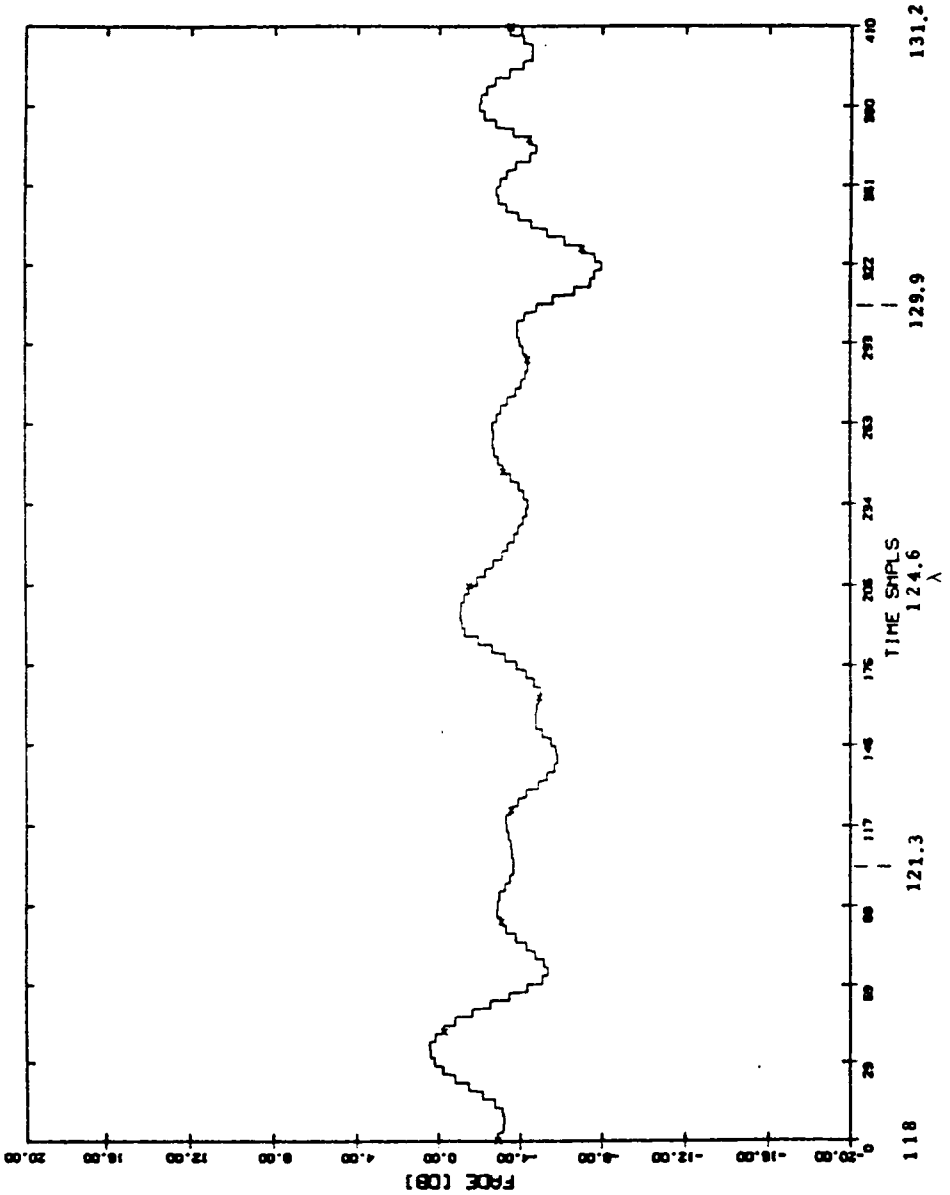

Figure 82. Expanded time scale showing fade depth for Fig.78 for 118.0 λ to 131.2 λ portion.

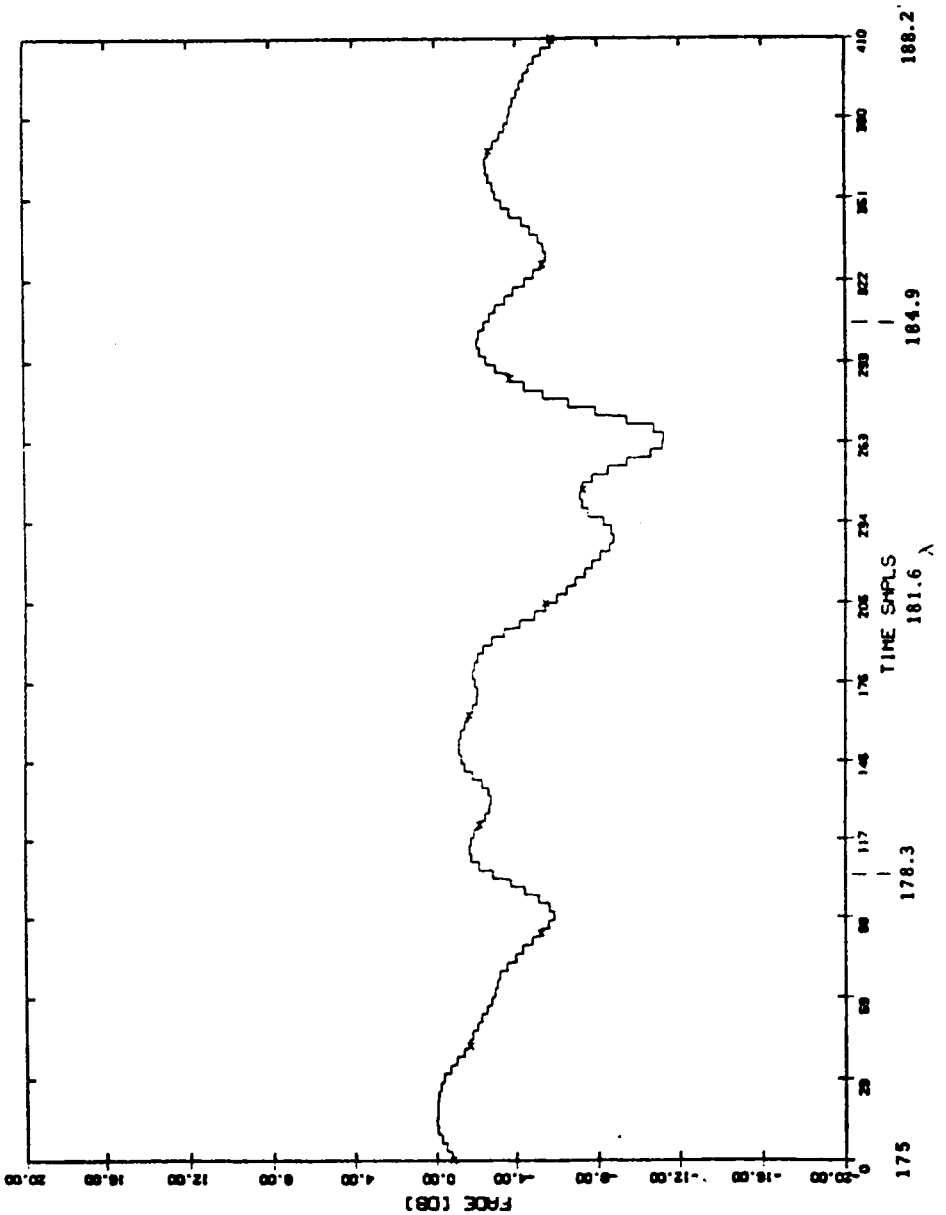

Figure 83. Expanded time scale showing fade depth for Fig.78 for 175.0 λ to 188.2 λ portion.

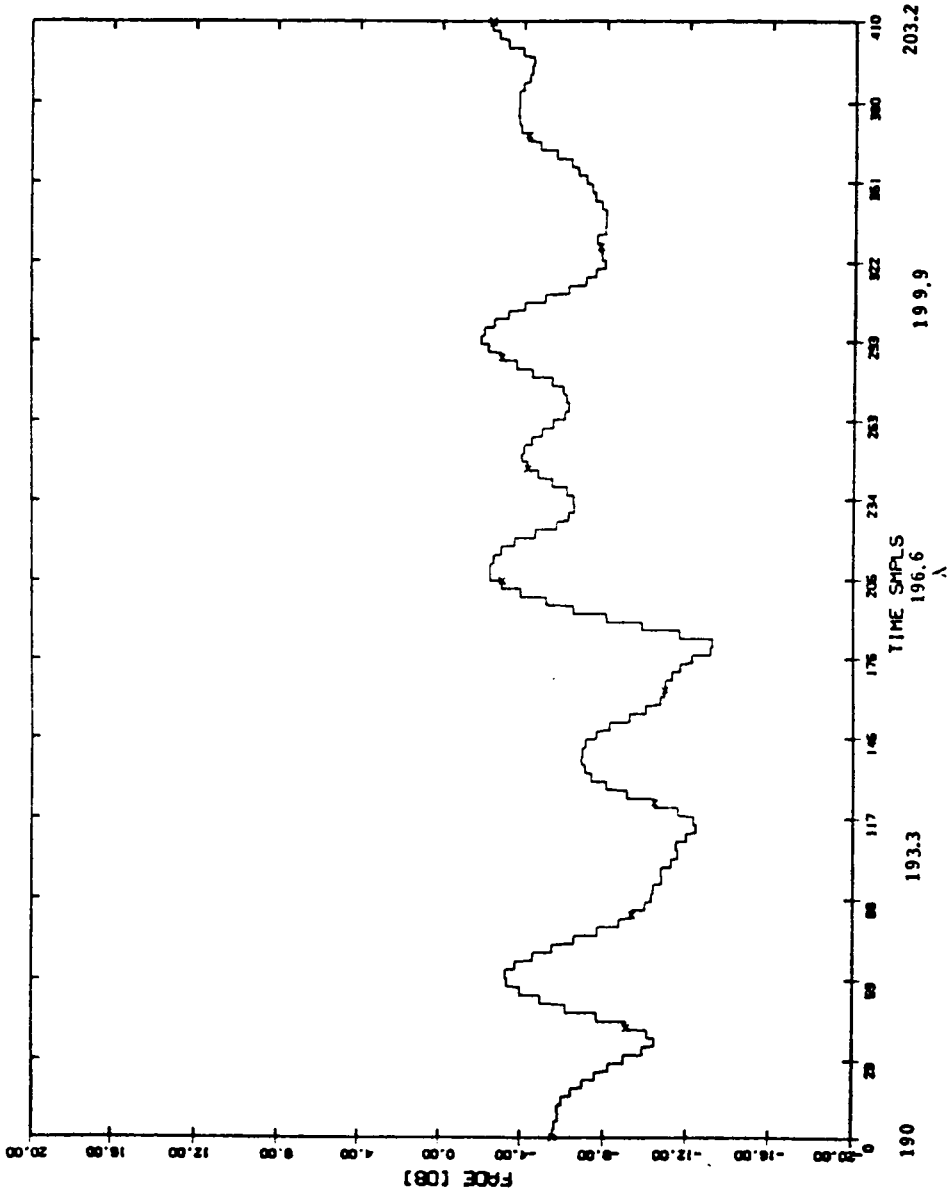

Figure 84. Expanded time scale showing fade depth for Fig.78 for 190.0 λ to 203.2 λ portion.

The five selected portions of fade depth were chosen to exhibit different fade characteristics to allow proper modeling of the LMSS channel.

Fig.85 shows the results of QPSK fading channel tests with results as average BER versus E_b/N_o ratio, when fades for the five 13.2 λ portions depicted in Fig.80 to Fig.84 are applied to the transmit filter output at 2.4 kbps. As can be seen from these curves, curve number 6 (results for 190.0 λ to 203.2 λ fade) shows the worst average BER performance, and curve number 2 (result of 40.0 λ to 53.2 λ fade) exhibits best average BER performance. These results are as expected when we compare the applied fade depth in Fig.80 and in Fig.84. Contrary to the small variation in fade depth centered around 0 dB in Fig.80 (fade of 40.0 to 53.2 λ), the fade in the interval 190.0 to 203.2 λ exhibits much more severe fading in the 0 dB to 13 dB range. Approximately 7 to 8 dB of E_b/N_o difference exists at the same BER between these two cases, and this gap gets larger at higher E_b/N_o ratios.

When we compare the curves numbered 3, 4, and 5, the relatively severe fade (curve number 5, fade portion of 175.0 to 188.2 λ) causes more degradation than the milder fades do (fade of 95.0 to 108.2 λ, and 118.0 to 131.2 λ), as expected.

If we compare the two extreme curves(number 6 and 2) in Fig.85 with the result of the modem back to back test (number 1 in the same figure), we can see that approximately 1 dB of additional E_b/N_o is needed to maintain the same BER as for the modem back to back test, even in the 40.0 to 53.2 λ portion fade case. This phenomenon is expected because there is still about 2 dB of fading in this portion as depicted in Fig.80. Comparison of curve number 6 (most severe fade for 190.0 to 203.2 λ) with the modem back to back test result confirms again that the severe fade causes more degradation than the mild fade.

Fig.86 shows the results of fading channel tests of coherent MSK when the same fades as were used in the coherent QPSK case (Fig.80 to Fig.84) are applied to the transmit filter output in the MSK system. When we look at the average BER performance denoted by the curves numbered 2 to 6 in Fig.86 (note that curve number 1 is the result of an MSK modem back to back test), the general trend in performance degradation is similar to the QPSK case, i.e, severe fades cause more degradation

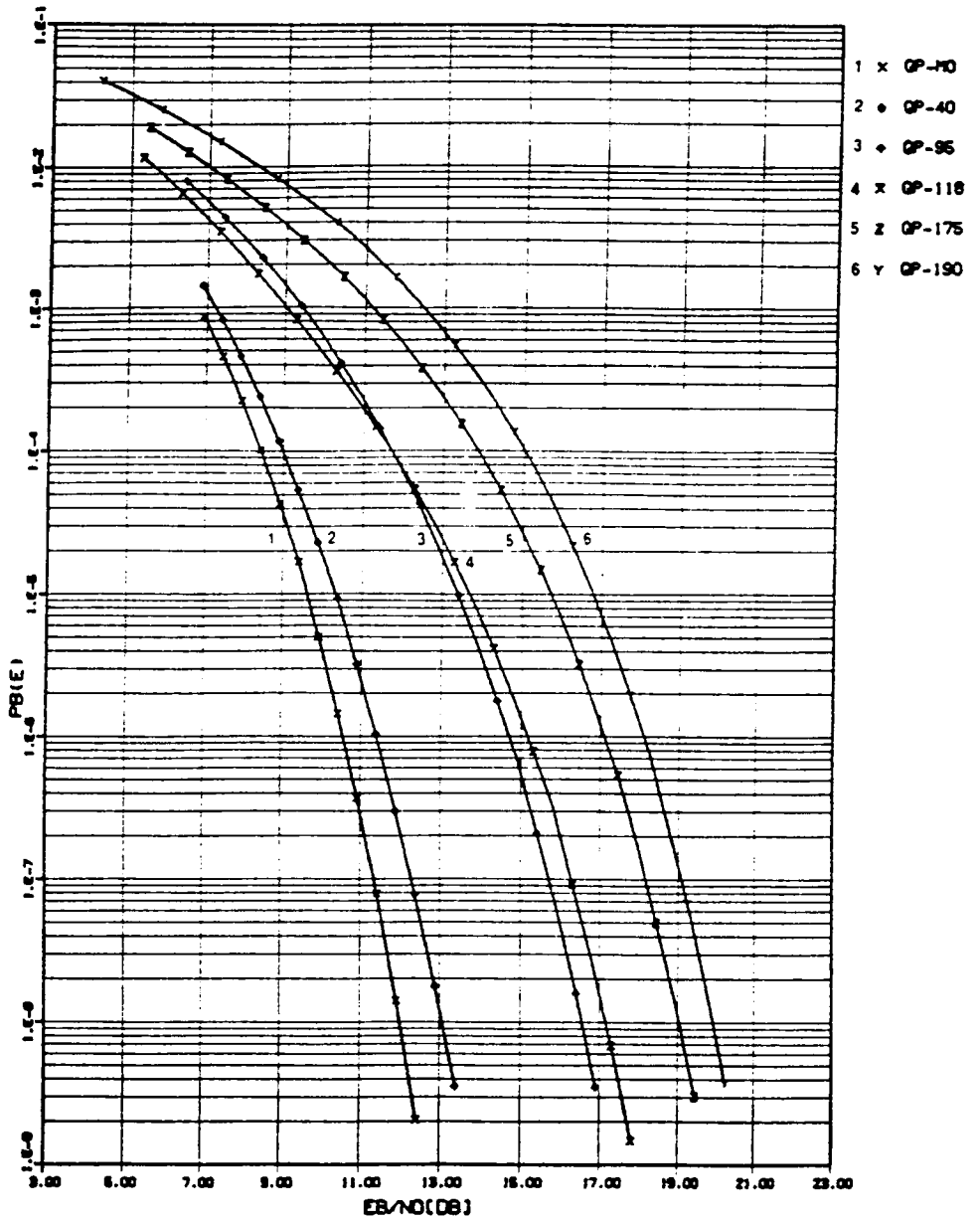

Figure 85. Average BER versus E_b/N_0 performance of coherent QPSK under fading, when fades of five 13.2 λ portions depicted in Fig.80 to Fig.84 are applied at the transmit filter output.

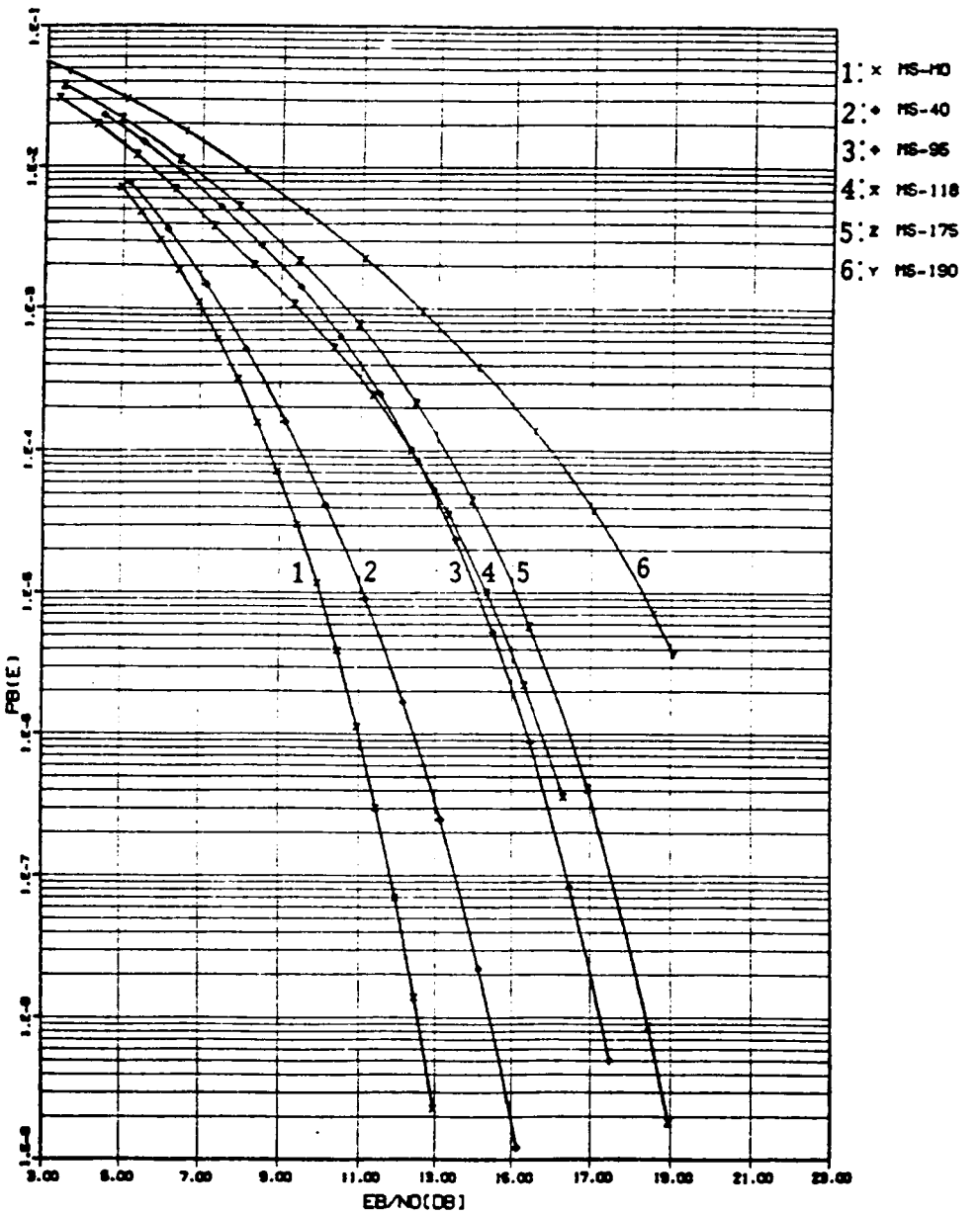

Figure 86. Average BER versus E_b/N_0 performance of coherent MSK under fading, when fades of five 13.2λ portions depicted in Fig.80 to Fig.84 are applied at the transmit filter output.

than the milder fade. However, the performance of MSK is generally inferior to QPSK, for the same applied fades. A similar result has already been observed from the comparison of modem back to back tests. However, the difference in degradation is not so large between the two modulation schemes under fading conditions, as can be seen from Fig.85 and Fig.86. At best 1 dB difference of E_b/N_o is seen for average BER ranges in the two graphs.

We have used the average BER as the major performance measure in the modem back to back tests and in fading channel tests, and average BER has been used in most digital communications systems. However, the measure of average BER may not be adequate to interpret the effect of fading in many cases, especially when there is a rapidly varying fade with a greater fade depth in a short time interval. Only the average value of bit error rate can be expressed by the average BER.

Bit by bit error probability can be used as an effective alternative to average BER, to investigate the effect of rapidly varying deep fades, in which the received sample value of each bit is directly calculated at a fixed E_b/N_o ratio. However, use of bit by bit error probability for the case of slowly varying or milder fades is not thought to be an effective method, because the effect of the fade will not be so evident for each specific bit in this case, contrary to the case of rapid, deeper fades.

Fig.87 to Fig.92 show the bit by bit error probability for coherent QPSK and MSK when three kinds of fades (characterized by their fade depth plots in Fig.81, Fig.83, and Fig.84) are applied to the transmit filter output at two fixed E_b/N_o ratios of 12 and 15 dB. For notational convenience, LOG (bit error probability) is used for the Y axis scales of all these plots.

Fig.87 and Fig.88 show the bit error probability for QPSK and MSK when the fade portion for 95.0 to 108.2 λ (Fig.81) is applied. Fig.89 and Fig.90. show the bit error probability for QPSK and MSK when the fade portion for 175.0 to 188.2 λ is applied. Fig.91 and Fig.92 illustrate the bit error probability of QPSK and MSK when the fade portion of 190.0 to 203.2 λ is applied.

The three cases of fading applied in these graphs can be classified into two categories. The fade in Fig.81 (from 95.0 to 108.2 λ) is a mixture of LOS signal and mild fade, while the fade depth of Fig.83

(from 175.0 to 188.2 λ) and Fig.84 (from 190.0 to 203.2 λ) are severe and include rapidly varying fades. In addition, the fade of Fig.84 is more severe than that of Fig.83.

Although many bit by bit plots are available, it is not easy to find the effect of fading with these plots alone. Comparison with the applied fade plot must be made for each case. To avoid complexity of explanation, we will confine the study of fading effects on bit error probability to a QPSK case only.

From the three bit error probability plots for QPSK, Fig.87, Fig.89, and Fig.91, we can find the obvious fact that the average error rate is lower for the case of Fig.87, where the fade in the time interval 95.0 to 108.2 λ was applied, and there is little fading. This fact can easily be confirmed from the average BER plot of Fig.85. In addition, it can also be confirmed for the MSK case when Fig.88, Fig.90, and Fig.92 are carefully reviewed along with the average BER plot for MSK, Fig.86.

The other fact we can confirm from these bit error probability plots is the fact that the bit by bit error rate gets lower as E_b/N_o gets higher, i.e, the error rate for 15 dB E_b/N_o is lower than that for the 12 dB case, regardless of the fade applied. This is also expected because higher E_b/N_o ratios mean that a lower level of noise was applied in the BER calculation. These phenomena can be easily observed from this series of plots, regardless of which modulation scheme was used.

To see the effect of fading more clearly, the bit error probability plot of Fig.91, and the corresponding fade plot, Fig.84 are overlapped in Fig.93. The fade depth applied in this plot is a portion of 13.2 λ, from 190.0 to 203.2 λ, from the 204.7 λ interval depicted in Fig.78.

In Fig.93, we can see the effect of a deep fade that occurs in a relatively short time interval. The bit by bit error plots for the two fixed E_b/N_o ratios of 12 and 15 dB follow closely the fade depth of the signal. In another way of saying, when there is a deeper fade, the error rate is high, and the error rate is lower when the fade is milder. Therefore, we can predict the effect of fading up to a certain point if the fading characteristics can be provided in the form of signal amplitude and phase, as was depicted in Fig.78 and Fig.79.

When we compare the performance of QPSK and MSK based on the simulation results for average BER and bit error probability, MSK is a little inferior to QPSK. However, in our simulation, much effort was given to make the simulation conditions the same for the two modulations, for convenience of comparison. This trial may not be adequate to assess the different modulation

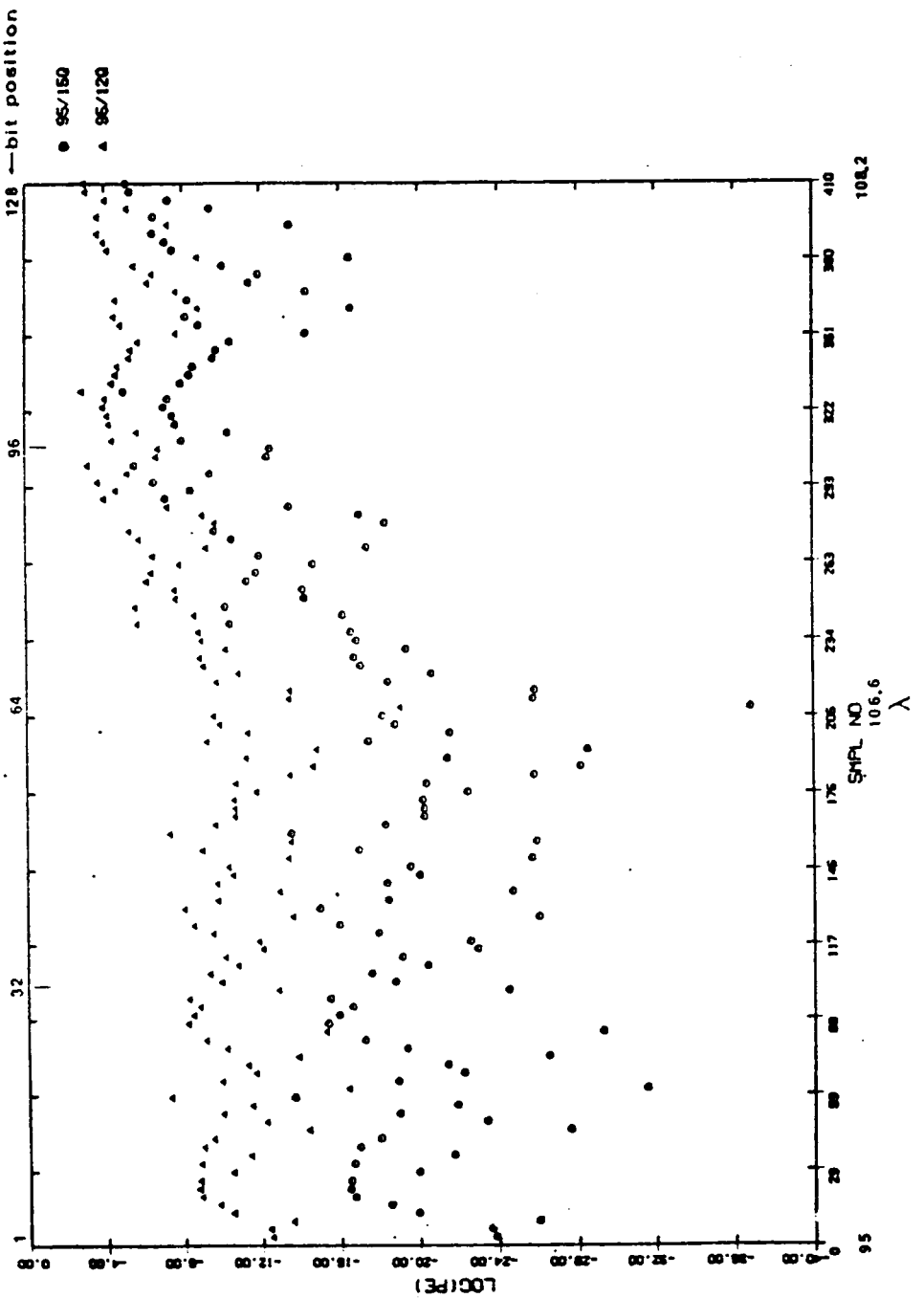

Figure 87. Bit error probability performance of coherent QPSK when the fade of Fig.81 (95.0 to 108.2 λ) is applied to the transmit filter output at a fixed E_b/N_o ratio of 12 and 15 dB.

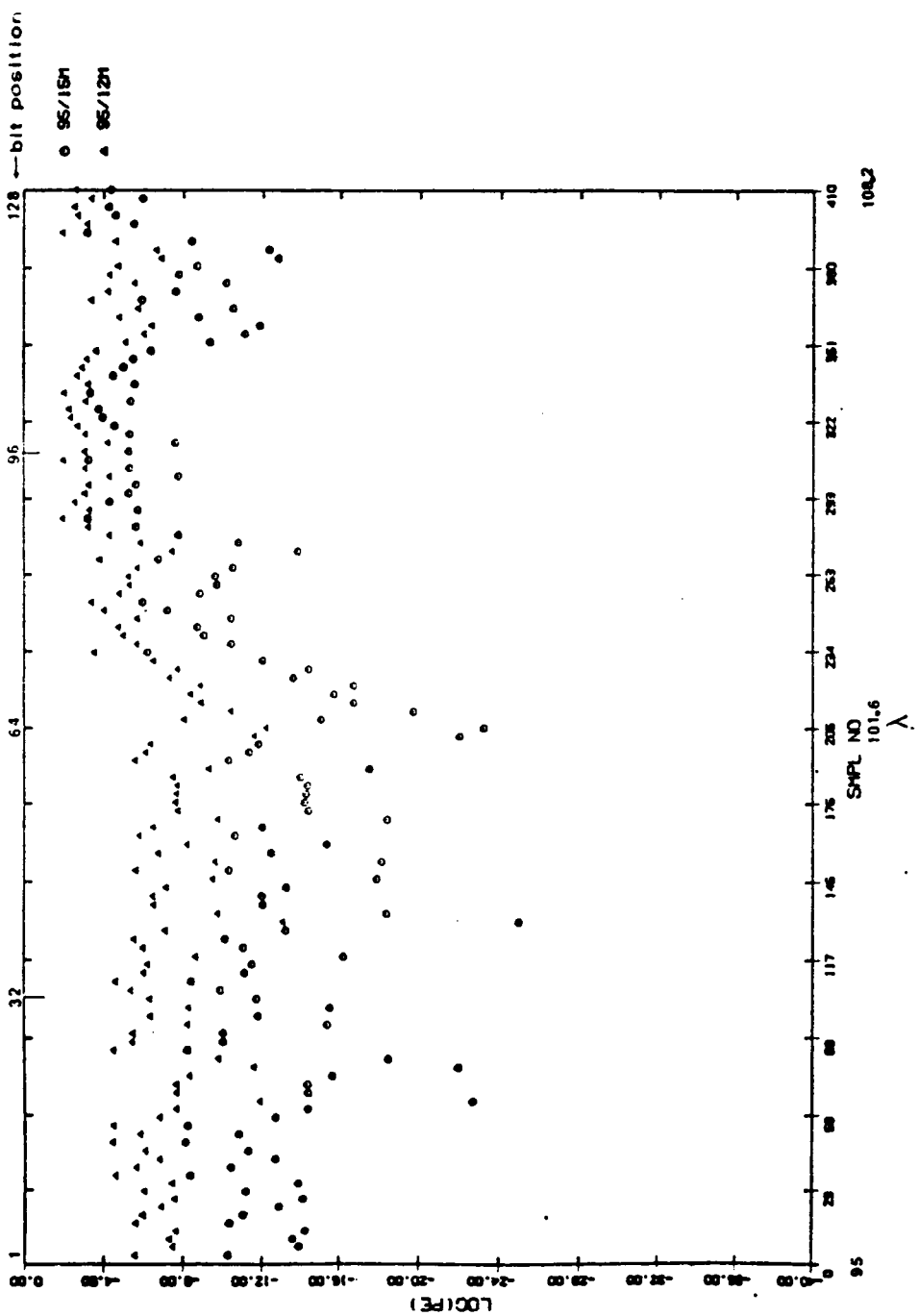

Figure 88. Bit error probability performance of coherent MSK when the fade of Fig.81 (95.0 to 108.2 λ) is applied to the transmit filter output at a fixed E_b/N_o ratio of 12 and 15 dB.

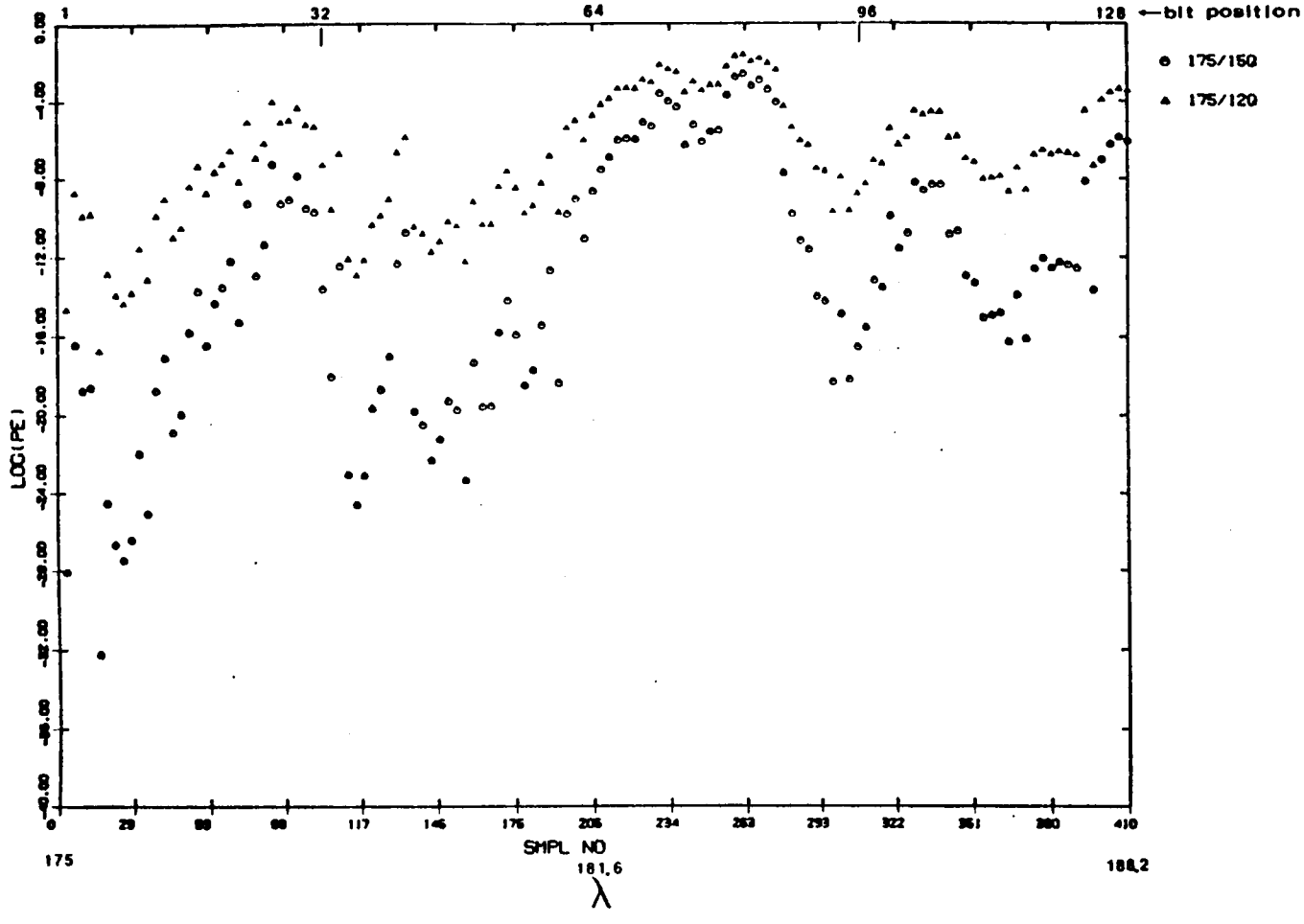

Figure 89. Bit error probability performance of coherent QPSK when the fade of Fig.83 (175.0 to 188.2 λ) is applied to the transmit filter output at a fixed E_b/N_o ratio of 12 and 15 dB.

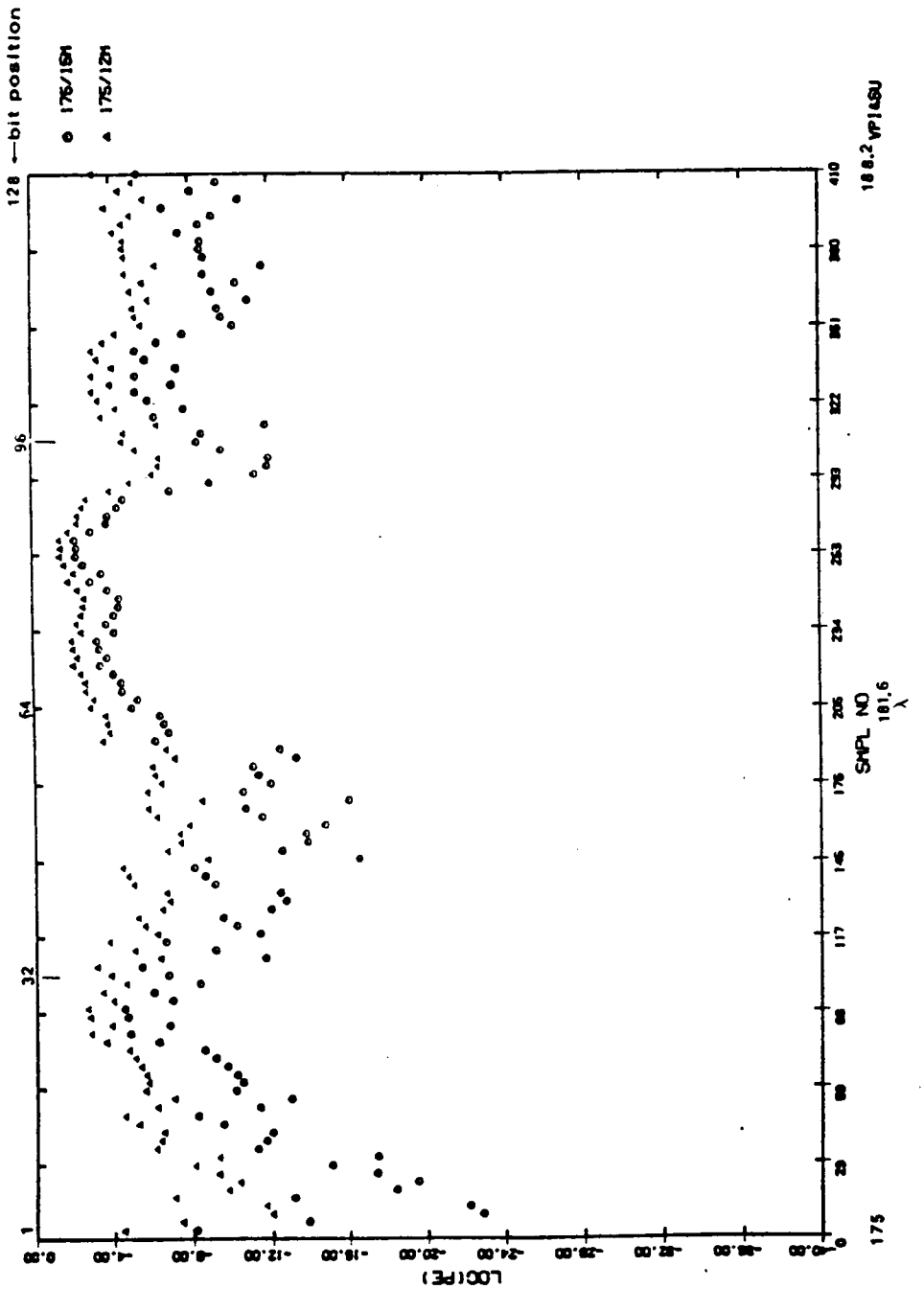

Figure 90. Bit error probability performance of coherent MSK when the fade of Fig.83 (175.0 to 188.2 λ) is applied to the transmit filter output at a fixed E_b/N_o ratio of 12 and 15 dB.

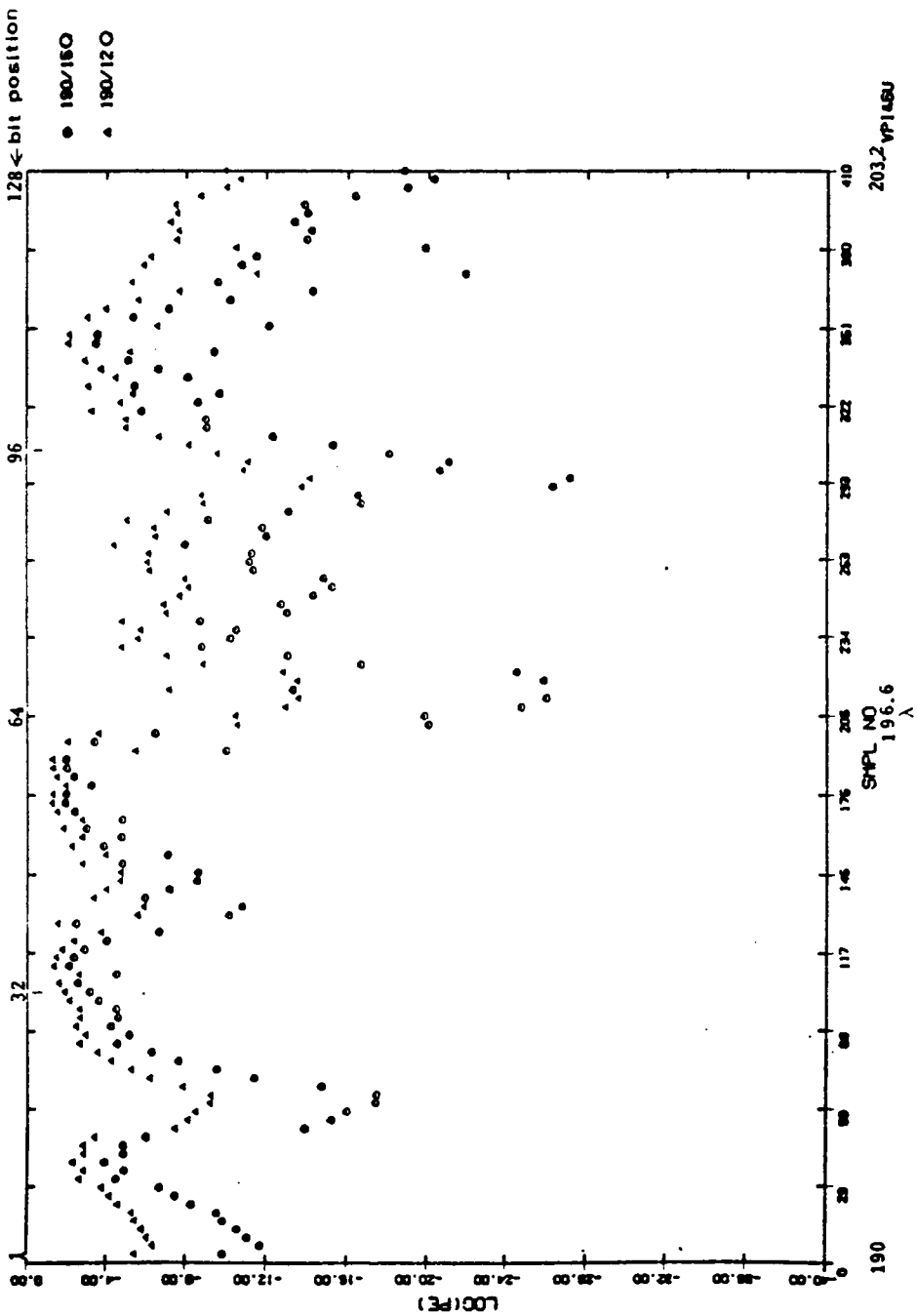

Figure 91. Bit error probability performance of coherent QPSK when the fade of Fig.84 (190.0 to 203.2 λ) is applied to the transmit filter output at a fixed E_b/N_o ratio of 12 and 15 dB.

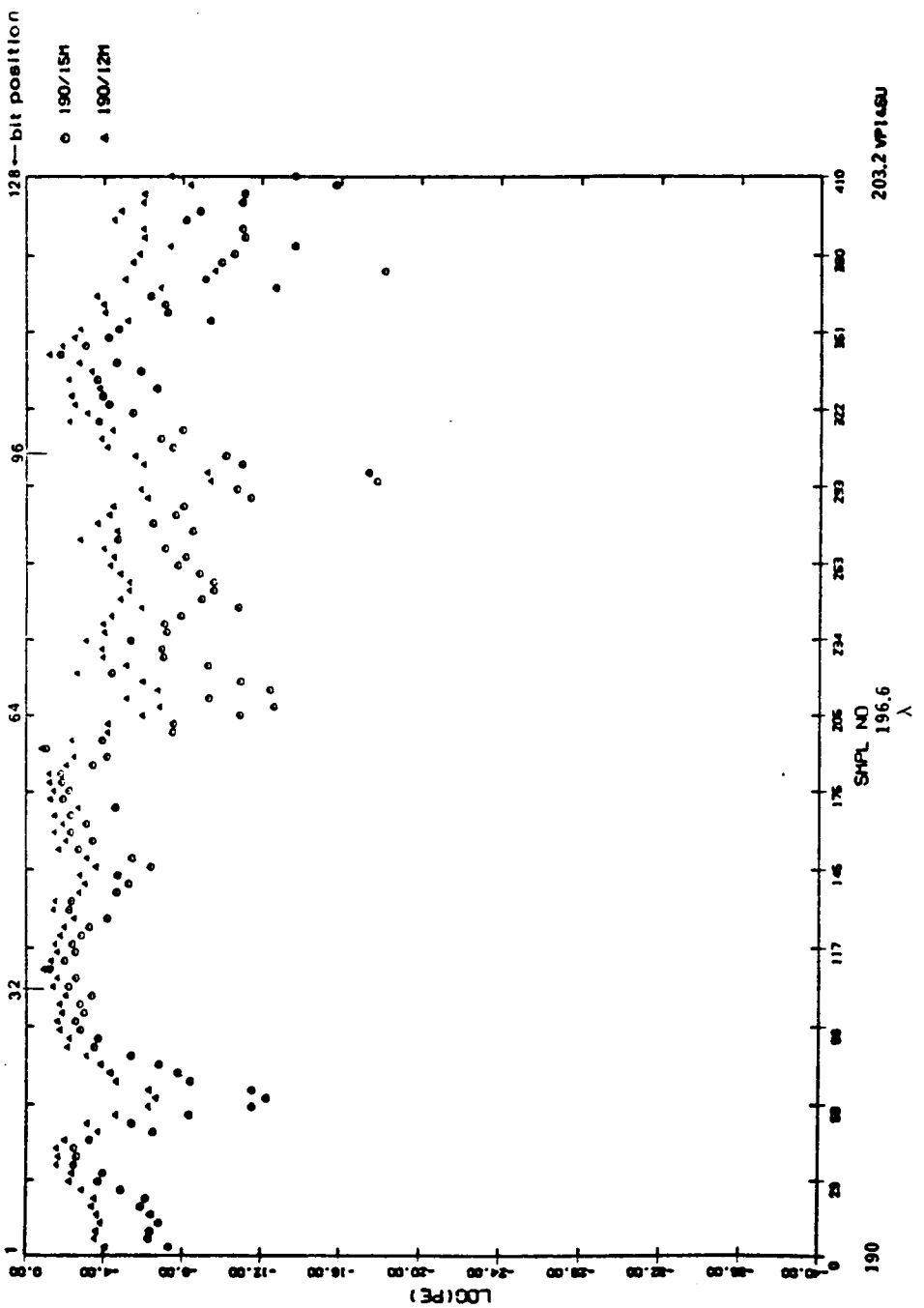

Figure 92. Bit error probability performance of coherent MSK when the fade of Fig.84 (190.0 to 203.2 λ) is applied to the transmit filter output at a fixed E_b/N_o ratio of 12 and 15 dB.

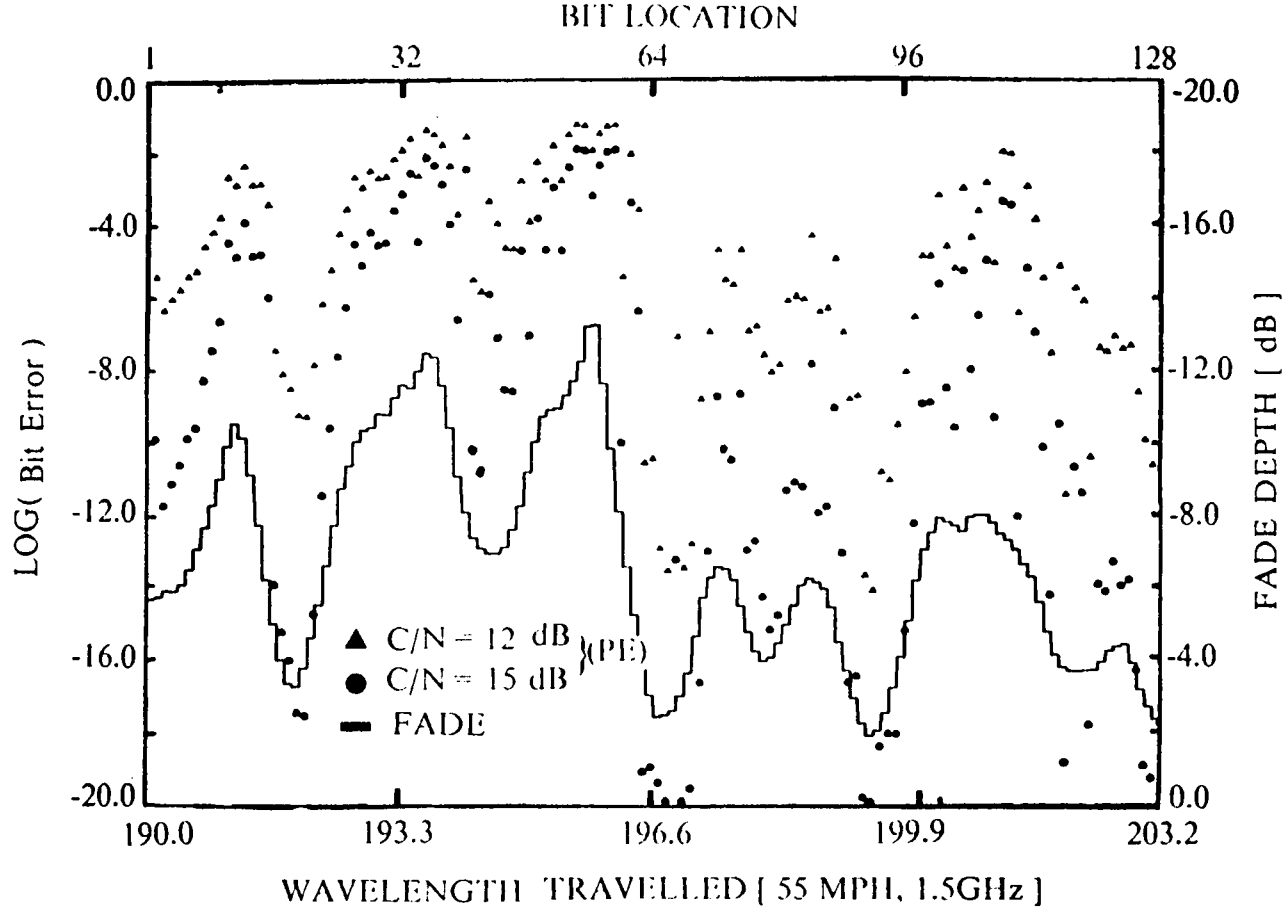

Figure 93. Overlapped plot of QPSK bit error probability and the applied fade depth (fade depth of Fig.84: 190.0 to 203.2 λ interval and corresponding bit error probability plot of Fig.91 are overlapped).

schemes because each scheme may exhibits its best performance only when its own advantages over other schemes are preserved by externally given system parameters.

6.3. Performance of Noncoherent TCM 8-PSK and DGMSK

For performance evaluation of the noncoherent digital modulation schemes, TCM 8-DPSK and DGMSK, the simulation programs 'LANSIM 2' and 'LANSIM 3' were used. Because of the relative complexity of the simulation procedures in TCM 8-DPSK and DGMSK, compared to the coherent schemes, several intermediate results are presented to enhance the understanding of the simulation flow.

Direct simulation (Monte-Carlo simulation), contrary to the analytic calculation of error rate used in the coherent QPSK and MSK case, allows the number of erroneous symbols or bits to be counted directly to calculate the symbol error rate or bit error rate.

However, the idea of average BER used in the coherent schemes cannot be applied in these schemes, because we do not know how many symbols must be simulated and evaluated to get the average symbol error rate or bit error rate by direct simulation. In addition, there are practical limitations in the simulation when a large number of symbols are used, such as long computation time and high cost. Because of these restrictions, only 6400 symbols (12800 bits) were generated and simulated for the modem back to back test of TCM 8-DPSK.

The preliminary results of the DGMSK simulation with 128 symbols under noise conditions exhibited an unexpectedly large number of errors, and we concluded that the simulation program did not work properly in some place, but we do not know why. So the results of the modem back to back test and fading channel test for DGMSK cannot be reported here. Only the intermediate results of the simulation procedures are included in this thesis.

Even in the TCM 8-DPSK case, the propagation simulator should provide a huge amount of diverse fading data, for as many symbols as are used in the simulation. But it cannot be fully

integrated in the channel simulator programs (LANSIM 2 and LANSIM 3) because modifications are still in progress. Therefore, results of the fading channel test for TCM 8-DPSK and DGMSK are also not reported here. Although the result of fading channel tests with a small number of transmitted symbols is possible, subsequent analysis based on this result is apt to be totally wrong, especially when direct simulation is employed, because too few symbols have been used to obtain a reliable error rate.

6.3.1. Intermediate Simulation Results

Fig.94 and Fig.95 show the simulation block diagrams of TCM 8-DPSK and DGMSK respectively. The optional propagation simulator, that will be used only for the fading channel test, is denoted by a dotted box in these diagrams.

Before we see the result of the modem back to back test of TCM 8-DPSK, let us see some of the intermediate results in the simulation. Fig.96 shows an example of the original 256 bit binary input data stream (corresponding to 128 2-bit symbols before coding) used both for TCM 8-DPSK and for DGMSK simulations, when an arbitrary seed of 226.8 is used for symbol generation. Once this input bit stream is encoded by the trellis encoder in TCM 8-DPSK, the mapped 128 symbols phases can be depicted as in Fig.97. Note that these phases are not differentially phase encoded yet. After the symbol to phase mapping in the transmitter in TCM 8-DPSK, the phases in Fig.97 are differentially phase encoded as depicted in Fig.98. Because of the phase addition in differential phase encoding, the phases are increasing as the number of symbols is increasing.

Contrary to the TCM 8-DPSK case, there is no need for differential encoding in DGMSK transmission, so the convolutionally encoded input data are directly forwarded to the Gaussian pre-modulation filter. Fig.99 shows the frequency response of Gaussian lowpass filter normalized to 1.0 when the BT product is 0.33. After the pre-filtering in DGMSK, we get the DGMSK instantaneous

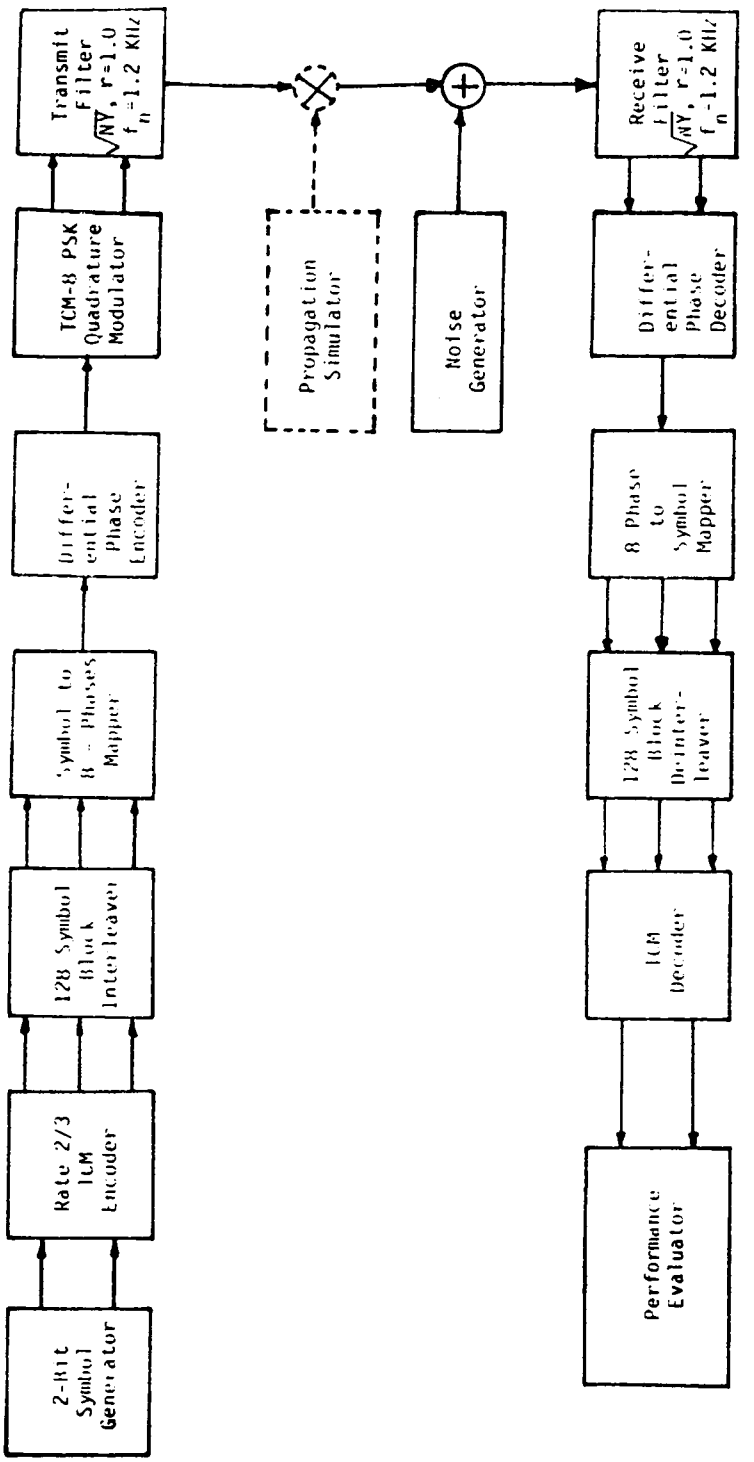

Figure 94. Simulation block diagram of TCM 8-DPSK used for the modem back to back test.

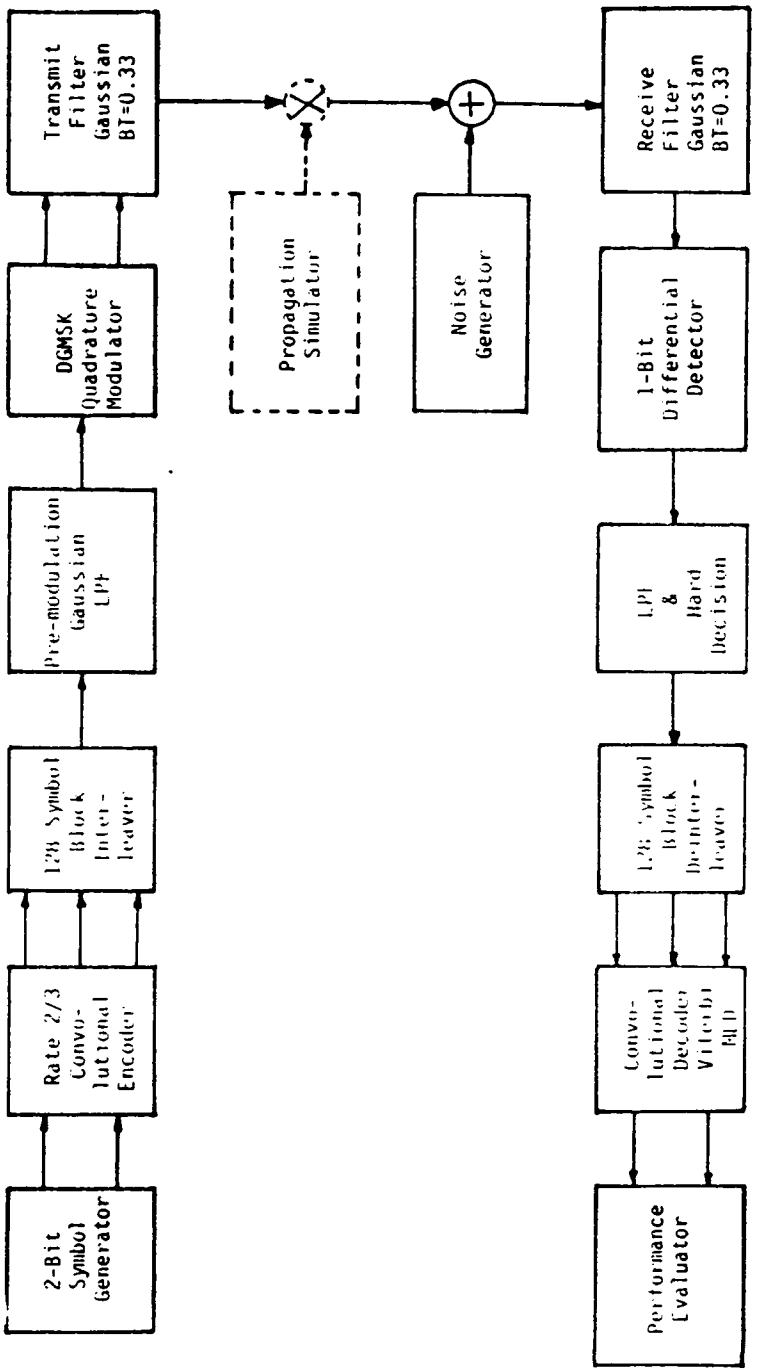

Figure 95. Simulation block diagram of DGMSK used for the modem back to back test.

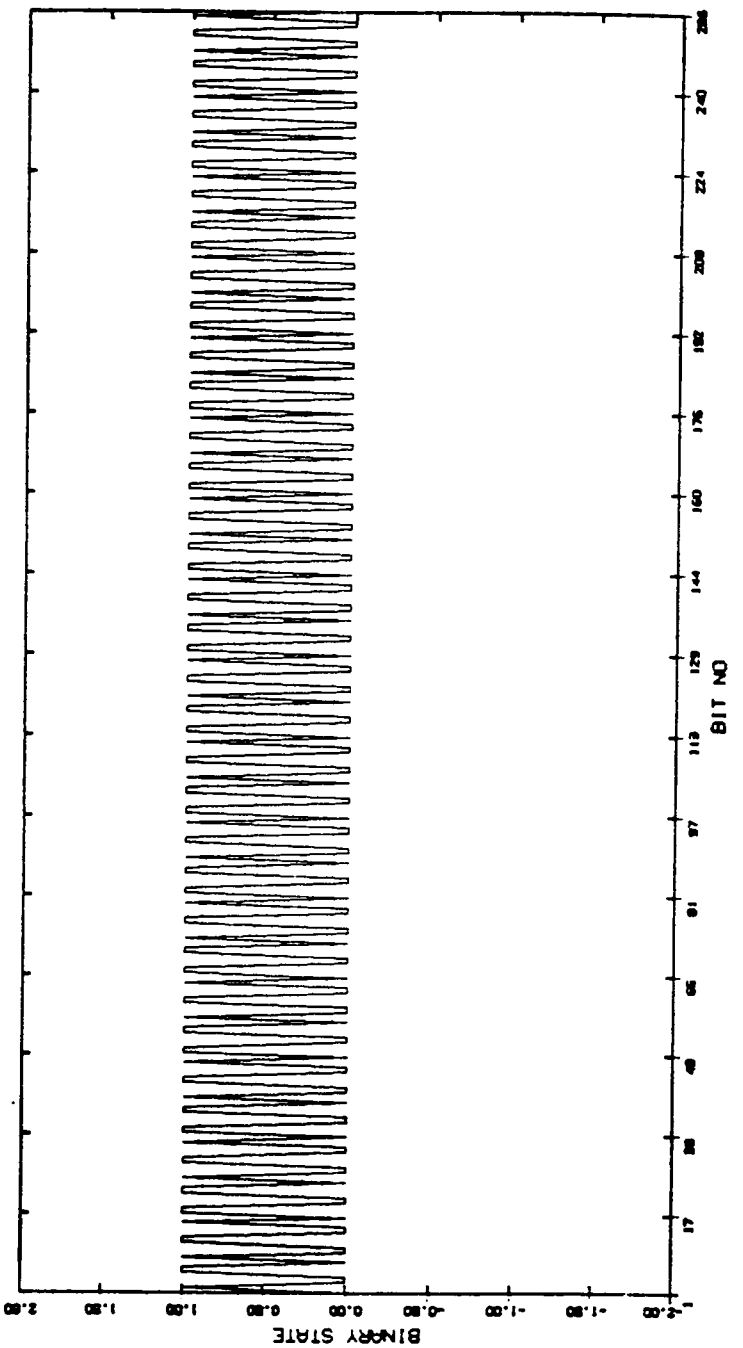

Figure 96. Example of simulated 256 bit (128 2-bit symbols) serial binary data stream used both for TCM 8-DPSK and for DGMSK.

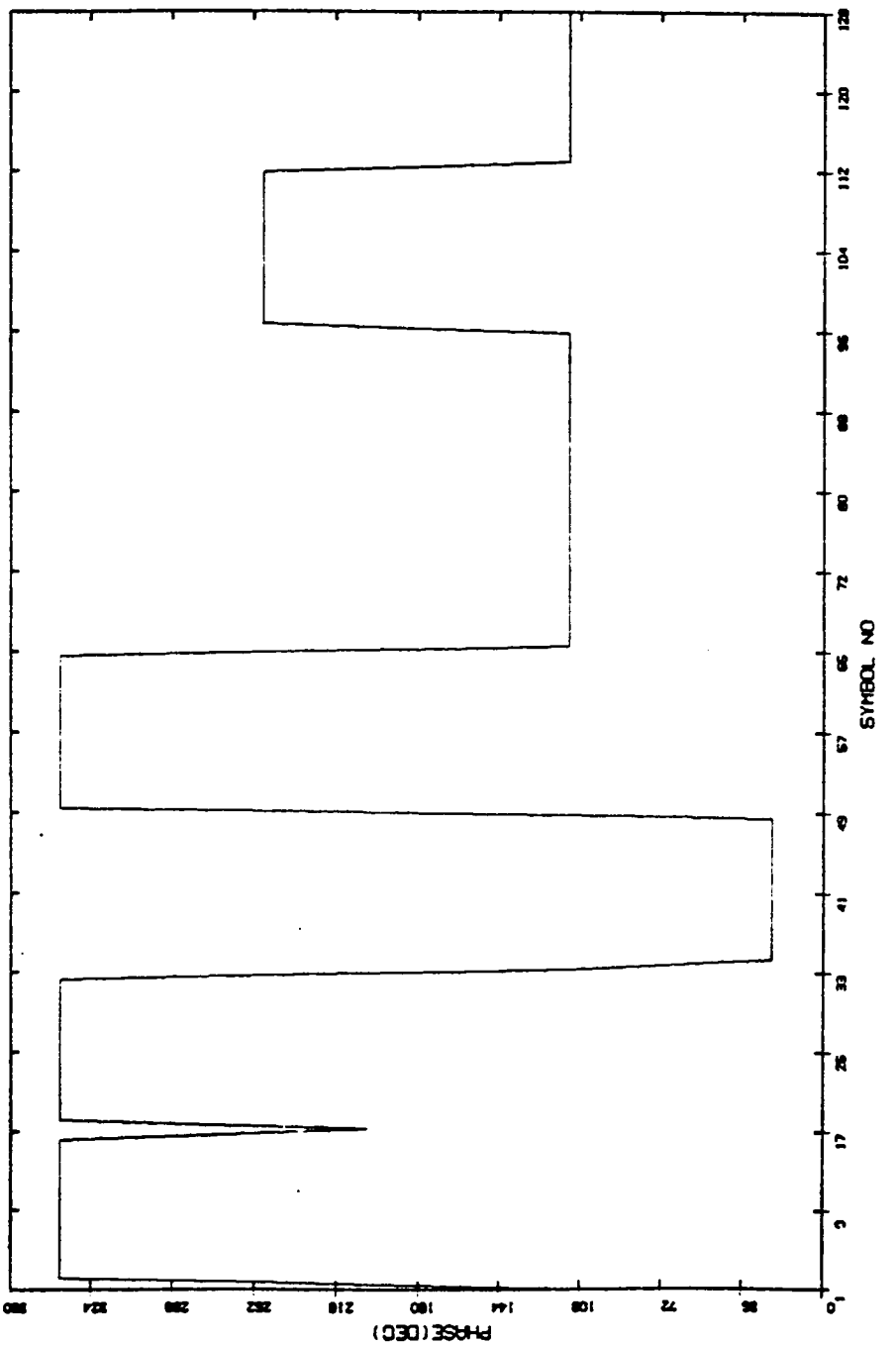

Figure 97. Mapped 128 3-bit encoded symbol phases of TCM 8-DPSK before differential phase encoding.

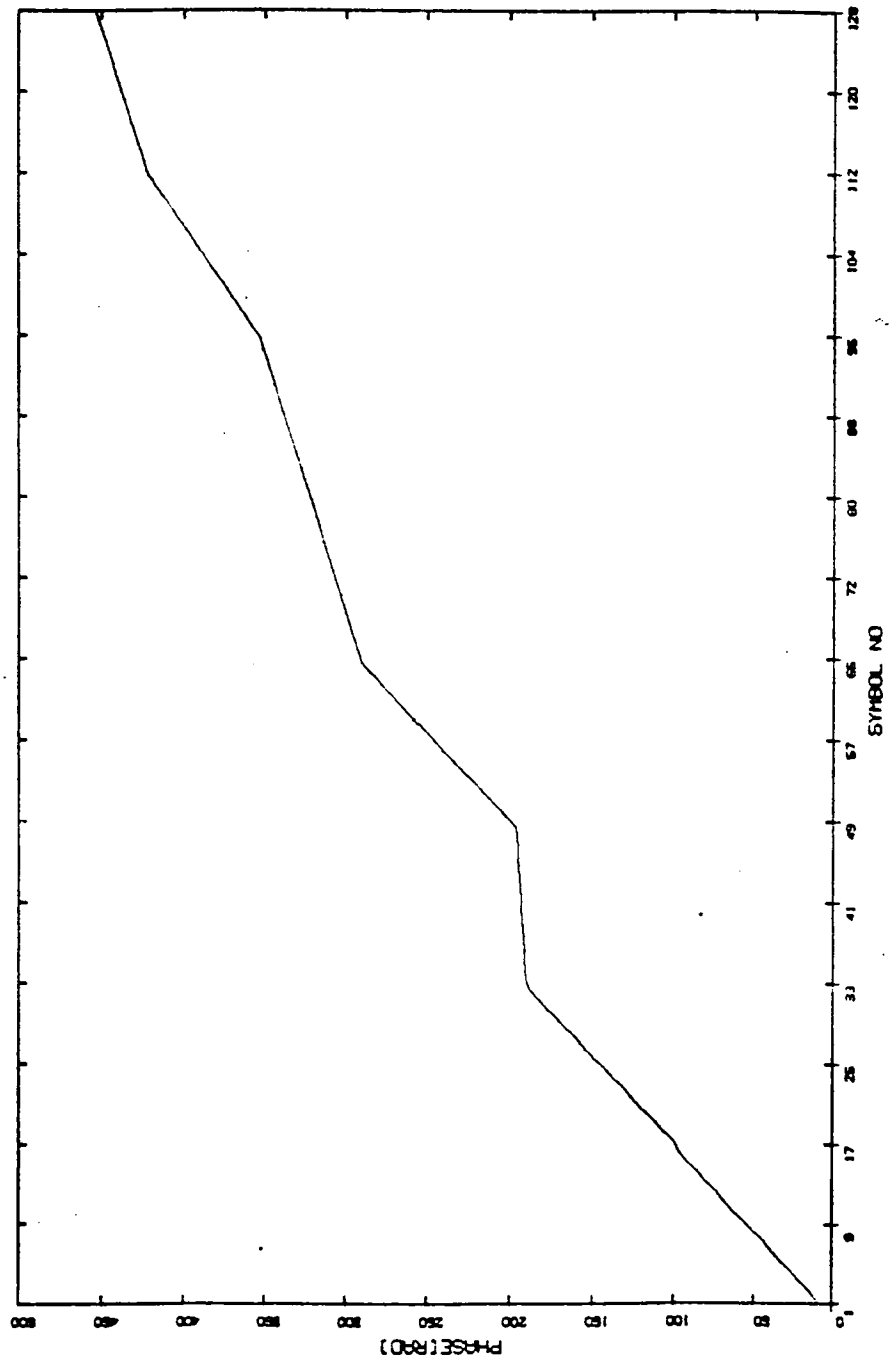

Figure 98. Differential encoded phases of TCM 8-DPSK when phases of Fig 97 are differentially phase encoded.

phase as depicted in Fig.100, in which we can see the continuously changing phases of the first 5 symbols when an initial phase of 0 radian is given.

After differential phase encoding, the TCM signal is modulated by the quadrature modulator. Fig.101 shows the time plot of the TCM 8-DPSK signal (I channel only) after the transmit filter. The filter was simulated by a square root raised cosine Nyquist filter with amplitude equalizer, with a roll-off factor r, of 1, for a Nyquist frequency of 1.2 KHz. In addition, we can see the result of noise addition to the modulator output in Fig.102. A carrier to noise ratio (C/N) of 6 dB was used in this case. As can be seen in this figure, random noise can change the shape of the transmitted signal amplitude.

If the modulator output of Fig.101 is faded and noise is added, we can see the result in Fig.103. In this case, the same fade of Fig.84 as was used in the QPSK and MSK case, was given. As can be seen from this figure, the signal amplitude is much different from the original transmitted plot in Fig.101.

In TCM 8-DPSK, the faded and noise-corrupted signal is forwarded to the receiver and this signal is differentially phase decoded. Fig.104 shows the result of differential phase decoding based on the method described in Table 5.4 in Chapter 5. The estimated phase in this diagram is used for the final phase to symbol mapping in the receiver. If we compare the estimated phase in Fig.104 with the original phase before differential phase encoding depicted in Fig.97, we can see the effects of noise and fade easily from the phase jitter.

6.3.2. Modem Back to Back Test of TCM 8-DPSK.

As was noted before, only the result of a TCM 8-DPSK modem back to back test is reported here. Fig.105 shows this result. This result was obtained from a cyclic run of the simulation program 'LANSIM 2'. Because only 128 symbols are generated and simulated in a single simulation cycle, 50 repetitive runnings were performed to simulate the transmission of 6400 symbols. To give randomness

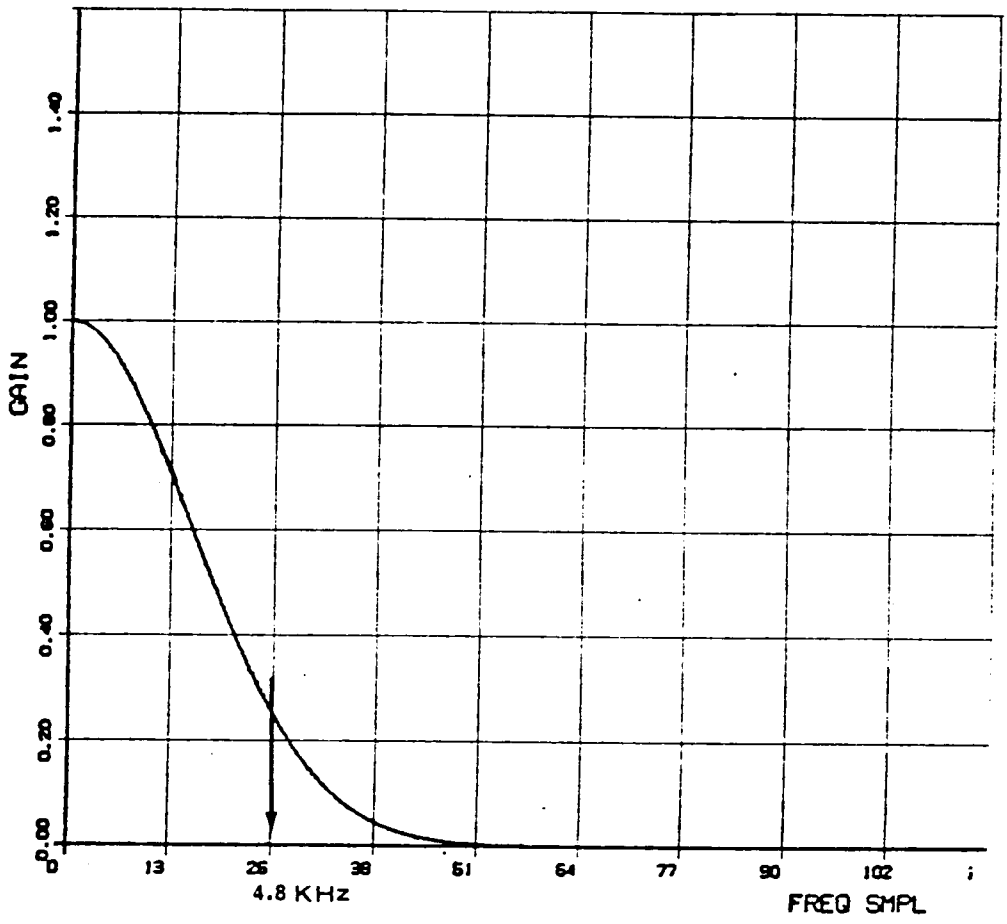

Figure 99. Frequency response of pre-modulation Gaussian lowpass filter (normalized to 1.0, BT = 0.33)

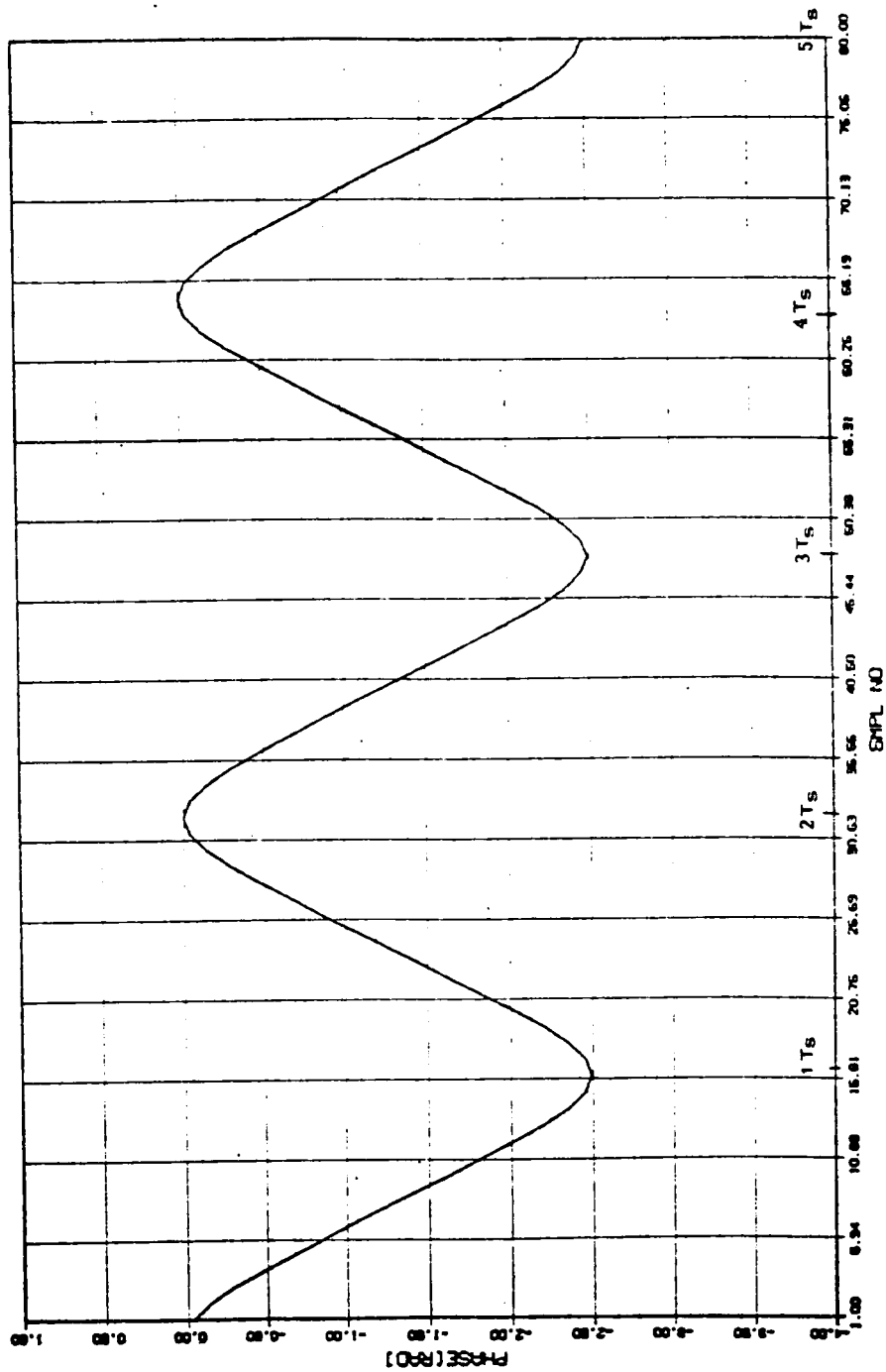

Figure 100. Example of DGMSK continuous, instantaneous phases of first 5 convolutionally encoded symbols after Gaussian lowpass filtering.

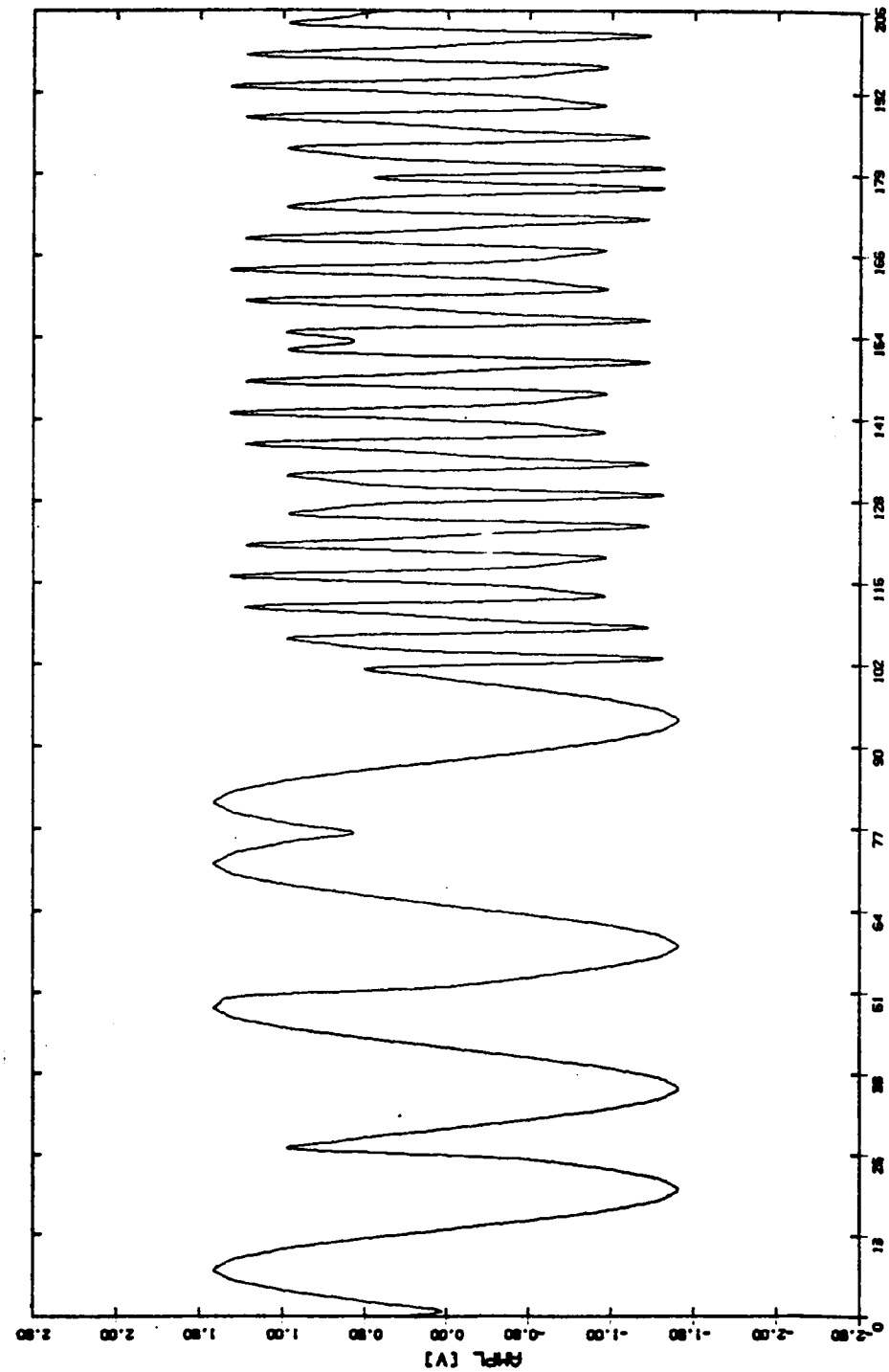

Figure 101. Time plot of the I channel signal of the modulator output of TCM 8-DPSK after transmit filtering by square root raised cosine Nyquist filter ($r = 1.0$, $f_n = 1.2$KHz)

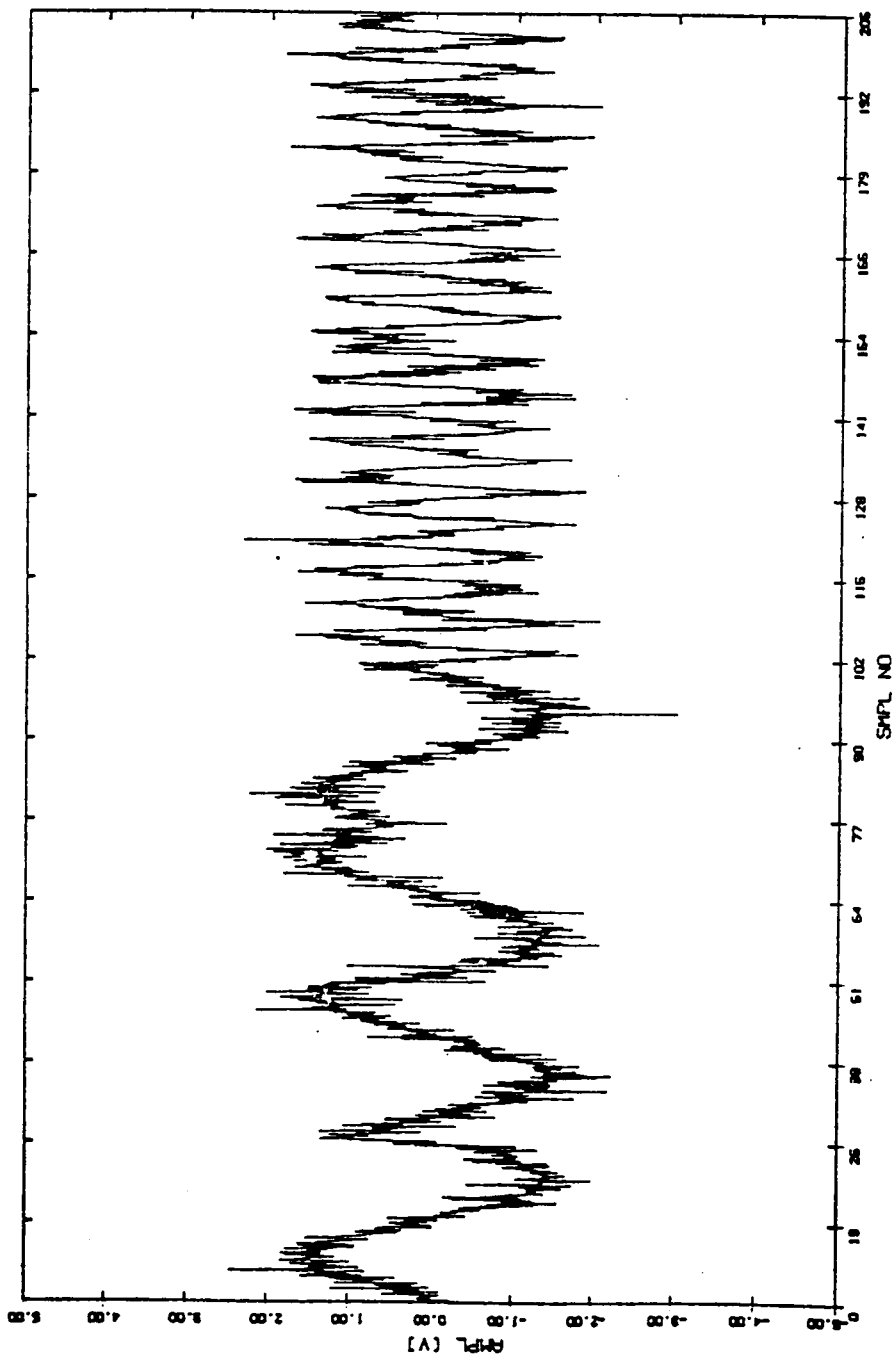

Figure 102. Example of the result of noise addition to the modulator output of Fig.101 (C/N = 6 dB).

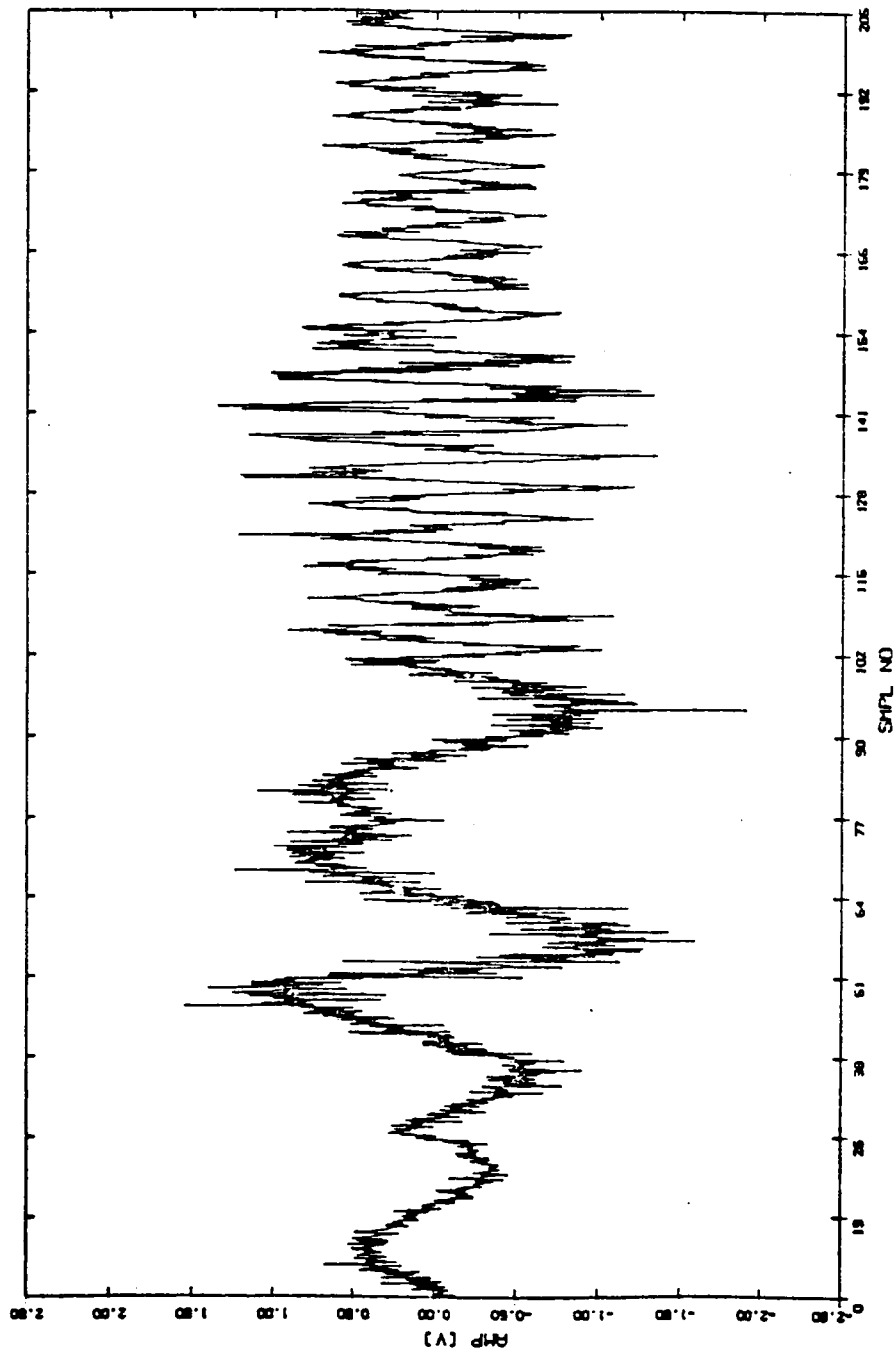

Figure 103. Example of the faded signal time plot (amplitude of the modulator output of Fig.101) after the fading and noise addition (C/N = 6 dB, fade of Fig.84 is used)

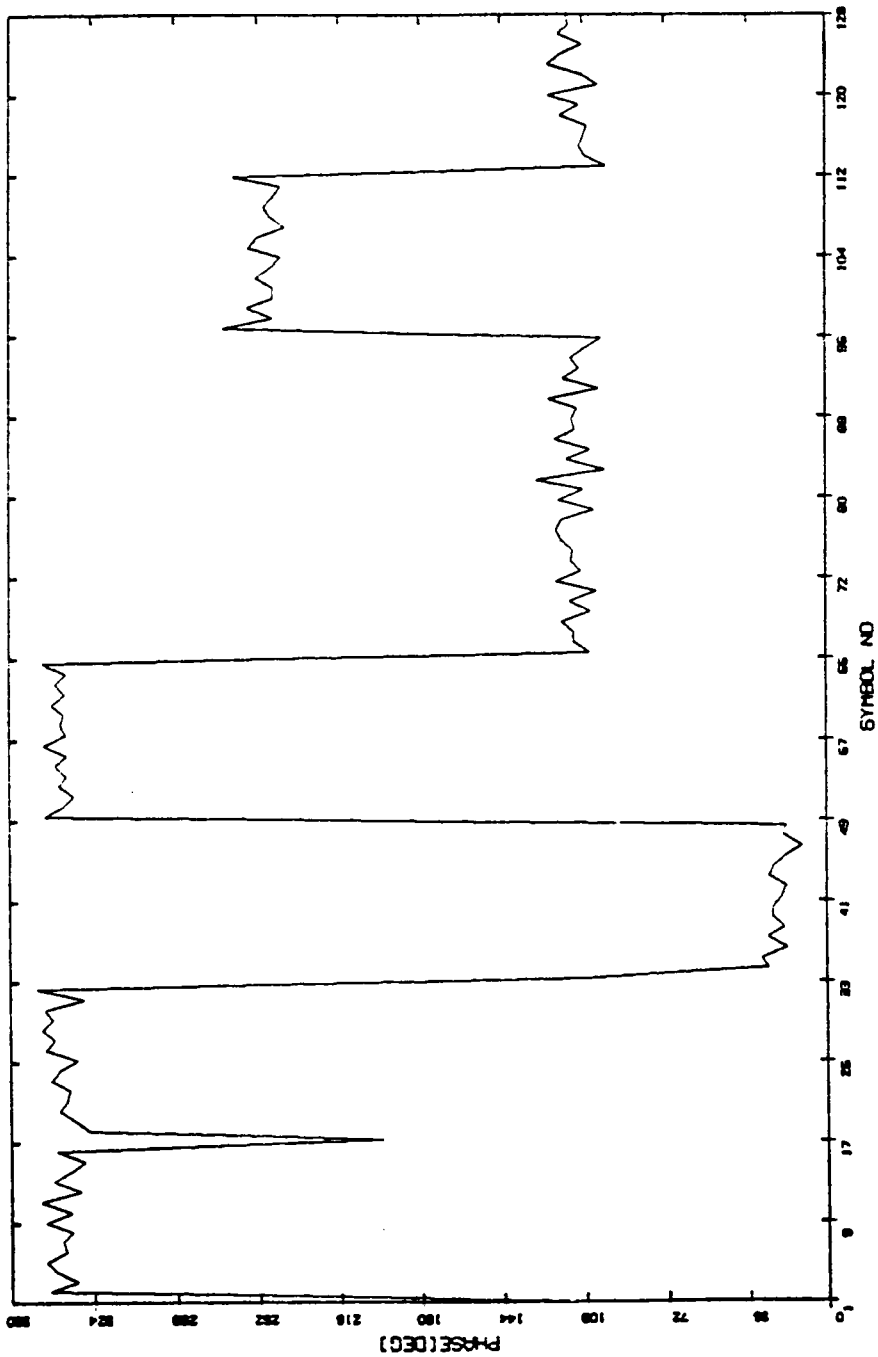

Figure 104. Estimated phases of TCM 8-DPSK after the differential phase decoding in the receiver (compare with the result of differential phase encoding in Fig.97).

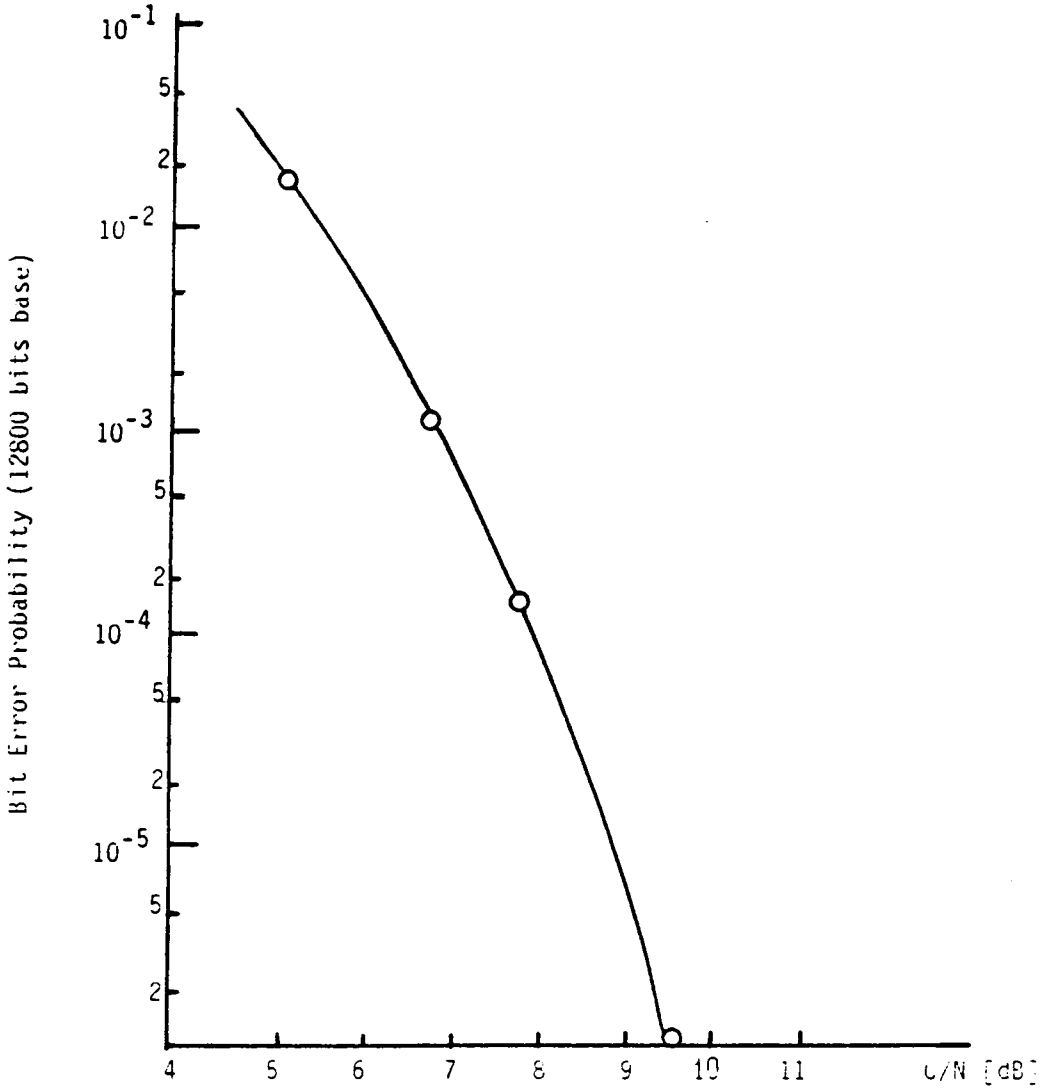

Figure 105. Result of TCM 8-DPSK modem back to back test with 6400 simulated symbols (12800 bits).

in the data sequence and in noise generation, seeds for the symbol generator and the noise generator were changed every 128 symbol unit.

Athough the modem back to back test result for TCM 8-DPSK is depicted in Fig.105, it is difficult to compare directly this result with other results in references or papers. This is because : first, the modem back to back test result obtained here is the average of a relatively small amount of data processing. So, the result obtained may differ from the results of a similar test, in which simulation of 6400 symbols are repeated many times. Therefore, the result depicted in Fig.105 is only one case of many other possible results. Second, we have used C/N ratios at the transmit filter output instead of E_b/N_o in our simulation, and we do not know how the performance in other results were measured. Third, results from other TCM 8-DPSK modem back to back tests using a similar simulation method cannot be found.

Therefore, it is too early to conclude whether our simulation result for the modem back to back test is correct or not at this point, and making a conclusion based on fewer symbols than 10^8 (to achieve a BER of 10^{-8}) seems to be very risky. However, the results should be accurate at error rates above $2x10^{-3}$, and probably down to 10^{-4}, since 6400 symbols were used in the tests.

6.4. Summary

Based on the system level models and the component level models described in Chapter 5, several simulation programs were written to simulate the LMSS channel.

The programs were : LANSIM 1 for coherent QPSK and MSK, LANSIM 2 for TCM 8-DPSK, and LANSIM 3 for DGMSK. With these programs, modem back to back tests, which are needed as a reference for further performance analysis, were performed first. Then fading channel tests were also performed to see the effect of fading in coherent QPSK and MSK cases only.

In the coherent QPSK and MSK case, modem back to back test results were generally in agreement with the theoretical performance, even though MSK was inferior to QPSK in the modem back to back performance. Fading channel test results of these coherent schemes evidently shows the effect of fading, i.e, when fading is severe, the average BER is bad. To see the effect of a fast varying fades, bit error probability was also calculated. The results of this test reveal that the specific bits in the severe fading region are more likely to be corrupted than the bits located in the milder fade. In general, MSK is inferior to QPSK, based on the results of the modem back to back test and fading channel test. However, the difference in the performance between these two coherent schemes is not large.

For the case of the noncoherent schemes, intermediate results of the simulation process were illustrated for ease of understanding of the simulation flow. However, only the result of the TCM 8-DPSK modem back to back test was reported here, because the program designed for DGMSK simulation does not yet work properly. In addition, the output of the propagation simulator that should be used for the fading channel test was not completely ready, so results of fading channel tests were also not reported. Although some fading channel tests were possible with a small number of simulated symbols, it was not considered desirable to make an analysis and evaluate the performances of TCM 8-DPSK and DGMSK based on such a small amount of data, especially when direct simulation was used as in the TCM 8-DPSK and DGMSK cases.

VII. Concluding Remarks

Performance of two satellite radio communication systems was examined by computer simulation. For the simulation of analog communications, a spread spectrum system using a chirp technique called coded multiple chirp was proposed. Its application as a spread spectrum overlay service on analog FM-TV was examined.

For the simulation of digital communications, four digital modulation schemes were selected for a through performance evaluation of a land mobile satellite system (LMSS) under fading conditions.

7.1. Chirp Spread Spectrum System and Overlay Service

There are many applications for low cost satellite communication links in which a large number of small terminals send data at a low rate to a central terminal. Spread spectrum is an important technique in any satellite communication system using very small antennas (VSAT's) because it provides a means for multiple access of a single communication channel with low interference to other users.

However, if conventional multiple access techniques are used, such as FDMA (Frequency Division Multiple Access) or TDMA (Time Division Multiple Access), the adjacent channel interference may be excessive. In this study, the capacity and performance of VSAT links overlaid on an occupied channel were investigated for the chirp system.

Chirp is a technique in which binary signals are represented by a rapid up or down sweep in frequency. The technique has been widely used in radars, but rarely for communications. We propose a system using multiple chirps to represent binary data 1's and 0's in an overlay service. The major advantage of chirp as a spread spectrum technique lies in the ease with which the chirp signal can be de-spread. De-spreading is achieved with passive dispersive filters, typically surface acoustic wave (SAW) devices, resulting in very much simpler receivers with no lock delay time at the receiver.

Multiple access with chirp is poor when only the slope of the chirp signal is varied. To improve multiple access capability, we proposed a system which we call "Multiple-Chirp", in which a sequence of fixed slope chirps is transmitted. The chirps can be up- or down-chirps, and various combinations of up and down slopes in a 16 or 32 bit word provide a means of identifying individual signals. Multiple access performance with multi-chirp is well below those of other spread spectrum techniques, and thus we do not recommend chirp for this purpose.

We investigated chirp for an overlay service in which data could be sent at a low rate over an FM-TV channel. The multi-chirp signal was designed to spread a 2.4 kbps data signal over a 5 MHz bandwidth using a 16-chirp word of up and down chirps. A major difficulty we encountered was a lack of published data on the spectrum of FM-TV signals. We simulated some typical and worst-case TV spectra so that we could assess the mutual interference problems for a chirp overlay system.

FM-TV presents a problem for a chirp overlay system because chirp is a frequency modulation technique and FM-TV receiver uses an FM demodulator to recover the TV signal. To assess the extent to which the overlay signal would cause interference, we simulated the response of a TV demodulator to a multi-chirp signal, and we were able to show that a 36 dB power ratio for TV to overlay signal would result in unnoticeable impairment of the TV video. For a thorough analysis of mutual interference effects when a multi-chirp signal was overlaid on the satellite TV channel, a 256 step random video waveform was used as a simulation model. The overlay signal power was set to a level

36 dB below that of the TV signal to ensure no impairment of the recovered TV video. Then, we varied the position of the 5 MHz wide chirp signal within the transponder band and calculated bit error rates for the data link.

Placing the chirp signal in the center of the transponder leads to very poor performance due to the concentration of TV signal energy there. When the chirp signal is moved towards the edge of the transponder, acceptable error rates are obtained. Data rates up to 25 kbps are achievable when the chirp signal is located at the edge of the transponder band. With smaller frequency offsets, data rates of 2.4 and 4.8 kbps would be possible. At C band, a 350 mW transmitter and 2.4 m satellite dish could send such a signal if the chirp frequency is offset at least 8 MHz from the TV video carrier.

We conclude that chirp is a feasible technique for an overlay service, in which a low data rate chirp signal is overlaid on top of an occupied FM-TV channel with a low power transmitter and minimal adjacent satellite interference, although capacity of the overlay circuit is small.

7.2. Land Mobile Satellite System (LMSS) under Fading

For the proper selection of a spectrally efficient modulation and fade resistant coding scheme in a land mobile satellite system (LMSS), four digital modulation techniques and a channel encoding scheme were selected and their performance under fading conditions was evaluated by computer simulation.

The selected digital modulation techniques were: coherent QPSK and MSK, and noncoherent TCM 8-DPSK and DGMSK with differential detection. A newly developed 16 state trellis code with a code rate of 2/3 was used for both the two noncoherent systems, whereas no channel encoding was employed for the two coherent systems. In addition, block interleaving and deinterleaving was used to protect against burst errors under fading conditions.

For computer simulation of the four digital modulation schemes, modeling was done at the system and component levels. Functional components were modeled in a modular structure for

modification and interconnection between modules. These were: a random symbol generator, a rate 2/3 TCM encoder and decoder, a 128 symbol block interleaver and deinterleaver, a differential phase encoder and decoder, filters, a noise generator, modems for the four different digital modulation schemes, and a performance evaluator for the average BER or symbol error calculation. An optional nonlinear TWTA simulation module was also designed.

Based on the specifications and component models, three separate simulation programs were designed. These were: LANSIM 1 for coherent QPSK and MSK, LANSIM 2 for noncoherent TCM 8-DPSK, and LANSIM 3 for noncoherent DGMSK. All simulations were performed in baseband by using the complex envelope of the modulated signal and by using frequency domain filters, that were simulated with their lowpass equivalents. For convenience and simplicity of simulation, constant zero phases was assumed in the filters.

For the performance evaluation, analytically calculated noise power at fixed $\frac{E_b}{N_o}$ ratios was inserted at the average BER calculation stage in the coherent QPSK and MSK cases, for indirect (or hybrid) simulation, whereas randomly generated noise at fixed C/N ratios was added to the modulated signal in noncoherent TCM 8-DPSK and DGMSK, for direct simulation.

The modem back to back test results of the coherent QPSK and MSK is in good agreement with theoretical performance in terms of average BER, although MSK is inferior to QPSK in general. However, the degree of relative degradation of MSK to QPSK is less than 0.5 dB of $\frac{E_b}{N_o}$ ratios at the BER range of 10^{-2} to 10^{-9}.

To see the effect of fading in coherent QPSK and MSK, two kinds of tests were performed. The first test was done to find the performance degradation of average BER when five fading characteristics were applied to the transmit filter output of coherent QPSK and MSK. These five fading characteristics were selected from W. Vogel's [50] data set, in which received signal levels were measured by a vehicle moving at 55 mph while receiving a 1.5 GHz signal transmission.

These five selected fading data sets represented some possible cases of fading in practical situations for an LMSS, such as a LOS signal, or a partially shadowed case. The length of each fading data set was arranged to match the simulation time required to process 128 symbols (2 bits/symbol) at 2.4 kbps.

The results of the first test, expressed in average BER, reveals that a large degradation occurs when there is a severe fade, while smaller degradation occurs for milder fades, as was expected. However, system performance expressed in average BER was not considered to be a sufficient measure if we want to see the effect of a fast varying fade during the simulation cycle. Therefore, individual bit error probability were calculated in the second test. Results of this test at the arbitrarily selected $\frac{E_b}{N_o}$ ratios of 12 and 15 dB showed that the bits in the severe fade were relatively much more often degraded than the bits in the mild fade. This degradation of bits transmitted during a deeper fade will result in burst errors if the fade duration is relatively long compared with the bit interval. To avoid this phenomenon, interleaving and deinterleaving must be used.

The results of the modem back to back test, and tests under fading, for coherent QPSK and MSK confirm that fading can degrade the system performance greatly, especially when the fade is severe. When we compare the relative performance of QPSK and MSK, MSK is inferior to QPSK in overall tests. It is not clear why this relative degradation happens at this moment. However, the relatively wider power spectrum of MSK signal may cause it to lose some of its power when the same type of modem filters are used both for QPSK and for MSK, and this fact may account for the degradation of MSK relative to QPSK in our simulation.

For the noncoherent TCM 8-DPSK and DGMSK cases, the simulation could not be completed because the propagation simulator that should provide the various fading data was not fully integrated into the channel simulator programs, LANSIM 2, and LANSIM 3. As a result, it was not possible to do the simulation under the various, lengthy fading conditions for the noncoherent schemes. Hence simulation under fading in noncohernt TCM 8-DPSK and DGMSK is left incomplete.

The preliminary results for DGMSK simulation with 128 symbols exhibited an unexpectedly large number of errors in noise, and we concluded that the DGMSK simulation program was not working properly.

So only the modem back to back test result of TCM 8-DPSK was reported. No fading channel test results for TCM 8-DPSK and DGMSK were available at the time of writing. Although fading channel tests with a small number of symbols were possible, analysis and performance evaluation based on

this small number of symbols was considered to be unreliable in the case of direct simulation. Hence, this approach was not used. However, we believe that the required simulation and the performance evaluation of noncoherent schemes under fading conditions can be done easily once the integration of the propagation simulator is completed.

The modem back to back test result for TCM 8-DPSK was obtained from repetitive simulation with 6400 symbol (12800 bits) transmission. However, comparison with other results in the published references was not easy, because we used C/N ratios rather than $\frac{E_b}{N_o}$ ratio for the calculation of bit error, and the published data were mostly obtained from analytical calculations, rather than the direct simulation we used. In addition, the obtained result is only one of many possible results when a large number of symbols are simulated. Therefore, it is not considered desirable to make a conclusion that TCM 8-DPSK works properly or not, with the modem back to back test result obtained so far.

Our conclusion, based on the simulation results obtained so far, is that coherent QPSK is better than coherent MSK in a fading channel. Comparison of coherent QPSK and MSK with noncoherent TCM 8-DPSK and DGMSK was not possible because simulation of the noncoherent schemes was not completed.

For further research, we recommend the following :

1. Use the ratio of the bit energy E_b and the noise power spectral density N_o in the case of TCM 8-DPSK and DGMSK, instead of C/N ratio, at the receive filter output for easy comparison with other published simulation results. For the bit energy calculation in TCM 8-DPSK, soft decision must be used for trellis decoding.
2. The differential detection in DGMSK must be done in bit units; either 1-bit or 2-bit detection is used. The differential encoding, based on the encoded (convolutional encoding) symbol, does not work properly when the signal to noise ratio is low, and fading is severe. The 2-bit differential detection will enhance the detection capability compared with the 1-bit case, because the phase

change between 2 bit intervals contains more accurate information for the correct decision of the received signal state.

3. Diversify the coding schemes by using different code rates, different code lengths, and different types of codes, such as block codes or specially designed burst error protection codes. The effects of fading can be analyzed more precisely for this diversity of coding, if fade duration and fade depth can be dynamically varied.
4. Increase the block interleaver size as far as possible, while keeping the transmission delay time as small as possible, for maximum burst error protection. For this, a thorough investigation of the average fade duration with the fade data to be used must be carried out.
5. Include a module that can simulate Doppler shift. To get the simulation results as close as possible to reality in an LMSS channel under fading, inclusion of the Doppler shift is necessary.

IIX. References

1. J. R. Klauder, et al. "The Theory and Design of Chirp Radars," Bell System Technical Journal, vol. 29, No. 4, July 1960, pp.745-809.

2. V. Ramanan, "An Asyncronous Multiple Access Scheme for Satellite Communications," Ph.D. Dissertation, Department of Electronic and Electrical Engineering, University of Birmingham, England, June 1983.

3. R. S. Berkowitz, Modern Radar, John Wiley, New York, NY, 1965.

4. C. E. Cook, M. Bernfeld, Radar Signals, Academic Press, New York, NY, 1967.

5. H. O. Ramp, E. R. Wingrove, "Principles of Pulse Compression," IRE Trans. Military Electronics, vol. MIL-5, April 1961, pp. 109-116.

6. R. C. Dixon, Spread Spectrum Systems, John Wiley, New York, NY, 1976.

7. M. R. Winkler, "Chirp Signals for Communications," IEEE WESCON Convention Record, 1962.

8. E. K. Holland-Moritx, J. C. Dute, and D. R. Brundage, "Swept Frequency Modulation, Proc. Nation. Electron. Conf. vol. 22, 1966, pp. 469-474.

9. A. J. Berni, W. D. Gregg, "On the Utility of Chirp Modulation for Digital Signaling," IEEE Trans. Comm., vol. COM-21, June 1973, pp. 748-751.

10. W. Hirt, S. Pasupathy, "Continuous Phase Chirp (CPC) Signals for Binary Data Communications," IEEE Trans. Comm. vol. COM-29, June 1981, pp. 836-858.

11. D. S. Dayton, "Coming to Grips with Multipath Ghosts," Electronics, vol. 40, Nov 1967, pp 104-108.

12. G. F. Gott, J. P. Newsome, "HF Data Transmission using Chirp Signals", Proc. Inst. Elec. Eng., vol. 118, Sept 1971, pp.1162-1166.

13. G. W. Barnes, D. Hirst, D. J. James, "Chirp Modulation System in Aeronautical Satellite," AGARD Conf. Proc., No. 87, Avionics in Spacecraft, Royal Aircraft Establishment, Rome, Italy, 1971.

14. Max Kowatsch, J. T. Lafferl, "A Spread-Spectrum Concept Combining Chirp Modulation and Pseudonoise Coding," IEEE Trans.Comm., vol. COM-30, No. 10, Oct 1983, pp. 1122-1142.

15. P. W. Baier, R. Simons, H. Waibel, "Chirp-PN-PSK Signale als Spread - Spectrum - Signalformen geringer Dopplerempfindlichkeit and grosser Signalformvielhalt," NTZ Archiv. vol. 3, Feb 1981, pp.29-33.

16. M. Kowatsch, F. J. Siefert, J. Lafferl, "Comments on Transmission System Using Pseudonoise Modulation of Linear Chirps," IEEE Trans. Aerosp. Electron. System, vol. AES-17, Mar 1981, pp.300-303.

17. R. Gold, "Characteristic Linear Sequences and Their Coset Functions," J. Soc. Ind. Appl. Math, May 1965.

18. T. Kasami, "Weight Distribution Formula for Some Class of Cyclic Codes," University of Illinois, Urbana, Rept. R-265, Apr. 1966.

19. C. E. Cook, "Pulse Compression - Key to More Efficient Radar Transmission," Proc. of IRE, vol. 48, Mar 1960, pp. 310-316.

20. B. A. Carlson, Communications Systems, McGraw Hill, New YorK 1975.

21. M. Cohn, W. L. Eastman, "A Class of Balanced Binary Sequence with Optimal Autocorrelation Properties" IEEE Trans. Inform. Theory, vol. IT-23, 1977, pp.38-42.

22. D. V. Sarwate, M. B. Pursley, "Crosscorrelation Properties of Pseudorandom and Related Sequences," Proc. of IEEE, vol. 68, No. 5, May 1980, pp.593-619.

23. D.V. Sarwate, "Bound on Cross-Correlation and Autocorrelation of Sequences," IEEE Trans. Inform. Theory, vol. IT-25, 1979, pp.720-724.

24. S. Stein, "Unified Analysis of Certain Coherent and Non-Coherent Binary Communications Systems," IEEE Trans. Inform. Theory, vol. IT-10, Jan 1964, pp.43-51.

25. C. W. Helstrom, "Resolution of Signals in White Gaussian Noise," Proc. IRE, vol. 43, Sept 1955, pp.1111-1118.

26. L. W. Couch II, Digital and Analog Communication Systems, MacMillan, New York, NY 1983, pp.362-364.

27. T. Pratt, C. W. Bostian, Satellite Communications, John Wiley, Inc., New York, NY 1986, pp.241-242.

28. R. M. Gagliardi, Satellite Communications, Lifetime Learning Publications, Belmont, CA, 1983, pp.248.

29. K. Feher, Digital Communications, Prentice-Hall, NJ, 1983, pp. 375-379.

30. F. G. Stremler, Introduction to Communication Systems, Addison-Wesley, Massachusetts, 1982, pp.338-341.

31. R. L. Freeman, Telecommunication Transmission Handbook, John Wiley, Inc., NY 1981, pp.194.

32. M. A. Maggenti, "Spread Spectrum Multiple Access and Overlay Service," M.S. Thesis, VPI&SU, Mar 1987.

33. D. M. Jansky, M. C. Jeruchim, Communication Satellite in Geostationary Orbit, Artech House, 1983, pp.482-485.

34. CCIR: XIV'th Plenary Assembly, Kyoto, Japan, vol.4, Report 464 on "Pre-emphasis Characteristics for Frequency Modulation Systems for FDM Telephony in the Fixed Satellite Service," Geneva, 1978.

35. "MSAT-X Quarterly", Jet Propulsion Lab., Pasadena, CA, no.1, Oct 1984.

36. G. H. Knouse, "Terrestrial/Land Mobile Satellite Considerations, NASA Plans, and Critical Issues", IEEE Trans. on Vehicular Technology, vol.VT-29, pp.370-374, Nov 1980.

37. G. H. Knouse and P. A. Castruccio, "The Concept of an Integrated Terrestrial/Land Mobile Satellite System", IEEE Trans. on Vehicular Technology, vol.VT-30, pp.97-101, Aug 1981.

38. F. Naderi, W. J. Weber and G. H. Knouse, "NASA's Mobile Satellite Communication Program; Ground and Space Segment Technology", Proceedings of the 35th Congress of The International Astronautical Federation, Lausanne, Switzerland, Oct 1984.

39. G. C. Hess, "Land Mobile Satellite Path Loss Measurements", Third Year ATS-6 Experiment Final Report, Motorola Inc., Schaumberg, IL, Sept. 6, 1978.

40. R. E, Anderson, R. L. Frey, J. R. Lewis, and R. T. Milton, "Satellite-Aided Mobile Communications: Experiment, Applications and Prospects", IEEE Trans. on Vehicular Technology, vol. VT-30, no.2, pp. 54-61, May 1981.

41. W. J. Vogel, and G. W. Torrence, "Measurement Results From a Balloon Experiment Simulating Land Mobile Satellite Transmissions", MSAT-X Report No. 101, Apr 1984.

42. D. Bodson, G. F. McClure, and S. R. McConoughey, editors. Land-Mobile Communications Engineering, IEEE Press, New York, 1984.

43. W. C. Jakes, Microwave Mobile Communications, Wiley, New York, 1974.

44. W. C. Y. Lee, Mobile Communication Engineering, Mcgraw Hill, New York 1982.

45. R. W. Huck, J. S. Butterworth, and E. E. Matt, "Propagation Measurement for Land Mobile Satellite Services", Proceedings of IEEE 33rd Vehicular Technology Conference, pp. 265-268, 1983.

46. J. S. Butterworth and E. E. Matt, "The characterization of Propagation Effects for Land Mobile Satellite Services", Proceedings of IEE International Conference on Satellite Systems for Mobile Communication and Navigation, London, pp. 51-54, June 1983.

47. J. S. Butterworth, "Propagation Measurements for Land-Mobile Satellite Services in the 800 MHz Band", Communications Research Centre, Department of Communications, Canada, Aug 1984.

48. J. S. Butterworth, "Propagation Measurements for Land-Mobile Satellite Services at 1542 MHz Band", Communications Research Centre, Department of Communications, Canada, Aug 1984.

49. J. S. Butterworth, "The Description and Evaluation of Mobile Communications Channel Simulator", Proceedings of the Propagation Workshop in Support of MSAT-X, JPL, Pasadana, CA, pp. 4.3-4.21, Jan 1985

50. W. J. Vogel, "PELMOSS Balloon Experiments", Proceedings of the Propagation Workshop in Support of MSAT-X, JPL, Pasadena, CA, pp. 1.5-1.18, Jan 1985.

51. G. C. Hess, "Land-Mobile Satellite Excess Path Loss Measurements", IEEE Trans. on Vehicular Technology, vol. VT-29, pp. 290-297, May 1980.

52. G. C. Hess, private communications, Nov. 15, 1984.

53. R. E. Anderson, R. L. Frey, and J. R. Lewis, "Satellite-Aided Mobile Communications Limited Operational Test in the Trucking Industry", Final Report for NASA Contract NAS5-24365(N81-20338), June 1979.

54. C. Loo, "A Statistical Model for Land Mobile Satellite Link", Proceedings of the 1984 IEEE International Communications Conferences ,pp. 588-594, 1984.

55. F. Davarian and J. Sumida, "Channel Simulator Tests Digital Mobile Radios", Microwaves and RF, vol.23, pp.115-118, Aug 1984.

56. F. Davarian, "JPL's Mobile Communications Channel Hardware Simulator ", Proceedings of the Propagation Workshop in Support of MSAT-X, JPL, Pasadena, CA, pp. 2.5-2.18, Jan 1985.

57. A. B. Samasi, A. B. Springett. J. C. Sumida, and J. J. Richter, "Land Mobile Satellite Service (LMSS) Channel Simulator: An End-to-End Hardware Simulation and Study of the LMSS Communication Link", JPL, Pasadena, CA, NASA-CR-173744, May 1984.

58. D.Divsalar, "Software Simulation of the LMSS Propagation Channel", Proceedings of the Propagation Workshop in Support of MSAT-X, JPL, Pasadena, CA, pp. 2.19-2.46, Jan 1985.

59. B. Trevor, "Ultra-High Frequency Propagation through Woods and Underbursh", RCA Review, vol. 5, pp. 97-100, July 1940.

60. W. J. Weissberger et al, "Radio Wave Propagation: A Handbook of Practical Techniques for Computing Basic Transmission Loss and Field Strength", Electromagnetic Compatibility Analysis Center, Report No. ECAC-HDBK-82-049, Sept 1982.

61. A. Weissberger, "An Initial Critical Summary of Models for Predicting the Attenuation of Radio Waves by Trees", ESD-TR-81-101, Electromagnetic Compatibility Analysis Center, Annapolis, MD, July 1982.

62. P. F. Sass, "Propagation Measurements for UHF spread spectrum mobile Communications", IEEE Trans. on Vehicular Technology, vol. VT-32, pp. 168-176, May 1983.

63. R. H. Lang, A. Schineider, F. J. Altman, and K. Truang, "UHF Radiowave .Propagation Through Forests", CyberCom Technical Report, CTR- 108-06, May 1984.

64. R. H. Lang, A, Schneider, S. Seker, and F. J. Altman, "UHF Radiowave Propagation through Forests", CyberCom Technical Reports, CTR-108-01, Sept 1982.

65. T. Tamir, "On Radio Wave Propagation in Forest Environments", IEEE Trans. on Antennas and Propagation, vol. AP-15, pp. 806-817, Nov 1967.

66. W. L. Stutzman, F. W. Colliver, and H. S. Crawford, "Microwave Transmission Measurements for Estimation of the Weight of Standing Pine Trees", IEEE Trans. on Antennas and Propagation, vol. AP-27, pp. 22-26, Jan 1979.

67. G. S. Brown, and W. J. Curry, "A Theory and Model for Wave Propagation through Foilage", Radio Science, vol.17, pp. 1027-1036, Sept- Oct 1982.

68. G. S. Brown, Seminar presented at VPI&SU on current research for rough surface scattering. May 1985.

69. J. A. Saxton and J. A. Lane, "VHF and UHF Reception and Effects of Trees and Other Obstacles", Wireless World, vol.61, pp. 229-232, may 1955.

70. H. T Head, "The Influence of Trees on Television Field Strengths at Ultra-High Frequencies", Proceedings of the IRE, vol. 48, pp. 1016-1020, June 1960.

71. A. H. Lagrone, "Propagation of VHF and UHF Electromagnetic Waves over a Grove of Trees in Full Leaf", IEEE Trans. on Antennas and Propagation, vol. AP-25, pp. 866-869, Nov 1977.

72. D. O. Reudink, "Estimates of Path Loss and Radiated Power for UHF Mobile Satellite Systems", Bell System Technical Journal, vol. 62, pp. 2493-2512, Oct 1983.

73. K. Bullington, "Radio Propagation Fundamentals", Bell System Technical Journal, vol. 36, pp. 114-122, May 1957.

74. P. L. Rice, "Some Effects of Buildings and Vegetation on VHF/UHF Propagation", IEEE Mountain West EMC Conference Record. pp.1-10, Nov 1971.

75. F. Davarian, "Channel Simulation to Facilitate Mobile-Satellite Communications Research", IEEE Trans. on Communications, vol. COM-35, No. 1, pp. 47-56, Jan 1987.

76. A. A.Saleh, "Frequency-Independent and Frequency Dependent Nonlinear Models Of TWTA", IEEE Trans. on Communication, vol. COM-29. No. 11. pp. 1715-1720, Nov 1981.

77. R. G. Schmier and C. W. Bostian, " Fade Duration in Satellite-Path Mobile Radio Propagation", Virginia Tech Report, EE SATCOM-86-5, Dec 1986.

78. A. J. Viterbi and J.K. Omura, Principles of Digital Communication and Coding, Mcgraw-Hill, New York, 1979.

79. K. Brayer, Data Communications via Fading Channels, IEEE Press, 1975.

80. R.G. Schmier, " Fade Durations in Satellite-Path Mobile Radio Propagation", M.S. Thesis, VPI&SU, Dec 1986.

81. W.T. Smith, " Statistical Modeling for Land Mobile Satellite Communications", M.S.Thesis, VPI&SU, Aug 1986.

82. P. Beckmann and A. Spizzichino, The Scattering of Electromagnetic Waves from Rough Surfaces, Pergamon Press, New York, 1963.

83. V. Jamnejad, " Ground Multipath in TOPEX's Precision Orbit Determination tracking System", JPL Interoffice Memo. 3365-84-003, JPL, Pasadena, CA, Jan 1985.

84. W.T. Smith and W.L.Stutzman, " Statistical Modeling for LMSS", VA Tech Report EE Statcom 86-3, Performed for JPL sponsored by NASA under Contract 956512, Aug 1986.

85. K. Kinoshita, M. Hata and H. Nagabuchi, " Evaluation of 16 Kbits/s Digital Voice Transmission on Mobile Radio", IEEE Trans. on Vehicular Technology, vol.VT-33, No.4, Nov 1984, pp 323-327.

86. T. Miki and M. Hata, " Performance of 16Kbits/s GMSK Transmission with Postdetection Selection Diversity in Land Mobile Radio", IEEE Journal on Selected Areas in Communications, vol. SAC-2, No. 4, July 1984, pp 512-517.

87. K. Hirade, K. Murota and M. Hata, " GMSK Transmission Performance in Land Mobile Radio", Conference Proceedings, GLOBALCOM 1982, pp 3.4.1-3.4.6.

88. M.K. Simon, and C. C. Wang, " Two-Bit Differential Detection of MSK", IEEE Conference, pp 22.3.1- 22.3.6. Not Specified.

89. M.K. Simon, and C. C. Wang, " Differential Detection of Gaussian MSK in a Mobile Radio Environment", IEEE Trans. on Vehicular Tech, vol.VT-33, Nov 1984, pp 309-pp320.

90. K.S. Chung, " Generalized Tamed FM and Its Application for Mobile Radio Communications", IEEE Journal on Selected Area in Communications, vol. SAC-2, No.4, July 1984, pp 487-497.

91. M. Rabzel and S. Pasupathy, " Spectral Shaping in MSK Type Signals", IEEE Trans. on Communications, vol. COM-26, No.1, Jan 1978, pp 189-195.

92. G. Ungerboeck, " Trellis Coded Modulation with Redundant Signal Sets Part I: Introduction", IEEE Communications Magazine, vol. 25, No. 2. Feb 1987, pp 5-11.

93. T. Masamura et al, " Differential Detection of MSK with Nonredundant Error Correction", IEEE Trans. on Communications, vol. COM-27, No. 6, June 1979, PP 912-917.

94. S. Pasupathy, " MSK: A Spectrally Efficient Modulation", IEEE Communications Magazine, vol. 19, No.4, July, 1979.

95. B.P. Lathi, Modern Digital and Analog Communication Systems, Holt Rinehart and Winston, New York, 1983.

96. M. K. Simon, " Double Symbol Error Rates for Differential Detection of Narrow Band FM", IEEE Trans. on Communications, vol. COM-33, No. 5, May 1985, pp 394-398.

97. J. L. Massy, " Coding and Modulation in Digital Modulations ", Proceedings of 1974 International Zurich Serminar on Digital Communications", Zurich, Switzerland, Mar 1974, pp E2(1)-E2(4).

98. G. Ungerboeck, " Trellis Coded Modulation with Redundant Signal Sets Part II: State of the Art", IEEE Communications Magazine, vol. 25, No. 2. Feb 1987, pp 12-21.

99. S. Lin , and D. J. Costello. Jr, Error Control Coding, Prentice- Hall, Englewood Cliffs, N.J, 1983.

100. JPL draft for TCM 8-PSK Transmitter. Mail Stop 238. JPL, Sept 1987.

101. S. Ogose, and K. Murita, " Differrentially Encoded GMSK with 2-bit Differential Detection", Trans. of IEEE Japan, vol. J64-B, No. 4, Apr 1981, pp 248-254.

102. R.W. Hamming, Coding and Informatiom Theory, 2nd Edition, Prentice- Hall, 1982.

103. L.C. Palmer, "Computer Modeling and Simulation of Communication Satellite Channels", IEEE Journal on Selected Area in Communications, vol. SAC-2, No.1, Jan 1984.

104. GTE private Communication, "Computer Simulation of QPSK Data Communication System ", Jan 1981.

105. R.E. Zimmer and R.L. Peterson, Digital Communications and Spread Spectrum Systyems, Macmillan Publishing Co. New York, 1985.

106. W. H. Press, et al. "Numerical Recipes: The Art of Scientific Computing", Cambridge University Press, Cambridge, 1986.

107. E.O. Brigham, The Fast Fourier Transform, Prentice-Hall, Englewood Cliffs, NJ 1974.

108. A.R. Kaye, D.A. George, and M.J. Eric, "Analysis and Compensation of Bandpass Nonlinearities for Communications", IEEE Trans. on Communications, vol.COM-20, Oct 1972.

109. P. Hetrakul and D.P. Taylor, "Nonlinear Quadrature Model for a Travelling Wave Tube Type ASmplifier", Electronics Letters, vol.11,Jan 1975, pp.364-374.

110. M.K. Simon and D. Divsalar, "The Performance of Trellis Coded Multilevel DPSK on a Fading Mobile Satellite Channel", Proceedings of Globalcom 87, Baltimore,MD, Oct 1987.

111. Junghwan Kim, "Performance Evaluation of Nonlinear Satellite Link by Computer Simulation", M.S Thesis, VPI&SU, Dec 1985.

112. W.J. Vogel, and E. K. Smith, "Propagation Considerations in Land-Mobile Satellite Reansmission", MSAT-X Report, No.105,NSAS-JPL, Pasadena, CA, Jan 1985.

113. W.S. Bradley and W.L. Stutzman, "Propagation Modeling for Land-Mobile Satellite Communications", Virginia Tech Report, EE Satcom 85-3, performed for JPL sponsored by NASA under Contract 956512, Aug 1985.

114. J.I. Marcum, Table of Q-Functions, RM-339, ASTIA Document Number AD 116551, The Rand Corporation, Jan 1950.

The vita has been removed from the scanned document